The Second International Conference

Materials Science and Nanotechnology

MSN-2024

ABSTRACT BOOK

BRICS 2024
RUSSIA

Ekaterinburg, Russia
27—30 August 2024

Ural Federal University
named after the first President
of Russia B.N.Yeltsin

УДК **538.9**
ББК 22.37
С-423

Materials Science and Nanotechnology (MSN-2024). Abstract Book of the Second International Conference (Ekaterinburg, August 27-30, 2024) Ekaterinburg, Ural Federal University, 2024- 198 с.
ISBN 978-5-9500624-7-6

Organizers

School of Natural Sciences and Mathematics, Ural Federal University named after the first President of Russia B.N. Yeltsin (UrFU)
http://www.urfu.ru

Ural Center for Shared Use “Modern Nanotechnology” UrFU
http://nanocenter.urfu.ru

Labfer Ltd.
http://www.labfer.com

Ferroelectric Laboratory, INSM UrFU
http://labfer.ins.urfu.ru

General chair

Prof. Vladimir Shur

Organizing committee

Vladimir Kruzhaev, Ural Federal University, Ekaterinburg, Russia
Alexander Sigov, MIREA - Russian Technological University, Moscow, Russia
Nikolai Mushnikov, M. N. Mikheev Institute of Metal Physics, Ekaterinburg, Russia
Leonid Korotkov, Voronezh State Technical University, Voronezh, Russia
Sergey Vakhrushev, Ioffe Institute, Saint-Petersburg, Russia
Alexander Vtyurin, Kirensky Institute of Physics, Krasnoyarsk, Russia
Xiaoyong Wei, Xi'an Jiaotong University, Xi'an, China
Le He, Soochow University, Jiangsu, China

Local organizing committee

Prof. Vladimir Shur	Ekaterinburg, Russia
Mrs. Elena Pelegova	Ekaterinburg, Russia
Mrs. Yana Mayorova	Ekaterinburg, Russia
Dr. Ekaterina Shishkina	Ekaterinburg, Russia
Mr. Eduard Linker	Ekaterinburg, Russia
Dr. Andrei Ushakov	Ekaterinburg, Russia
Dr. Victoria Pryakhina	Ekaterinburg, Russia

ISBN 978-5-9500624-7-6
9 785950 062476

ББК 22.37

Ural Federal University
named after the first President
of Russia B.N. Yeltsin

MSN-2024 sponsors

Ostec-ArtTool Ltd.
https://www.arttool.ru

nanometric

Avesta Ltd.
https://avesta.ru/

АВЕСТА
ЛАЗЕРЫ И ОПТИЧЕСКИЕ СИСТЕМЫ

TUTORIAL LECTURES

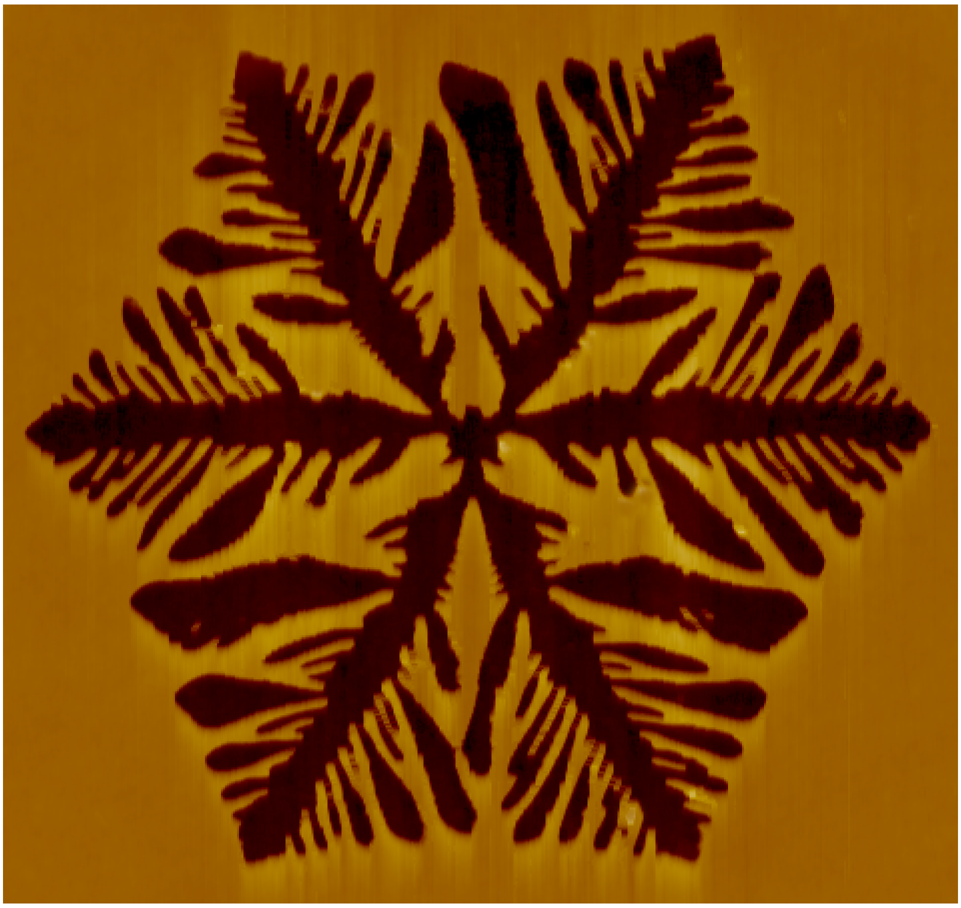

Geometric ideas in condensed matter physics

A. Pyatakov

Lomonosov Moscow State University, Moscow, Russia

pyatakov@physics.msu.ru

"All my physics is nothing else but geometry" used to say Descartes, and two centuries later Pierre Curie formulated a principle: "it is the dissymmetry that creates the phenomena".

In this lecture on the example of the new topical class of materials, van der Waals media, it is shown how bending of the material creates the electric polarization and magnetization, and how the curvilinear geometry manifest itself in the magnetization distribution. The analogues of geometrical extrema problems in magnetism will also be discussed on the example of the shape of bubble domains and stripe magnetic domain structure "refraction" in the electric field.

Towards quantitative piezoresponse force microscopy measurements: theory and experiment

D.O. Alikin

School of Natural Sciences and Mathematics, Ural Federal University, 620000, Ekaterinburg, Russia, denis.alikin@urfu.ru

Piezoresponse force microscopy (PFM) is a local method for measuring converse piezoresponse with exceptionally high spatial resolution in micro- and nano-objects, where macroscopic measurement techniques fail. PFM thus becomes the only viable method to quantify the piezoelectric coefficients in such materials. In PFM, an electric field is applied to the scanning probe microscopy probe, which has a radius of tens of nanometers, creating a highly inhomogeneous electric field. This complexity makes PFM measurements more challenging compared to those involving a uniform electric field and related electromechanical deformation in the piezoelectric capacitor.

PFM measurements encounter several uncertainties, including significant impacts from electrostatic forces, voltage drop across the tip-surface interface, and mechanical clamping of the oscillating surface. In this tutorial, we discuss approaches to quantify PFM, aiming to obtain reliable and calibrated piezoresponse values and extract information about polarization orientation and switching behavior. Addressing this complex problem involves tackling technical challenges as well as experimental and theoretical issues. We explain how to set up PFM experiments to collect reliable data and discuss the theoretical framework for evaluating piezoelectric coefficients from PFM data. State-of-the-art data processing techniques in PFM spectroscopy and microscopy are illustrated. We also introduce a fully quantitative "global-excitation" mode in PFM, which allows accurate recovery of the piezoelectric coefficients in the micro-scale objects.

The authors are grateful for financial support of the Ministry of Science and Higher Education of the Russian Federation (state task FEUZ-2023-0017). The work was performed using the equipment of the Ural Center for Shared Use "Modern Nanotechnologies" UrFU (reg. No. 2968).

Rational data processing in scanning probe microscopy

I. Yaminsky

Lomonosov Moscow State University, Moscow, Russia

yaminsky@nanoscopy.ru

The unique capabilities of scanning probe microscopy (SPM), including super-resolution imaging, nanomanipulation, and the ability to operate under physiological conditions, have opened up exciting research opportunities in biology and biomedicine. SPM imaging applied to biological objects allows us to reveal the fine structure of cells at the nanolevel and how they change during life, including under the influence of various drugs.

Often, such dynamic events can introduce additional distortions into images, which the experimenter can get rid of using special applications. This report discusses the functions of FemtoScan Online software in relation to processing probe microscopy images, improving image quality, reducing noise and increasing the information content of data.

Construction of functional nanomaterials from amino acids and peptides

P.S. Zelenovskiy

School of Natural Sciences and Mathematics, Ural Federal University, 620000 Ekaterinburg, Russia

zelenovskiy@urfu.ru

Amino acids and peptides represent a convenient tool for construction of functional materials for biomedical, energy, and nanotechnological applications. Interest in them originates from their natural biocompatibility, chemical diversity, self-assembly and functionalization capabilities, and impressive physical properties. All this is possible due to a wide range of oriented non-covalent interactions available for amino acids and inaccessible to most of inorganic materials. Understanding the details of these interactions makes it possible to design specific amino acid sequencies for the targeted creation of materials with various, predetermined properties.

This tutorial reviews the chemical and structural features of amino acids and short peptides, the types of chemical interactions between them, and also, on the example of glycine, diphenylalanine and other di- and tripeptides, demonstrates methods for creating materials of various dimensionalities (0D nanospheres, 1D nanotubes, 2D crystals and films, 3D crystals), and indicate ways to control their mechanical, piezoelectric, pyroelectric, and optical properties.

The author is grateful for the financial support by the Ministry of Science and Higher Education of the Russian Federation (state task FEUZ-2023-0017).

1. E. Gazit, *Chem. Soc. Rev.* **36**, 1263 (2007). DOI: 10.1039/b605536m
2. A.C. Mendes, et al., *WIREs Nanomed. Nanobiotechnol.* **5**, 582 (2013). DOI: 10.1002/wnan.1238
3. L. Adler-Abramovich, E. Gazit, *Chem. Soc. Rev.* **43**, 6881 (2014). DOI: 10.1039/c4cs00164h
4. P. Makam, E. Gazit, *Chem. Soc. Rev.* **47**, 3406 (2018). DOI: 10.1039/c7cs00827a
5. S. Guerin, A. Stapleton, et al. *Nat. Materials* **17**, 180 (2018). DOI: 10.1038/NMAT5045
6. J. Zhang, S. Guerin, et al., *Bio-Des. Manuf.* **5**, 529 (2022). DOI: 10.1007/s42242-022-00186-3

INVITED PRESENTATIONS

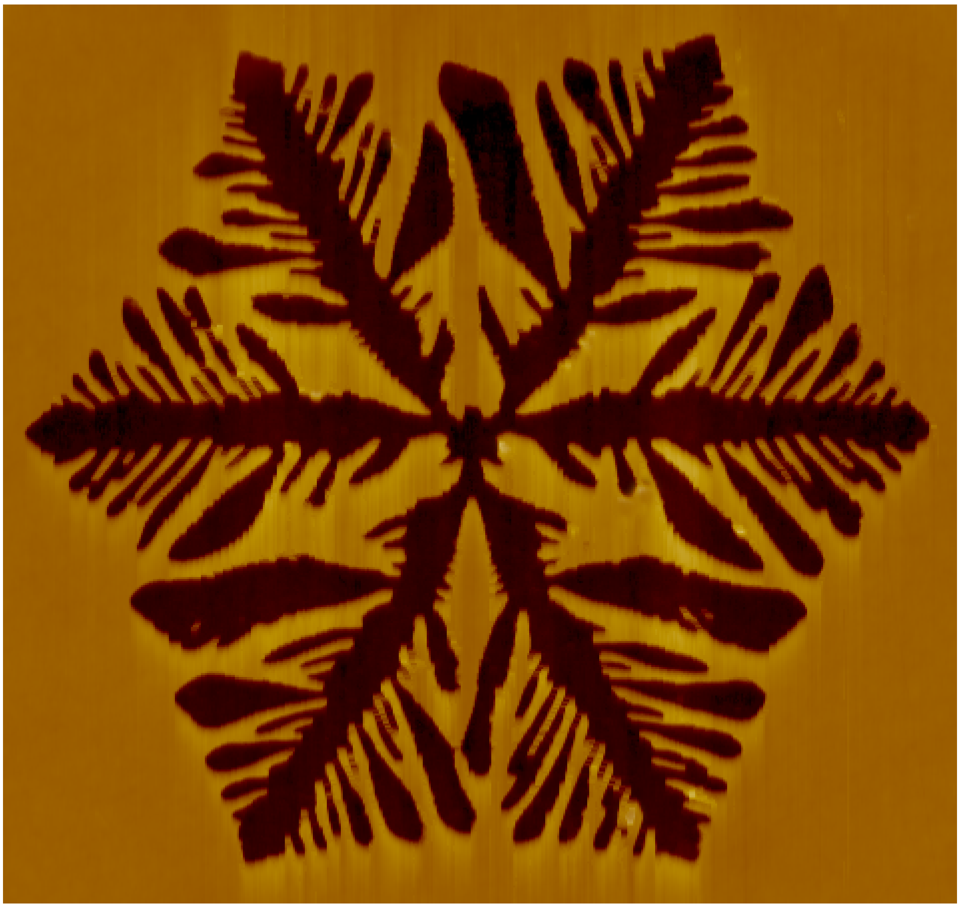

I1

Ultrafast laser technologies in bulk nano- and micro-characterization of doped semiconductors

S.I. Kudryashov[1,2], M.S. Kovalev[1,2]

[1] *Lebedev Physical Institute, 119991, Moscow, Russia*
[2] *Bauman State Technical University, 105005, Moscow, Russia*

kudryashovsi@lebedev.ru

Selective non-linear technologies, utilizing parametrically-generated spectrally-tunable ultrashort laser pulses, enable quantitative measurements and spatial mapping of functional impurities at the ppt-level in ultrapure diamonds, silicon and silicon nitride for vis-IR single-photon, photosensing and lasing nanophotonic applications.

These results were obtained in the framework of the State task № FSFN-2024-0019.

I2

The structural transformation of DUT-4 metal-organic framework

A.S. Krylov

Kirensky Institute of Physics FRC KSC SB RAS, 660036, Krasnoyarsk, Russia
shusy@iph.krasn.ru

Metal-Organic Frameworks (MOFs) have revolutionized the field of crystal engineering, and solid-state chemistry is unique materials, which can transform their crystal structure from a dense, nonporous to a highly porous, open state and vice versa as a response to external stimuli. They are bistable or multistable crystalline materials with long-range structural ordering, a reversible transformability between crystalline phases, and permanent porosity [1]. MOF exhibit wide variety of properties attractive for a variety of applications.

It was reported early that the Raman spectra comparison revealed a significant difference in the low-wavenumber region for different pore forms of DUT-8(Ni) [2]. This characteristic spectral feature is a basis for rapid, and routinely applicable Raman based technique for characterization of different switchable MOF phases and for in situ evaluation and analysis of them by the spectral profile [3].

Here we report *in situ* studying DUT-4 with confocal Raman and FTIR spectroscopy and PXRD at ambient conditions revealed first-order phase transition between the original ordered and distorted phases. We experimentally confirmed the threshold behavior of the transition, as well as the effect of exposure time and humidity. Synchronous thermal analysis and Raman spectroscopy have proven experimentally that the transition is reversible and that the initial state can be restored by holding it in a vacuum condition. The vacuum storing time depends on the vacuum level. Comparing the structure of the distorted phase (according to the PXRD) with MIL-69, raises the question of a potential transformation of DUT-4 to MIL-69 upon the action of humidity. According to Raman spectroscopy data, the chemical structure is stable during transition, as the spectra before and after the transition are the same. We also analyzed the phase transition optically and electronically, confirming the high potential of using DUT-4 as a new phase change material for sensing and optoelectronic applications [4].

The study of the structural behaviour of metal-organic frameworks (MOFs) under hydrostatic pressure is a thriving area. The goal of active research is the identification of overarching composition-structure principles, including both properties of technological relevance and material behaviour of academic interest, such as material stability criteria, mechanical properties, pressure-induced phase transitions, negative compressibilities, and guest-dependent high-pressure structural responses [5]. Pressure-induced emission enhancement (PIEE) is a new phenomenon that has attracted much attention in recent years for improving the solid-state emission efficiency of MOFs. Experiments under high hydrostatic pressure conditions have shown that there is an effect of pressure-induced emission enhancement in the DUT-4 MOF with increasing pressure.

1. A. Schneeman, V Bon, I Schwedler, et al. *Chem. Soc. Rev.* **43**, 6062 (2014).
2. A. Krylov, A. Vtyurin, P. Petkov, et al. *Phys. Chem. Chem. Phys*. **19**, 32099 (2017).
3. S. Ehrling, I. Senkovska, V. Bon, et al. *Mater. Chem. A.* **7**, 21459 (2019).
4. A.S. Krylov, S.A. Shipilovskikh, S.N. Krylova, et al. *Dalton transaction* **53**, 3459 (2024).
5. A. Krylov, I. Yushina, E. Slyusareva, et al. *Phys. Chem. Chem. Phys*. **24**, 3778 (2022).

I3

The structure, thermal, elastic and dielectric properties of nanocrystalline Rb_2ZnCl_4, embedded in nanosize porous matrices

L.N. Korotkov[1], L.S. Stekleneva[1], I.N. Flerov[2], E.A. Mikhaleva[2], E. Rysiakiewicz-Pasek[4], M.S. Molokeev[2,3], V.S. Bondarev[2,3], M.V. Gorev[2,3]

[1]Voronezh State Technical University, Voronezh, 394000 Russia

l_korotkov@mail.ru

[2]Kirensky Institute of Physics, Krasnoyarsk, 660036 Russia

[3]Institute of Engineering Physics and Radio Electronics, Siberian Federal University, Krasnoyarsk, 660041 Russia

[4]Wrocław University of Science and Technology, 50-370 Wrocław, Poland

The Rb_2ZnCl_4 crystal is a well-known ferroelectric with incommensurate phase. At present its physical properties have been well studied theoretically and experimentally. However, investigations concerning of the size effect in this crystal have not been carried out. The purpose of this work was to study, over a wide temperature range, the crystal structure, dielectric, elastic and thermal properties of nanosized crystallites of rubidium tetrachlorozincate embedded into porous dielectric matrices.

The experimental results showed a slight shifting of the incommensurate-phase transition temperature T_i in the Rb_2ZnCl_4 particles embedded in porous silicon oxide matrices with an average pore size of 5, 46 and 320 nm and porous aluminum oxide matrices with an average pore size of 90 and 300 nm compared to a bulk single-crystal sample rubidium tetrachlorozincate.

Along with this, it was found that the temperature of ferroelectric phase transition in embedded Rb_2ZnCl_4 is approximately 50 K higher than in the bulk material.

The temperature dependences of dielectric permittivity ε, elastic modulus and internal friction, obtained for studied nanocomposite materials within a broad temperature range, are characterized by a wide temperature hysteresis. Observed irreversibility of $\varepsilon(T)$ dependences indicate the nonergodicity of the state realized in the Rb_2ZnCl_4 – SiO_2 and Rb_2ZnCl_4 – Al_2O_3 composite materials.

A study of the dielectric response dispersion for a composite Rb_2ZnCl_4 – SiO_2 revealed an increase in the dispersion depth $\Delta\varepsilon$ when the sample is cooled, due to an increase in the concentration of “relaxers” and an increase in the value of their dipole moment. This gives reason to assume that in the composite, with decreasing temperature, starting from T_i, there is a continuous nucleation of polar structures and an increase in their dipole moment, similar to what occurs in ferroelectrics with a diffuse phase transition. Analysis of the features of the dielectric response showed that a domain structure is formed in the ferroelectric phase of Rb_2ZnCl_4 particles, the mobility of which near the freezing temperature T_f obeys the empirical Vogel-Fulcher relation.

I4

Scanning probe microscopy of living neurons and nervous tissue

I.V. Yaminsky[1,2]

[1]*Lomonosov Moscow State University, Faculty of Physics, 119991, Moscow, Russia*
yaminsky@nanoscopy.ru

[2]*Advanced Technologies Center, 119311, Moscow, Russia*

Scanning probe microscopy has become smart enough to study the most sophisticated matter – network of living neurons and nervous matter [1]. At least two techniques have prominent advantages in the visualization of living biological objects – atomic force microscopy and scanning capillary (ion-conductance) microscopy. Environmental conditions (temperature, liquid composition) provide the success of long lasting experimental observations.

Advances in scanning capillary microscopy (SCM) in studies of living objects have generated interest in this technique: over its 30 years of existence, more than 300 articles and numerous reviews describing the development of SCM have been published. The growth of dendrites and axons and the dynamics of actin in living cells have been visualized, changes in the volumes of nerve cells during migration have been measured, changes in the structure of the cell membrane during endocytosis of nanoparticles have been studied, the topography and stiffness of living fibroblasts have been assessed, and more [2]. This report reviews recent advances in the observation of living neurons using scanning probe microscopy.

In our scientific group we have developed FemtoScan Xi models of scanning capillary microscope. Usually the FemtoScan Xi microscope is installed on the optical inverted microscope. The technical solution, which includes a compact optical microscope and a capillary microscope with a planar scanner, is shown in Figure 1.

Figure 1. Mechanical system of FemtoScan Xi scanning capillary microscope. Precision movement range in X, Y, Z axes – 50 µm, 50 µm, 30 µm; movement accuracy – 0.05 nm. The range of smooth automated movement in X and Y axes is 12 mm. Built-in inverted optical system provides bottom view of the sample and capillary tip.

Probe microscopy has taken the first, albeit confident, steps in the study of networks of living neurons. At the same time, new results, achievements and discoveries in the field of brain research are still ahead.

1. P. Novak, C. Li, A.I. Shevchuk, et al. *Nature methods* **6**, 279 (2009)
2. T.O. Sovetnikov, A.I. Akhmetova, et al. *Bio-Medical Engineering* **57**, 250 (2023).

I5

Transport of small molecules through peptide nanochannels

P. Zelenovskiy[1,2], M. Soares[3], V. Yuzhakov[1], L. Mafra[3], F. Figueiredo[2]

[1]*School of Natural Sciences and Mathematics, Ural Federal University, 620000 Ekaterinburg, Russia*
zelenovskiy@urfu.ru

[2]*Department of Physics and CICECO−Aveiro Institute of Materials, University of Aveiro, 3810-193 Aveiro, Portugal*

[3]*Department of Chemistry and CICECO−Aveiro Institute of Materials, University of Aveiro, 3810-193 Aveiro, Portugal*

Self-assembling peptide nanotubes can serve as channels for the transportation of small molecules or ions with high diffusion coefficients [1]. Charged amine and carboxylic functional groups at the internal surface of such nanochannels significantly affect the molecular motion, sometimes giving it complex and intricate shapes. In this work, we present a study of water and ammonia molecules motion through diphenylalanine (FF) nanotubes with the pore size below 1 nm under the action of pressure and temperature gradients.

A combination of single crystal X-ray diffraction, solid-state nuclear magnetic resonance (NMR) spectroscopy, and dynamic vapour sorption (DVS) measurements was used to analyse water diffusion inside FF nanochannels. The obtained results indicate the formation of two independent flows in the nanochannels: a conventional axial flow located around the nanotubes axis and a helical flow located near the peptide shell [2]. These two flows are independent of each other and their diffusion coefficients differ by several orders of magnitude (1.5×10^{-10} m^2s^{-1} and 4×10^{-12} m^2s^{-1}, respectively). The molecular dynamics simulations have confirmed the trajectory of the helical flow being dictated by the screw-like distribution of the functional groups within the channel walls, while its flux is governed by external water vapour pressure.

At the next step of the research, water molecules in the FF nanotubes were partially substituted by the ammonia (NH_3) molecules, and their diffusion under the thermal gradient was studied *in situ* by confocal Raman microscopy. Due to the stronger adhesion of NH_3 molecules to the peptide shell, the temperature gradient leads to an inhomogeneous density of molecules resulting in pressure difference and the molecular movement from the denser region (cold) to the less dense (hot). Local variations of NH_3 concentration allowed estimating the ammonia thermal diffusion coefficient $D = 5.9\times10^{-12}$ m^2s^{-1} and the thermal conductivity coefficient $\lambda \approx 3.78\times10^{-4}$ $W\ m^{-1}\ K^{-1}$ which is comparable with that of keratin nanofibres (4.62×10^{-4} $W\ m^{-1}\ K^{-1}$ [3]).

P.Z. is grateful for the financial support by the Ministry of Science and Higher Education of the Russian Federation (state task FEUZ-2023-0017). The equipment of the Ural Center for Shared Use “Modern nanotechnology” Ural Federal University (Reg. No. 2968) was used.

1. P.S. Zelenovskiy et al., *ACS Appl. Mater. Interfaces* **12**, 27485 (2020).
2. P. Zelenovskii et al., in press.
3. Y. Xue, S. Lofland, X. Hu, *Polymers,* **11** 456 (2019).

Ferroelastic switching in $Hf_{0.5}Zr_{0.5}O_2$ films

A.A. Chouprik[1], M.V. Spiridonov[1], I.G. Margolin[1]

[1]*Moscow Institute of Physics and Technology, 141701, Dolguprudny, Russia*
chouprik.aa@mipt.ru

Ferroelectricity is demanded in many device concepts in electronics, energy and microsystems engineering. The performance of ferroelectrics-based devices is determined by either out-of-plane or in-plane polarization, or out-of-plane or in-plane piezoelectric strain. For instance, the out-of-plane polarization component determines the performance of ferroelectric memories. On the other hand, the in-plane piezoelectric strain of the ferroelectric layer dictates the magnetization of an adjacent magnetic material in layered magnetoelectric systems composed of a ferroelectric and a magnetic material. Therefore, the establishment of the polarization components and tensorial piezoelectric strain as well as their changes during polarization reversal, is vital for further progress of ferroelectrics-based devices.

Real prospects for the practical implementation of innovative devices opened up after the discovery of ferroelectricity in thin hafnium oxide films, due to their perfect compatibility with silicon technology and a number of unique properties. This material has found applications in many fields, including conventional and flexible non-volatile memories, building blocks for neurocomputing architectures, piezoelectric microelectromechanics devices and energy harvesters. Despite the significant progress in HfO_2 applications, the origin of ferroelectric and piezoelectric properties that determine the performance of the above devices remains controversial and unclear. In particular, the mechanism of polarization reversal in hafnium oxide and the tensorial piezoelectric behaviour, which are inextricably coupled, are still not addressed, which limits both the improvement of demonstrated devices and the development of new devices.

In this work, the nanoscopic nature of the polarization vector rotation over polycrystalline $Hf_{0.5}Zr_{0.5}O_2$ (HZO) film during polarization switching in a ferroelectric capacitor is revealed using a combination of two techniques, specifically, *in situ* synchrotron X-ray microdiffraction and *in situ* vector piezoresponse force microscopy (PFM). With the vector PFM, the polarization vector is found to be flipped by 180° in most of the HZO film, which is consistent with a single polar axis of orthorhombic phase that determines the ferroelectric properties of HZO. However, a rather large fraction of the capacitor is also occupied by nanoregions of ferroelastic (non-180°) switching, which are explained by the effect of the local mechanical stress emerged in a result of crystallization annealing. On the other hand, ferroelastic switching manifests itself as a reversible change in the structural properties at polarization switching revealed by *in situ* synchrotron X-ray microdiffraction. Namely, a reversible change in the fractions of orthorhombic phase grains with orientation (002), (202) and (022) is observed during polarization switching. An irreversible change in the lattice constant of orthorhombic phase grains with orientation (002) and the evolution of the relative fractions of grains with orientation (002), (202) and (022) are observed during the wake-up procedure. The latter results indicate a significant role of ferroelastic switching of the film in the wake-up phenomenon, which is consistent with the results previously obtained by transmission electron diffraction [1].

Several components of the piezoelectric tensor of the HZO film have been measured using a new method to quantify the vector PFM technique. It is found that the shear piezoelectric coefficient is twice as large as the piezoelectric coefficient (-1.9 and -0.9 pm/V, respectively), which is in agreement with recent theoretical works.

The experimental insights can be useful for fundamental understanding of the ferroelectric and piezoelectric properties of hafnium oxide, and have a potential to trigger a new versions ferroelectrics-based devices.

The work was financially supported by the Russian Science Foundation (Project No. 20-19-00370, https://rscf.ru/en/project/20-19-00370/).

1. M. Lederer, C. Mart, B. Volkmann, et al. *Appl. Phys. Lett.* **123**, 022903 (2023).

I7

Brillouin light scattering in barium strontium niobate thin films

A.M. Pugachev

Institute of Authomation and Electrometry RAS, Novosibirsk, 630090 Russia,
apg@iae.nsk.su

Ferroelectric thin films of barium strontium niobate have been studied. SBN 75 films were deposited on a sapphire substrate by high-frequency sputtering in pure oxygen at a pressure of 2 Pa and a temperature of 950°C. The deposition time varied from 2 to 4 hours. Annealing was carried out in air at a temperature of 1150 C. The samples were synthesized at the St. Petersburg State Electrotechnical University. A much thicker SBN50 film was also studied, deposited by RF sputtering on a Sp/ITO substrate at the Institute of Automation and Electrometry SB RAS, Novosibirsk. The Brillouin scattering spectra were measured on a six-pass scanning Fabry–Perot interferometer.

Brillouin scattering spectra were measured in thin films of barium strontium niobate. It has been shown that as the film thickness decreases, the peak of the LA mode broadens and satellites appear in accordance with previously proposed model [1, 2]. Fitting the experimental spectra according to the model proposed in [1, 2] made it possible to determine the film thickness. The structure and thickness of the film were additionally studied using a scanning electron microscope TM 3000 Hitachi and using IR reflection spectra on a Vortex 80 Fourier IR spectrometer. The results obtained from processing the Mandelstam – Brillouin spectra were confirmed by studies on a scanning electron microscope and measurements of a periodic frequency components in the IR reflectance spectra.

In annealed thin films, the Brillouin scattering spectra exhibit an anomalous peak, which cannot be explained by the presence of the TA mode due to a violation of the selection rules. This is evidenced by the results obtained in various spectral geometries. It is shown that this peak is caused by the resonant excitation of acoustic vibrations on microscopic granules during film annealing and causes a decrease in the quality factor in the vicinity of 17 GHz.

Some part of the experiments was performed in the multiple-access center “High-Resolution Spectroscopy of Gases and Condensed Matter” in IA&E SBRAS (Novosibirsk, Russia).

The study was supported by the Russian Science Foundation No. 23-22 00205.

1. J.R. Sandercock, *Phys. Rev. Lett.* **29**, 1735 (1972).
2. A.A. Passeri, A. Di Michele, I. Neri, et al., *Biomaterials Advances* **147**, 213341 (2023).

I8

Phase transition in PYN-*x*BT (*x* < 0.1) ceramics – Raman scattering data

A.N. Vtyurin[1], A.N. Krylov[1], M.S. Molokeev[1], G. Li[2], B. Teng[2]

[1] *Kirensky Institute of Physics, 660036,Krasnoyarsk, Russia*
vtyurin@iph.krasn.ru

[2] *Shanghai Institute of Ceramics, 201899, Shanghai, China*

Complex lead-based perovskite compounds with the general formula of $A_2B(1)B(2)O_6$ have been of fundamental and practical interest for many years [1]. They exhibit several types of interesting dielectric properties depending on the degree of the B-site cationic ordering and compositions. Structure of Pb_2YbNbO_6 [PYN] is highly ordered enough to be a prototype for spectroscopic studies, so its lattice dynamics can be investigated by varying its compositions [2]. PYN undergoes the first order phase transition from the paraelectric (cubic) phase to antiferroelectric (orthorhombic) phase around 493 K due to the antiparallel displacement of Pb ions [3]. In [4] it was shown that small amount of ferroelectric substitution may effect this transition temperature considerably, and it reveals brightly in Raman spectra. So here we report results of Raman scattering investigation of PYN-*x*BT ceramics p–T phase diagram at small (below 5%) amount of $BaTiO_3$ substitution.

The spectra in the 180° geometry were recorded with a Horiba Jobin Yvon T64000 spectrometer equipped with a liquid nitrogen-cooled charge-coupled device detection system in subtractive dispersion mode. Ar+ ion laser Spectra-Physics Stabilite 2017 with $\lambda = 514.5$ nm and 5 mW power on a sample was used as an excitation light source. The heated high-temperature diamond anvil cell (HTDAC) device of gas membrane Diacell μ Scope DAC HT(G) type (EasyLab, UK) with diamond IIa anvils, electrical resistive heating, water-cooling casing, and Ar gas blowing was used for Raman study of processes at simultaneously high p and T. Limit p–T parameters in the work volume of the given HT-DAC device are equal to 20 GPa and 800 K. A stainless steel gasket with an initial thickness of 0.25 mm is used in this DAC. Holes with a diameter of about 180–200 μm were drilled in the gaskets preindented to a thickness of about 86 μm, for measuring at pressures up to 15 GPa. The pressure was monitored by the shift of the 5D0_7F0 fluorescence band of Sm2+ ion in a small $SrB_4O_7{:}Sm^{2+}$ crystal placed in the vicinity of the sample within the experimental error of about 0.05 GPa. The temperature was monitored using a type K thermocouple in contact with the gasket and diamond anvil. A mixture of methanol–ethanol alcohols in 4:1 parts has been used as a hydrostatic pressure transmission media.

Transition temperature was controlled by position of Raman line at about 800 cm^{-1} that corresponds to longitudinal vibrations of oxygen ions at Yb–O–Nb bonds [4]. This line goes up gradually under heating in the lower frequency phase and jumps sharply at the transition point. Pressure applied shifts this transition point down closer to ambient temperatures. Complete pressure – temperature diagram is built for this range of concentrations.

1. M.E. Lines, A.M. Glass, Principles and Application of Ferroelectrics and Related Materials (Clarendon, Oxford), 1977.
2. J.-H. Kim, K.S. Koh, W.K. Choo, *Integr. Ferroelectr.* **47**, 11 (2002).
3. H. Lim, H.J. Kim, W.K. Choo, *Jpn. J. Appl. Phys*. **34**, 5449 (1995).
4. S.-J. Ahn, J.-J. Kim, J.-H. Kim, W.K. Choo, *Integr. Ferroelectr.* **67**, 159 (2004).

I9

The change of the domain wall shape as a result of ion beam irradiation in lithium niobate

A.R. Akhmatkhanov, E.A. Pashnina, A.S. Slautina, M.A. Chuvakova, V.Ya. Shur

School of Natural Sciences and Mathematics, Ural Federal University, 620002, Ekaterinburg, Russia
andrey.akhmatkhanov@urfu.ru

Lithium niobate (LN, $LiNbO_3$) single crystals with tailored periodical domain structures (PDS) are one of the main platforms for nonlinear laser wavelength conversion applications. Advances of domain engineering in LN stimulated the development of new applications of tailored domain structures in other fields beyond nonlinear optics. One of these emerging fields is ferroelectric lithography – the technique of creation of artificial patterns on the surface of ferroelectric crystal by selective deposition of material on domains of different signs or domain walls [1-3]. As the ferroelectric template in this case can be potentially used for replication of large number of functional patterns, the problem of correction of the initially created domain structure arises.

From the other hand, the studies of domain wall shape change induced by local switching in the vicinity of this wall represents important fundamental problem of ferroelectric physics. This problem was studied previously during local switching by biased or grounded conductive tip of scanning probe microscope (SPM) in congruent LN single crystals [4]. It was demonstrated that scanning by grounded SPM tip across the plane macroscopic domain wall leads to nanoscale perturbations on the wall and appearance of nanodomains near the wall. However, the change of domain wall shape as a result of field application by a stationary biased SPM tip was not studied in detail.

We present the study of the shape change on the polar surface and in the bulk of the walls of lamellar domains as a result of local switching by focused ion-beam. PDS are created by two methods: (i) electric-field poling using photolithographically defined electrodes and (ii) ion-beam poling.

The dot irradiation of Z+ areas near the walls of lamellar domains leads to the formation of faceted or rounded hexagonal domains. For e-field PDS additional formation of nanodomain ensembles was observed. We have revealed two types of domain wall shape changes induced by irradiation: (1) merging of the hexagonal domain with the domain wall for Z+ areas; (2) formation of rounded distortion of the domain wall for Z– areas [5]. For Z+ areas irradiation, the domain wall distortion was described by a simple model of independent growth of isolated domain with its subsequent merging with static domain wall [5]. For Z– surface irradiation, the domain wall shift increases linearly with the distance between the irradiation dot and the wall. It was revealed that the merging of the growing hexagonal pyramidal domain and lamellar domain can be obtained in the bulk even for absence of merging at the surface [5].

All obtained results have been explained within a kinetic approach to the domain wall motion by step generation. The switching field consists of inputs produced by: (i) the charges injected during dot irradiation into the photoresist layer and crystal bulk, (ii) the charges injected during the creation of i-beam PDS, (iii) the bound charges (depolarization field) [5]. The transition of the shapes of isolated domains and wall distortions from faceted to rounded one with field increase was attributed to the transition from determined step generation to stochastic one.

For practical applications these results provide guidelines for correction of created domain structure. It is shown that better correction accuracy (smaller feature size) is obtained when local switching is realized outside of the created domain (that is on Z+ surface).

The research was made possible by the Russian Science Foundation (Project № 21-72-10160). The equipment of the Ural Center for Shared Use “Modern nanotechnology” UrFU was used.

1. A. Blázquez-Castro, A. García-Cabañes, M. Carrascosa, *Appl. Phys. Rev.* **5**, 041101 (2018).
2. L. Lv, F. Zhuge, F. Xie, et al., *Nature Comm.* **10**, 3331 (2019).
3. A. Haußmann, A. Gemeinhardt, M. Schröder, et al., *Langmuir* **33**, 475 (2017).
4. A.V. Ievlev, A.N. Morozovska, V.Ya. Shur, et al., *Phys. Rev.* **91**, 214109 (2015).
5. E. Pashnina, A. Slautina, A. Akhmatkhanov, et al., *J. Adv. Dielect.*, 2450015 (2024).

I10

Spintronics – MRAM and beyond

K.A. Zvezdin

New Spintronic Technologies Moscow, Russia
k.zvezdin@nst.tech

Interest in spintronic heterostructures based on magnetic tunnel junctions (MTJs) is primarily caused by the possibility of their effective use for recording and storing information. In recent years, Magnetic RAM has begun to be actively introduced into various areas of industry, primarily in the automotive, becoming an indispensable technical solution for the new generation of automotive chips. However, the applied opportunities offered by spintronics is not limited to this. The microwave dynamics of magnetization in such structures is of particular interest. It has been shown the possibility to generate an alternating (microwave) signal constant spin-polarized current in MTJs excited by spin-polarized direct current [1]. Based on this effect, a new generation of alternating signal generators for telecommunication devices are being developed. Of no less interest is the opposite effect – the spin-transfer diode [2]. When an alternating spin-polarized current with a frequency close to the resonant one is passed through the MTJ, a constant voltage component appears. It can be obviously used for signal detection. In the first works, the efficiency of rectifying an alternating signal did not exceed 1.4 mV/mW. In 2014, sensitivity of a spin-transfer diode at room temperature of 12000 mV/mW was experimentally demonstrated [3] through the use of a constant bias current. Subsequently, it was demonstrated a possiblity toenhance the microwave sensitivity up to 210,000 mV/mW [4-5].

The development of spin-transfer diodes from the first experiments to prototype microwave devices are covered in the talk. An opportunities and methods for increasing the microwave sensitivity are shown and the physical mechanisms behind this are explained. The possibilities of resonant frequency engineering and the transition to broadband rectification are discussed. The influence of magnetic distribution on the features of rectification is considered. Finally, possible practical applications of the mentioned effects are discussed.

1. S.I. Kiselev et al., *Nature* **425**, 380 (2003).
2. A. Tulapurkar et al., *Nature* **438**, 339 (2005).
3. S. Miwa et al., *Nat. Mater.* **13**, 50 (2014).
4. B. Fang et al., *Nat. Commun.* **7**, 11259 (2016).
5. L. Zhang et al., *Appl. Phys. Lett.* **113**, 102401 (2018).

I11

Light-only domain switching in ferroelectrics

V.Ya. Shur

School of Natural Sciences and Mathematics, Ural Federal University, 620000, Ekaterinburg, Russia
vladimir.shur@urfu.ru

The brief review of achievements and recent progress in the all-optical domain switching in various ferroelectrics realized without any application of the electric field will be presented. The main attention has been paid to recently discovered all-optical domain switching in the crystal bulk by applications of near-IR femtosecond laser irradiation, which can be used for creation of the periodical domain structures and three-dimensional nonlinear photonic crystals [1].

Nonlinear photonic crystals (NPCs) represent the media with spatially modulated nonlinear susceptibility coefficient $\chi(2)$. The created stable structures allow to realize frequency conversions of laser beams by means of quasi-phase matching, which allows to realize Second Harmonic Generation (SHG) and Optical Parametric Oscillators (OPO) with record efficiency [2]. The tailored periodical domain structures with modulation of the $\chi(2)$ sign can be created in nonlinear optical ferroelectrics. The most popular method for domain patterns creating is electrical field poling (EFP) using the electrodes with proper geometry for field applying [2]. However, the most significant drawback of EFP is inability to create 3D domain structures.

The all-optical poling of ferroelectric crystals by pulse laser irradiation is considered now as a promising alternative of EFP. Two variants of these approach have been realized using strongly absorbable and non-absorbable light. The first method was based on UV and far IR irradiation strongly absorbed in the surface layer. The absorbed energy stimulates nonuniform heating and subsequent cooling thus stimulating appearance of pyroelectric field strong enough for domain switching [3-5]. The spatial distribution of the pyroelectric field leads only to domain nucleation at the surface and their growth in polar direction and doesn’t allow creating of 3D structures of intra-volume domains. This drawback has been overcome recently using of tightly focused irradiation of the femtosecond laser with wavelength in the NIR range. The main idea of this method is based on the high enough multiphoton absorption of the light from the transparent spectral range due to the extremely high light intensity in the focusing region. In 2015 for the first time such domain switching was demonstrated in ferroelectric lithium niobate ($LiNbO_3$, LN) crystals [6]. The further works widely expended the number of ferroelectrics used for 2D and 3D domain patterning [1].

We study formation of the domain structures in the single crystals of uniaxial high-quality lithium niobate $LiNbO_3$ and lithium tantalate $LiTaO_3$ family as the most frequently used nonlinear optical materials by local irradiation and linear scanning [7-9]. The created domain structure has been imaged at the surface and in the bulk using various complimentary methods. The main attention was paid imaging in the bulk by Cherenkov-type confocal Second Harmonic Generation [10]. We suppose that the domain formation near the focus point is caused by depolarization field appeared around the microtracks and subsequent growth is caused by pyroelectric field occurring during nonuniform temperature change [9]. The creation of the three-dimensional nonlinear photonic crystals and periodical domain structures in the bulk was demonstrated [7-9].

The equipment of the Ural Center for Shared Use “Modern nanotechnology” Ural Federal University (Reg.№ 2968) was used. The research was made possible by Russian Science Foundation (Project № № 24-12-00302).

1. Y. Sheng, X. Chen, T. Xu, S. Liu, R. Zhao, W. Krolikowski, *Photonics* **11**, 447 (2024).
2. V.Ya. Shur, A.R. Akhmatkhanov, I.S. Baturin, *Applied Physics Review*, **2**, 040604 (2015).
3. V.Ya. Shur, D.K. Kuznetsov, E.A. Mingaliev, et al., *Appl. Phys. Lett.* **99**, 082901 (2011).
4. V.Ya. Shur, E.A. Mingaliev, M.S. Kosobokov, et al., *J. Appl. Phys.* **127**, 094103 (2020).
5. V.Ya. Shur, M.S. Kosobokov, A.V. Makaev, et al., *Acta Materialia*, **219**, 117270 (2021).
6. X. Chen, P. Karpinski, V. Shvedov, et al., *Appl. Phys. Lett.* **107**, 141102 (2015).
7. S. Kudryashov, A. Rupasov, M. Kosobokov, et al., *Nanomaterials*, **12**, 4147 (2022).
8. B.I. Lisjikh, M.S. Kosobokov, A.V. Efimov, D.K. Kuznetsov, et al., *Ferroelectrics*, **604,** 47 (2023).
9. B.I. Lisjikh, M.S. Kosobokov, A. Turygin, A.V. Efimov, V.Ya. Shur, *Photonics*, **10**, 1211 (2023).
10. Y. Sheng, A. Best, H.J. Butt, W. Krolikowski, et al., *Opt. Express* **18**, 16539 (2010).

I12

Moderate fields, maximum potential: Achieving high records with temperature-stable energy storage in lead-free BNT-based ceramics

L. Jin

Electronic Materials Research Laboratory, Key Laboratory of the Ministry of Education, School of Electronic Science and Engineering, Xi'an Jiaotong University, Xi'an 710049, China
ljin@mail.xjtu.edu.cn

The increasing awareness of environmental concerns has prompted a surge in the exploration of lead-free, high-power ceramic capacitors. Ongoing efforts to develop lead-free dielectric ceramics with exceptional energy-storage performance (ESP) have predominantly relied on multi-component composite strategies, often accomplished under ultrahigh electric fields. However, this approach poses challenges in insulation and system downsizing due to the necessary working voltage under such conditions. Despite extensive study, bulk ceramics of $(Bi_{0.5}Na_{0.5})TiO_3$ (BNT), a prominent lead-free dielectric ceramic family, have seldom achieved a recoverable energy-storage (ES) density (W_{rec}) exceeding 7 J/cm^3. This study introduces a novel approach to attain ceramic capacitors with high ESP under moderate electric fields by regulating permittivity based on a linear dielectric model, enhancing insulation quality, and engineering domain structures through chemical formula optimization. The incorporation of $SrTiO_3$ (ST) into the BNT matrix is revealed to reduce the dielectric constant, while the addition of $Bi(Mg_{2/3}Nb_{1/3})O_3$ (BMN) aids in maintaining polarization. Additionally, the study elucidates the methodology to achieve high ESP at moderate electric fields ranging from 300 to 500 kV/cm. In our optimized composition, $0.5(Bi_{0.5}Na_{0.4}K_{0.1})TiO_3$-0.5(2/3ST-1/3BMN) (B-0.5SB) ceramics, we achieved a W_{rec} of 7.19 J/cm^3 with an efficiency of 93.8% at 460 kV/cm. Impressively, the B-0.5SB ceramics exhibit remarkable thermal stability between 30 and 140°C under 365 kV/cm, maintaining a W_{rec} exceeding 5 J/cm^3. This study not only establishes the B-0.5SB ceramics as promising candidates for ES materials but also demonstrates the feasibility of optimizing ESP by modifying the dielectric constant under specific electric field conditions. Simultaneously, it provides valuable insights for the future design of ceramic capacitors with high ESP under constraints of limited electric field.

I13

Crystallization kinetics of rare-earth doped $BiFeO_3$ thin films

E.B. Araújo, M.A.M. Teixeira, F.B. Minussi

Department of Physics and Chemistry, São Paulo State University, 15385-000 Ilha Solteira, Brazil
eudes.borges@unesp.br

Multiferroic materials have attracted great attention due to their numerous physical properties and potential technological applications. The so-called magnetoelectric coupling is a fascinating aspect of multiferroics, in which a magnetic field can tune electrical polarization and an electric field can tune magnetization. This is an advantage over conventional magnetic materials, as their magnetism in multiferroic materials can be controlled using electric fields. Bismuth ferrite ($BiFeO_3$) is a prototype multiferroic material that exhibits ferroelectric ($T_C \sim 1103$ K) and antiferromagnetic ($T_N \sim 643$ K) phases at room temperature, has G-type antiferromagnetic due to the local spin ordering of Fe^{3+} that forms a cycloidal spiral spin structure, present a large ferroelectric polarization at room temperature, and is considered as the most attractive for photovoltaic applications among ferroelectric materials due to its narrow bandgap ($E_g \sim 2.7$ eV). Despite the promising material to develop new concepts of photovoltaic, spintronic, and magnetoelectric devices, among others, a large leakage current often observed in $BiFeO_3$ thin films at room temperature has been a significant obstacle among some problems that limit the practical technological applications of this multiferroic. Doping the Bi^{3+} or Fe^{3+} by ions of comparable ionic sizes has often been used to modulate the physical properties of the $BiFeO_3$. Rare earth ions with different ionic radii have been especially used for doping the A site to change physical properties and to investigate possible new compositions. In my talk, I will review recent advances and perspectives on doping $BiFeO_3$ thin films with rare earth to control their physical properties. In addition, a systematic study on the synthesis, crystallization kinetics, and characterization of $BiFeO_3$ thin films doped with different rare earth ions (La, Sm, Nd, and Pr) will also be presented. Based on the results of doping Bi^{3+} site with multiple ions, the prospects for obtaining $BiFeO_3$ thin films with complex compositions will be discussed.

I14

Designing new room temperature magnetoelectric materials

J.A. Eiras[1], M.S Alkathy[1], F.L. Zabotto[1], M.H. Lente[2], E.B. Araujo[3], I.A. dos Santos[4]

[1]*Depto. de Física, Universidade Federal de São Carlos, São Carlos, SP CEP 13565-905, Brasil eiras@df.ufscar.br*

[2]*Instituto de Ciência e Tecnologia, Universidade Federal de São Paulo, São José dos Campos, SP*

[3]*Depto. Física, Universidade Estadual de São Paulo, Ilha Solteira, SP*

[4]*Depto. Física, Universidade Estadual de Maringá, Maringá, PR*

The magnetoelectric coupling (MEC) which enabling to control a magnetic state using electric field (or polarization control by using magnetic field) has been investigated to design of novel low power electronic devices. This phenomenon provides a direct route for electrically controlled magnetism or alternately a ferroelectricity that can be tuned by magnetic field. Magnetoelectric coupling (MEC) can be observed as well in single phase as in composites multiferroic materials (which can combine two or more ferroic order parameters (namely ferroelectricity, ferromagnetism and ferroelasticity in a single phase). The search for materials presenting high MEC at room temperatures has attracted considerable research activities in the last decade due to its wide range of potential applications in spintronic, data storage, sensors, and electrically tunable microwave devices with low power consumption.

Although the high technological interest, there are only a few single-phase materials that present multiferroic and magnetoelectric coupling at room temperature. Most of these compounds present order coexistences only at low temperatures. Moreover, the magnetoelectric coupling in single-phase compounds is usually weak due to their low remanent magnetization. Obtain a single-phase multiferroic displaying a large magnetization controllable by an electric field at 300 K remain a challenge.

As a strategy to search for new single phase room temperature multiferroics an alternative is the doping or modification of ferroelectrics with high Curie temperature (T_C) with magnetic and heterovalent elements.

In this talk results obtained for room temperature multiferroic magnetoelectric $(1-x)Pb(Zr_{0.53}Ti_{0.47})O_3–xPb(Fe_{0.5}Nb_{0.5})O_3$, $0.10 \leq x \leq 0.35$ ($PZT_{1-x}PFN_x$) solid solutions and lead free bismuth layered compounds (bismuth titanate-BIT based ceramics of $Bi_{3.25}A_{0.75}Ti_{3-x}(Co, Fe)_{x/2}O_{12}$, where A=La, Nd or Sm and x=0, 0.1, 0.2, 0.3, 0.4), synthesized through the conventional oxide mixture process, will be presented. The influence of iso- and heterovalent doping in the structural, dielectric, ferroelectric, magnetic and magnetoelectric properties will be discussed. It is noticed that in ($PZT_{1-x}PFN_x$) the magnetoelectric coupling and its nature are anomalously dependent on the PFN concentration, resulting from the contributions of a linear magnetoelectric and a paramagnetoelectric coupling.

A consistent magnetoelectric response was found for the compositions PZT-10PFN, PZT-30PFN, and PZT-35PFN, which exhibit the coexistence of ferromagnetic and ferroelectric ordering. The origin of the multiferroicity and the magnetoelectric coupling is explained by considering the presence and evolution of complex defects and magnetic nanoregions caused by PFN addition.

In single phase bismuth layered bulk ceramics (bismuth titanate-BIT based ceramics of $Bi_{3.25}A_{0.75}Ti_{3-x}(Co, Fe)_{x/2}O_{12}$, where A=La, Nd or Sm and x=0, 0.1, 0.2, 0.3, 0.4) it was observed that heterovalent (Co, Fe) co-doping promotes ferromagnetic ordering, still maintaining a high ferroelectric spontaneous polarization. The room temperature multiferroic state (ferroelectric and ferromagnetic), consequently, promotes the magnetoelectric coupling. Experimental results of multiferroic state and magnetoelectric coupling are discussed and correlated with changes in the electronic structure, octahedral distortions (tilting angles and bond lengths), and oxygen vacancies formation.

I15

Magnetoelectric properties of small particles with inhomogeneous magnetization

R.F. Mamin, T.S. Shaposhnikova

Zavoisky Physical-Technical Institute, FRC Kazan Scientific Center of RAS, 420029, Kazan, Russia
mamin@kfti.knc.ru

Materials with magnetoelectric properties have attracted widespread attention due to their potential use in various devices. New materials with magnetoelectric characteristics interesting for practical applications have been obtained. Note that these properties are often observed in multiferroics [1, 2]. In this work, within the framework of a phenomenological model, the possibility of a magnetoelectric effect in systems with inhomogeneous magnetic ordering is considered. The occurrence of electric polarization in small magnetic particles of various shapes with inhomogeneous magnetization has been studied. Inhomogeneous distribution of magnetization leads to inhomogeneous electrical polarization. The result of the action of a uniform external magnetic field on magnetic particles leads to a change in electrical polarization, resulting in a magnetoelectric response. The specific form of expressions for electric polarization and magnetoelectric response is determined by the inhomogeneous distribution of magnetization in the particles. Magnetoelectric response is observed at various directions of the external magnetic field, but a non-zero average magnetoelectric response appears only for some field directions.

1. N.A. Spaldin, R. Ramesh, *Nat. Mater*. **18**, 203 (2019).
2. A.P. Pyatakov, A.K. Zvezdin, *Physics – Uspekhi* **55**, 557 (2012).

I16

Surface energy of domain walls as a universal concept in materials science and beyond

A.P. Pyatakov

M.V. Lomonosov Moscow State University - Leninskie gori, MSU, 119991, Moscow, Russia
pyatakov@physics.msu.ru

The surface tension due to additional energy associated with interfaces or boundary lines is a universal concept widely used in theoretical models of material science as well as for models of “nonmaterial” issues like geographical dialects distribution [1].

In micromagnetism the surface energy of magnetic domain walls is one of the major factors determining the size and shape of magnetic domains. For magnetoelectric media in particular, its value depends not only on exchange stiffness and anisotropy like it was in classical micromagnetism [2], but also on the electric polarization in the medium [3] as well as its topography [4]

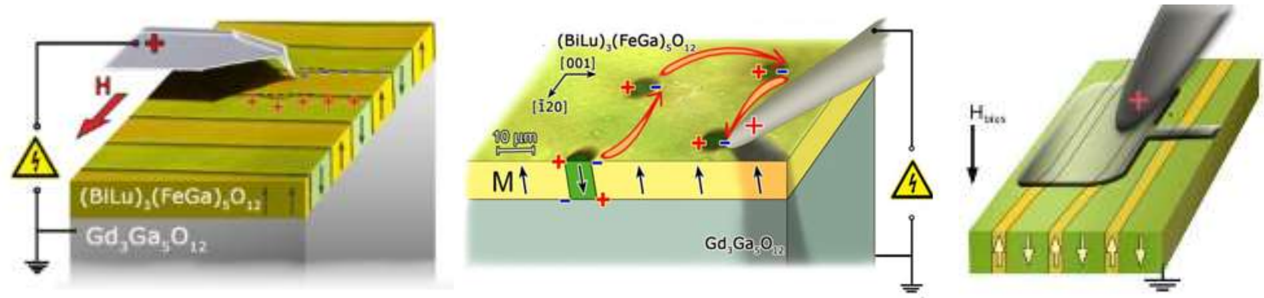

Figure 1. The manifestations of the electric-field induced domain wall surface energy modulation: a) he effect of domain wall attraction/repulsion; b) bubble domain nucleation c) domain wall refraction

This report will be focused on various manifestations of the electric-field induced domain wall surface energy modulations (Fig.1) such as the effect of electric field-driven domain wall motion [3], the effect of electric field-controlled bubble domain nucleation (Fig. 1) as well as the effect of the domain structure refraction on the stripe electrode [5]. The effect of the “dynamical multiferroicity” on a ferroelectric domain wall will also be considered [6].

The support by Russian Science Foundation grant #23-22-00162 is acknowledged.

1. J. Burridge *Phys. Rev. X.* **7**, 31008 (2017).
2. L.D. Landau, J.S. Bell, M.J. Kearsley, et al., *Electrodynamics of Continuous Media* (Pergamon, Amsterdam) Vol. 8 (1984).
3. A.P. Pyatakov et al, *Topics in Applied Physics* **138**, 129 (2021).
4. N. Hedrich et al, *Nature Physics* **17**, 574 (2021).
5. A.A. Podkletnova, et al., *JETP Lett.* **118**, 262 (2023).
6. D.M. Juraschek et al., *Phys. Rev. Lett.* **123**, 127601 (2019).

Ferroelectric-ferromagnetic composites for sensing and biomedicine

A.L. Kholkin

Department of Physics & CICECO – Aveiro Institute of Materials, 3810-193, Aveiro, Portugal
kholkin@ua.pt

Magnetoelectric (ME) effect is defined as a linear coupling between polarization and magnetic field (direct effect) and between magnetization and electric field (converse effect). This effect has been of immense interest in the scientific community over the past years [1]. Unlike ME of single-phase multiferroics, numerous ME composites, combining elastically coupled piezoelectric and magnetostrictive phases, have been shown to yield very strong ME effects even at room temperature. These structures also offer a great flexibility in the sense that a large number of parameters may be tuned independently including the materials properties of the constituent phases and the connectivity between them. Consequently, these composites are nowadays very close to a range of promising applications including: DC and AC magnetic vector field and electric current sensors, magneto-electro-elastic energy harvesters, multiple-state memory devices, micro-sensors in read heads, transformers, spinners, diodes, spin-wave generators, electrically tunable microwave filters, and various biomedical devices.

In this work, the fabrication and characterization of several types of novel ME composite transducers will be presented including magnetic/piezoelectric cantilevers for environmental (mechanical+magnetic) energy harvesting [2], sensitive magnetic field sensors, and various ME composites (scaffolds) for tissue regeneration, drug delivery, and remotely induced catalysis. These include piezoelectric fibers with embedded magnetic nanoparticles, ME nanorods, and core-shell ME spherical nanoparticles. These composites are characterized by excellent biocompatibility and biodegradability and show large ME response mediated by the remote magnetic field. Scaffold morphology, molecular and phase composition, crystalline structure, surface potential, and local piezoresponse were studied [3]. Core-shell structures based on $MnFe_2O_4$ and $(Ba,Ca)(Zr,Ti)O_3$ were synthesized by mild hydrothermal synthesis and surface modification [4]. These structures were used for the removal of water pollutant (rhodamine B) with more than 95% efficiency under AC magnetic field of only 150 mT. Other examples of the biomedical applications of ME composites will be presented in this talk.

1. S. Kopyl et al. *Materials Today Bio* **12**, 100149 (2021).
2. J.V. Vidal et al, *IEEE Trans. Ultrason. Ferroelectr. & Freq. Control* **67**, 1219 (2020).
3. R.V. Chernozem et al, *Nano Energy* **89**, 106473 (2021).
4. R.V. Chernozem et al, *Small*, 2302808 (2023).

I18

Sustainable MXene- Ferrite based nanocomposites for environmental remediation

M. Khanuja

Centre for Nanoscience and Nanotechnology, Jamia Millia Islamia, New Delhi-110025, India
manikakhanuja@gmail.com

Sol-gel auto combustion and hydrothermal technique were used to construct a highly effective composite catalyst (MZF) ornamented on MXene ($Ti_3C_2T_x$) sheets with magnetic zinc ferrite nanoparticles ($ZnFe_2O_4$). The synthesized catalyst exhibits exceptionaladsorption performance for the removal of terephthalic acid (TPA) from wastewater as compared to the pristine $ZnFe_2O_4$ (ZnF) and MXene (MX). MZF catalyst 97.4, 82.5, 76.0 and 69.4% of removal efficiency at 20, 50, 70 and 100 mg/L concentration of TPA in 20 minutes, which is ~9 fold higher than pristine ZnF.The structural, morphological and functional group analysis of preparedsamples were characterized by X-ray diffraction (XRD), field emission scanning electron microscopy (FESEM), Fourier transform infrared spectroscopy (FTIR). The higher surface area, greater porosity, low charge transfer resistance, and enhanced carrier concentration as determined by Branuaer Emmet Teller (BET), electrochemical impedance spectroscopy (EIS), and Mott-Schottky (MSK) analysis were the reasons for the improved removal efficiency in the case of MZF catalyst. Free radical production in the absence of light is also beneficial to enhanced elimination efficiencies as analyzed from electron paramagnetic resonance (EPR) analysis. The results obtained from zeta potential with auto titration, time correlated single photon counting decay (TCSPC) also favors the removal efficiency of TPA by MZF catalyst. The formation of free radicals under dark conditions are also in support of removal rates. The magnetic nature of catalyst helps in the collection of samples after adsorption with any loss as explained on the basis of vibrating sample magnetometer (VSM) technique. The mechanism of degradation of TPA by MZF was explained through kinetic studies. In order to meet Sustainable Development Goal 6, this work will provide important scientific contributions to researchers working on wastewater treatment.

I19

Additive manufacturing of magnetic materials

A.S. Volegov[1,2], S.V. Andreev[1], O.A. Golovnia[1,2], A.A. Golubyatnikova[1], V.E. Maltseva[1],
D.S. Neznakhin[1], N.V. Selezneva[1], E.A. Stepanova[1], A.N. Shalaginov[1]

[1] *Ural Federal University named after the first President of Russia B.N. Yeltsin, 620002, Yekaterinburg, Russia*
alexey.volegov@urfu.ru

[2] *Institute of Metal Physics UB RAS, 620108, Yekaterinburg, Russia*

The development of power engineering and robotics, miniaturization of high-tech devices containing electric motors and actuators, as well as electric transport require an increase in the production of permanent magnets and simultaneous improvement or optimization for specific technical tasks of their magnetic hysteresis properties. Due to eddy currents, the temperature of permanent magnets used in generators and electric motors exceeds room temperature and often reaches 400÷450 K. Since the Curie temperature of $Nd_2Fe_{14}B$ compounds is relatively low, their coercive field depends on the temperature in the range from room temperature and above, the main way to improve the properties of magnets for motors and generators is to increase the coercivity in the entire temperature range below the Curie temperature. Magnets based on Nd-Fe-B alloys are mainly produced by sintering, which allows to obtain simple shapes of magnets in the form of rectangular parallelepipeds, cylinders, prisms, horseshoes, etc. These shapes imply the use of complex assemblies. Such shapes imply the use of complex assembly procedures in the manufacture of magnetic systems. The use of additive manufacturing technologies currently allows to create products from structural materials of complex, almost arbitrary shapes and is used mainly in the field of space technologies. In the field of functional materials, there is a pronounced lag between the properties of materials manufactured using additive technologies and the properties obtained as a result of decades-old technological processes.

The talk will describe the approaches to additive manufacturing of permanent magnets and magnetically soft elements with and without organic binder used worldwide. The approach realized by the authors to additive manufacturing of permanent magnets with high coercivity without using heavy rare-earth metals will be described in detail. The essence of the approach is to use a mixture of powders of a eutectic alloy based on 3d-4f-metals with an alloy consisting of highly anisotropic grains of $Nd_2Fe_{14}B$ or Sm-Fe-Ti phase with $ThMn_{12}$ structure. The eutectic alloy performs two functions: (i) a binding function to create a permanent magnet body from the powder and (ii) a function of effective separation of nanoscale grains of $Nd_2Fe_{14}B$ phase, suppressing the exchange interaction between the grains. The realization of the proposed approach allowed us to obtain permanent magnets with coercivity up to 19.5 kOe in the case of the main phase like $Nd_2Fe_{14}B$ and 3 kOe in the case of the $SmFe_{11}Ti$ phase. The report will contain detailed results of the study of the phase composition, microstructure and magnetic properties of the obtained samples.

The work on fabrication and investigation of magnetic hysteresis properties of hard magnetic materials fabricated by selective laser melting was financially supported by RSF (grant No. 21-72-10104), magnetically soft materials - within the framework of the Priority 2030 program.

I20

Magnetic nanostructure for THz photonics

E.D. Mishina[1], A.M. Buryakov[1], M.V. Sapozhnikov[2], V.L. Preobrazhensky[1,3]

[1]*MIREA - Russian Technological University, 119454 Moscow, Russia*
mishina_elena57@mail.ru

[2]*Institute for Physics of Microstructures RAS, Nizhny Novgorod, Russia*

[3]*Prokhorov General Physics Institute of RAS, Moscow, Russia*

The generation of terahertz (THz) radiation is of great technological importance for many applications, such as non-destructive diagnostics, imaging, ultrafast computing, wireless communication, and direct control of material order parameters. For comprehensive applications, analogously to UV-visible-IR photonics, a comprehensive variety of THz photonic instruments has to be developed: THz sources and detectors, filters, modulators, etc. There are four main groups of THz sources, which can be excited by femtosecond visible or near IR laser: nonlinear organic and inorganic crystals, semiconductor antennas and spintronic emitters. Spintronics emitters are mainly based on magnetic/non-magnetic nanolayers. In such structures, THz radiation is excited by a femtosecond laser pulse due to the mechanism of the inverse spin Hall effect, which ensures the conversion of ultrafast spin photocurrent into a transverse charge current. The main advantages of spintronic emitters are wide spectrum of generated THz pulses (up to 30 THz [1]) and tunability by magnetic field. Here we present magnetic nanostructures with in-plane anisotropy that enable internal manipulation of THz wave amplitude and polarization by magnetic field strength.

Two types of magnetic nanostructures were fabricated: the bilayer Co(3nm)/Pt(3nm) and spin valves Co(1,8nm)/Pt(3nm)/Co(1,8nm)/IrMn(5nm). The structures were deposited by magnetron sputtering on a glass substrate in an argon atmosphere and room temperature. The deposition process was carried out under an applied magnetic field of 400Oe, aligned in the plane of the samples. Magnetic field assisted fabrication enabled the creation of an easy magnetization axis in the same as magnetic field direction. To measure the parameters of THz generation we utilized the conventional method of THz time-domain spectroscopy [2]. For THz wave parameters control, the samples were put in an in-plane magnetic field.

In the Co/Pt bilayer, magnetic field should be directed along the hard axis. Then by the magnetic field ramp within the anisotropy field, magnetization rotates by 180^o without changing its value. It gives rise to the THz wave polarization rotation by 180^o as well while its amplitude remains constant. Thus, the proposed structure is a pure polarization rotator.

In the spin valves, magnetic field should be directed along the easy axis of magnetization. The for two types of valves mechanisms are different. In Co/Pt/Co/IrMn structure, antiferromagnetic IrMn layer provides pinning of magnetization direction in the neighboring Co layer. For unmagnetized structure, magnetization in two Co layers is directed oppositely. Then charge currents are parallel and enhances the generated THz field. When magnetic field higher than coercive field H_C, is applied to the structure, magnetizations in two Co layers become parallel. Then the charge currents from two sources, directed antiparallel, cancel each other, resulting in almost zero THz field. Modulating magnetic field provides modulation of THz wave amplitude with very high efficiency.

In this study we propose the route to control the polarization and amplitude of the THz wave magnetic nanostructures using specially constructed nanostructures. The key point of the developed spintronic emitters is the in-plane anisotropy. Applying ultrabroadband THz radiation and femtosecond laser pulses to spintronic and magnetic structures provides new insights into fundamental spintronic processes. On the other hand, exciting applications for spintronic information processing and THz photonics emerge.

The work is supported by Russian Science Foundation (#23-19-00849).

1. T. Seifert et al, *Nature Photonics* **10**, 483 (2013).
2. A. Buryakov et al, *Appl. Phys. Lett.* **123**, 082404 (2023).

I21

Interaction between a relaxation mode and soft acoustic phonon in the relaxor ferroelectric $Na_{1/2}Bi_{1/2}TiO_3$

S.G. Lushnikov[1], N.K. Derets[1], A.I. Fedoseev[1], J.-H. Ko[2], Seiji Kojima[3]

[1]Ioffe institute, 194021 St. Petersnurg, Russia
sergey.lushnikov@mail.ioffe.ru

[2]Hallym University, 24252, Chuncheon, Korea

[3]University of Tsukuba, Tsukuba 305-8573, Japan

This work presents the results of study of behavior of low frequency part of the vibration spectra of $Na_{1/2}Bi_{1/2}TiO_3$ (NBT) crystals within a temperature range from 110 K to 850 K. Measurements were carried out by means of Brillouin light scattering on longitudinal, quasi-longitudinal and transverse (TA) acoustic phonons with a wave vector $\mathbf{q}_{ph} \parallel [100]$, $\mathbf{q}_{ph} \parallel [010]$ and $\mathbf{q}_{ph} \parallel [110]$, regarding a cubic phase of NBT. Additionally, the behavior of quasi-elastic light scattering in the corresponding directions in the crystal was analyzed.

We reveal that the maximal anomalies of the vibrational and electron degres of freedom, as well as the manifestations of the strength of their interaction, are associated with the characteristic temperatures of this material. The first type of anomalies peak at $T_3^* \sim 565$ K, which correspond to the onset of the high-temperature electronic fluctuations in the M-point of the Brillouin zone. The temperature range of the second anomalies type is between T_3^* and $T_2^* \sim 655$ K, where high temperature M-type fluctuations compete with the low-temperature diffuse mode in the R-point. Phonon anomalies are manifested in the softening of its frequencies and the strength of electronic fluctuations is reflected in its intensity. The qunatum interplay between discrete phonon peak and continuum of electronic excitations results in the asymmetric Fano shape of the Brillouin spectra (Fig.1). The anomalies of vibrational and electronic spectra are maximal at the temperatures where Fano asymmetry parameter q approaches unity, indicating the strongest qunatum electron-vibrational mixture and, thus, pointing to the decisive role of the electron-lattice interplay in the crosover between different phases of relaxor materials.

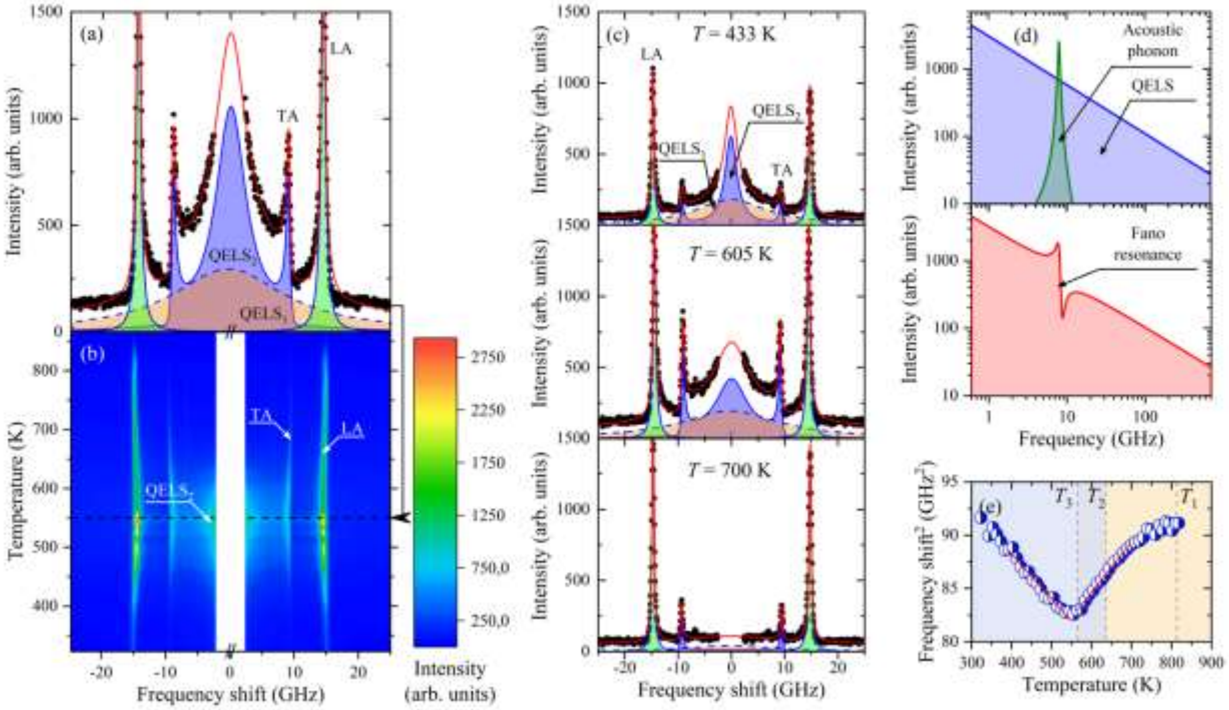

Figure 1. Brillouin spectra in NBT crystals vs temperature (a-c) and “softening” TA acoustic phonon at phase transformations in NBT (e).

I22

Magnetic irreversibilities, microwave nonreciprocity and ultrafast magnetization dynamics in multiferroic $FeCr_2O_4$ spinel

R.V. Yusupov, R.G. Batulin, M.A. Cherosov, A.V. Petrov, B.F. Gabbasov, K.V. Vasin,
A.G. Kiiamov, A.L. Zinnatullin, M.V. Eremin

Kazan Federal University, 420008 Kazan, Russia
Roman.Yusupov@kpfu.ru

Great attention has long been paid to the applied and fundamental studies of crystals with the spinel structure. These materials reveal a broad variety of useful properties: strong hardness, low thermal conductivity, stability at high temperatures. Modern studies of these compounds are stimulated by magnetoelectric effects discovered in them [1]. Compounds $FeCr_2S_4$, $FeCr_2O_4$, $NiCr_2O_4$ and FeV_2O_4 belong to the spinel family and have a high cubic symmetry at or slightly above the room temperature, but are distinguished by an orbital degeneracy of the iron, nickel of vanadium ions at definite spinel structure sites. This endows a system with an additional degree of freedom (compared, e.g., with $CoCr_2O_4$) and therefore increased complexity in magnetic and dielectric properties. Magnetoelectric effects of a still unclear origin were detected in the ferrimagnetic phase of $FeCr_2S_4$ [2,3]. The temperature dependences of the magnetic-order-induced electric polarization in $FeCr_2O_4$ and FeV_2O_4 are reported in [4,5] and [6], respectively.

Most of the reported studies have been performed on the polycrystalline powder samples, and it looks that many interesting effects are masked or averaged out in such materials. Here, we report on our recent achievements in a synthesis of high-quality single crystals of $FeCr_2O_4$ spinel, its unusual magnetic and electromagnetic properties as well as the recent results of femtosecond optical and magnetooptical studies.

The sample was synthesized with a high-temperature solid-state reaction from the stoichiometric mixture of the ferrous oxalate FeC_2O_4 and chromium oxide Cr_2O_3. The known problem of iron oxidation from the Fe^{2+} state to Fe^{3+} state was inhibited by the decomposition of FeC_2O_4 compound to FeO, CO_2 and CO, the latter creating the reducing atmosphere in the synthesis chamber. The polycrystalline ingot then was used for a single crystal growth by the optical floating zone method. A near-absence of the Fe^{3+} ions either in the powder sample or in a single crystal has been verified by the Mössbauer spectroscopy [7]. Specific heat and magnetic susceptibility measurements revealed anomalies at 138 K, 65 K and 38K inherent for $FeCr_2O_4$ and corresponding to the onsets of the orbital ordering in the Fe^{2+}-ion sublattice, global collinear ferrimagnetic order and a spiral modulation of the magnetic order [8], respectively.

The last two are revealed also in the temperature dependence of the magnetic susceptibility. The shape of the $M(T)$ curve varies qualitatively with the magnitude of an applied magnetic field, and two additional anomalies were observed at ~ 44 K and ~ 21 K that we associate with the magnetic-field induced rearrangement of the magnetic structure or modification of the magnetocrystalline anisotropy. A qualitatively similar observation in the $FeCr_2S_4$ isostructural sulfide compound was recently reported in [9]. The magnetic moment per unit cell at any temperature and a magnetic field less than 9 T doesn't exceed a value $1.25\mu_B$, which is less than $2\mu_B$ expected for a collinear ferrimagnetic arrangement between the Fe^{2+} and Cr^{3+} sublattices. This clearly shows that the magnetic structure of $FeCr_2O_4$ is more complicated. The shape of the hysteresis curves changes from narrow classic-one above 21 K to a butterfly-like below this temperature, with a pronounced irreversibility in the magnetic field range of $|B| < 5$ T.

Magnetic resonance study in the X microwave band has revealed a complex spectrum consisting of a minimum of 2 wide absorption bands that varied with temperature and was observed only in the temperature range of 21 ÷ 65 K. Interestingly, the orientation dependence investigation showed that the spectrum of a rectangular parallelepiped shaped sample with the faces perpendicular to the cubic <100> directions is not reproduced on the sample rotation by 180 degrees but rather demonstrates only a 360-degree periodicity. As either the crystalline structure or a shape symmetry is not lower than orthorhombic, we associate the described observation with the microwave non-reciprocity. The last is discussed in terms of the interference of the electric-dipole and magnetic-dipole transitions characteristic to multiferroic materials [10].

Ultrafast studies were performed with the use of the 1-kHz regenerative amplifier Legend-USP and the optical parametric amplifier (OPA) TOPAS (Coherent, USA) in the conventional pump-probe arrangement. For pump the light at 800 nm (1.55 eV) was used, and the probe wavelength was either the second harmonic, 400 nm (3.10 eV) or the output of the OPA tuned to the wavelengths in the range of 1700 ÷ 2200 nm (0.75 ÷ 0.55 eV). Probing at 3.10 eV corresponds essentially to the Mott-Hubbard-like excitation of the Cr^{3+} ions from the ground $^4A_2$ to excited $^4T_2$ state while with probing in the mid-IR we addressed the Fe^{2+} subsystem via the $^5E \rightarrow {}^5T_2$ single-ion transition. Two kinds of the probing light characteristics were studied: intensity variation due to the reflectivity modification and the rotation of the polarization plane due to the magnetooptical Kerr effect (TR-MOKE).

Reflectivity transients on probing at 400 nm reveal the signals with characteristic amplitude variation with temperature that allows to associate them with an establishment of the orbital and the magnetic orders. Thus, on cooling below 150 K, the signal with exponential rise and decay appears that indicates that the orbital order melts on the timescale of 1.5 ps and recovers on ~ 180 ps rate. On further cooling, additional components appear below 70 K that are identical to the components of the TR-MOKE transients observed only in the ferrimagnetic state; therefore, these responses originate from partial melting and recovery of the magnetic order that occur at the timescales of ~20 ps and ~800 ps at 10 K, respectively.

Interestingly, the time-resolved MOKE with probing at 2000 nm wavelength shows a behavior different from that observed at 400 nm. The signals are composed of two rising components. The faster one has a timescale that varies from 25 to 55 ps in the temperature range of 5 ÷ 35 K, then changes a sign and gets faster, varying from 5 to 15 ps on approaching the Neel temperature. The slow rising component has a time constant of 800 ps at 5 K and gradually becomes faster, approaching a value of 200 ps at 55 K. Magnetic order recovery is much longer though is fully restored within 2 ms, a period between the pump laser pulses.

Thus, we see that the magnetic order probed at different wavelengths reveals rather different characters, which, in our opinion, indicates significantly independent magnetic structures of the simpler Cr^{3+}-ion sublattice and more complicated Fe^{2+} sublattice. The slow (~ 800 ps) component of the Fe^{2+} sublattice dynamics may originate from the magnetic structure rearrangement mentioned above [10].

1. A. Sundaresan, N.V. Ter-Oganessian, *J. Appl. Phys.* **129**, 060901 (2021).
2. J. Bertinshaw, C. Ulrich, A. Günther et al., *Sci. Rep.* **4**, 6079 (2014).
3. L. Lin, H.X. Zhu, X.M. Jiang, et al., *Sci. Rep.* **4**, 6530 (2014).
4. K. Singh, A. Maignan, C. Simon, et al., *Appl. Phys. Lett.* **99**, 172903 (2011).
5. A. Maignan, C. Martin, K. Singh, et al., *J. Solid State Chem.* **195**, 41 (2012).
6. Q. Zhang, K. Singh, F. Guillou, C. Simon, et al., *Phys. Rev. B* **85**, 054405 (2012).
7. R. Batulin, M. Cherosov, A. Kiiamov, et al., *Magnetochemistry* **8**, 86 (2022).
8. G. Shirane, D.E. Cox, S.J. Pickart, *J. Appl. Phys.* **35**, 954 (1964).
9. L. Prodan, S. Yasin, A. Jesche, et al., *Phys. Rev. B* **104**, L020410 (2021).
10. R.V. Yusupov, M.A. Cherosov, B.F. Gabbasov, et al., *JETP Lett.* **115**, 167 (2022).

I23

Large electromechanical coupling in Zr-doped ceria

A. Frenkel[1], Y. Qi[2], E. Wachtel[3], D. Ehre[3], I. Lubomirsky[3]

[1]*Dept. of Materials Science and Chemical Engineering, Stony Brook University, Stony Brook, NY 11794, USA*

[2]*Dept. of Physics, Brown University, Providence, RI 02912, USA*

[3]*Dept. of Molecular Chemistry and Materials Science, Weizmann Institute of Science, Rehovot, 7610015, Israel*

We have investigated the electrostriction (ES) effect in Zr-doped ceria ($Zr_xCe_{1-x}O_{2-\delta}$) ceramics. ES is a second order electromechanical response, *i.e.*, strain, $\boldsymbol{u}$, is proportional to $\mathbf{M}\cdot\mathbf{E}^2$, where **E** is the applied electric field and **M** is the longitudinal electrostriction strain coefficient. Large ES in ceria has generally been associated with oxygen vacancies (V_o) which provide charge compensation for aliovalent dopants or for cerium reduction (Ce^{3+}). The ES induced by V_o is restricted to frequency <1 Hz and low saturation strain ($|u_{sat}|$ <15 ppm). Doping CeO_2 with Zr results in a large ES strain coefficient, reaching $|M|=10^{-16}$ m^2/V^2 for x=0.1, without formation of V_o. This effect persists to frequency ≥3 kHz with |u| ≥220 ppm, making $Zr_{0.1}Ce_{0.9}O_2$ competitive with the best commercial electrostrictor (PMN-PT15), but with ~100 times lower dielectric permittivity and three-fold higher elastic modulus. |**M**| of Zr-doped ceria increases exponentially with Zr content for x=0-0.1, suggesting that the contribution of Zr-ions to electrostrictive strain is collective. However, such collective motion does not lead to a phase transition even at 123 K, implying that interaction between Zr-ions is neither sufficiently strong nor sufficiently long-range to produce freezing of the displacement, an effect that has been observed for perovskite relaxors. XAS data, DFT modelling and *ab initio* molecular dynamics (AIMD) calculations demonstrate that elastic dipoles formed by Zr-doping are dynamic. In the absence of an E-field, $[ZrO_8]$-local bonding units remain, on average, centered with respect to the second (cation) coordination shell. Due to bond anharmonicity displacement of Zr by an E-field requires less energy than displacement of the host cations, resulting in a large dynamic elastic dipole. This polarizable elastic dipole gives rise to large electrostrictive strain and constitutes the first example of non-classical electrostrictors (NCES) relying solely on substitutional point defects.

I24

The impact of domain wall conductivity on domain growth in ferroelectric single crystals

D.O. Alikin, M.S. Kosobokov, A.P. Turygin, V.Ya. Shur

School of Natural Sciences and Mathematics, Ural Federal University, 620000, Ekaterinburg, Russia, denis.alikin@urfu.ru

Polarization reversal in ferroelectric materials is governed by a delicate interplay between polarization dynamics and screening processes at the surface, in the material bulk, and at the domain walls. Inevitably, charged domain walls (CDWs) emerge and propagate in the material bulk during polarization reversal, raising questions about the mechanisms of their charge compensation. Basic electrostatic considerations of the nucleation of domains with CDWs lead to the Landauer paradox, where the depolarization energy appears exceedingly high while expanding the domain into the bulk requires charge compensation at the CDWs to screen the depolarization field [1]. This paradox can be partially resolved in the pre-electrode area by assuming charge injection from the electrode, as suggested by Molotskii et al. [2] and further developed by Jiang et al [3]. However, the mechanisms of the depolarization field screening during the evolution of the CDWs in the bulk of the ferroelectric crystal remain unclear, particularly where conductivity is negligibly small for many classical ferroelectrics.

Here by exploring the kinetics of the tip-induced polarization switching at the nonpolar surfaces of uniaxial ferroelectrics, we demonstrated significant asymmetry in the forward growth of the domains with “head-to-head” and “tail-to-tail” domain walls, which we rationalized based on the insight into the dynamics of the polarization screening. We both experimentally demonstrate and theoretically confirm that the conductivity of domain walls notably impacts the kinetics of forward domain growth during polarization reversal and the stability of the resultant domains. We've analyzed the asymmetry of the surface potential distribution on domains with CDWs after local polarization switching via scanning probe microscopy on the non-polar ferroelectric surface of the MgO-doped lithium niobate, attributing it to the heightened charge diffusion at the surface induced by the conductivity of the walls. Furthermore, we've simulated the scenario of screening charge redistribution along the CDWs, showcasing its critical role in the stability of the created ferroelectric domains.

The reported study was funded by the Russian Science Foundation (grant 23-72-01074). The equipment of the Ural Center for Shared Use “Modern nanotechnology” Ural Federal University (Reg.№ 2968) was used.

1. R. Landauer, *J. Appl. Phys.* **28**, 227 (1957).
2. M. Molotskii, R. Kris, G. Rosenman, *J. Appl. Phys.* **88**, 5318 (2000).
3. A.-Q. Jiang, H.J. Lee, C.S. Hwang, T.A. Tang, *Phys. Rev. B* **80**, 024119 (2009).

ORAL

PRESENTATIONS

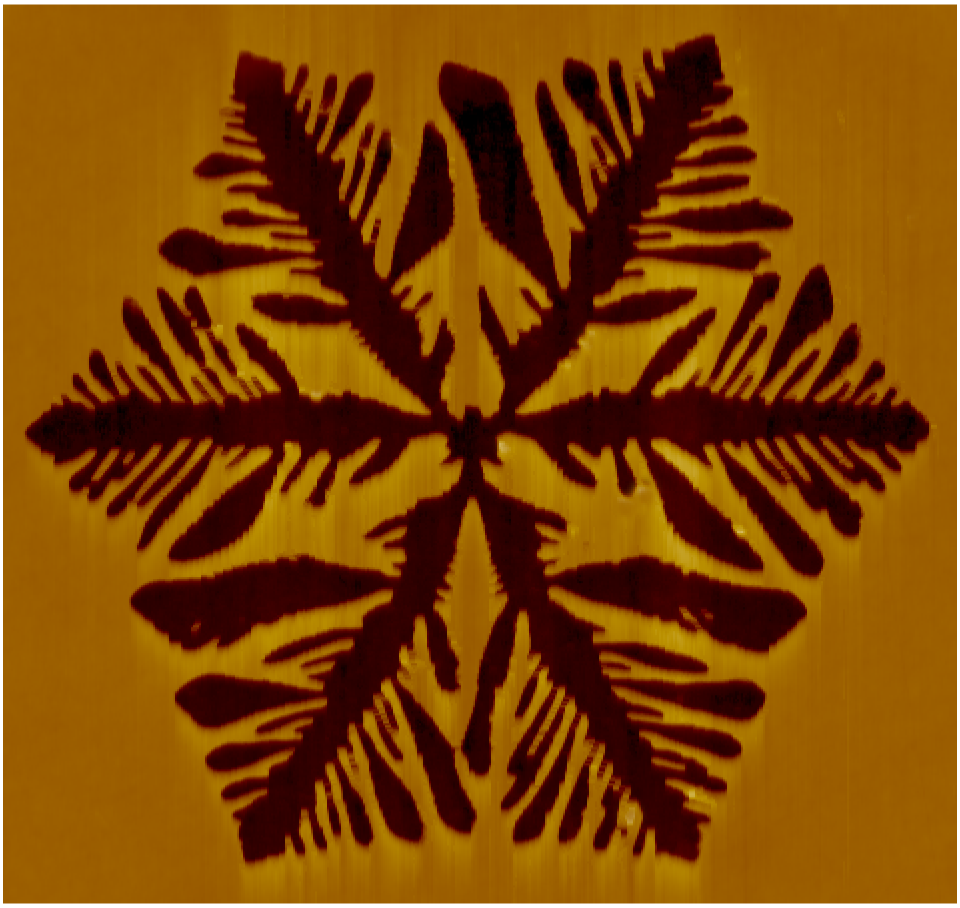

Optical method for the study of the pyroelectric phenomena in lithium niobate

S.M. Shandarov[1], K.M. Mambetova[1], A.I. Aksenov[1], L.N. Orlikov[1], N.I. Burimov[1], A.S. Ivanov[1], E.A. Chekh[1], M.A. Bryushanin[2], I.A. Sokolov[2]

[1]*Tomsk State University of Control Systems and Radioelectronics, 634050, Tomsk, Russia*
stanislavshandarov@gmail.com

[2]*Ioffe Physical-Technical Institute, 194021, St. Petersburg, Russia*

The high pyroelectric properties of lithium niobate are effectively used to accelerate of charged particles and to generate X-ray radiation and neutrons during the heating/cooling cycles [1−3]. Electron pulses generated by pyroelectric effects have a sporadic character with weakly studied time parameters. In ref. [4] it was obtained that for assembly with coaxial geometry and for cylindrical lithium niobate sample in the heating/cooling cycles at atmospheric pressure the sporadic discharge pulses having current in maximum from 45 mA to 600 mA, duration about 15 ns, and rise time from 1 to 1.9 ns are registered.

We have studied the peculiarities of an electric discharge generation between Z-faces of lithium niobate crystals with a thickness of 12.2 mm and a diameter of 17 mm, and a semitransparent conductive anode, which have been accommodated in the cylindrical copper cup. All experiments were realized at atmospheric pressure for temperature range from 24 to 110 ºC. The heating of this cup was performed by resistive heater with rate of 10 K/min whereas in the cooling cycle a free decrease of temperature has been used. The grounded anode was placed above upper Z-face of crystal at a distance of 5 mm or 10 mm.

The registration of the changes in the crystal attendant the electric discharges realized by using a reflection of laser beam with wavelength of 532 nm from the two parallel faces of a sample, $Z+$ and $Z-$, representing optical Fabry-Perot cavity. The time dependences for intensity of reflected light beam have been registered by using a pin photodiode BWP34 that was connected through an emitter follower to the input of broadband digital oscilloscope Keysight DSO-X 3102T (1 GHz). At the variations of a temperature, we observed as the slowly changes in the intensity of reflection beam connected with thermos-optic effect and pyroelectric generation of electric field in the crystal [5] as well as the abrupt jumps of such field on the values $\Delta E(t)$. There is reason to believe that these abrupt jumps of electric field $\Delta E(t)$ in the lithium niobate crystal caused by the electric discharges between one and a semitransparent anode.

By using the known relationship for reflection coefficient from Fabry-Perot cavity and for linear electrooptic effect in lithium niobate we have estimated from the mass of experimental date that the magnitudes of the abrupt jumps ΔE may be taken the values from 0.6 kV/cm to 1.4 kV/cm. Also, it has been established that time duration of abrupt jumps not exceed the value of 1 μs.

This study was funded by the Ministry of Science and Higher Education of the Russian Federation within the framework of the state order for 2023-2025 (job-order FEWM-2023-0012).

1. G. Rosenman, D. Shur, Y.F. Krasik, et al., *J. Appl. Phys*. **88**, 6109 (2000).
2. J.A. Geuther, G. Danon, *Appl. Phys. Lett.* **90**, 174103 (2007).
3. M. Ali, P. Karataev, A. Kubankin, et al., *Nucl. Instr. and Methods in Phys. Res. A* **1061**, 169134 (2024).
4. K.M. Mambetova, S.M. Shandarov, S.I Arestov, et al., *J. Instrumentation* **17**, 04008 (2022).
5. J. Parravicini, J. Safioui, V. Degiorgio, et al., *J. Appl. Phys,* **109**, 033106 (2011).

O2

Electronic and optical properties of LKGT crystal: DFT calculations

S.N. Krylova

Kirensky Institute of Physics Federal Research Center KSC Siberian Branch Russian Academy of Sciences, 660036, Krasnoyarsk, Russia
slanky@iph.krasn.ru

The $Li_2K_4TiOGe_4O_{12}$ (LKGT) crystal has a wide transparency range from 0.28 to 5.8 μm, a high laser damage threshold of 910 MW/cm2 (1064 nm, 6 ns, 15 Hz) and a moderate second harmonic generation (SHG) response, ~2 × KDP at 1064 nm [1]. In addition, this compound also exhibits slight anisotropic thermal expansion. The physical properties of the crystal indicate that $Li_2K_4TiOGe_4O_{12}$ is a stable nonlinear optical material in the mid-IR range. $Li_2K_4TiOGe_4O_{12}$ crystallizes in the non-centrosymmetric and polar tetragonal space group *P4nc* (No. 104) [1]. The structure of LKGT crystal in in yz-plane is presented in Figure 1.

The purpose of this work was to theoretically study the optical and electronic properties of this new interesting material in order to establish a connection between the physical properties and the structure of this compound.

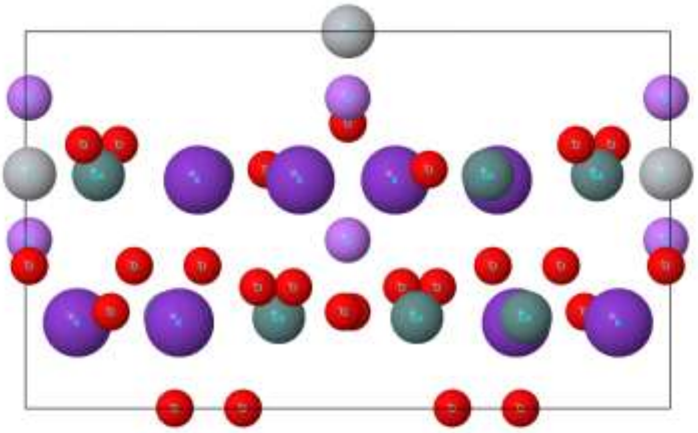

Figure 1. The $Li_2K_4TiOGe_4O_{12}$ crystal structure in yz-plane.

Theoretical modeling was carried out within the framework of plane waves based on density functional theory in the CASTEP software package [2]. To optimize the geometry and calculate the physical properties of the crystal, the PBEsol (GGA) functional was used. [3, 4]. This functional includes the dependence of energy on electron density and its gradient.

As a result of the work, dispersion curves in the first Brillouin zone were calculated. The tetragonal crystal structure was shown to be stable. The electronic structure of the crystal was also studied. In particular, the electronic structure in the first Brillouin zone (valence band, conduction band) and the density of electronic states were constructed. Basic optical properties (dielectric function, loss function, conductivity, reflectivity, absorption function) were simulated.

1. J. Xu, H. Wu, H. Yu, et. al., *Chemistry of Materials* **32**, 906 (2019).
2. S.J. Clark, M.D. Segall, et. al., *Z. Kristallogr. -Crystalline Materials* **220**, 567 (2005).
3. J.P. Perdew, K. Burke, M. Ernzerhof, *Phys. Rev. Lett.* **77**, 3865 (1996).
4. J.P. Perdew, A. Ruzsinszky, G.I. Csonka, et. al., *Phys. Rev. Lett.* **100**, 136406 (2008).

O3

Characterization of the PVA-based polarizers doped with carbon nanostructures

N.V. Kamanina[1,2,3], L.O. Fedorova[2,3], S.V. Likhomanova[1,2,4]

[1]*Lab for Photophysics of Nanostructured Materials and Devices, Vavilov State Optical Institute, St.-Petersburg, Russia*

[2]*St.-Petersburg Electrotechnical University ("LETI"), St.-Petersburg, Russia*

[3]*Petersburg Nuclear Physics Institute, National Research Center «Kurchatov Institute», Gatchina, Russia*

[4]*St.-Petersburg State University of Aerospace Instrumentation, St.-Petersburg, 190000, Russia*
nvkamanina@mail.ru

Among wide groups of the organic materials used to make the thin-film polarizers polarizer's elements the PVA (polyvinyl alcohol) occupy a special place because of their large atomic weight (responsible for the flexibility), ease of the integration into any optoelectronic circuit and good functioning in the visible and near-infrared spectral range, which can compete with the Glan and Nicolas volumetric prisms. Different scientific teams are investigated the doped PVA materials with the Al_2O_3, TiO_2, SnO_2 nanoparticles doping [1-3]. Before we have studied PVA matrix with the carbon nanotubes [4,5], that predicts the future doping of the PVA by different carbon-based sensitizers. The results of a current study are discussed how the carbon-based nanoparticles influence on the basic properties of a PVA polymer matrix. Good transparency for the parallel light components, large polarization ability, improved mechanical characteristics is established. The accent is made on the fullerenes, shungites, and graphene oxide nanoparticles, which are used as the PVA effective sensitizers. Some comparative results for these polarizers are shown in Figure 1. It should be noticed that the different stretching of the film in the stretching machine was used. Data presented in Figure 1 corresponded to the large value of the stretching, of about 3.5 times.

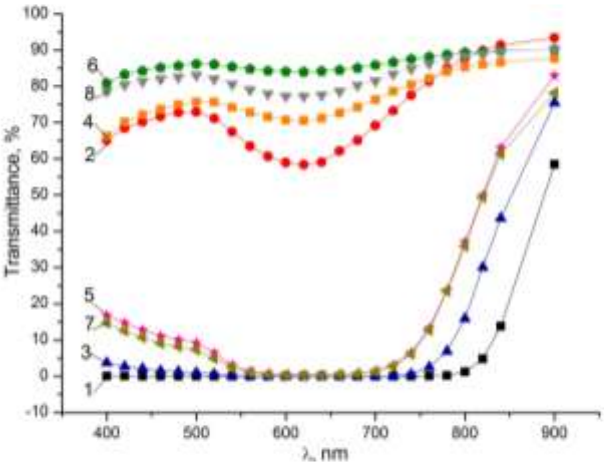

Figure 1. The transmittance of the parallel (*T* par.) and orthogonal (*T* orth.) light component for the thin-film polarizers with the stretching of 3.5 times (long). Curves are the followings: 1 - *T* orth. pure PVA, 2 - *T* par. pure PVA, 3 - *T* orth. PVA+0.1 wt.% GrO, 4 - *T* par. PVA+0.1 wt.% GrO, 5 - *T* orth. PVA+0.1 wt.% C_{70}, 6 - *T* par. PVA+0.1 wt.% C_{70}, 7 - *T* orth. PVA+0.1 wt.% Shungite; 8 - *T* par. PVA+0.1 wt.% Shungite.

It should be mentioned that the introduction of the carbon-based nanoparticles can provoke the increase of the parallel light component transmittance; thus the polarization ability will be increased as well. This research reveals the advantages to use the carbon-based structured thin-film light polarizers based on a PVA matrix as the independent optoelectronic element.

This research is supported by Russian Scientific Fond, project No. 24-23-00021 (2024-2025).

1. B. Canimkurbey, C. Cakirlar, S.P. Mucur, et al. *J. Mater. Sci.: Mater. Electron.* **30**, 18384 (2019).
2. T.A. Abdel-Baset, *J. Mater. Sci.: Mater. Electron.* **31**, 15960 (2020).
3. R.J. Sengwa, P. Dhatarwal, *J. Mater. Sci.: Mater. Electron.* **32**, 9661 (2021).
4. N.V. Kamanina, S.V. Likhomanova, P.Ya. Vasilyev, et al., *Tech. Phys.Lett.* **37**, 1165 (2011).
5. Patent RU 2 498 373 C2. Polarizing films for the visible range of light with a nanostructured surface based on carbon nanotubes and nanofibers. 2013. Patent holder: S.I. Vavilov State Optical Institute. Authors: N.V. Kamanina, P.Ya. Vasiliev, V.I. Studenov.

O4

Coupling lab-based AFMs with ultrafast in-situ Nanocalorimetry in view of building a lab-on-a-chip platform for characterization of nanogram-sized samples

A.F. Akhkiamova, A.F. Abukaev, A.P. Melnikov, I.I. Rulev, D.A. Ivanov

NUST MISIS, 119049, Moscow, Russia
azigy@mail.ru

This research is methodologically focused on the in-situ combination of nanocalorimetry (NC) and atomic force microscopy (AFM) to enable simultaneous and quantitative determination of the surface features and thermal properties of a vast range of nano-sized and/or thinfilm materials. The high heating and cooling rates provided by the Nanocalorimetry (NC) sensor based on micro-electro-mechanical-systems (MEMS), allow unveiling the complex temperature-dependent micro/nano-structural evolutions occurring in semicrystalline polymers, as well as in polymer nanocomposites and thin films designed for organic photovoltaics applications. Among the many possible scientific targets, we concentrate on crystallization and melting of semi-rigid poly(trimethylene terephtalate) (PTT) and similar semicrystalline polymers.

Further development of MEMS-based ultrafast calorimetry coupled to AFMs lead to a new experimental platform for combined physico-chemical characterization of nanogram-sized samples. This was achieved via the know-how developed for the integration of nanocalorimetry with the AFMs. These instruments significantly expand the possibilities of scanning probe microscopy in terms of analysis of topography and surface properties of thin films and nano-objects used in functional nanomaterials. Importantly, the NC/AFM combination will enable quantitative investigation of multiple thermal transitions in nanogram-sized specimens, thus yielding information on e.g. the temperatures and enthalpies of the phase transitions, the degree of crystallinity, and the glass transition temperatures, which will enhance our understanding of the information delivered by simultaneous AFM imaging.

The methodological and scientific developments driven by this research will be beneficial for a broad scientific community working in the field of functional nanomaterials and polymer nanocomposites. We believe that this work will enhance the interest of a growing user community for in-situ combinations of novel emerging characterization techniques, thus contributing to the possible development of a future lab-on-a-chip platform.

This research was funded by state support with the K1-2022-035 project in the framework of the strategic academic leadership program “Priority 2030”.

O5

The onset of tip-surface contact in AFM force curve measurements

I.A. Morozov, R.I. Izumov

Institute of Continuous Media Mechanics UB RAS,614013, Perm, Russia
ilya.morozov@gmail.com

Accurate determination of the beginning of the contact between the tip of the atomic force microscope (AFM) probe and the surface in force measurements is necessary both for calculating the constants of non-contact interactions and for determining the structural and mechanical properties of the materials. In an air environment the contact is preceded by a rapid jump of the tip to the surface due to the attractive forces. If a surface is not deformed by a probe of a given stiffness, the end of the jump (minimum of the deflection of the cantilever) is taken as the onset of the contact. In this work, it is shown that the contact of the tip with the deformable surface occurs before the completion of the jump. In this case, it is reasonable to use the point of the extreme velocity of deflection as the onset of the contact.

The rapid jump of the AFM probe to the surface under the action of van der Waals forces to (deformable) viscoelastic materials as well as to a rigid substrate was investigated with various approach velocities and probes of different stiffness. The velocity of the cantilever deflection becomes very high just before the tip contacts with the surface. This causes loss of significant points of the interaction curve; the high probe-sample approach velocity amplifies the problem even more. Therefore, the rate of data acquisition has a major impact on the accuracy of measurement of the onset of the tip-surface contact. The accuracy is also affected by the viscoelastic properties of the surface and the probe, Hamaker constant and experiment settings.

Calculations using a dynamic mass-spring model of the interaction of the tip with the viscoelastic material have shown that the high deflection velocity and the low rate of data acquisition (bandwidth) are the reasons for significant errors in determining the contact from the experimental force curve. In most cases, the observed point of contact is lower than the actual one (under certain conditions, the opposite situation is also possible) and the measurement error is at least 50% (depending on the experimental settings, the properties of the probe and the material). The uncertainty in the detection of the contact is due to the penetration of the tip into the deformable material immediately after the contact that is caused by the inertia and adhesion forces. In the experiments where the precise determination of the contact is required (study of non-contact interactions or the properties of the thin films) it is recommended to use the highest possible data acquisition rate (30 kHz and more), probes of moderate stiffness and approach not exceeding than 5...10 µm / s.

The contact with the rigid surface located in the vicinity of the completion of the jump (the minimum of the deflection). Contact with deformable materials occurs before this point, namely in the point of the extreme deflection velocity. Note, that the regular AFM-measurements usually overestimate this position.

The work was supported by Russian Science Foundation, project 23-22-00064.

O6

Correlation of local ferroelectric and resistive properties in $BaTiO_3$-films studied by scanning tunneling microscopy

N.V. Andreeva[1], A.E. Petukhov[2], E.A. Ryndin[1], O.Y. Vilkov[3]

[1]*Department of Micro- and Nanoelectronics, St. Petersburg Electrotechnical University 'LETI', St. Petersburg, Russia*
nvandr@gmail.com

[2]*Research Park St. Petersburg State University, St. Petersburg, Russia*

[3]*Department of Solid State Electronics St. Petersburg State University, St. Petersburg, Russia*

An approach to the study of the relationship between local ferroelectric (FE) and resistive properties in nanolayered memristive compositions based on epitaxial BaTiO3 films (BTO-films) using scanning tunneling microscopy (STM) and spectroscopy (STS) under ultra-high vacuum conditions, with a higher spatial resolution on nanometer-scale, has been developed.

Using tunnel current, exponentially decaying with distance, as a feedback control parameter, ensures the possibility of local ferroelectric property investigation with STM. Due to the change in the height of 'STM-probe - BTO-surface' potential barrier happened at FE-polarization reorientation, the distribution of FE-properties over the BTO-film surface could be visualized on the results of topology measurements.

Experimental and theoretical investigations of the correlation between resistive and FE properties in thin epitaxial BTO-films in STO (substrate) / LSMO (bottom electrode) / BTO (FE film, 3 nm) compositions in the temperature range of 30 ÷ 300 K have been carried out. It is shown, that when studying the correlation of local resistive and FE properties in BTO-films using probe techniques (including conductive atomic force microscopy and piezoresponse force microscopy), the contribution of the free BTO-surface under certain conditions replaces the resistance switching conditioned by the BTO-film properties. This effect is related to the participation of the surface charge density in the screening of polarization charges, distorting the results of local resistive property studies [1, 2].

An approach to investigating the correlation between local resistive and FE properties in epitaxial BTO- films using the voltage sweep of the working point in STM scanning, at the experimental level, and the results of first-principles calculations, at the theoretical level, has been developed. To analyze the local resistive properties, a model of current transfer has been developed [3], in which tunneling through an asymmetric potential barrier was considered as the dominant transport mechanism and the contribution of the potential drops due to the peculiarities of polarization charge screening at the BTO-interfaces were taken into account. Based on the comparative studies of simulated and experimental *I-V* curves, the possibility to separate the contributions of the BTO-film resistive state, BTO-surface states, and the orientation of the FE polarization to the local resistive properties of the STO/LSMO/BTO-compositions has been established.

This research was funded by Russian Science Foundation, grant number 21-79-20073.

1. Y. Kim, C. Bae, K. Ryu et al., *Appl. Phys. Lett.* **94**, 3 (2009).
2. N.V. Andreeva, E.A. Ryndin, Y.A. Demin et al., *Int. Conf. Electr. Eng. Photonics* (EExPolytech), St. Petersburg, Russian Federation (2022).
3. N.V. Andreeva, A.E. Petukhov, O.Y. Vilkov et al., *Nanomaterials* **11**, 3323 (2021).

O7

НАУЧНО-ИССЛЕДОВАТЕЛЬСКОЕ ОБОРУДОВАНИЕ КОМПАНИЙ NANOMETRIC И OSTEC

И.Л. Прусаков

ООО «Остек-АртТул», г. Москва

prusakov.i@ostec-group.ru, info@arttool.ru

Компания Nanometric осуществляет поставки иностранного измерительного оборудования на территории РФ и стран СНГ. Наиболее востребованным прибором для исследовательских задач в продуктовой линейке Nanometric стал оптический профилометр модели IntoM OP100 (Рис. 1а), реализованный по оптической схеме интерферометра Мирау. Прибор применяется для микротопографии образцов, позволяет оценить морфологию поверхности, измерить параметры шероховатости, кривизны и пр. (Рис. 1б).

Специалисты Nanometric произвели более 20-ти инсталляций профилометра IntoM OP100 с 2022 года. Nanometric осуществляет официальную гарантийную, постгарантийную и методическую поддержку пользователей. С уходом ряда иностранных производителей с рынка РФ OP100 заинтересовал множество научно-исследовательских организаций привлекательным соотношением цены и характеристик, а также наличием официальной сервисной службы.

История группы компаний Остек началась более 30 лет назад и на данный момент Остек является крупнейшим инжиниринговым предприятием в России и странах СНГ. Департамент научно-исследовательского оборудования комплексно оснащает заводские и исследовательские лаборатории современными решениями в области оптической и электронной микроскопии, рентгенофлуоресцентного и рентгенофазового анализа, колебательной спектроскопии, металлографии, пробоподготовки к различным методам анализа и др.

В 2024 году стала доступна к приобретению новая модель настольного сканирующего электронного микроскопа (СЭМ) EM-40 (Рис. 1в) от корейского производителя COXEM Co., Ltd. Новинка стала логичным продолжением «бестселлера» EM-30 (более 60-ти инсталляций в РФ и СНГ с 2018 года), сохранив преимущества предшественника (надежное исполнение основных узлов, простота в обслуживании, высокое качество изображения на уровне с термоэмиссионными полноразмерными СЭМ, удобное ПО с множеством регулировок и настроек, наличие опций и специализированных систем пробоподготовки для различных задач пользователей). В новом, еще более компактном настольном СЭМ EM-40 максимальное увеличение достигло 250 тыс. крат (против 150 тыс. у EM-30), появилась моторизация столика образцов по оси Z, что делает позиционирование еще более удобным для оператора. В приборе добавлена возможность многоступенчатой регулировки давления в камере образцов, а технология сверхбыстрой обработки сигналов позволяет достичь частоту обновления изображения в 13 кадров/секунду.

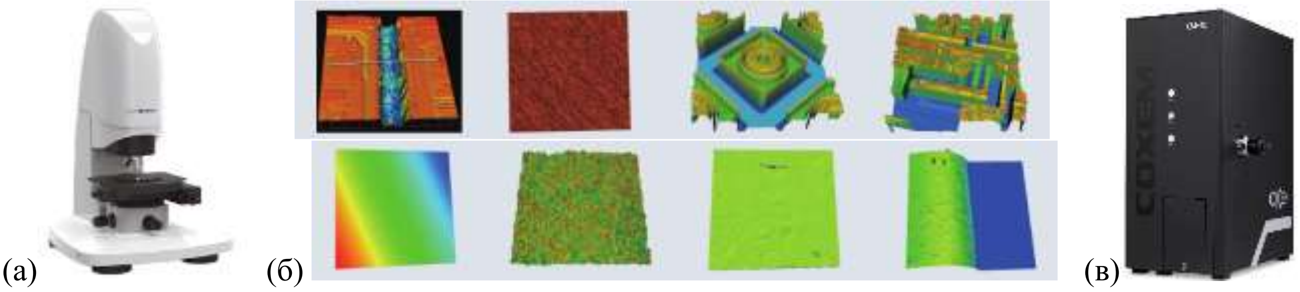

(а) (б) (в)

Рис. 1. (а) Интерферометр IntoM OP100, (б) морфология поверхностей, (в) СЭМ EM-40

O8

Synthesis of silver nanoparticles with controllable sizes on dielectric surfaces in a plasma-chemical process initiated by gyrotron radiation

E.A. Obraztsova[1,2], N.N. Skvortsova[1], V.D. Stepakhin[1], V.D. Borzosekov[1], A.V. Sokolov[1],
V.D. Malakhov[1], A.V. Knyazev[1], E.G. Voronova[1], N.K. Kharchev[1], N.S. Akhmadullina[2],
O.N. Shishilov[3], N.G. Gusein-zade[1]

[1]*Prokhorov General Physics Institute of the Russian Academy of Sciences, Moscow, Russia*
e.a.obraztsova@gmail.com

[2]*Moscow Institute of Physics and Technology, Dolgoprudny, Moscow Region, Russia*

[3]*A.A. Baikov Institute of Metallurgy and Material Science, Russian Academy of Sciences, Moscow, Russia*

[4]*MIREA – Russian Technological University, Institute of Fine Chemical Technologies, Moscow, Russia*

Nanostructured silver coatings are perspective for a wide range of applications. Well-known antimicrobial activity of silver makes it especially attractive for development of bio-medical materials. Among its perspective industrial applications are silver-based catalysts. In this work we suggest a procedure of nanosized Ag particles deposition on a dielectric surfaces or micrometer-sized particles in a plasma-chemical process. We illustrate it by deposition of silver nanoparticles on aluminum oxide microparticles in a plasma-chemical process initiated by gyrotron in a mixture of precursor powders. Synthesis was carried out on a specialized stand using a powerful pulsed gyrotron. The description of the experiment, the conditions for the development of a microwave discharge, and the evolution of process parameters in the reactor are described in detail in. [1-4]. In this work, materials were obtained from mixtures of silver and aluminum oxide precursor powders. The size of the synthetized nanostructured silver could be controlled through the synthesis conditions and varied from tens of nanometers to micrometers as shown in Figure 1.

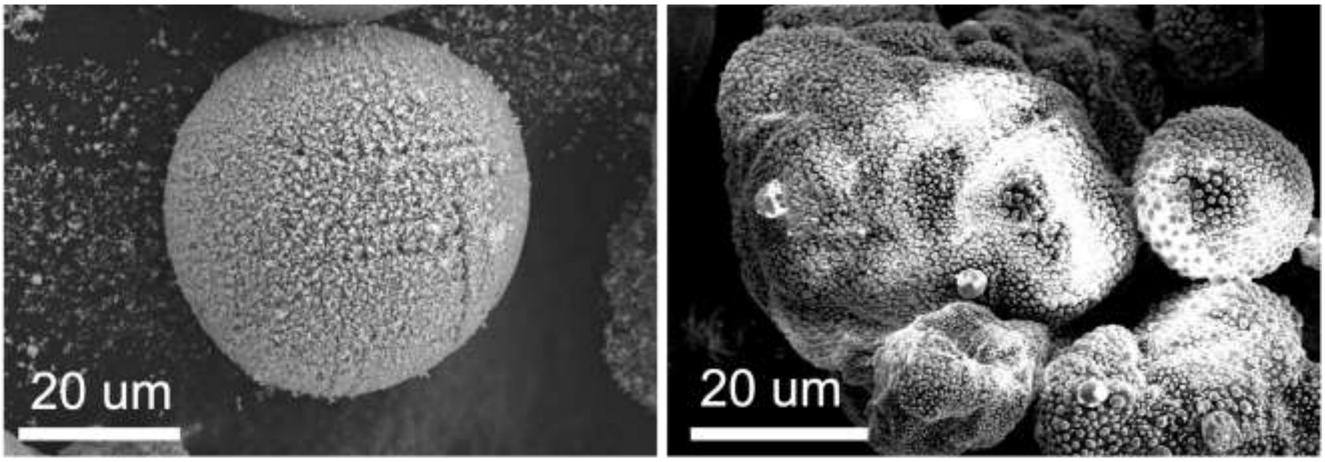

Figure 1. Scanning electron microscopy images of aluminum oxide particles covered by nanostructured silver in different experimental conditions.

1. A.V. Litvak, G.G. Denisov, M.Y. Glyavin, *IEEE J. Microwaves* **1**, 1 (2021).
2. N.K. Kharchev, G.M. Batanov, et al., *Rev. Scientific Instruments* **84**, 013507 (2013).
3. G.V. Ukryukov, D.V. Malakhov, et al., *Inzhenernaya Fizika* **2**, 27 (2017).
4. N.N. Skvortsova, D.V. Malakhov, et al., *JETP Lett.* **106**, 262 (2017).

O9

Properties of Zinc-substituted and Manganese-substituted Hydroxyapatite

V.S. Bystrov[1], E.V. Paramonova[1], L.A. Avakyan[2], S.V. Makarova[3], N.V. Bulina[3]

[1]*Institute of Mathematical Problems of Biology - Branch of Keldysh Institute of Applied Mathematics, Russian Academy of Sciences, Pushchino, Russia*
vsbys@mail.ru
[2]*Physics Faculty, Southern Federal University, Rostov-on-Don, Russia;*
[3]*Institute of Solid State Chemistry and Mechanochemistry, Siberian Branch, RAS, Novosibirsk, Russia*

Hydroxyapatite (HAP) is wide used material as ceramics powders and coating films on the implants and fillers in various biomedical applications [1]. The cationic substitutions in the structure of HAP greatly affect its physical properties, biocompatibility and survival of implants and fillers based on HAP introduced into the body [2,3]. In this work, the properties of Zinc-substituted and Manganese-substituted HAP structures were studied by calculations using density functional theory (DFT) methods in combination with experimental mechanochemical synthesis studies. Basic data on the initial configuration of the cation-substituted HAP at the different concentrations of the introduced Zn and Mn cations and the high-precision DFT calculations method using the PBE(GGA) and HSE hybrid functional, are presented earlier in a similar work [4] on the Mg-substituted HAP studies. The results showing good data agreement: the parameters and volume of the HAP-Zn and HAP-Mn unit cell decrease with an increase of Zn and Mn substitutions with variations for Ca1 and Ca2 positions.

For Zn-cation substitutions in HAP the electronic energy levels were found to depend on the Zn concentration and the positions of the calcium ions being replaced. In this case, the HAP-Zn band gap E_g experiences a jump of 0.6–0.8 eV with the introduction of one zinc ion per supercell, and then decreases and reaches values below the initial E_g value by 0.5–0.6 eV for substitutions in the Ca1 positions, and by 0.8–0.9 eV for substitutions in the Ca2 positions. It has been shown that the energy of substitution has a complex dependence on the concentration of the substituent and the replacement of calcium ions with zinc occurs predominantly in the Ca2 position over the entire concentration range.

For Mn-substitutions in HAP, a significant difference in the change of the electronic and optical properties has been established with the introduction of Mn into HAP in compare with Zn, as well as with Mg [3]. It is shown that new electronic energy levels appear inside the band gap E_g of HAP-Mn, while in HAP-Zn and HAP-Mg not any energy levels inside band gap, only change of the E_g width was observed. Moreover, depending on the Mn concentration and change the photo-excitation energy of HAP, making its effective value E_g* less than the band gap Eg in the initial pure HAP, and generally changing the photo-electronic properties of HAP. Here, at low concentrations $x = 0.1 – 0.5$, the values of E_g* ~ 5.5 eV for Mn/Ca1 substitutions and E_g* < 5.0 eV for Mn/Ca2 substitutions. Then at $x = 0.75$ there is a decrease and a minimum of E_g* ~ 4.5 eV is observed with a slight rise at $x = 1.0$ for almost both types of substitutions. On average, the level of E_g* ~ 4.8 eV (at E_g ~ 7.3 eV) for nMn/Ca2 substitutions, while for nMn/Ca1 we have E_g* ~ 5.4 eV (at E_g ~ 7.4 eV). In addition, HAP-Mn exhibits an important magnetic properties proportional to the amount of the introduced Mn (each Mn atom gives 5 Bohr·mag/cell), which is not observed in HAP-Zn and HAP-Mg. It was established that the formation energy of the substitutions Mn/Ca depend on the Ca position (Ca1 or Ca2) and on the Mn concentration, with preference in Ca2. For the case charged calcium substitutions with Mn^{3+} and Mn^{4+} ions are more likely in the Ca1 position, while substitutions with Mn^{2+} ions are more preferable at the Ca2 position. For Mn-substitutions in HAP, IR spectra were also calculated, and it was found that the main changes are observed in the libration vibrations of the OH group ν_L. When replacing at the Ca1 position (Ca is far from the OH-channel), the ν_L mode is split into two, one of which is dominant in intensity and shifted to the left by ~17 cm^{-1}. When replacing at the Ca2 position (near the OH-channel wall), the ν_L mode is divided into three well-defined parts, shifted to the right with respect to the mode in the ideal HAP. These results are in good agreement with experimental observations.

This research was funded by the Russian Science Foundation (RSF), grant No. 21-12-00251.

1. S.V. Dorozhkin, *Mater. Sci. Eng. C Mater. Biol. Appl.* **55**, 272 (2015).
2. M. Šupova, *Ceram. Int.* **41**, 9203 (2015).
3. V. Bystrov, E. Paramonova, L. Avakyan, et al., *Nanomaterials* **11**, 2752 (2021).
4. V.S. Bystrov, E.V. Paramonova, L.A. Avakyan, et al., *Materials* **16**, 5945 (2023).

O10

AFM investigation of biomaterials for dsRNA delivery into plant cells

A.I. Akhmetova[1,2,3], E.V. Popova[1,2], V.E. Tikhomirova[1,2], I.Yu. Ilyina[1], O.A. Kost[1,2], I.V. Yaminsky[2,3]

[1]Shemyakin and Ovchinnikov Institute of Bioorganic Chemistry, Moscow, Russia
akhmetovaai@my.msu.ru

[2]Lomonosov Moscow State University, Faculty of Physics, Faculty of Chemistry, Moscow, Russia
[3]Advanced Technologies Center, Moscow, Russia

Compared to other high-resolution imaging techniques such as stimulated spontaneous emission depletion microscopy (STED), photoactivated localisation microscopy (PALM), stochastic optical reconstruction microscopy (STORM), scanning and transmission electron microscopy, AFM has unique advantages for simultaneously imaging living biological structures and measuring their mechanical properties under aqueous conditions, making AFM particularly suitable to study the biointerfaces and biomechanics.

This work explores options for nanoplatforms for the delivery of biologically active compounds, including double-stranded RNA (dsRNA), into plant cells based on chitosan. Using atomic force microscopy, morphological characteristics of nanoparticles and chitosan solution were determined, arrangement on the substrates of graphite and mica was visualised, and geometric dimensions were assessed for further investigation of their ability to form complexes with dsRNA [1,2].

The chitosan particles were derived from chitosan lactate with an average molecular weight of 5 kDa via ionotropic gelation with sodium tripolyphosphate (STPP) (Fig.1a). 2D and 3D images of chitosan particles were selected, then the parameter values were determined using FemtoScan Online software:

- P – perimeter, length of the object’s border in the XY plane,
- S – area occupied by the object in projection onto the XY plane,
- RMS – object height dispersion (roughness).
- H – maximum height of the object.
- <H> – average height of the object.
- D – average diameter of the object.

A solution of the same chitosan with a concentration of 0.83 mg/ml was prepared by dissolving chitosan in distilled water and treating in an ultrasonic bath for 30 minutes while heating to 50°C. On the AFM images of chitosan solution we can observe film made from a fine fraction, height approximately 12 nm, average roughness 0.9 nm, root mean square roughness is about 1.2 nm (Fig. 1b). Individual large particles 6-10 nm in diameter are distinguishable.

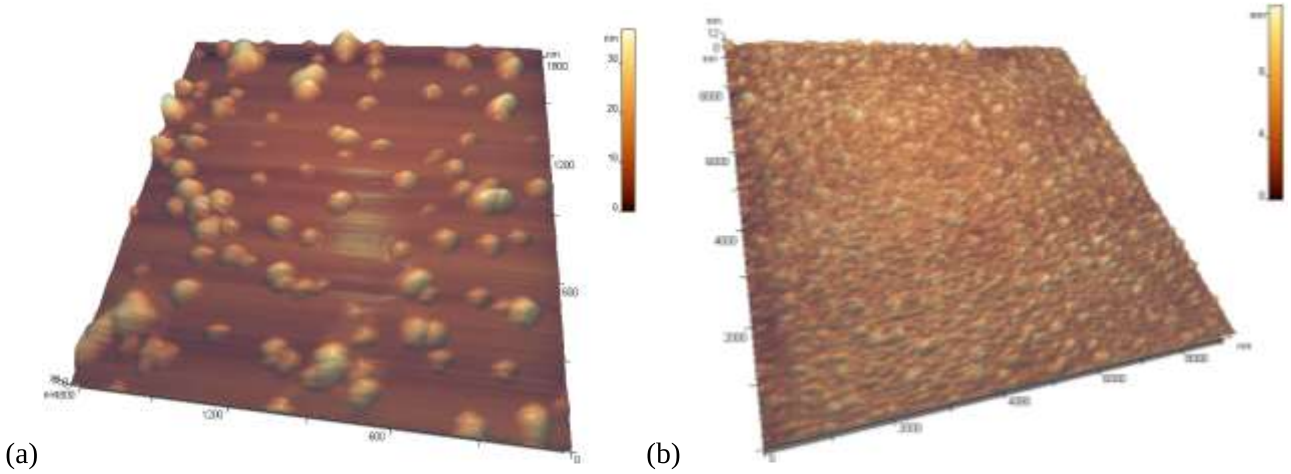

(a) (b)

Figure 1. (a) AFM image of chitosan particles, (b) AFM image of chitosan solution.

Using AFM, the ability of chitosan particles to form complexes with dsRNA was confirmed (Fig. 2). To form carrier-dsRNA complexes, dsRNA and particle suspensions were mixed in an

Eppendorf tube and kept on ice for 30 minutes. To study the complexes, 0.5 µl of a dsRNA:carrier sample in a 1:5 ratio was applied to the substrate. The morphology of the observed objects changed significantly compared to control samples of chitosan particles. The average diameter increased to 284 ± 56, the maximum height increased threefold to 63 ± 5 nm, and the average height doubled to 32 ± 3 nm. The roughness of the complexes increased threefold to 15±6 nm. At the same time, the particle sizes in complexes with dsRNA (P, S, H, <H>) increased compared to the control sample of chitosan particles (Table 1). The radius of the complex was 200 nm, the height was about 80 nm. (Fig. 2).

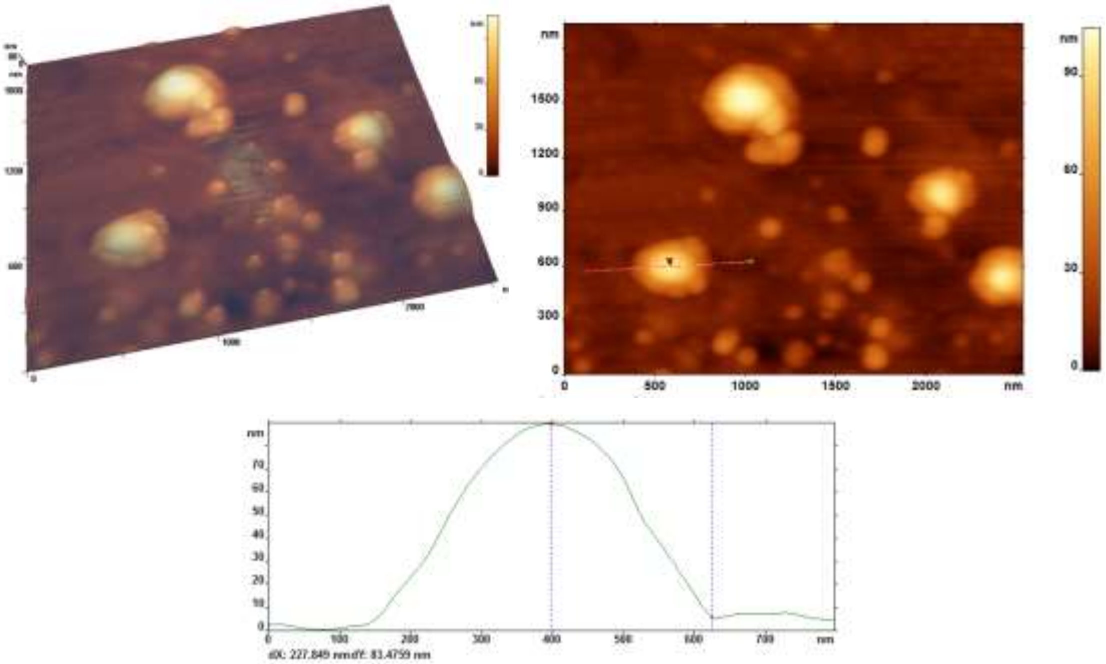

Figure 2. Complexes of chitosan particles with dsRNA: 3D and 2D mages and a cross-section

Table 1. Parameters of carriers determined by AFM.

Sample	Chitosan nanoparticles	dsRNA with chitosan nanoparticles
P, nm	875±75	970±145
S·10^3, nm^2	57±10	74±15
RMS, nm	4±1	15±6
H, nm	20±5	63 ±5
<H>, nm	14±4	32±3
D, nm	270±22	284±56

Despite great progress in the use of chitosan in the field of medicine and pharmaceuticals, the use of chitosan-based delivery systems in agriculture is still limited. In this work, 3D images of chitosan particles and solution were obtained. The dsRNA complexes topography was characterized using AFM: when chitosan nanoparticles interacted with dsRNA, the morphology of the sample changed, and the size and roughness of the observed objects increased, which may indicate the formation of dsRNA-chitosan nanoparticles complexes. Thus, chitosan nanoparticles can be promising carriers for delivering dsRNA into plant cells.

The work was carried out with the financial support of the Russian Science Foundation (project No. 23-74-30003).

1. A.I. Akhmetova, E.V. Popova, *News of the Academy of Sciences. Chemical series* **73**, 2024.
2. A.I. Akhmetova, I.V. Yaminsky, *Nanoindustry* **16**, 2023.

O11

Mechanical stresses in spherulitic PZT thin films

I.P. Pronin[1], E.Yu. Kaptelov[1], M.V. Staritsyn[2], A.S. Semenov[3], V.P. Pronin[4]

[1] *Ioffe Institute, St. Petersburg, Russia*
Petrovich@mail.ioffe.ru

[2] *CRISM "Prometey", Kurchatov Institute, St. Petersburg, Russia*

[3] *Peter the Great St. Petersburg Polytechnic University, St. Petersburg, Russia*

[4] *Herzen State Pedagogical University, St. Petersburg, Russia*

The spherulitic microstructure is inherent in many polycrystalline thin-film materials. As a rule, such a structure is formed as a result of crystallization from an amorphous state. It is accompanied by a change in the density of thin films, an appearance of tensile mechanical stresses in the film plane, and a rotation of the crystal lattice [1-2]. In this work, peculiarities of microstructure and physical properties induced by mechanical stresses in radially radiant spherulitic thin PZT films were studied.

Thin PZT films were formed by two-stage RF magnetron method. After deposition, the amorphous films were annealed at 580°C to form a perovskite phase, and differed in the sizes of the spherulite blocks. REM image of block microstructure and linear rotation of crystalline lattice along radial line are presented in Figure 1. It was observed that gradient of lattice rotation (and mechanical stresses) was lineally depended on spherulitic block square and changed in the vicinity from 0.5 to 1.5 deg/μm.

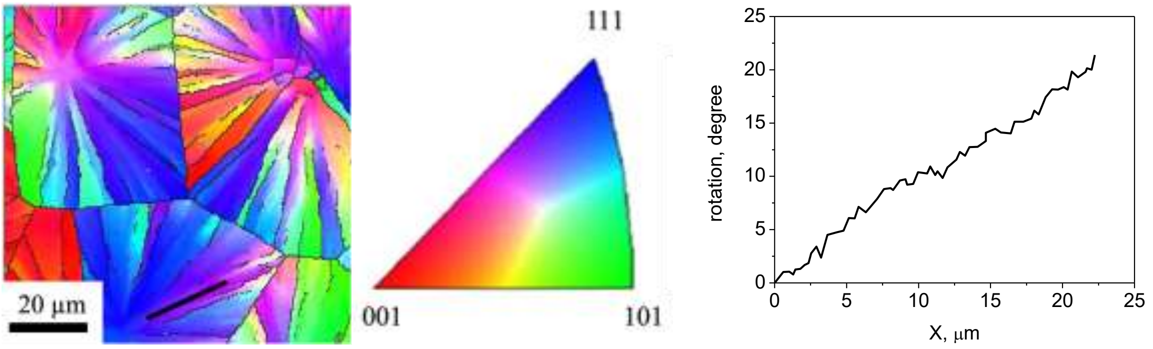

Figure 1. Map of crystalline orientations of spherulitic blocks in thin PZT film (to the left) and linear dependence of crystalline lattice rotation (to the right).

A further increase in the block size led to the appearance of internal high-angle boundaries and partial relaxation of tangential lateral mechanical stresses, accompanied by a decrease in the lattice rotation gradient. Figure 2 demonstrates a sceme of lattice rotation with periodical formation of structural dislocations.

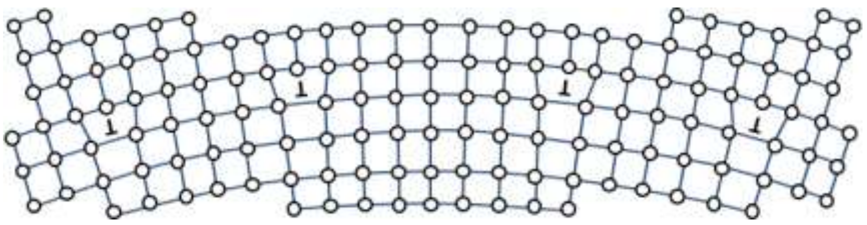

Figure 2. A sceme of crystalline lattice rotation under an action of lateral mechanical stresses.

Data on the study of dielectric properties of thin films and their changes with increasing size of spherulitic blocks are presented and analyzed. Estimates of the magnitude of tensile mechanical stresses have been made.

1. V.Yu. Kolosov, A.R. Thölén, *Acta Materialia* **48**, 1829 (2000).
2. E.J. Musterman, V. Dierolf, H. Jain, *Int. Journ. of Applied Glass Science* **13**, 402 (2022)

O12

Physical properties and radiation hardness of piezoelectric ceramics after neutron irradiation

E.P. Smirnova[1], A.V. Sotnikov[1,2], P.A. Pankratiev [1], V.N. Klimov[3], E.G. Guk [1],
N.V. Zaitseva[1],V.G. Zalesskii[1], E.E. Mukhin[1]

[1]Ioffe Institute, St-Petersburg, Russia
esmirnoffa@gmail.com

[2]Emperor Alexander I St. Petersburg State Transport University (PGUPS), St. Petersburg, Russia

[3]Central Research Institute of Structural Materials Prometey, National Research Centre Kurchatov Institute, St.-Petersburg, Russia

Piezoelectric ceramics have a number of potential applications in fusion reactors as sensors (strain) and actuators (control and positioning). Designs and specifications for new devices for plasma and reactor diagnostics based on piezoelectric ceramics need to be developed in together with the progress towards practical fusion reactors.

At the same time, research into the effect of neutron irradiation on piezoceramics is currently limited. Published data on the effect of fast neutrons on barium titanate and lead zirconate titanate based piezoceramics indicate threshold damage levels 7.6 x 10^{10} n/cm^2 and 3.6 x 10^{18} n/cm^2, respectively [1]. The harsh conditions caused by a thermonuclear reaction are accompanied with an intense neutron and gamma radiation with expected fluence at piezoceramic elements location $\sim 10^{19}$ n/cm^2 ($E > 0.1$ MeV) in the case, for example, of International Thermonuclear Experimental Reactor (ITER) experimental program [2]. This circumstance stimulates the study of other compositions.

Post-irradiation life-test of high temperature piezoelectric ceramics $BiScO_3 – PbTiO_3$ is presented. Irradiation of the ceramic samples was carried out in the WWR-M reactor of B.P. Konstantinov PNPI, NRC "Kurchatov Institute". The total irradiation fluence of $5 \cdot 10^{19}$ n/cm^2 ($E > 0.1$ MeV) was achieved.

X-Ray study indicates anisotropic radiative lattice expansion in the ceramics with an increase in tetragonality (lattice parameter ratio c/a) by 0.47%. In contrast, radiation expansion of the interface electrode-ceramics layer demonstrates a decrease in tetragonality that may indicate the initial stage of structure degradation.

The scanning electron microscope (SEM) study showed the presence of radiation-stimulated diffusion of the electrode into the ceramics volume. Additionally, the SEM images and the corresponding grain sizes histograms revealed microstructure stability as well as domain structure reflecting the existence of a tetragonal ferroelectric phase in the grains after irradiation.

A study of the dielectric properties versus temperature of piezoceramics before and after irradiation showed an increase in Curie temperature T_c by 10°C that is associated with the increase in crystal lattice tetragonality [3]. Electromechanical properties demonstrate a decrease in the mechanical quality factor Q_m by 3.8 times after irradiation, that can be explained by segregation of both point and structural defects resulting from irradiation. The reduction of piezoelectric constants by about 25% after irradiation takes place as well.

Criteria for resistance of piezoelectric ceramics to high fluences of neutron radiation are discussed.

1. A. Holmes-Siedle, L. Adams, Handbook of Radiation Effects, Oxford University Press Inc, NY, 614 (2002).
2. E.E. Mukhin, V.M. Nelyubov, V.A. Yukish, et al., *Fusion Eng. Des.* **176**, 113017 (2022).
3. Z. Liu, H. Wu, Y. Yuan, et al, *Current Opinion in Solid State and Materials Science* **26**, 101016 (2022).

O13

Numerical analysis of effective temperature coefficients of nanostructured porous piezoceramics under various polarization models

A.V. Nasedkin

Southern Federal University, Rostov-on-Don, Russia
avnasedkin@sfedu.ru

A fairly large number of papers are devoted to the study of thermoelectroelastic (pyroelectric) composite materials, and in particular, porous materials. However, porous piezomaterials with a nanosized pore structure have been studied to a much lesser extent. Meanwhile, the properties of nanomaterials differ quite significantly from the properties of similar materials of ordinary sizes. To explain the nanoscale effect, various theories have been developed based on the methodologies of molecular dynamics, surface stresses, nonlocal models, etc. Here, in continuation of previous investigations to determine the effective moduli of nanostructured thermoelectroelastic composites, homogenization methods based on solving stationary boundary value problems are considered, and to take into account the scale factor, the generalized Gurtin-Murdoch theory is used [1, 2], according to which surface thermoelectroelastic fields are introduced at the interface boundaries.

The complete set of effective moduli was determined as a result of the finite element solution of homogenization problems as follows. First, a finite element representative volume of a porous composite with a random porosity structure was constructed. In this volume, interface finite elements were placed at the pore boundaries, considering the nanoscale effect. For the interface elements, surface moduli were specified that were different from the bulk material moduli, which, when dimensionless in space, depended on the characteristic pore size. From the solution of boundary value problems under appropriate boundary conditions, the averages over volumetric elements and over surface elements of the stress and of the electrical induction fields were determined, and from them, from the energy balance conditions, the effective moduli of the homogenized medium were calculated.

A special feature of our investigation is the consideration of the inhomogeneous polarization field in a representative volume of porous piezoceramics. To do this, the result of polarization of a representative volume of the composite is preliminarily modeled in a simplified linear formulation, which is as follows. First, the problem of electrostatics for a dielectric composite is solved regarding the action of an electric field along the macropolarization axis. The solution to this problem gives inhomogeneous fields of electric field strength and electric induction, from which, in accordance with the adopted model, the inhomogeneous polarization field is determined. Various models of the dependence of inhomogeneous material moduli of piezoceramics on the polarization field were considered [3]: homogeneous properties; inhomogeneous properties depending only on the direction of the polarization vector; inhomogeneous properties depending on the magnitude and direction of the polarization vector.

The results of numerical experiments made it possible to analyze the dependences of effective stiffness moduli, piezoelectric moduli, dielectric constants, temperature stress coefficients and pyroelectric constants on polarization models, pore nanosizes, percentage of pores and relative areas of interface boundaries.

Author acknowledges the support of the Russian Science Foundation (grant number No. 22-11-00302), https://rscf.ru/project/22-11-00302/, at the Southern Federal University.

1. A. Nasedkin, *Ferroelectrics* **509**, 57 (2017).
2. A. Nasedkin, *Mathematical Applications in Continuum and Structural Mechanics, Advanced Structured Materials* **127**, Eds. F. Marmo, S. Sessa, E. Barchiesi, M. Spagnuolo. (Springer, Cham), 13 (2021).
3. A.V. Nasedkin, A.A. Nasedkina, Y.V. Tolmacheva, *Comput. Contin. Mech.* **16**, 476 (2023).

! O14

Mechanochemical imprint lithography: direct patterning of C-C covalent grafts

X. Xie[1], Sh. Long[1], A. Nashchekin[2], L. Chi[1,3], Y. Fang[1,4], O. Ivasenko[1,3]

[1]*Institute of Functional Nano & Soft Materials (FUNSOM), Soochow University, , Suzhou, PR China*
ivasenko@suda.edu.cn

[2]*Characterization of Materials and Structures of Solid State Electronics Laboratory, Ioffe Institute, St.-Petersburg, Russia*
[3]*Jiangsu Key Laboratory of Advanced Negative Carbon Technologies, Soochow University, Suzhou, Jiangsu, PR China*
[4]*Jiangsu Key Laboratory for Carbon-Based Functional Materials & Devices, Soochow University, Suzhou, Jiangsu, PR China*

Graphene-based materials [1] are renowned for their exceptional properties, including remarkable strength, conductivity, and flexibility. Graphene on different supports, graphite, graphene oxide and carbon quantum dots are just some of the diverse examples of such materials, that find numerous applications in electronics, energy storage, chemo- and bio sensors, catalysis, etc. The performance optimization of graphene-based materials for specific application to a great extent is defined by our abilities to functionalize the interfacial graphene layers. Ideally, we should be able to control not only the surface density and chemical type of functional groups but also their distribution and patterning. Several successful strategies have been developed towards this goal, however many of them either lack flexibility in varying patterns [2,3] or require expensive and elaborate protocols [4,5], not readily accessible to non-specialist working in relevant interdisciplinary fields. Here, we present a simple, convenient and versatile approach for multicomponent patterned functionalization of graphene surfaces [6].

We have discovered that patterned polydimethylsiloxane (PDMS) stamps can spatio-selectively brake $C_{(graphene)}$-$C_{(aryl)}$ bonds where PDMS is pressed to the surface of covalently functionalized graphene layers. The pattern of degrafting can be easily tuned by the imprint parameters (microstructure of PDMS stamp, contact pressure, offset rotation, etc.). When combined with sequential multicomponent grafting, this mechanochemical imprint lithography (MCIL) offers convenient and versatile multicomponent patterned functionalization of graphene-based surfaces (Fig. 1).

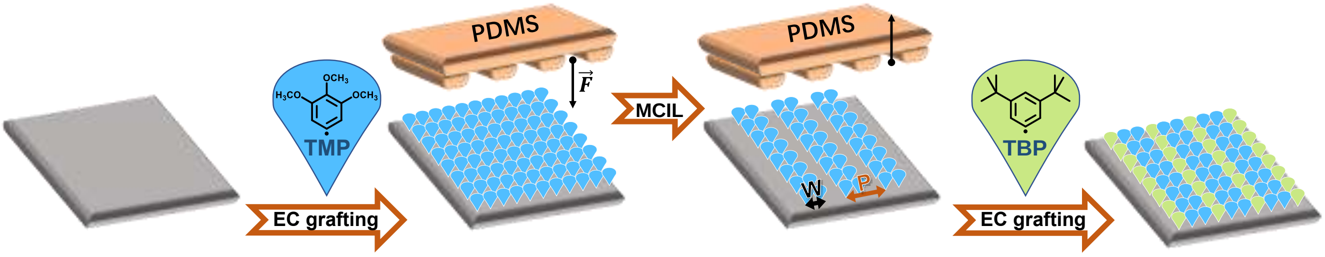

Figure 1. An example workflow diagram for multicomponent patterned grafting of graphene surface.**Ошибка! Закладка не определена.**

Highly accessible (low cost, inexpensive equipment, no specialized knowledge/expertise), MCIL could enable the in-house design of custom multi-functional micropatterned surface for advanced studies in a broad range of highly interdisciplinary research fields including interfacial physical chemistry, supramolecular chemistry, development of (bio)sensors, crystal engineering, stimuli-responsive systems, scanning probe microscopy, nanotechnology, etc.

1. V. Georgakilas, J. A. Perman, J. Tucek, et al., *Chem. Rev.* **115**, 4744 (2015).
2. Z. Xia, F. Leonardi, M. Gobbi, et al., *ACS Nano* **10**, 7125 (2016).
3. H. Van Gorp, P. Walke, A. M. Bragança, et al., *ACS Appl. Mater. Interfaces* **10**, 12005 (2018).
4. T. Wei, M. Kohring, H. B. Weber, et al., *Nat. Commun.* **12**, 552 (2021).
5. M. C. Rodríguez González, A. Leonhardt, H. Stadler, et al., *ACS Nano* **15**, 10618 (2021).
6. X. Xie, Sh. Long, L. Chi, Y. Fang, O. Ivasenko, *submitted* (2024).

O15

Domain shape evolution during local switching in the crystals of triglycine sulfate family

A.P. Turygin[1], V.A. Shikhova[1], M.S. Kosobokov[1], A.R. Akhmatkhanov[1], O.M. Golitsyna[2],
S.N. Drozhdin[2], O.N. Sergeeva[3], V.Ya. Shur[1]

[1]School of Natural Sciences and Mathematics, 620000, Ural Federal University, Ekaterinburg, Russia
anton.turygin@urfu.ru

[2]Voronezh State University, 394018, Voronezh, Russia

[3]Tver State University, 170000, Tver, Russia

Triglycine sulfate ($[NH_2CH_2COOH]_3 \cdot H_2SO_4$, TGS) is one of the most intensively studied ferroelectrics, which is used for creation highly sensitive infrared receivers and detectors due to its high dielectric and pyroelectric properties [1]. TGS has a low Curie temperature $T_C \approx 49^oC$. Deuteration of TGS leads to an increase in the Curie temperature and improvement of the pyroelectric properties [2]. However, the kinetics of the domain structure of TGS crystals in a highly non-uniform field created by a conducting probe of a scanning probe microscope has not been studied in detail.

Single crystals of pure and deuterated TGS were investigated in this work. The samples of deuterated triglycine sulfate (DTGS) had a ferroelectric phase transition temperature of 59°C. The degree of deuteration was about 80%. The surface of the studied samples was prepared by cleaving the crystals along the cleavage plane (010), perpendicular to the polar axis *b*. The thickness of the studied samples was about 1.5 mm. Moreover, the samples of DTGS with in-plane polarization with thoroughly polished were studied.

Local polarization switching in single-domain and polydomain crystals of the TGS family was experimentally investigated. In single-domain crystals, the formation of lenticular domains with significant anisotropy of the growth rate along the *a* and *c* axes caused by different nucleation mechanisms was detected [3]. The formation of chains of isolated domains was detected for scanning by SPM probe with a constant voltage [4]. It was shown that in polydomain crystals, the shape of the partially switched region is determined by the dominant screening mechanism [5].

The obtained dependences of domain sizes on switching pulse parameters are typical for ferroelectric crystals: linear on amplitude (voltage) and logarithmic on duration. The formation of isolated domain arrays during scanning is considered from the point of view of the formation of a comb-shaped blind domain with charged domain walls in the crystal bulk. The strong anisotropy of the domain growth in polydomain crystals has been attributed to current limited wall motion mechanism in TGS with anisotropic bulk conductivity. The obtained results demonstrate the key role of the screening processes in the creation of periodic domain structures and open the way to further improvement of domain engineering methods using scanning probe microscopy.

The research was made possible by the Russian Science Foundation (Project No. 24-12-00302). The equipment of the Ural Center for Shared Use “Modern nanotechnology” Ural Federal University (Reg. No. 2968) was used.

1. R.B. Lal, A.K. Batra, *Ferroelectrics* **142**, 51 (1993).
2. M. Banan, R.B. Lal, A. Batra, *J. Mater. Sci.* **27**, 2291 (1992).
3. A.P. Turygin, M.S. Kosobokov, O.M. Golitsyna et al., *Appl. Phys. Lett.* **119** 262902 (2021).
4. A.P. Turygin, V.A. Shikhova, M.S. Kosobokov et al., *J. Adv. Diel.* 2350030 (2023).
5. A.P. Turygin, V.A. Shikhova, M.S. Kosobokov et al., *ACS Appl. Electron. Mater.* **4**, 5215 (2022).

O16

Angular misorientation of the nanodomains in relaxed antiferroelectric heterostructures

A.E. Ganzha[1], Y. Si[2], Z. Chen[2], Y. Dong[3], Z. Luo[3], M.A. Kniazeva[1], R.G. Burkovsky[1]

[1]Peter the Great Saint-Petersubrg Polytechnic University, St.-Petersburg, Russia

[2]School of Materials Science and Engineering, Harbin Institute of Technology, Shenzhen, Guangdong, China.

[3]National Synchrotron Radiation Laboratory, University of Science and Technology of China, Hefei, Anhui, China

alexander.ganzha@gmail.com

Functional dielectrics occupy a significant niche in modern industry. For a wide class of such materials, practically significant properties are determined by the presence of structural phase transitions. Due to the phase switching in thin-film heterostructures of such materials, it is possible to implement a number of promising electromechanical, electrocaloric, energy storage and memory devices [1-3]. However, in some materials, such as $PbZrO_3$, when going from bulk to thin films, strong deformations of lattice and presence of defects caused by the lattice mismatch between the film and the substrate leads to modification of film properties. For example, in the $PbZrO_3/SrRuO_3/SrTiO_3$ heterostructure, a field-induced long-period intermediate phase with ↑↑↑↑ ↓↑↑↓ ordering of the lead subsystem is formed [4]. Such phase is not observable without defect-induced spatial heterogeneity of the material. A notable feature of the intermediate phase is the dominant role of the heterophase contact between the domains of the intermediate and the antiferroelectric phase. but in order for the energy of heterophase boundaries to have a significant role in stabilization of intermediate phase, there must be many such boundaries.

In accordance with this, the need to understand the nature of nanodomain configurations in films is obvious. Our first step in characterization of domain configurations in thin films is the comparison of the shapes of the intensity distributions of Bragg reflections of the $PbHfO_3/SrRuO_3/SrTiO_3$ heterostructure with the model of an undeformed bulk antiferroelectric $PbHfO_3$. By analyzing the differences between experiment and theory, it is possible to reveal the reasons behind modified shape of the reflections.

We conducted an experimental study of the shape of the reflection on the magnitude of the transferred momentum (BL02U2 SSRF in Shanghai, China). It was possible to identify two components of the broadening of the Bragg reflections. One of the components does not depend on the magnitude of the transferred momentum and is associated with the average linear dimensions of nanodomains in the structure (Fig. 1a) which are estimated at approximately 22 nm. Its amplitude is higher compared to our previously obtained results from X-ray nanoscopy [5]. It might be logical since the size of the beam is much larger compared to X-ray nanoscopy, so the smaller domains are indistinguishable. It is worth mentioning that there is also a component associated with strains but we were unable to reliably separate it from the domain size effect.

The second component strongly depends on the transferred momentum and is associated with the angular misorientation of the domains due to tilts around the normal to the film surface (Fig. 1a). By assessing the intensity of Bragg reflections at half maximum in different directions, we were able to estimate the magnitude of angular misorientation around the film normal and along its surface (Fig. 1b). It can be seen that despite the strong relaxation of the film through dislocations, strong nanoinhomogeneous deformation fields remain in the relaxed volume, preventing the natural rotation of nanodomains around the film normal.

Another interesting observation is that the distribution of domain inclination angles obeys a Gaussian distribution with parameters that can be associated with the characteristics of spontaneous strains of single-crystal samples (Fig. 2a).

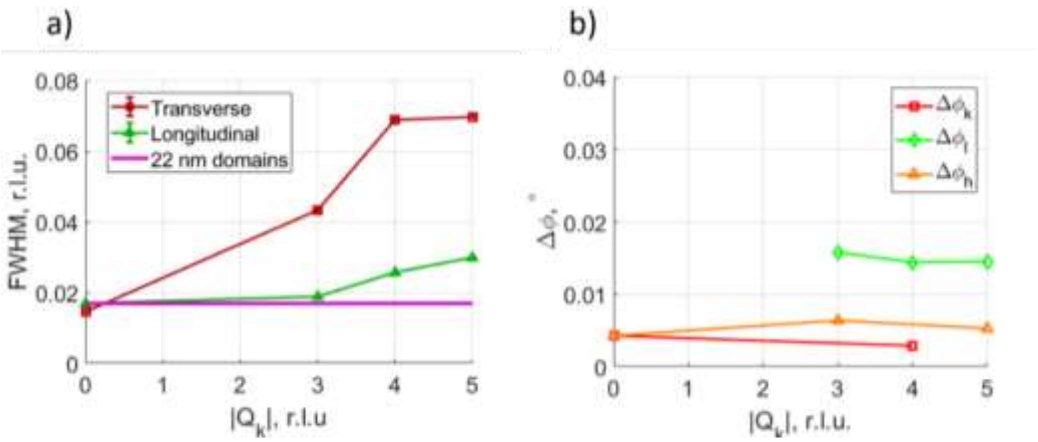

Figure 1. (a) The transverse (perpendicular to the modulation wave) (squares) and longitudinal (along the modulation wave) (triangles) FWHM of Q = (004), Q = (0-31), Q = (0-44), and Q = (0-51) Bragg reflections along [010] direction. The longitudinal FWHM contains info about nanodomains size (purple line) and show the strains influence of higher |Q$_k$|. The transverse FWHM contains info about angular misorientation of the domains due to tilts around the surface normal. It is worth mentioning that the reason for Q = (0-44) (|Q$_k$| = 4) being a bit outside the linear dependence is the contribution of tilts along the films' surface. (b) The magnitude of angular misorientation around the film normal (squares and triangles) and along its surface (diamonds) of Bragg reflections along [010] direction.

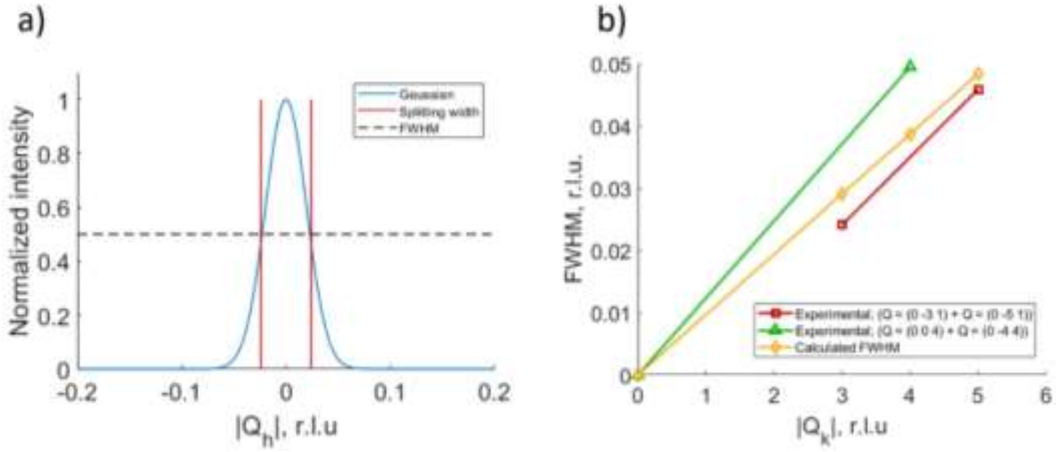

Figure 2. (a) Comparison of the Gaussian function which describes the statistics of microtwisting (blue line), with the width of the theoretical splitting due to spontaneous strains of single-crystal samples (red line) using the example of peak Q = (0 -5 1) in [1 0 0] direction. (b) Comparison of the half-width of the Gaussian function in the [100] direction (squares and triangles) with the width of the theoretical splitting (diamonds).

This observation is not consistent with classical domain compatibility theory, despite some degree of similarity. The real angular distribution of domain inclinations should not be Gaussian-like. If this was the case, then, according to the meaning of the Gaussian distribution, the vast majority of domains would not experience rotation relative to the film normal. Taking it into account, the next logical step is to combine the experimental results with the free energy function simulations in order to clarify how the around-the-normal domain tilts, which arise from the pursuit of domain mechanical compatibility, get simultaneously relaxed on going towards the interface.

A.E. Ganzha, M.A. Kniazeva, R.G. Burkovsky acknowledge the support of Russian Science Foundation (Grant 20-72-10126).

1. K. Vorotilov, A. Sigov, *Phys. Solid State* **54**, 894 (2012).
2. F. Zhang, H. Zhang, S. Krylyuk, et al., *Nature Mater* **18**, 55 (2019).
3. J. Karthik, L.W. Martin, *Appl. Phys. Lett.* **99**, 3 (2011).).
4. R.G. Burkovsky, G.A. Lityagin, A.E. Ganzha, et al., *Physical Review B* **105**, 125409 (2022).
5. J.E. Flores Gonzales, A.E. Ganzha, M.A. Kniazeva, et al., *J. Appl. Crystallogr.* **56**, 3 (2023).

O17

Ultra-high electric field-induced strain of sodium bismuth titanate-based lead-free ferroelectric ceramics

R.Y. Jing, X.Y. Wei, L. Jin

Electronic Materials Research Laboratory, Key Laboratory of the Ministry of Education & International Center for Dielectric Research, School of Electronic Science and Engineering, Faculty of Electronic and Information Engineering, Xi'an Jiaotong University, Xi'an, 710049, China
ryjing@xjtu.edu.cn

Micro-displacement actuators based on the electric-field induced strains of ferroelectric ceramics occupy an important position in the field of ultra-precision positioning and machining due to their high accuracy and fast response. As one of the most promising functional materials to replace lead-based ferroelectric ceramics, bismuth titanate sodium ($Bi_{1/2}Na_{1/2}TiO_3$, BNT)-based lead-free ferroelectric ceramics have attracted much attention because of their excellent electric field-induced strain performance. The development of BNT-based lead-free ceramics with high performance and high temperature stability is one of the current research hotspots in the field of ferroelectric materials.

In this work, the typical chemical modification methods of obtaining large strain and extrinsic factors affecting the large strain are discussed. The relationship between strain performance and intrinsic structure is analyzed, the intrinsic mechanism of giant strain generation is clarified, and ultra-high electric field-induced strains obtained by novel doping methods and atomic-scale defect engineering are presented.

O18

Novel approaches to manufacture optical transparent and luminescent nanoceramics

O.L. Khasanov, V.D. Paygin, E.S. Dvilis, D.T. Valiev, S.A. Stepanov

National Research Tomsk Polytechnic University, 634050, Tomsk, Russia
khasanov@tpu.ru

The main results of R&D concerning methods of consolidation of $MgAl_2O_4$, ZrO_2-Y_2O_3, $Y_3Al_5O_{12}$ optical transparent, luminescent nanostructured and functional graded ceramics doped with rare-earth ions as luminescence activators have been reported [1-10].

The novel approaches include international patented methods of dry nanopowder compaction by control of the friction forces to provide a density uniform distribution and perfect microstructure of optical ceramics, as well as spark plasma sintering in combination with mentioned methods to improve the optical transparency of ceramics having increased aspect ratio.

The R&D were supported by many projects of the Russian Science Foundation, Russian Foundation for Basic Research, research contracts, including the State task "Science" (project FSWW-2023-0011).

The R&D were implemented using the equipment and facilities of the Centre for Share Use “Nanomaterials and Nanotechnologies” of Tomsk Polytechnic University (http://ckp-rf.ru/ckp/3140).

1. D. Valiev, S. Stepanov, et al., *Ceram. Int.* **50**, 19374 (2024).
2. D. Valiev, S. Stepanov, et al., *Optik* **295**, 171499 (2023).
3. V. Paigin, E. Dvilis, et al., *Opt. Mater.* **128**, 112332 (2022).
4. S. Stepanov, O. Khasanov, et al., *Radiation Phys. Chem.* **189**, 109736 (2021).
5. S. Stepanov, O. Khasanov, et al., *Ceram. Int.* **47**, 6608 (2021).
6. V. Paigin, E. Dvilis, et al., *Appl. Sci.* **11**, 1304 (2021).
7. O. Khasanov, E. Dvilis, et al., *Ultrason. Sonochem.* **50**, 166 (2019).
8. O. Khasanov, E. Dvilis, et al., *Phys. Status Sol. C* **10**, 918 (2013).
9. O.L. Khasanov, E.S. Dvilis, *Adv. Appl. Ceram.* **107**, 135 (2008).
10. O.L. Khasanov, E.S. Dvilis, et al., *J. Eur. Ceram. Soc.* **27**, 749 (2007).

O19

Microstructure, complex electromechanical parameters and dispersion characteristic of ferroelectrically hard piezoceramics

A.N. Rybyanets[1], I.A. Shvetsov[1], N.A. Shvetsova[1], D.I. Makarev[1], N.A. Kolpacheva[2]

[1]*Southern Federal University, 344090, Rostov-on-Don, Russia*
arybyanets@gmail.com

[2]*Don State Technical University, 344000, Rostov-on-Don, Russia*

Ferroelectrically hard PZT materials are primarily used in high-power acoustic applications. The advantages of these materials are their moderate permittivity, large piezoelectric coupling factors, high mechanical qualities, and very good stability under high mechanical loads and operating field strengths. Low dielectric losses facilitate their continuous use in resonance mode with only low intrinsic heating of the component. Especially high-power acoustic applications benefit from the properties of hard piezo materials. Examples of their fields of application include ultrasonic cleaning (typically in the kHz frequency range), the machining of materials (ultrasonic welding, bonding, drilling, etc.), ultrasonic processors (e.g., to disperse liquid media), the medical sector (ultrasonic tartar removal, surgical instruments, etc.) and sonar technology. Meanwhile, the requirements for the characteristics of high-frequency medical ultrasonic transducers have changed drastically in recent years because of the emergence of new fields of application, primarily, focusing ultrasound transducers of high intensity (HIFU) for ultrasonic ablation and therapy systems [1]. The emergence of new high-frequency applications and meeting their specific demands stimulates the development and improvement of piezoelectric materials and technologies for their manufacture.

This paper presents the results of an experimental study of the microstructure peculiarities, complex electromechanical parameters and their frequency dependences for PZT-type hard piezoelectric ceramics of the composition $PbTi_{0.41}Zr_{0.49}Nb_{0.057}Zn_{0.023}W_{0.008}Mn_{0.012}O_3$ + 0.1 m% GeO_2. We used the standard synthesis and sintering methods for the piezoceramics fabrication. The complex elastic, dielectric, and electromechanical parameters of the piezoceramics elements were measured at radial and thickness extensional modes of standard piezoceramic discs using impedance analyzer Agilent 4294A (Agilent Technologies, USA) and the PRAP software. To study the frequency dependences of the complex parameters of experimental samples in the range from 2 up to 50 MHz, we used the previously developed method of analysis of piezoelectric resonance spectra at the fundamental frequency and higher-order resonances of thickness extensional modes. Microstructural studies were performed on polished and chipped surfaces of porous piezoceramics samples using the scanning electron microscopes (JEOL JSM-6390LA and TM-100, Hitachi).

As the result of SEM microstructure analysis, it was found that the hard piezoceramics are characterized by low porosity $P \approx 3\%$, dense and chaotic packing of grains with straight and curved crystallite boundaries, and an average size of $R \approx 2$ μm. This grain structure provides low attenuation of resonant vibrations and ultrasonic waves in the high-frequency range.

It was found, that the ferroelectrically hard piezoelectric ceramics of the composition $PbTi_{0.41}Zr_{0.49}Nb_{0.057}Zn_{0.023}W_{0.008}Mn_{0.012}O_3$ + 0.1 m% GeO_2. possess a unique combination of electromechanical parameters and characterized by moderate permittivity at very low dielectric loss, large piezoelectric coupling factors, very low attenuation and dispersion of ultrasonic waves over a wide frequency range up to 50 MHz, and can be used in high-frequency ultrasonic transducers for medical equipment and non-destructive testing.

The study was financially supported by the Russian Science Foundation Grant No. 24-22-00063, https://rscf.ru/project/24-22-00063/ at the Southern Federal University.

1. A.N. Rybyanets, A.A. Naumenko, N.A. Shvetsova, et al., *Advanced Materials: Manufacturing, Physics, Mechanics and Applications* (NY: Springer Proceedings in Physics), 621 (2016).

O20

Depolarization effect in functional memory structures based on ferroelectric $Hf_{0.5}Zr_{0.5}O_2$

I.A. Savichev, A.A. Chouprik

Moscow Institute of Physics and Technology (national research university),141700, Dolgoprudny, Russia
ilya.savichev@phystech.edu

Since 2008, hafnium oxide has been integrated into the microelectronics industry as a gate high-k dielectric [1]. Three years later, the unexpected discovery of ferroelectricity in doped hafnium oxide increased the applied importance of this material [2]. The most promising of the potential applications is in the field of non-volatile memory, where the current dominant concept (flash-memory) has reached its physical limit. It has been theoretically and experimentally confirmed that ferroelectric memory has a significantly larger endurance, lower power consumption and high read-write speed compared to the still prevailing flash-memory [3]. However, ferroelectric memory has a significant disadvantage, namely, it exhibits limited information storage time.

Among known concepts of ferroelectric memory, a ferroelectric field-effect transistor (FeFET) advantages due to non-destructive information readout and simple architecture, which allows high scalability and high information capacity. The key element of the FeFET concept is the metal-ferroelectric-semiconductor (MFS) functional structure. The use of a technology-compatible ferroelectric hafnium oxide on silicon is the most promising approach for implementing FeFETs into modern industry.

In HfO_2-based FeFETs, the limited information storage time is determined by the depolarization effect of the ferroelectric, which consist in polarization backswitching driven by the depolarization field emerging in a poled MFS structure. Depolarization effect leads to suppression of one of two polarization states and stabilization of second polarization state. In a result, output and transfer characteristics of FeFET devices are shifted along voltage axis, memory window degrades with time, the information storage time is limited and in the worst case, the memory effect is absent at all. Therefore, the decrease in the magnitude of the depolarization field and the rate of its increase after the polarization switching help to improve the storage time of information in ferroelectric-based memory devices.

In this work, the depolarization effect in functional structures $Si/Hf_{0.5}Zr_{0.5}O_2/TiN$ is studied and approaches to reduce this effect are proposed and analyzed. It is shown that the depolarization effect is caused by the charging surface states at the silicon-$Hf_{0.5}Zr_{0.5}O_2$ interface, and the depolarization dynamics is determined by the charging dynamics. It is revealed that the depolarization rate depends significantly on the thickness of the $Hf_{0.5}Zr_{0.5}O_2$ layer (in the range from 5 to 10 nm) and the presence and thickness of an interface SiO_x layer. The effect of passivation annealing in hydrogen and nitrogen atmospheres under different conditions on the density of surface states and depolarization rate of the ferroelectric is studied. Finally, an approach to fabricate a functional MFS structure based on $Hf_{0.5}Zr_{0.5}O_2$ film for FeFET applications with maximum state retention time is proposed.

The work was financially supported by the Ministry of Science and Higher Education of the Russian Federation (agreement No. 075-03-2024-117, project No. FSMG-2022-0031).

1. S. Natarajan, M. Armstrong, M. Bost, et al., International Electron Devices Meeting, 2008. *IEEE Int.* **3** (2009).
2. T.S. Böscke, J. Müller, D. Bräuhaus, et al., *Appl. Phys. Lett.* **99**, 102903 (2011).
3. D.S. Jeong, R. Thomas, R.S. Katiyar, et al., *Rep. Progr. Phys.* **75**, 076502 (2012)

O21

Structure, dielectric, ferroelectric and piezoelectric properties of modified lead-free perovskite ceramics

E.D. Politova[1], G.M. Kaleva[1], A.V. Mosunov[2], S.Y. Stefanovich[2], S.A. Ivanov[2],
N.V. Sadovskaya[3], D.A. Kiselev[4], T.S. Ilina[4]

[1] *N.N.Semenov Federal Research Center for Chemical Physics, RAS, Moscow, 119991, Russia, politova@nifhi.ru*

[2] *Lomonosov Moscow State University, Moscow, Moscow, 119991 Russia,*

[3] *SRC «Crystallography and Photonics» RAS, Moscow 119333 Russia,*

[4] *National University of Science and Technology "MISiS", Moscow 119049 Russia,*

Lead-free perovskite oxides promising for development of materials for various applications based on perovskites $(K_{0.5}Na_{0.5})NbO_3$ (KNN), $BaTiO_3$ (BT), $BaZrO_3$ (BZ), $NaNbO_3$ (NN), $(K_{0.5}Bi_{0.5})TiO_3$ (KBT) and $(Na_{0.5}Bi_{0.5})TiO_3$ (NBT) were intensively studied last years in order to replace the widely used Pb-based ones.

We studied influence of cations substitutions and preparation conditions on phase content, structure, microstructure, dielectric, ferroelectric, and local piezoelectric properties of KNN and NBT compositions from Morphotropic Phase Boundaries modified by BT, NN, KNN, and KBT oxides up to 10 mol %.

Ceramic samples were prepared by the solid-state reaction method at temperatures up to 1450 K and characterized using X-ray Diffraction (XRD), Scanning Electron Microscopy (SEM), Second Harmonic Generation (SHG), Dielectric Spectroscopy (DS) and Piezoresponse Force Microscopy (PFM) methods.

The unit cell volume changes and crystallite size distributions were observed by the XRD method in ceramics. In NBT-BT samples increase in the volume-weighted crystallite size distribution function was observed with KBT additive increasing, thus indicating to changes in relative content of polar nanoregions in tetragonal nonpolar matrix.

Ferroelectric phase transitions at ~ 400 – 700 K were confirmed by the DS and SHG methods. Decrease in temperatures of phase transitions was observed in the NBT- and KNN-based samples with additives content increasing. In NBT-based ceramics effects of dielectric relaxation were observed at temperatures > 800K caused by formation of oxygen vacancies in compositions with aliovalent substitutions.

Using the PFM method increase in effective d_{33} piezoelectric coefficient in some ceramics studied correlated with increase in dielectric permittivity and spontaneous polarization values was observed at the room temperature thus confirming improvement of functional properties and prospects of new lead-free piezoelectric and electrocaloric materials development on the base of modified KNN- and NBT-based compositions.

The work was supported by the Russian Foundation for Basic Research (Project 21-53-12005).

1. G.M. Kaleva, E.D. Politova, S.A. Ivanov, et al., *Inorg. Mater.* **59**, 202 (2023).
2. G.M. Kaleva, E.D. Politova, A.V. Mosunov, et al., *Crystallogr. Rep.* **68**, 818 (2023).
3. E.D. Politova, G.M. Kaleva, S.A. Ivanov, *Ferroelectrics* **605**, 73 (2023).
4. G.M. Kaleva, E.D. Politova, A.V. Mosunov, *Russ. J. Phys.Chem. A* **97**, 965 (2023).

O22

Conducting antiferromagnets and antiferromagnetic multiferroics for spintronics

Z.V. Gareeva[1], A.K. Zvezdin[2,3,4]

[1]*Institute of Molecule and Crystal Physics, Subdivision of the Ufa Federal Research Centre of the Russian Academy of Sciences, 450075, Ufa, Russia*

[2]*Prokhorov General Physics Institute of the Russian Academy of Sciences, 119991, Moscow, Russia*

[3]*P.N. Lebedev Physical Institute of the Russian Academy of Sciences, 119991 Moscow, Russia*

[4]*'New spintronic technologies' Limited Liability Company, 121205, Skolkovo, Moscow, Russia*

In recent years, the concept of antiferromagnetic spintronics has seen active development [1], driven by the technological potential offered by antiferromagnetically ordered materials in modern technologies. The stability of antiferromagnets against external magnetic fields, high-speed magnetization dynamics, and excellent transport properties render these materials attractive for use in random access memory devices, including as components of spin-tunneling magnetoresistive elements [2]. The multifunctionality of antiferromagnets is also ensured by their variety of electrical properties.

In this work, we will focus on two types of antiferromagnetic materials prospects for spintronics applications: conducting antiferromagnets exemplified by CuMnAs and Mn_2Au, known from recent studies of high-speed domain wall dynamics [2, 3] and antiferromagnetic multiferroics based on $BiFeO_3$ compounds, prospect of application in magnetoelectric (ME) - spin orbit (SO) logic devices [4]. Within the framework of the general theory for investigating the physical properties of antiferromagnets, developed by Soviet scientists [5-7], see also Chapter 14 in Ref. [8], based on the knowledge of spatial symmetry groups of crystals we elaborate the approach for analysis of the spin dynamics of conducting antiferromagnets and consider the possible magnetic structures and their interaction with spin-polarized currents.

Concerning the MESO logics we consider the principle of operations of MESO-based logic devices; discuss the physical mechanisms, responsible for converting charge into spin in ME input and spin to charge in SO output; and simulate magnetization reversal processes in ME component of MESO. To address this, we develop a model of magnetization switching in ME heterostructures, focusing attention on the exchange – coupling mechanisms between multiferroics (MF) and ferromagnetic (FM) layers and the impacts given by non-collinear magnetic phases such as spin cycloids emerging in multiferroic films at definite conditions. As an example, we take well - studied multilayers, combining such FMs as metals (Co, CoFe, Ni and permalloy), half metals (e.g. Fe_3O_4) and insulators (iron garnets, $BaTiO_3$,) coupled with MFs ($BiFeO_3$, Cr_2O_3, Ruddlesden – Popper structures).

The ability to incorporate a number of factors (such as the geometry and dimensions of the system, the presence of several phases, interfacial interactions and energy-efficient external influences) makes developed approach promising for studying ME heterostructures and their compatibility with spin-orbit switching schemes. Hybrid magnetoelectric – spin orbit (MESO – like) systems play an important role in pursuit of low - energy consuming devices and expected to provide ultra-fast dynamics and ultra-low power consumption.

The support of Ministry of Science and Higher Education of the Russian Federation, Agreement No. 075-11-2022-046 is kindly acknowledged.

1. V. Baltz, et al., *Rev. Mod. Phys.* **90**, 015005 (2018).
2. P. Wadley, et al., *Science* **351**, 587 (2016).
3. K. Olejník, et al., *Nat. Commun.* **8**, 1 (2017).
4. S. Manipatruni, et al., *Nature* **565**, 35 (2019).
5. E.A. Turov, V.V. Nikolaev, *Phys. Usp.* **48**, 431 (2005).
6. И.Е.Дзялошинский, *ЖЭТФ* **46**,1420 (1964).
7. А. С. Боровик-Романов, *Лекции по низкотемпературному магнетизму*. Москва, Институт Физических Проблем им. П.Л. Капицы РАН, 55с. 2010.
8. А.К. Звездин, В.М. Матвеев, А.А. Мухин, А. И. Попов. *Редкоземельные ионы в магнитоупорядоченных кристаллах*. Москва. Наука. 295 с. 1985.

O23

Magnetic ordering transition in Al doped GdNiSi

R.D. Mukhachev[1], A.G. Kuchin[1], A.V. Lukoyanov[1,2]

[1]M.N. Mikheev Institute of Metal Physics of Ural Branch of Russian Academy of Sciences, 620108, Ekaterinburg, Russia
r.d.mukhachev@imp.uran.ru

[2]Institute of Physics and Technology, Ural Federal University, 620002, Ekaterinburg, Russia

Our theoretical calculations of the electronic structure and magnetic properties of GdNiSi with the Al doping have been performed within the framework of the DFT+U method. The magnetic properties were found to change drastically at the Al concentrations x ≥ 0.1, namely, the antiferromagnetic (AFM) ordering of the Gd magnetic moments as the ground state changes to the ferromagnetic (FM) one [1].

In our study, for the intermetallic GdNiSi compound, various types of FM and AFM orderings in the gadolinium sublattice were considered. The electronic structure and magnetic orderings were investigated using the DFT+U method for an exchange–correlation functional approximated in the generalized gradient approximation form (GGA-PBE). Strong electron correlations in the 4f shell of gadolinium were taken into account within GGA+U for the Coulomb parameter equal to 6.7 eV and Hund parameter equal to 0.7 eV. Structural parameters for the calculations were taken from the experimental data [2].

It was found for pristine GdNiSi that the most stable in terms of minimum total energy is the antiferromagnetic ordering with different directions of Gd magnetic moments, which corresponds to the G-type AFM. In GdNiSi, this ordering is with the Gd moments being aligned antiferromagnetically in ‘‘W slabs’’ and ferromagnetically in ‘‘$BaAl_4$ blocks’’ [3]. The ferromagnetic ordering is only 0.0003 Ry higher in total energy in pure GdNiSi. In the self-consistent DFT+U calculations, the total magnetic moment of $GdNiSi_{1-x}Al_x$ was found to be solely formed by the Gd ion, and Ni, Si are either non-magnetic or have negligible magnetic moments 0.02 μ_B at Si and 0.1 μ_B at Ni, similar to the previous studies. Let us further consider the replacement of a small number of silicon atoms with aluminum atoms, a change in the magnetic ordering in $GdNiSi_{1-x}Al_x$ occurs. In $GdNiSi_{1-x}Al_x$ ($x = 0.1 – 0.3$) it was found that even at concentrations as low as $x = 0.1$. The energy difference in these cases ranges from 2.32 ($GdNiSi_{0.7}Al_{0.3}$) to 4.02 ($GdNiSi_{0.8}Al_{0.2}$) meV/f.u. It is possible to estimate the transition point for the Al concentration x equal to 0.024, i.e. 2.4% Al, which is very close to $x = 0$. The ferromagnetic ordering in the Gd sublattice is more favorable in total energy as the ground state which can be ascribed to the shortening of Gd-Gd distances and the oscillating behavior of the Ruderman–Kittel–Kasuya–Yosida interaction in the Al-doped compositions.

Thus, the electronic structure of of $GdNiSi_{1-x}Al_x$ demonstrates significant changes in the vicinity of the localized Gd 4f states that confirms the presence of the antiferro-to-ferromagnetic transition using our first-principles calculations for Al $x \geq 0.1$ in agreement with the previous experimental results [2]. The concentration-driven magnetic transition is promising for the Gd-based compounds and will motivate further research. Therefore, further study of their properties may be useful for various environmentally sustainable applications.

This study was supported by the grant of Russian Science Foundation No 24-22-00066, https://rscf.ru/en/project/24-22-00066/.

1. R.D. Mukhachev, A.V. Lukoyanov, A.G. Kuchin, *Pis'ma v ZhETF* **119**, 764 (2024).
2. G. Yao, G. Zeng, Q. Wang, W. Cui, *J. Magn. Magn. Mater.* **585**, 170918 (2023).
3. S.P. Platonov, A.G. Kuchin, A.S. Volegov, et al., *Phys. B: Cond. Matter* **685**, 416060 (2024).

O24

Structure, dielectric and piezoelectric properties of solid solutions 0.7$BiFeO_3$ – 0.3(Ba,Sr)TiO_3

D.V. Karpinsky[1,2], S.I. Latushko[1,2], D.V. Zheludkevich[1,2], M.V. Silibin[1]

[1] *National Research University of Electronic Technology "MIET", Zelenograd, Russia*

[2] *SSPA «Scientific-Practical Materials Research Centre of NAS of Belarus», Minsk, Belarus*
karpinsky@physics.by

Promising materials for creating new electroceramic compounds are lead-free multiferroics based on bismuth ferrite, which is due to the high temperatures of phase transitions into magnetically ordered and ferroelectric states. It is known that chemical substitution of bismuth and iron ions in $BiFeO_3$ makes it possible to control the crystal structure of the compounds and thus to modify their physical properties. In this abstract, the features of the “rhombohedral-cubic” concentration phase transition in the system of solid solutions 0.7$BiFeO_3$ – 0.3($Ba_{1-x}Sr_x$)TiO_3 with $0 \leq x \leq 0.3$ are investigated. The obtained data presents the results of studies of the crystal structure, carried out by X-ray diffraction and Raman spectroscopy, and the piezoelectric properties of the compounds. Based on the data obtained, the structural state of the compounds was studied as a function of the concentration level and the type of the dopant ions, the region of the concentration stability of the polar rhombohedral phase, which determines the piezoelectric properties of solid solutions based on bismuth ferrite, was determined.

Crystal structure analysis.

X-ray phase analysis of the samples indicates the absence of impurity phases in all studied compounds with an accuracy of the error of the research method (~ 1%). X-ray diffraction analysis, carried out by the Rietveld method, made it possible to determine the nature of the change in the crystal structure with a change in the concentration of the dopant ions (Sr). It has been established that the initial compound with $x = 0$ is characterized by a two-phase structural state in which a polar rhombohedral structure (space group *R3c*) and a cubic structure (space group *Pm-3m*) coexist, with a dominance of the cubic phase being, the volume fraction of the rhombohedral phase is ~ 15%. An increase in the concentration of Sr ions leads to a structural transition to a single-phase cubic state (Figure 1), while a decrease in the values of structural parameters and, accordingly, in the unit cell volume occurs. The decrease in parameters is associated with the smaller ionic radius of strontium ions (1.18Å) compared to barium ions (1.35Å), while the iron ions Fe^{3+} and titanium Ti^{4+} have similar ionic radii in the octahedral environment - 0.645Å and 0.605Å, respectively.

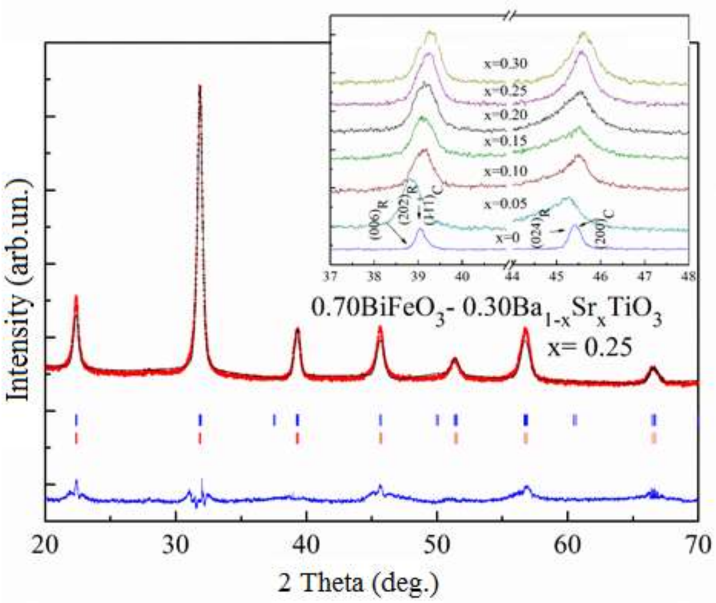

Figure 1. X-ray diffraction patterns obtained for compounds 0.7$BiFeO_3$-0.3($Ba_{1-x}Sr_xTiO_3$) recorded at room temperature. The inset shows the concentration driven evolution of the diffraction reflections recorded for compounds $0 < x < 0.3$.

An increase in the concentration of Sr ions leads to a significant decrease in the volume fraction of the rhombohedral phase; diffraction patterns of compounds with $x \geq 0.2$ were refined using a single-phase structural model with cubic symmetry of the structure. The Raman spectra obtained for all studied compounds contain active Raman phonon modes, which indicates the presence of non-centrosymmetric distortions in the crystal structure of solid solutions. Phonon modes E(1TO), E(2TO), A1(1TO) and A1(2TO) (not presented) are characteristic of rhombohedral distortions and are caused by polar vibrations of bismuth and iron (and titanium) ions in oxygen polyhedra. The frequencies of these modes, as well as their intensity, practically do not change with increasing concentration of strontium ions, which is due to the presence of rhombohedral distortions, including in compositions that are single-phase according to X-ray diffraction studies. Thus, structural studies carried out by Raman spectroscopy indicate the presence of local clusters with submicron sizes, characterized by rhombohedral distortions of the structure in solid solutions with $x > 0.2$.

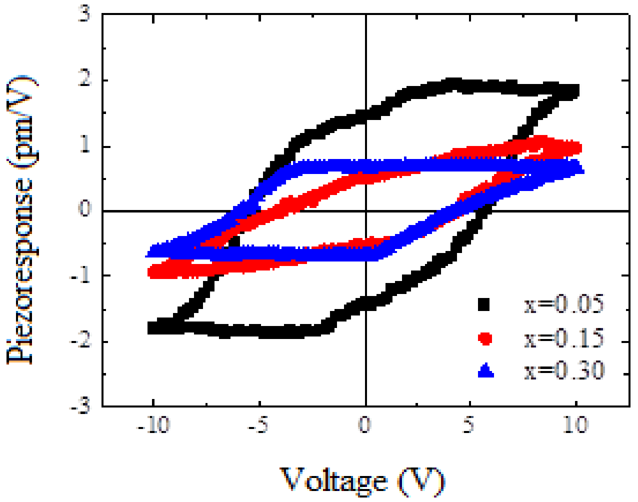

Figure 2. Piezoelectric hysteresis loops for the studied compositions.

Piezoelectric properties measurements. The data obtained by force microscopy method made it possible to visualize the domain structure of the compounds, while all the studied samples were characterized by the presence of polar clusters with an arbitrary direction of the polarization vector. Studies of switching the direction of polarization made it possible to estimate the value of the minimum voltage sufficient to change the direction of polarization to the opposite one - for all the studied compounds, a voltage of +/– 10 V is sufficient to repolarize local areas of the sample surface. The value of the piezoelectric coefficient d_{33} decreases significantly with increasing concentration of strontium ions, so in a composition with $x = 0.05$ $d_{33} \sim 2$ pm/V, in a solid solution with $x = 0.3$ the value $d_{33} \sim 0.8$ pm/V.

So, concluding we have to note, that the solid solutions of the $0.7BiFeO_3 – 0.3(Ba_{1-x}Sr_x)TiO_3$, obtained by solid-phase reactions, are characterized by a two-phase structural state at $0.0 < x < 0.2$. An increase in the concentration of strontium ions leads to a decrease in the proportion of the rhombohedral phase, which is accompanied by a decrease in the values of the structural parameters; the structure of compositions with $x \geq 0.2$ is single-phase cubic. The “rhombohedral-cubic” concentration phase transition is diffuse in nature and is caused by the difference in the ionic radii of Ba c ions (r_{Ba} = 1.35 Å) and Sr ions (1.18 Å). Studies carried out using Raman spectroscopy and piezoelectric response force microscopy indicate the presence of clusters with a rhombohedral structure with characteristic submicron dimensions in compositions with $x \geq 0.2$.

The research was supported by the Russian Science Foundation (23-19-00347).

O25

Structure and properties of proton exchange waveguides in lithium niobate-tantalate single crystals

A.V. Sosunov[1], I.V. Petukhov[1], A.R. Kornilicyn[1], A.A. Mololkin[2]

[1]*Perm State University, 614990 Perm, Russia*

[2]*National University of Science and Technology MISiS, 119049, Moscow, Russia*
alexeisosunov@gmail.com

The mixed single crystals of lithium niobite-tantalate (LNT) have recently attracted increasing attention from scientists due to the ability to control their characteristics by changing the composition. These unique materials can find their application in integrated photonics, electro- and acousto-optics, sensors, quantum technologies and nonlinear interactions. This work is devoted to study the structure and properties of the proton exchange waveguides in new mixed LNT single crystals.

The crystal was grown by the Czochralski method from the $LiNb_{0.97}Ta_{0.03}O_3$ charge in Pt crucibles at the Institute of Microelectronics Technology and High Purity Materials of the Russian Academy of Sciences using an upgraded NIKA-3M system [1]. The experimental samples LNT had a size of 10×10×1 mm^3 and *X*- and *Z*-cut crystallographic directions.

Proton exchange (PE) was done in leak-free zirconium reactor in pure molten benzoic acid at 180-210°C during 2 hours. TEM technic, XRD, IR-spectroscopy, prism coupling method, optical microscopy and profilometry were used as research methods.

Results:

1) *Waveguide profile*

The increment of refractive index has a step profile for *X*- and *Z*-cut samples Δn_e=0.08-0.10, which is 0.01-0.02 less than for lithium niobate crystals. In this case, the depth of the waveguides increases (Fig. 1, inset in the upper right corner).

2) *Unit cell parameters*

The lattice parameters of LNT samples after PE change greatly. The crystal lattice is stretched. The results obtained are important in describing the destruction of the surface during PE.

Table 1. Unit cell parameters

Unit cell parameters, Å	$LiNbO_3$	$LiNb_{0.97}Ta_{0.03}O_3$	PE 190°C, 2h. [$LiNb_{0.97}Ta_{0.03}O_3$]
a	5.147	5.145±0.001	5.200±0.001
c	13.849	13.848±0.001	13.902±0.001

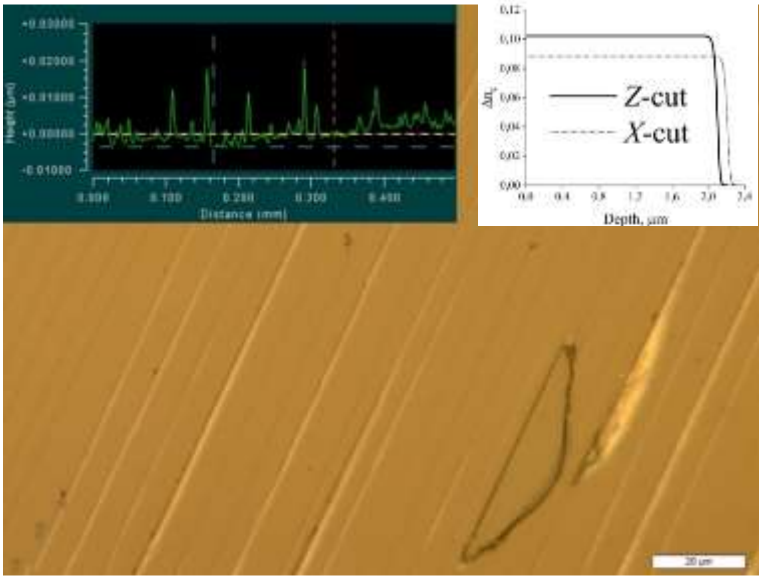

Figure 1. Surface damage during PE process and step-waveguide profile

3) Surface damage

For non-polar samples of lithium niobate and mixed crystals, in contrast to polar ones, surface damage is observed in the form of parallel oriented cracks (Fig. 1). The generality of the microstructure results indicates a relationship with crystallographic orientation [2]. The results of optical profilometry (Fig. 1 inset in the upper left corner), the height of the line cracks can reach almost 20 nm. At the same time, etching areas between lines until 5 nm is observed.

4) Phase analysis

According to XRD analysis and IR spectroscopy, β_1 and β_2 phases [3] are formed during direct PE ($\varepsilon \approx 3.5\text{-}5.0 \times 10^{-3}$). However, for the *X*-cut, relative deformations ε of the β_2-phase with $\varepsilon \approx 10.7 \times 10^{-3}$ are observed, unlike to the *Z*-cut LNT.

5) Energy Activation

The activation energy E_a and coefficient D_0 were determined from the Arrhenius equations and Fick's law (Fig. 2). The calculated E_a and D_0 of proton diffusion in mixed crystals indicate a more intense process than in lithium niobate and tantalate single crystals.

Table 2. Kinetic parameters

Sample [$LiNb_{0.97}Ta_{0.03}O_3$]	D_0, μm^2/h	E_a, eV	E_a, eV [$LiNbO_3$]
X-cut	1.2×10^6	0.59	0.8
Z-cut	3.0×10^6	0.65	0.9

Key physical parameters of the proton diffusion process were determined in mixed crystals. These parameters significantly depend on the composition and homogeneity of the samples. For mixed crystals, the PE process is more intense, i.e. higher diffusion coefficients, as well as crystal lattice deformation, unlike for lithium niobate.

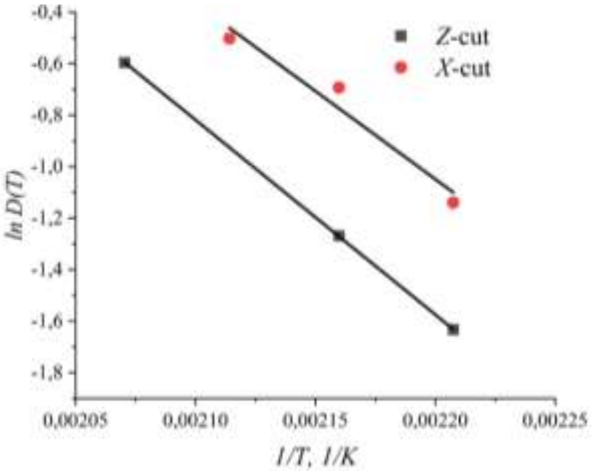

Figure 2. Arrhenius function of proton diffusion into LNT

This work was funded by RSF and Perm Region [grant number 24-22-20097].

1. E.V. Zabelina, A.A. Mololkin, N.S. Kozlova, et al., *Crystallogr. Rep.* **68**, 1173 (2023).
2. P.J. Matthews, A.R. Mickelson, S.W. Novak, *J. Appl. Phys.* **72**, 2562 (1992).
3. Yu.N. Korkishko, V.A. Fedorov, *Crystallogr. Rep.* **44**, 237 (1999).

Influence of plasma flows on the functional properties of piezoelectric materials

G.Yu. Sotnikova[1], G.A. Gavrilov[1], V.Yu. Goryainov[1], R.S. Passet[1], A.A. Vorob'ev[2], A.V. Sotnikov[2]

[1]*Ioffe Institute, 194021, St. Petersburg, Russia*
G.Sotnikova@mail.ioffe.ru

[2]*Emperor Alexander I St. Petersburg State Transport University (PGUPS), 190031, St. Petersburg, Russia*

Plasma flow irradiation, being an effective way of predetermined influence on the structure of materials, significantly expands the experimental capabilities of studying their properties. Such investigations are in demand both for studying the behavior of various functional materials under extreme operating conditions, and for exploring the possibility of controlling their performance characteristics. Currently, the main interest is related to the search for structural materials for reactors in the rapidly developing field of thermonuclear energy [1]. At the same time, plasma technologies are widely used for microstructuring the surfaces of various materials to improve their mechanical properties and increase their resistance to external influences. In modern semiconductor industry, plasma Smart-cut technology is used to create thin layers and structures for new nano- and microelectronics components, radiation- and high temperature resistant integrated circuits, various kinds of sensors and high-quality solar cells. Note that similar studies in the field of ferroelectric and piezoelectric materials, which are widely used as basic elements for creating high-quality ultrasonic transducers and electromechanical actuators, are quite few in number and are devoted mainly to the effect of neutron radiation on the functional properties of piezoelectric ceramics [2, 3].

This contribution presents both an experimental approach and a setup for a comprehensive study of the influence of different plasma particles and plasma flow energy (thermal load) on the electrophysical properties of ferroelectric and piezoelectric materials. The experimental setup based on the plasma accelerator of the Ioffe Institute of the Russian Academy of Sciences and original radiation (pyrometric) techniques, characterized by high spatial and temporal resolution [4, 5].

Using this advanced setup, experimental samples of Russian-made single crystals and ceramics were irradiated by pulsed hydrogen and helium plasma flows: particle energy up to 200 eV, integral fluence up to 10^{23} m^{-2}, flow energy 0.1 MJ/m^2, pressure 0.15 MPa. A dynamic analysis of the temperature response of the sample surface was carried out with a 1 μs time resolution directly during plasma exposure. The results of studies of modification of the composition and structure of the surface layers of experimental samples under various types of plasma exposure are presented. The main material parameters (dielectric constant, piezo- and elastic constants, mechanical quality factor and electromechanical coupling coefficient) of lithium niobate single crystal and CTS-19 and CTSNV-1 piezoceramics were measured before and after exposure.

The results obtained are discussed within the framework of existing models that take into account the influence of the modified surface layer.

The work was carried out with partial support from the Russian Science Foundation, grant No. 24-19-00716.

1. X. Litaudon et al., *Nucl. Fusion* **57**, 10 (2017).
2. D. Simeone et al., *Mater. Res.*, **30**, 1495 (2015).
3. E. Mukhin et al., *Tech. Phys. Lett.*, **48** ,12, (2022).
4. A.V. Voronin, V.Yu. Goryainov, V.K. Gusev, *Tech. Phys.* **65**, 987 (2020).
5. A.V. Voronin et al., *Tech. Phys*. **68**, 580 (2023).

O27

Optical scanner based on cascaded domain structure in PMN-PT single crystals

A.D. Ushakov[1], I.A. Kipenko[1], M.A. Chuvakova[1], A.R. Akhmatkhanov[1],
X. Liu[2], X. Wei[2], V.Ya. Shur[1]

[1]*School of Natural Sciences and Mathematics, Ural Federal University, 620000, Ekaterinburg, Russia, bddah@ya.ru*

[2] *Electronic Materials Research Laboratory, Key Laboratory of the Ministry of Education and International Center for Dielectric Research, Xi'an Jiaotong University, 710049, Xi'an, China*

In this study, we present the results of fabrication of the optical scanner prototype with the engineered cascaded domain structure within the multiaxial ferroelectric PMN-PT single crystal.

It is known that the working characteristic of the effect is the birefringence induced by the electric field $\Delta n(E)$. The induced change in the refractive index can be used to change the direction of the beam in space, i.e. to create the optical scanners. Thus, the distribution of radiation in the far field (beam direction) can be controlled using just the electrical voltage.

Recently, the six-layer cascaded domain engineered optical phased array was proposed and embodied in the bulk lithium niobate single crystal [1]. The demonstrated capability of beam steering with frequency up to 3 MHZ opens a prospect for optical phased arrays and related applications utilizing such cascaded domain engineering techniques. Considering the high value of the electro-optic coefficient of PMN-PT ($\langle r \rangle$ = 41 pm/V) [2, 3], it was proposed to manufacture prototypes of cascade optical scanners based on this material.

We used the [001]-cut $0.62\mathrm{Pb(Mg_{1/3}Nb_{2/3})O_3}$-$0.38\mathrm{PbTiO_3}$ single crystals possessing the tetragonal symmetry. The samples were switched into a quasi-single-domain state before the optical scanner prototype making. The cascaded domain structure was made using the original method. The resulted domain structure was visualized in bulk using the second harmonic generation microscopy (Fig. 1a,b). The deflecting performance of the optical scanner prototypes was estimated as $2{,}5\cdot10^{-4}$ deg/V/mm (Fig. 1c) which is close to the result obtained in CLN [1].

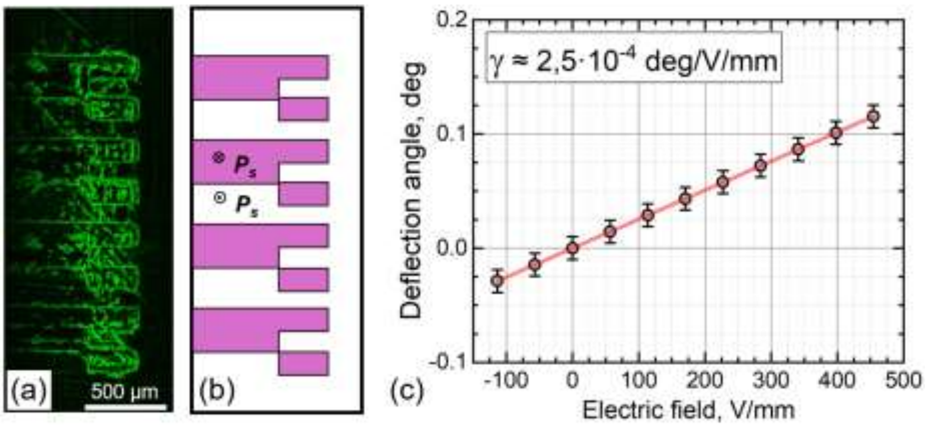

Figure 1. (a) SHG microscopy image and (b) corresponding schematic of the cascade domain structure last layer. (c) Deflecting performance of the optical scanner prototype based on PMN-PT.

The authors are grateful for financial support of the Ministry of Science and Higher Education of the Russian Federation (state task FEUZ-2023-0017). The work was performed using the equipment of the Ural Center for Shared Use "Modern Nanotechnologies" UrFU (reg. No. 2968).

1. J. Li, Y. He, H. Zheng, et al., *Appl. Phys. Rev.* **10**, 031413 (2023).
2. Q. Hu, R. Yang, Y. Zhao, et al., *Appl. Phys. Lett.* **115**, 222901 (2019).
3. X. Wan, H. Luo, X. Zhao, et al., *Appl. Phys. Lett.* **85**, 5233 (2004).

O28

Study of the heat capacity of the relaxor ferroelectric $PbNi_{1/3}Nb_{2/3}O_3$ in a wide temperature range

N.K. Derets, N.Yu. Mikhailin, T.A. Smirnova, S.G. Lushnikov

Ioffe Institute, 194064 St. Petersburg, Russia
nikita.derets@gmail.com

This comprehensive study investigates the heat capacity of the relaxor ferroelectric lead nickel niobate $PbNi_{1/3}Nb_{2/3}O_3$ (PNN) across an extensive temperature range, from cryogenic temperatures up to temperatures well above the Curie point. A large family of crystals with the perovskite structure $AB'B''O_3$ (A = Pb) with complex replacement of the tetravalent ion in the B-position by two ions of different valences exhibit unique physical properties of relaxor ferroelectrics [1]. Relaxor ferroelectrics (hereinafter referred to as relaxors), for example, $PbMg_{1/3}Nb_{2/3}O_3$ (PMN), are characterized by the temperature dependence of the dielectric constant in the form of broad frequency-dependent maxima, which, in the general case, are not associated with a structural phase transition. The temperature region in which wide temperature-dependent anomalies in the dielectric response are observed is called the diffuse phase transition region. Compounds of this family, as well as solid solutions based on them, have gigantic dielectric and piezoelectric coefficients, which are widely used in industry.

In the family of relaxors, a separate group of crystals can be distinguished in which one of the ions in the B-position is magnetically active. The combination of the magnetic properties of ferro- and antiferromagnets and the polar properties of relaxors allows us to consider this group of crystals as promising multifunctional materials, called multiferroic relaxors. The poorly studied $PbNi_{1/3}Nb_{2/3}O_3$ (PNN) single crystal can be considered a potential candidate for multiferroic relaxors. Understanding the thermodynamic behavior of these materials is crucial for optimizing their performance in practical applications.

The heat capacity measurements were conducted by relaxational calorimetry using physical property measurements system (PPMS) technique to ensure accurate and reliable data from 2 K up to 400 K. Heat capacity anomaly associated with phase transition at 200 K observed in Brillouin scattering [2] in the material was not observed in our measurements.

Additionally, at low temperatures, the heat capacity of a single crystal exhibits non-Debye behavior. In the temperature dependences $C_p(T)/T^2$ of PNN single crystal, a maximum is observed at a temperature $T \sim 17$ K. This maximum can be associated with the Einstein oscillation mode. Another explanation of the appearance of this peak may be the difference between real density of states in the crystal from predicted by the Debye theory.

Furthermore, the implications of our findings extend to the broader field of physics of condensed matter, where the understanding of thermal and dielectric properties is essential for the advancement of technology. The insights gained from this study of PNN's heat capacity can be used to design and synthesize of new relaxor ferroelectrics with enhanced performance characteristics. This research represents a step forward in the quest to understand the nature of relaxor ferroelectrics and their unique physical properties.

1. G.A. Smolenskii, V.A. Bokov, V.A. Isupov, et al., *Ferroelectrics and Related Materials* (Gordon and Breach, New York, 1984).
2. H.J. Fan, M.H. Kuok, S.C. Ng, et al., *J. Appl. Phys.* **91**, 4, 2262 (2002).

O29

Kinetics of polarization reversal with conducting domain walls: An application to lithium niobite crystals

B. Sturman[1], N. Masnev[2], E. Podivilov[1]

[1]*Institute of Automation and Electrometry of RAS, 630090 Novosibirsk, Russia*
sturman@iae.nsk.su

[2]*Landau Institute for Theoretical Physics of RAS, 142432, Moscow Region, Chernogolovka, Russia*

Ferroelectric polarization reversal is a vast developing research area [1]. Reversal of the spontaneous polarization P occurs at electric fields E much smaller than the depolarization field via nucleation of needle-like critical domains and their subsequent fast-forward and lateral growth. The classical models for the domain formation energy [2,3] deal with the dielectric case (no DW conduction). They lead to non-realistically high energies and are not consistent with the law $t_R \propto \exp(E_*/E)$ for the reversal time. Recently, DW conduction was discovered and explored in many materials to become a general ferroelectric effect [4]. It was found [5] that the DW conduction strongly influences the domain energy.

We show that account for the DW conduction in lithium niobite (LN) crystals leads to the exponential $\exp(-E_{n,l}/E)$ field dependences for the rates of domain nucleation (n) and lateral (l) growth with characteristic fields $E_{n,l}$ comparable with E_* and the ratio $E_n/E_l \approx 5$ controlled by the crystal point symmetry. Modeling of the reversal kinetics shows distinct stages of nucleation, lateral growth, and coalescence. The reversal time follows, in line with experiment [6], the field law $t_R \propto \exp(E_*/E)$ with $E_* \approx 35$ kV/mm. An important ingredient of our theory is the assertion that the DW conduction not only significantly lowers the critical domain formation energy W_*, but also provides the necessary E_n/E dependence on the applied electric field. This result was missed earlier in [5].

Figure 1 gives an illustration of our modelling of the domain reversal kinetics as applied to SLN crystals. It corresponds to the surface energies 3 and 15 erg/cm^2 relevant to neutral and maximally charged DW sections, respectively.

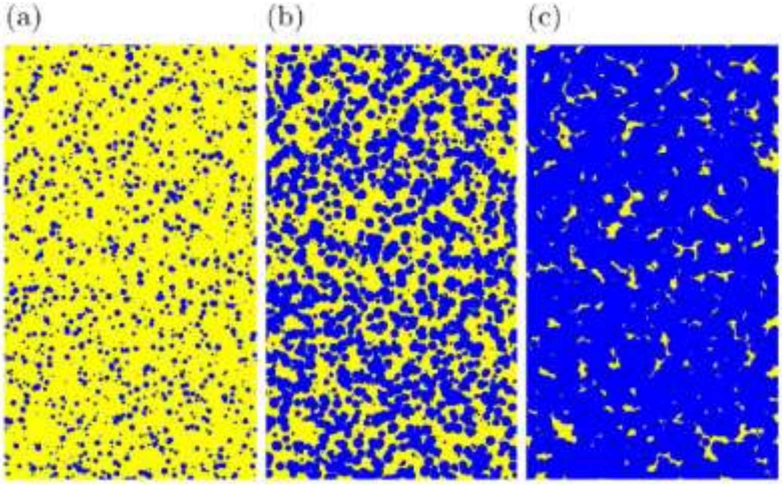

Figure 1. Illustration of domain patterns for an SLN crystal at $E = 4$ kV/mm. The cases (a), (b), and (c) correspond to time $t = 19$, 33, and 50 s. They are relevant to the stages of nucleation, lateral expansion, and coalescence. Blue color indicates the inverted domain areas.

Further modeling results include self-similarity of kinetic curves at different values of E, hysteresis loops at different ramping times, and a link between E_* and the coercive field E_c.

1. A.K. Tagantsev, L.E. Cross, J. Fousek, *Domains in Ferroic Crystals and Thin Films* (Springer, 2010).
2. R. Landauer, *J. Appl. Phys.* **28**, 227 (1957).
3. R. C. Miller, G. Weinreich, *Phys. Rev.* **117**, 1460 (1960).
4. P. Bednyakov, B. Sturman, T. Sluka, et al., *NPJ Comput. Mater.* **4**, 65 (2018).
5. B. Sturman, E. Podivilov, *JETP Letters* **116**, 246 (2022).
6. A. Kuroda, S. Kurimura, Y. Uesu, *Appl. Phys. Lett.* **69**, 1565 (1996).

O30

Experimental and theoretical aspects of Mn-Pt-Al based alloys

S.S. Samatham[1], A.K. Patel[2], A.V. Lukoyanov[3], P.D. Babu[4], K.G. Suresh[5]

[1]*Department of Physics, Chaitanya Bharathi Institute of Technology, Gandipet, Hyderabad 500 75, India*
shanmukharao_physics@cbit.ac.in

[2]*Research Centre for Magnetic and Spintronic Materials, National Institute for Materials Science, Tsukuba, Ibaraki 305 0047, Japan*

[3]*M.N. Mikheev Institute of Metal Physics of Ural Branch of Russian Academy of Sciences, 620108 Ekaterinburg, Russia*

[4]*UGC-DAE Consortium for Scientific Research, Mumbai Center, BARC Campus, Mumbai 400085, India*

[5]*Magnetic Materials Laboratory, Department of Physics, Indian Institute of Technology Bombay, Mumbai 400 076, India*

Understanding and exploration of magnetic materials that exhibit functional properties play critical and crucial role in designing the materials for future technological and industrial applications. In particular, theoretical calculations in combination with experimental results lead to a comprehensive approach. Out of numerous materials repository, Heusler alloys got their unique place for their rich physical and magnetic phenomena along with functional properties such as large and asymmetric magnetoresistance for spin-valve applications, giant adiabatic change in temperature and magnetic entropy for magneto-refrigeration applications, half-metallic nature for spintronics applications etc. In our study, we present Mn-Pt-Al based Heusler alloys Mn_2PtAl [1] and MnPtAl using experimental and theoretical methods.

Mn_2PtAl and MnPtAl are synthesized using arc melting method. The magnetization measurements were carried out using physical property measurement system. X-ray diffraction measurements were performed at room temperature. These alloys are found to crystallize in hexagonal Ni_2In type structure ($P6_3/mmc$) with lattice parameters of $a = b = 4.34$ Å, and $c = 5.47$ Å and $a = b = 4.33$ Å and $c = 5.63$ Å, respectively as shown in Figure 1. Magnetization (M-H) isotherms of Mn_2PtAl at low temperatures are asymmetric exhibiting exchange bias. On the other hand, MnPtAl shows compensated antiferromagnetic behavior.

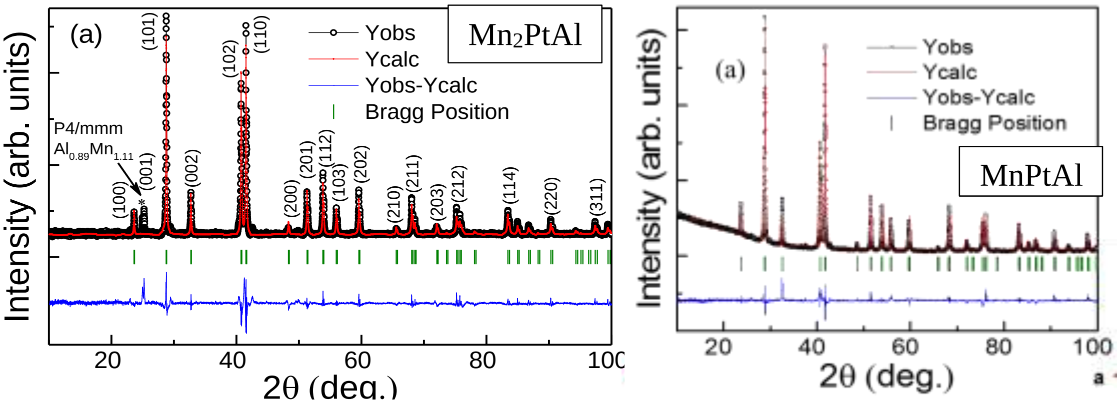

Figure 1. Rietveld refined X-ray diffraction patterns of (a) Mn_2PtAl and (b) MnPtAl.

The theoretical electronic structure calculations for Mn_2PtAl reveal the ferrimagnetic ground state of Mn_2PtAl and the Mn ions with total magnetization of 0.15 m_B/f.u. resulting from the antiferromagnetically arranged Mn moments of 3.9 and -3.9 μ_B/Mn. The calculated exchange interaction parameters for the Mn_2PtAl alloy demonstrated the AFM coupling between the nearest neighbor Mn ions along the c axis and the competing FM next-nearest neighbor interaction of the comparable value, also corresponds to the Mn ions along the c axis. The similar values of the Mn ions 3.7 and -3.7 μ_B/Mn were also calculated for MnPtAl. However, the ground state for MnPtAl is found as the antiferromagnetic one with the zero total moment. The values of the total magnetic moment calculated for both compounds are found in good agreement with the experimental magnetization measurements.

1. A.K. Patel, S.S. Samatham, A.V. Lukoyanov, et al., *Phys. Chem. Chem. Phys.* **24**, 29539 (2022).

O31

Stability of ferroelectric domains created by local switching on non-polar cut MgOLN

M.S. Kosobokov, A.P. Turygin, S.A. Melnikov, D.O. Alikin, V.Ya. Shur

[1]*School of Natural Sciences and Mathematics, Ural Federal University 620002, Ekaterinburg, Russia*
mihail.kosobokov@urfu.ru

Polarization reversal in ferroelectric materials initiates the formation of domains where polarization aligns with the applied electric field, inevitably leading to the emergence and further evolution of charged domain walls (CDWs) [1] CDWs have unique functional properties that significantly differ from the bulk properties of the material [2]. For example, they have several orders of magnitude higher electrical conductivity and can be created or changed in a material using an external electric field. The electrical properties of domain walls are determined by their topology and depend on the properties of the ferroelectric and the electrode materials used to switch polarization [3,4]. However, a comprehensive understanding of the mechanisms governing the kinetics of CDWs and their stabilization is still lacking.

In this work, we conduct both experimental and theoretical investigations into the phenomenon of ferroelectric domains stability and its correlation with CDWs enhanced conductivity at Y-cut of the single crystal of the Lithium Niobate doped with Magnesium (MgO:LN). Here, local polarization switching experiments by the SPM probe were performed with further visualization of the surface potential distribution $V(x, y)$ at the domain using Kelvin probe force microscopy (KPFM) and visualization of the reversed domain pattern using piezoresponse force microscopy (PFM). Solution of physics-based inverse problem of calculating the surface charge density distribution $\sigma(x,y)$, from $V(x, y)$ and depolarization field spatial distribution (E_{dep}) have been performed by COMSOL Multiphysics software (Fig. 1). The spatial distribution of the electric field has been calculated for a wedge-shaped domain for both conductive walls and non-conductive walls.

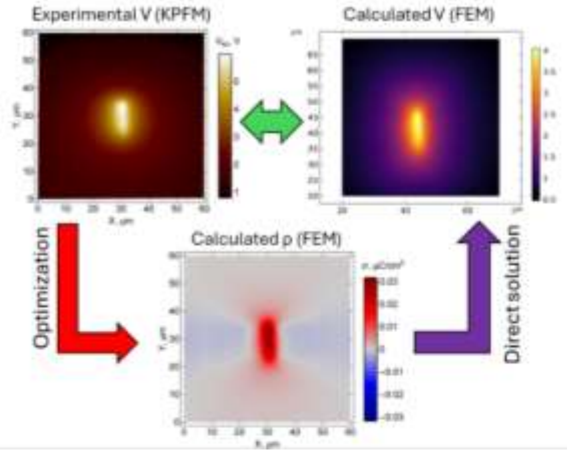

Figure 1. Scheme of the solution of physics-based inverse problem using FEM and optimization in COMSOL Multiphysics software.

Study of charge decay time dependence revealed the difference in stability of ferroelectric domains with “head-to-head” and “tail-to-tail” CDWs, in addition, for the first time we were able to contactless visualize the process of backswitching of unstable “tail-to-tail” domains before it disappeared. The calculated distribution of the polar component of the depolarization field on the domain wall made it possible to explain the stability of domains with conducting walls (“head-to-head”) and the instability of domains with non-conducting domain walls (“tail-to-tail”).

The reported study was funded by the Russian Science Foundation (grant 23-72-01074). The equipment of the Ural Center for Shared Use “Modern nanotechnology” Ural Federal University (Reg. № 2968) was used.

1. V.Y. Shur, A.R. Akhmatkhanov, I.S. Baturin, *Appl. Phys. Rev.* **2**, 040604 (2015).
2. E.A. Eliseev, A.N. Morozovska, G.S. Svechnikov, et al, *Phys. Rev. B* **83**, 235313 (2011).
3. Y. Qian, Y. Zhang, J. Xu, G. Zhang, *Phys. Rev. Appl.* **17**, 044604 (2022).
4. J.P. McConville, et al., *Adv. Funct. Mater.* **30**, 2000109 (2020).

O32

Phase transitions in $PbZrO_3$ from molecular dynamics simulations

A.V. Motseyko[1], N.V. Ter-Oganessian[1,2]

[1]*Southern Federal University, 344090, Rostov-on-Don, Russia*

[2]*Peter the Great Saint Petersburg Polytechnic University, 195251 St. Petersburg, Russia*
e-mail: teroganesyan@sfedu.ru

Calculations of the physical properties of ferro- and antiferroelectric perovskites using the density functional theory (DFT) are usually in good agreement with experiments, however, due to the resource-intensive calculations, they are limited to a small number of atoms (~100) and short times over which the evolution of the system is studied. In recent years, large-scale modeling of much larger systems (10^3 – 10^6 atoms) using molecular dynamics methods has been actively developing. This is due to the need to describe and understand, for example, the properties of domain structure and interaction of domains, various heterostructures (thin film/substrate, superlattices), polar and chemically ordered nanoregions in relaxors, topological states in polar nanostructures [1-3]. At the initial stage of development of such modeling, equivalent Hamiltonians were used [4], the parameters of which were determined using DFT. The adequacy of this approach, however, is limited by the choice of collective modes of atomic displacements, which are taken into consideration.

The main problem of modeling using the molecular dynamics method is the choice of interatomic interaction potential. In recent years, major efforts have been aimed at developing machine-learning interatomic potentials. The purpose of this work is to develop machine-learning potentials for $PbZrO_3$ and study the phase transitions in it with a change in temperature and under the influence of an external electric field using the molecular dynamics method. To solve these problems, in this work we used the moment tensor potentials [5], which provide a very good ratio of interatomic potential development and calculation speed and the resulting accuracy.

This work was financially supported by the RSF-DST Joint project (Russian Science Foundation Project No. 24-42-02025).

1. L.W. Martin, A.M. Rappe, *Nature Rev. Mater*. **2**, 16087 (2017).
2. J. Junquera, Y. Nahas, S. Prokhorenko, et al., *Rev. Mod. Phys*. **95**, 025001 (2023).
3. A.A. Bokov, Z.-G. Ye, *J. Mater. Sci*. **55**, 16451 (2020).
4. S. Prosandeev, D. Wang, W. Ren, et al., *Adv. Func. Mater*. **23**, 234 (2013).
5. I.S. Novikov, K. Gubaev, E.V Podryabinkin, et al., *Mach. Learn.: Sci. Technol*. **2**, 025002 (2021).

O33

Interplay of charge, orbital, spin and lattice degrees of freedom in orthonickelates

A.S. Moskvin

Ural Federal University, 620083, Ekaterinburg, Russia
alexander.moskvin@urfu.ru

Rare-earth orthonickelates $RNiO_3$ (R = rare-earth, or yttrium Y) belong to a wide class of Jahn-Teller magnets, compounds based on Jahn-Teller (JT) 3d- and 4d-ions with configurations of the $t_{2g}^{n1}e_g^{n2}$ type in a highly symmetrical octahedral, cubic, or tetrahedral environment and with ground state orbital *E*-doublet [1,2]. These are compounds based on tetra-complexes with the configuration d^1 (Ti^{3+}, V^{4+}, Cr^{5+}), low-spin (LS) configuration d^3 (V^{2+}, Cr^{3+}, Mn^{4+}), and high-spin (HS) configuration d^6 (Fe^{2+}, Co^{3+}), octa-complexes with HS-configuration d^4 (Cr^{2+}, Mn^{3+}, Fe^{4+}, Ru^{4+}), low-spin configuration d^7 (Co^{2+}, Ni^{3+}, Pd^{3+}), as well as octa-complexes with configuration d^9 (Cu^{2+}, Ni^{1+}, Pd^{1+}, Ag^{2+}). The class of JT-magnets includes a large number of promising materials that are the focus of modern condensed matter physics, such as β-Sr_2VO_4, $(Sr,Ba)_3Cr_2O_8$, CrO, CrF_2, manganites $RMnO_3$, oxoferrates $(Ca,Sr)_2FeO_4$ $(Ca,Sr)FeO_3$, $(Ca,Sr)_3Fe_2O_7$, ruthenates RuO_2, $(Ca,Sr)_2RuO_4$ $(Ca,Sr)RuO_3$, $(Ca,Sr)_3Ru_2O_7$, a wide range of ferropnictides (FePn) and ferrochalcogenides (FeCh), Na_5CoO_4, 3D nickelates $RNiO_3$, $(Li,Na,Ag)NiO_2$, cuprates CuO, CuF_2, K_2CuF_4, $KCuF_3$, 2D cuprates (La_2CuO_4, ...) and nickelates $RNiO_2$, silver-based compounds AgO, AgF_2, $KAgF_3$, Cs_2AgF_4. These materials have a rich spectrum of unique properties from various types of magnetic and charge ordering to metal-insulator transitions and superconductivity.

The lifting of the orbital *E*-degeneracy in the high-symmetry "progenitor" JT-magnets can be associated with the conventional Jahn-Teller effect, which, as a rule, leads to the formation of a low-symmetry insulating antiferromagnetic (La_2CuO_4, $KCuF_3$, $LaMnO_3$) or ferromagnetic (K_2CuF_4) phase with an orbital order (OO-insulator). A competing mechanism for removing orbital degeneracy in JT magnets is "anti-Jahn-Teller", "symmetric" *d-d*-disproportionation according to the scheme $d^n + d^n \rightarrow d^{n+1} + d^{n-1}$, assuming the formation of a system of electronic d^{n+1} and hole d^{n-1} centers, differing by a pair of electrons/holes [2]. We argue that the unusual properties of a wide class of JT-magnets with different crystal and electronic structures, with an unusual charge and magnetic order can be explained within a unified scenario [2]. Anti-JT disproportionation in all these JT-magnets leads to the formation of a system of effective local composite spin-singlet or spin-triplet, electron or hole S-type bosons “moving” on magnetic or nonmagnetic lattice, which can be found in various localized or delocalized, magnetic or nonmagnetic phase states, including unconventional charge or spin-charge orders, spin-singlet (cuprates, nickelates) or spin-triplet (manganites, FePn/Ch, ruthenates) superconducting state. All the JT-magnets are strongly correlated systems in the sense that they cannot be adequately described within the framework of density functional band theory (DFT) methods (or their hybrid and $+\,U$ extensions) and beyond DFT methods are required for the correct description of materials properties.

In this work we propose a generalized model of effective charge triplets to describe the electronic structure and phase diagrams of a JT magnet of the $RNiO_3$ type, which involves considering a certain highly symmetrical “progenitor” configuration with ideal NiO_6 octahedra, the low-energy state of which is formed by the $[NiO_6]^{10-,9-,8-}$ charge triplet (nominally $Ni^{2+,3+,4+}$) with different spin and orbital ground states. We associate the three charge states of the NiO_6 cluster with three projections of the pseudospin Σ=1 and use the familiar spin algebra to describe the charge degree of freedom.

Formally the local pseudospin $\Sigma = 1$ presupposes the presence of eight (three “dipole” and five “quadrupole”) independent operators and corresponding local charge order parameters. In irreducible components these are $\hat{\Sigma}_0 = \hat{\Sigma}_z;\;\; \hat{\Sigma}_{\pm} = \mp\frac{1}{\sqrt{2}}(\hat{\Sigma}_x \pm i\hat{\Sigma}_y);\;\; \hat{\Sigma}_z^2;\;\; \hat{\Sigma}_{\pm}^2;\;\; \hat{T}_{\pm} = \frac{1}{2}\{\hat{\Sigma}_z, \hat{\Sigma}_{\pm}\}$. Operators $\hat{P}_0 = (1 - \hat{\Sigma}_z^2)$; $\hat{P}_{\pm} = \frac{1}{2}\hat{\Sigma}_z(1 \pm \hat{\Sigma}_z)$ are actually projection operators onto charge states with pseudospin projection M = 0, ±1, respectively, and averages $\langle\hat{P}_0\rangle$, $\langle\hat{P}_{\pm}\rangle$ are actually local densities for corresponding charge states. The operators $\hat{\Sigma}_{\pm}$ and $\hat{T}_{\pm}$ change the pseudospin projection by ±1. The operator $\hat{\Sigma}_{\pm}^2$ changes the pseudospin projection by ±2, so it can be considered as the creation/annihilation operator of an effective composite boson. The corresponding local averages $\langle\hat{\Sigma}_{\pm}\rangle$, $\langle\hat{T}_{\pm}\rangle$, $\langle\hat{\Sigma}_{\pm}^2\rangle$ will describe various versions of the “off-diagonal” charge order, in particular, the coherent metallic and superconducting states. Taking into account the spin and orbital states for the charge components, we must expand the on-sight local Hilbert space to a "pseudospin-orbital-spin octet":

$$|1M;\Gamma\mu;Sm\rangle\ (|\,10;E_g\mu;\tfrac{1}{2}\nu\rangle;\ |1-1;A_{1g}0;1m\rangle;\ \ |1+1;A_{1g}0;00\rangle), \qquad (1)$$

where $\mu = 0;2, \nu = \pm\frac{1}{2}, m = 0;\pm1$ ($|E_g0\rangle \propto d_{z^2}, |E_g2\rangle \propto d_{x^2-y^2}$), and consider the JT magnet in the general case as a system of such “octets”. This approach will allow us to take into account in the most general form the effects of competition between different degrees of freedom. In the simplest “atomic” limit, we neglect the effects of one- and two-particle charge transfer, so that the effective Hamiltonian of the JT magnet takes the form

$$\hat{H}_{at} = \hat{H}_{ch} + \hat{H}_{el-lat} + \hat{H}^{eff}_{spin}\,, \qquad (2)$$

where

$$\hat{H}_{ch} = \Delta\sum_i \hat{\Sigma}^2_{iz} + \sum_{i>j} V_{ij}\hat{\Sigma}_{iz}\hat{\Sigma}_{jz} - \mu\sum_i \hat{\Sigma}_{iz} \qquad (3)$$

is the effective Hamiltonian of charge interactions (local and nonlocal correlations), μ chemical potential, determined from the condition of the constant value $\sum_i\langle\hat{\Sigma}_{iz}\rangle$ (deviation from a half-filling). The value and sign of the parameter $\Delta = \frac{1}{2}U$ (U is the effective parameter of local correlations) are of fundamental importance for JT magnets. Large positive values of U make disproportionation energetically unfavorable and stabilize the JT center, leading to local/cooperative JT ordering with orbital order (OO) and, as a rule, to a magnetic insulator state. Large negative values of U (negative-U model) make anti-JT disproportionation energetically favorable, leading to the formation of a system of electron and hole centers with a wide range of possible phase states, including the insulating charge-ordered phase (CO-insulator). Within a two-sublattice (A, B) model we introduce two parameters: $n = \frac{1}{2}(\langle\Sigma_{zA}\rangle + \langle\Sigma_{zB}\rangle)$; $l = \frac{1}{2}(\langle\Sigma_{zA}\rangle - \langle\Sigma_{zB}\rangle)$ of uniform and staggered charge order, respectively.

The effective Hamiltonian of linear electron-lattice interaction includes two fundamentally important contributions for charge states with pseudospin projection M=0, that is, for the JT center, and M=±1, that is, for electron/hole centers, respectively:

$$H_{el-lat} = V_E\sum_i \hat{P}_0(\hat{v}^E_i\cdot Q^E_i)\,\hat{P}_0 + a\sum_i(\hat{\Sigma}^2_{iz} + \lambda\hat{\Sigma}_{iz})Q^{A_{1g}}_i\,,$$

where the first term is the contribution of the JT interaction with the local displacement mode Q^E ($Q^{E0} \propto d_{z^2}, Q^{E2} \propto d_{x^2-y^2}$), V_E is the JT interaction constant, and the matrices $\hat{v}^{E0}, \hat{v}^{E2}$ on the basis of states $|E_g0\rangle$ и $|E_g2\rangle$ coincide with the Pauli matrices $\hat{\sigma}_z$ and $\hat{\sigma}_x$, respectively [1]. The second term is the interaction with the local fully symmetric (breathing) displacement mode for charge states with pseudospin projection M=±1, a and λ are the electron-lattice interaction constants. In the two-sublattice model, it is necessary to distinguish the contribution of uniform and staggered displacement modes: $Q_\pm = \frac{1}{2}(Q_A \pm Q_B)$. The effective spin Hamiltonian includes both terms typical of systems of s=1/2 JT centers [1] and terms typical of S=1 JT magnets with anti-JT disproportionation, which can be represented as $\hat{H}^{eff}_{spin} = \hat{P}_{-1}\hat{H}_{spin}\hat{P}_{-1}$, where $\hat{P}_{-1}$ is the corresponding projection operator and the spin Hamiltonian

$$\hat{H}_{spin} = \sum_{i>j} J_{ij}(\hat{\boldsymbol{S}}_i\cdot\hat{\boldsymbol{S}}_j) + \sum_{i>j} j_{ij}(\hat{\boldsymbol{S}}_i\cdot\hat{\boldsymbol{S}}_j)^2 + \sum_{i>j}\boldsymbol{d}_{ij}[\hat{\boldsymbol{S}}_i\times\hat{\boldsymbol{S}}_j] + \hat{V}_{an} \qquad (4)$$

includes bilinear and biquadratic isotropic exchange, Dzyaloshinskii-Moriya interaction, and symmetric spin anisotropy.

To illustrate the capabilities of the developed approach, we consider a simple theory of the insulator-to-metal transition in orthonickelates as a CO-NO melting transition, as well as the effect of pressure and isotopic substitution.

The research was supported by the Ministry of Education and Science of the Russian Federation, project No. FEUZ-2023-0017.

1. К.И. Кугель, Д.И. Хомский, *УФН* **136**, 621 (1982).
2. A.S. Moskvin, *Magnetochemistry* **9**, 224 (2023).

O34

Drift of domain walls in iron garnet plates with magnetic compensation temperature

L.A. Pamyatnykh, M.S. Lysov, D.S. Mekhonoshin, S.E. Pamyatnykh, L.Yu. Agafonov, G.A. Shmatov

Ural Federal University, 620083, Ekaterinburg, Russia
Lidia.Pamyatnykh@urfu.ru

The results of experimental study and numerical simulation of the drift of domain walls (DW) in iron garnet plates with magnetic compensation temperature T_K are reported, which is topical in connection with possible interesting dynamic effects in ferrimagnets [1].

The results of study of the oscillations and drift of the DWs in a harmonic magnetic field $H = H_0 sin(2\pi ft)$ for frequencies f between 30 and 1200 Hz and amplitudes H_0 up to 500 Oe obtained for iron garnet $(TbErGd)_3(FeAl)_5O_{12}$ (111)-plate are presented. Sample parameters: plate thickness $L = 50$ μm, saturation magnetization $M_s = 40$ Gs, constants of cubic and uniaxial magnetic anisotropy are $K_1 = -3.4\cdot 10^3 erg/cm^3$ and $K_u = 5.5\cdot 10^3$ erg/cm^3, respectively. Stroboscopic technique was used to study the dynamics of the domain structure [2].

In the temperature region of magnetic compensation, a spin-reorientation phase transition was established, which took place by rotation of the magnetization vector Ms in the domains. The conditions for the drift of stripe domains of various magnetic phases at $T < T_K$ and $T > T_K$ are established. The dependences of the stripe domains drift velocity V_{dr} on the amplitude of the external field H_0 for different temperature values are obtained (Fig. 1).

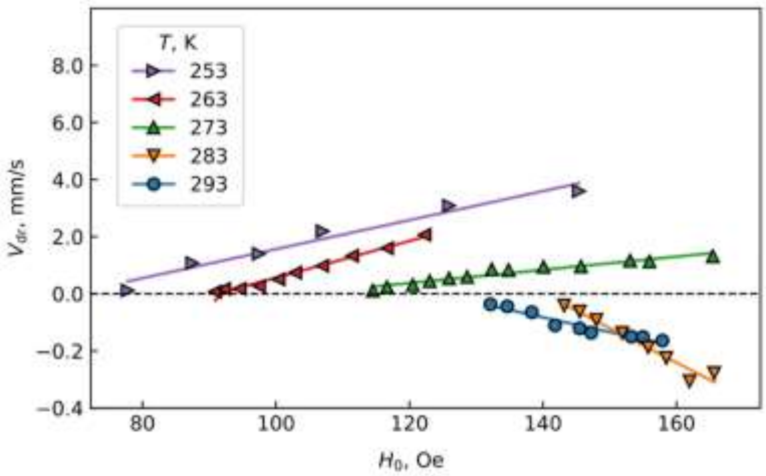

Figure 1. The dependences of the drift velocity of the stripe domains on the amplitude of the harmonic magnetic field at $T > T_K$.

A feature of the dynamic behavior of the stripe domain structure at $T > T_K$ is a change in the direction of drift to the opposite in a narrow temperature range of 273 – 283 K. A possible reason for the change in the direction of the DW drift is a change in the direction of the gradient of the internal field in the sample with a change in temperature [3].

The research was carried out with the financial support of the Ministry of Science and Higher Education of the Russian Federation within the framework of the state assignment (topic FEUZ-2023-0020).

1. Z.V. Gareeva, X.M. Chen, *JETP Letters* **114**, 215 (2021).
2. L.A. Pamyatnykh, D.S. Mekhonoshin, S.E. Pamyatnykh, et al., *Fizika Tverdogo Tela* **61**, 483 (2019).
3. L. Pamyatnykh, M. Lysov, S. Pamyatnykh, G. Shmatov, *J. Magn. Magn. Mater.* **542**, 168561 (2022).

POSTER PRESENTATIONS

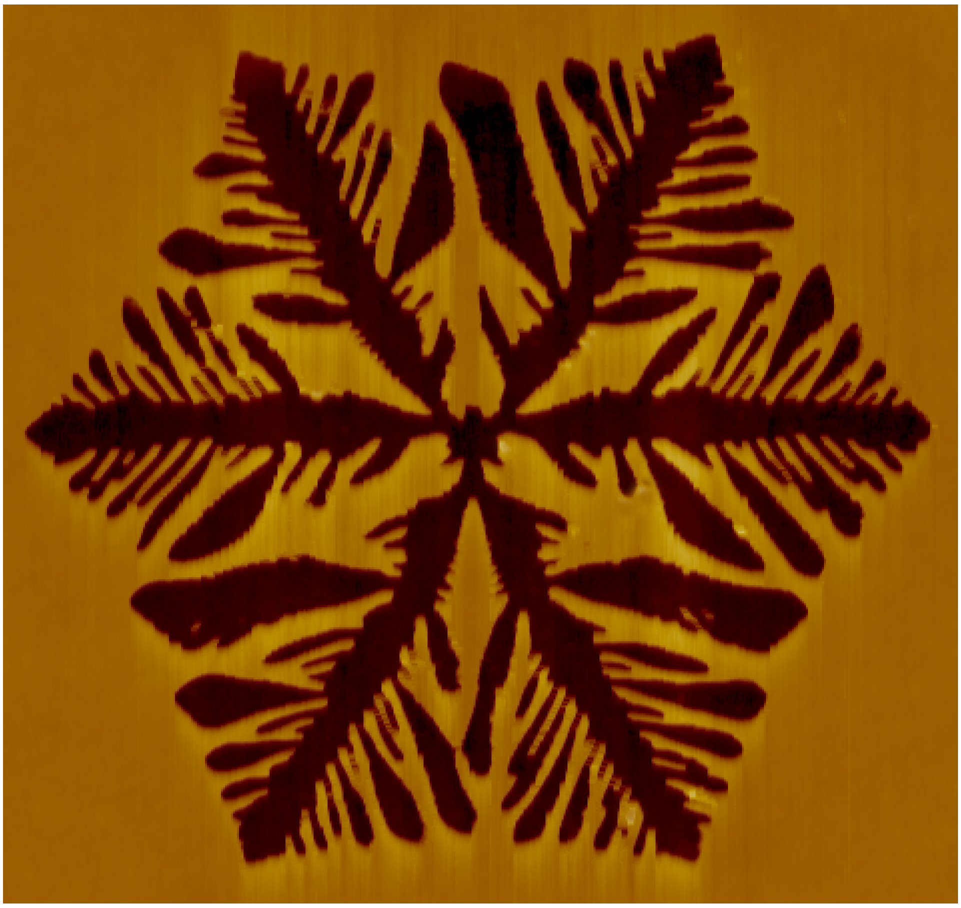

P1

Reversible characteristics of dielectric properties in cobalt-containing ferroelectric ceramics (1-x)$Ba_{0.95}Pb_{0.05}TiO_3$+xCo_2O_3

S.R. Al Saedi[1], R.V. Dikov[2], L.V. Zhoga[1], A.V.Sopit[1]

[1]*Volgograd State Tecnical University, 400074, Volgograd, Russia*

[2]*Volgograd State Socio-Pedagogical University, 400001, Volgograd, Russia*
romanodc@yandex.ru

In this work, the reversible dielectric constant in cobalt-containing ferroelectric ceramics is studied. Ferroelectric ceramic samples were prepared from high-frequency oxides using traditional two-stage solid-phase synthesis technology. Measurements of the dielectric response on plane-parallel samples of size S = 15 mm^2 (coated with silver electrodes) and thickness d = 0.5 mm were carried out using a bridge method device with in a weak alternating field with a frequency of 1 kHz and with a stepwise supply constant bias field $E_=$ with a step 1 kV/cm.

Figure 1 illustrates the reversible dependences for two ferroelectric ceramic compositions with cobalt oxide concentration x=0 and x=0.3 wt%. It was found that in the composition of ceramics $Ba_{0.95}Pb_{0.05}TiO_3$ does not contain cobalt, in addition to the maxima $\varepsilon'(E_=)$, corresponding to the coercive fields $\pm E_c$, for some values of the bias field $|E_=| > |\pm E_c|$ at the increasing and decreasing of $E_=$, the local minima of $\varepsilon'(E_=)$ appears. These minima are likely due to the clamping effect of the antiparallel domain structure, known as the Drougard-Young effect. The presence of cobalt into ferroelectric ceramics leads to the fact that in the used interval $E_=$ local minima $\varepsilon'(E_=)$ disappear. At the same time, the diffusion of the maxima $\varepsilon'(E_=)$ in this region of E_c increases with a simultaneous increasing the values E_c.

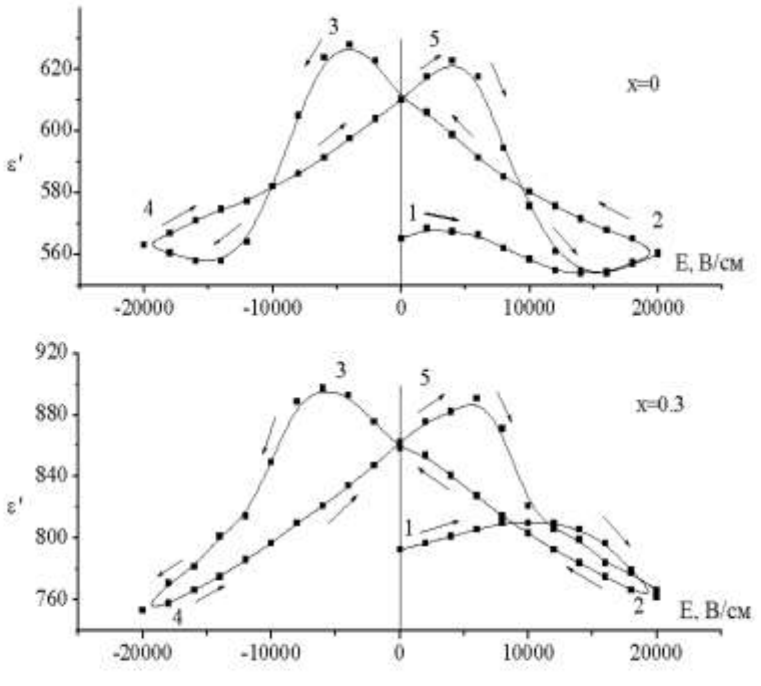

Figure 1. Reversive dependences of $\varepsilon'(E_=)$ in $(1-x)Ba_{0.95}Pb_{0.05}TiO_3+xCo_2O_3$ compounds (x = 0 and 0.3 wt%) at T = 25°C.

P2

Photoelectric response of KNN ferroelectric ceramics doped with barium titanate

S.R. Al Saedi, A.V. Sopit, L.V. Zhoga

Volgograd State Technical University, 400074, Volgograd, Russia
sandrej74@mail.ru

Interest in the study of processes occurring in disordered ferroelectric materials is due to their wide application in various electronic devices and devices for converting light energy into electrical energy. The investigation of the photosensitive characteristics of lead-free ferroelectric ceramics based on potassium niobate (KNN) is a promising direction in the search for materials that can be used in the development of non-volatile memory devices that using non-destructive readout techniques [1].

The aim of the present work is to study the effect of $BaTiO_3$ additives on the behavior of photoresponse in short-circuited KNN-based ferroceramic samples when illuminated with light at room temperature.

The studies were carried out on polycrystalline ceramic samples of KNN-based with different concentrations of barium titanate (KNNS7–*x*BT, where x = 0; 2 and 4 mol%) [2] for the form of plate 0,5 mm thick with silver electrodes obtained by burning a silver-containing paste. The method of measuring the photocurrent is described in [3].

Figure 1 demonstrates that, as the concentration of barium titanate increases, there is a notable augmentation in photocurrent, both within the transition region and the steady-state current region (curves 1). Analysis of the acquired outcomes suggests that the magnitude of photocurrent is significantly influenced by remaining polarization, which rises at room temperature as the concentration of *x*BT increases.

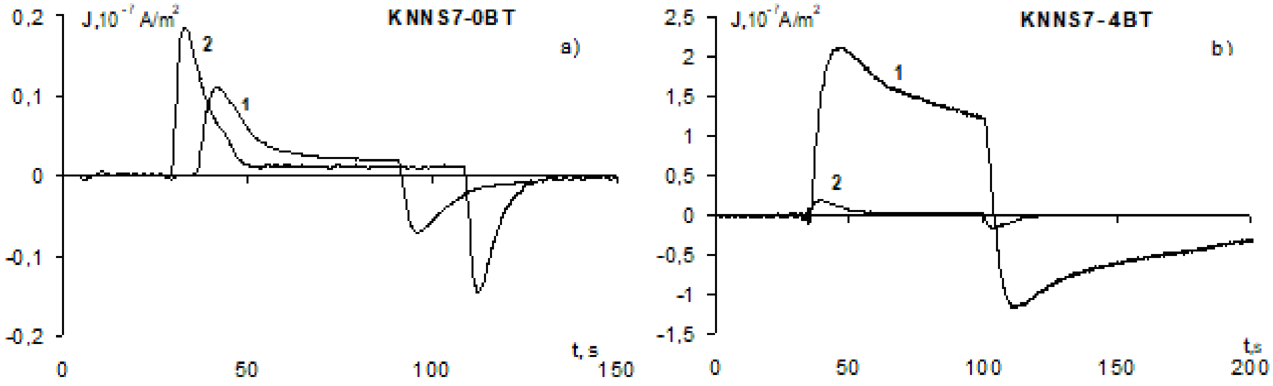

Figure 1. Photocurrent density kinetics of the KNNS7-*x*BT ferroelectric ceramics at room temperature. Curves: 1 - before heating, 2 - after heating the samples to the temperature of the TFP region.

It is shown that after heating the KNNS7-0BT sample to a temperature a few degrees below the structural phase transition temperature (SPT) [4], the steady-state photocurrent values decrease (curve 2a), caused by partial depolarization of the sample. At the same time, the increase in photocurrent in the peak region can be explained by the increase in the concentration of non-equilibrium charges induced by light. Apparently, the emergence of current carriers is facilitated by the decrease in the depth of the charge traps after heating the sample. Heating the KNNS7-4BT sample to the temperature a few degrees above the SPT temperature causes the photoresponse to disappear (curve 2b) obviously due to sample depolarization.

The mechanisms responsible for the photocurrent behavior both in the transition region and in the steady-state photocurrent region are discussed.

1. R.M. Magomadov, *Avtoref. dr. f.-m. sciences: 01.04.07.* (Grozny), 25 (2014).
2. I. Smeltere, *Summary of the doctoral thesis* (Riga: RTU), 27 (2012).
3. V.K. Yarmarkin, *Phys. Solid State* **42**, 511 (2000).
4. A.I. Burchanov, S.R. Al Saedi, K. Bormanis, *Ferroelectrics* **591**, 26 (2022).

Structural features of nonstoichiometric solid solutions of Pb(B’$_{1/3}$B”$_{2/3}$)O$_3$-based relaxor ferroelectrics

A.S. Alaverdova, A.R. Lebedinskaya

Academy of Architecture and Arts, Southern Federal University, 344090, Rostov-on-Don, Russia
Alexandra_2001@rambler.ru

Currently, the attention of scientists around the world is drawn to the study of unusual and unique properties of ferroelectrics with a diffuse phase transition, which are called relaxor ferroelectrics. Most relaxors are ternary oxides with a perovskite structure and are characterized by a composition of the A(B’$_{1/3}$B”$_{2/3}$)O$_3$ type. Particular interest in this class of compounds is due to the fact that they can be the basis for the creation of a new generation of functional materials for the needs of microelectronics, piezotechnics, computer technology, etc.[1] However, despite the more than half-century history of their fairly active research, a clear understanding of the relationship between the unique physical properties of relaxors and the structural features that determine them has not yet been achieved.

It has been established that relaxors Pb(B’$_{1/3}$B”$_{2/3}$)O$_3$ are characterized by a nonstoichiometric arrangement of atoms in the B-sublattice [2,3]. The size of the nonstoichiometry region depends on many factors, such as the size of the atoms and their nature of interaction. The key question is how nonstoichiometry affects the observed physical properties. Many experiments have shown that the properties of compounds are affected not by the nonstoichiometric atoms themselves, but by the defects that are formed as a result of deviations from stoichiometry. physical properties of these compounds [3,4].

The purpose of this work was: firstly, to study the possible types of violations that arise in these structures in the B-sublattice and oxygen octahedra using the example of crystals and solid solutions based on lead magnoniobate; secondly, building a model of the distribution and interaction of these structural defects in the crystal lattice of compounds such as Pb(B’$_{1/3}$B”$_{2/3}$)O$_3$ in order to understand the possible mechanisms of emerging structural and phase transformations [5].

Differences in the ionic radii and valences of the B′ and B″ cations affect the degree of disorder. With a larger difference between these values, the degree of ordering is higher, which is manifested in X-ray diffraction experiments in the form of superstructural reflections. It has now been established that the formation of the relaxor state and the temperature broadening of the relaxor maximum of dielectric constant are directly influenced by an increase in the degree of disorder. It has been shown that atomic disorder is not decisive in the dynamics of the perovskite crystal lattice. Based on the results of our own research and literature data, we assessed the presence in the structures under consideration of two mechanisms for the occurrence of crystal lattice distortions: due to changes in the relative position of BO$_6$ octahedra relative to each other and the occurrence of crystal lattice defects due to the presence of oxygen vacancies [2,6].

1. G.A. Smolensky, A.I. Agranovskaya, V.A. Isupov, *Solid State Physics* **1**, 990 (1959).
2. A.R. Lebedinskaya, A.G. Rudskaya, *IOP Conf. Ser.: Mater. Sci. Eng.* **1008**, 012061 (2020).
3. P.V. Kovtunenko, *Physical chemistry of solids: Crystals with defects* (M.: Higher School), 352 (1993).
4. V.P. Zlomanov, *Soros Educational J.* **7**, 29 (2001).
5. A.Yu. Gufan, *Solid State Phys.* **47**, 1097 (2005).
6. Yu.D. Tretyakov, *Soros Educational J.* **4**, 35 (1999).

P4

Preparation and ferroelectric properties of pyrochlore-free $Pb(Mg_{1/3}Nb_{2/3})O_3$-based solid solutions

A.S. Alaverdova[1], A.R. Lebedinskaya[1], A.G. Rudskaya[2], Yu.V. Kabirov[2]

[1]*Academy of Architecture and Arts, Southern Federal University, 344090, Rostov-on-Don, Russia*
[2]*The Department of Physics, Southern Federal University, 344090, Rostov-on-Don, Russia*
Alexandra_2001@rambler.ru

Lead magnoniobate $PbMg_{1/3}Nb_{2/3}O_3$ (PMN) has traditionally been a model object for studying the physical properties of ferroelectric relaxors. The main reason for studying ferroelectric relaxors is to understand the relationship between observed physical properties and structural characteristics.

The starting PMN-containing solid solutions can be synthesized in two ways: 1) using solid-phase synthesis, in which compounds are formed during a solid-phase reaction at high temperatures (below the melting point); 2) using chemical synthesis [1].

Only the perovskite PMN phase has the properties of a ferroelectric relaxor. It has been reliably established that the most important role in the correct course of solid-phase synthesis is played by the following indicators of the initial components: dispersion of the initial substances, their modification, synthesis temperature and synthesis time.

The main method for the synthesis of complex lead-containing oxides is the thorough grinding and mixing of these oxides into a mixture, and then pressing the resulting mixture into tablets, which are then fired at temperatures of 700 - 1000°C. For lead magnoniobate, this synthesis method is not ideal, because impurity phases in the form of pyrochlore appear during the firing process, which deteriorate the properties of PMN [1].

Mixtures of the initial oxides PbO, MgO, Nb_2O_5, corresponding to the compositions $(1-x)PbMg_{1/3}Nb_{2/3}O_3 - xPbMg_{1/2}Nb_{1/2}O_{2,75}$ with $0 \leq x \leq 1$ with a step of $\Delta x = 0.1$ were ground in ethyl alcohol for 60 minutes and pressed into tablets with a diameter of 10 mm and a height of 2 mm.

The next stage of the oxide solid-phase synthesis of lead magnoniobate in the perovskite phase is the activation of the reagents by changing the thermal history, which makes it possible to change its crystal structure, or rather its type. The samples obtained at the previous stage were fired at a temperature T = 880°C for 3 hours (with a heating time from room temperature of 1 hour) in an air atmosphere without the use of any backfill [2].

We studied the features of each stage of the solid-phase synthesis of lead magnoniobate in order to increase the yield of the perovskite phase during solid-phase oxide synthesis. It was found that when the samples are heated to a temperature of 650°C, no reactions occur in the system. With further heating to 700°C, the pyrochlore phase is formed, and at 850°C the perovskite phase is formed. With a further increase in temperature, the amount of perovskite phase continues to increase. During the synthesis, the dependence of the completeness of the synthesis of lead magnoniobate on the composition of the charge and the firing temperature was obtained.

The effect of excess lead oxide on the synthesis results was determined. It turned out that excess PbO affects, firstly, an increase in the density of the samples, and secondly, the contribution of intergranular layers to the dielectric constant of the ceramic.

1. G.A. Komandin, O.E. Porodinkov, A.A. Bush, et al., *Solid State Physics* **59**, 2343 (2017).
2. A.R. Lebedinskaya, A.G. Rudskaya, *Abst. Book Int. Conf. Materials Science and Nanotechnology* (MSN-2023) 152 (2023).

P5

Band structure topology and magnetic properties of GdNiSb and GdSb compounds

S.T. Baidak[1,2], R.D. Mukhachev[1], A.V. Lukoyanov[1,2]

[1] *M.N. Mikheev Institute of Metal Physics, Ural Branch, Russian Academy of Sciences, 620108, Ekaterinburg, Russia*

[2] *Institute of Physics and Technology, Ural Federal University, 620002, Ekaterinburg, Russia*
baidak@imp.uran.ru

Ternary GdNiSb and binary GdSb compounds have been investigated in terms of their electronic, optical properties and band structures using DFT+U method. This method allowed us to correctly account for strong electron correlations in the 4f shell of the rare earth elements [1]. The conducted calculations demonstrated that GdNiSb is a semiconductor with an indirect gap from high-symmetry point Γ to X with the value of 0.26 eV. Additional calculations with spin-orbit coupling included resulted in the increase of the band gap to 0.38 eV in GdNiSb. It was also demonstrated in our additional calculations for the compressed unit cells that a semiconductor-to-metal transition occurs in GdNiSb with specific topologically non-trivial states for some volumes of the unit cell. The binary GdSb compound is found to be a semimetal with the hole and electron pockets near high-symmetry points Γ and X, as can be seen from the Fermi surfaces. We also found good agreement of the experimental and theoretical conductivity for both GdSb [2] and GdNiSb [3]. Thus, our theoretical results for topological features in the DFT+U band structure, optical and magnetic properties demonstrate that the combination of Gd and Sb in quantum materials may result in promising properties. This study was funded by the grant of Russian Science Foundation No 22-42-02021.

1. S.T. Baidak, A.V. Lukoyanov, *Int. J. Molecular Sci.* **24**, 8778 (2023).
2. Yu.V. Knyazev, Yu.I. Kuz'min, S.T. Baidak, et al., *Solid State Sci.* **136**, 107085 (2023).
3. Yu.V. Knyazev, S.T. Baidak, Yu.I. Kuz’min, et al., *Opt. Quant. Electron.* **56**, 650 (2024).

P6

Spin waves in nanoscale lateral coupled ferromagnetic and magnonic structures

V.V. Balayeva, M.A. Morozova

Saratov State University named after N.G. Chernyshevsky, 410012, Saratov, Russia
vkonda2000@mail.ru

Spin waves are promising information carriers due to their weak attenuation and short wavelength, which makes it possible to create much smaller nanoscale devices for data processing. [1]

The structures under study are laterally bound ferromagnetic films and magnonic crystals made of yttrium iron garnet (YIG) $Y_3Fe_5O_{12}$. The thickness of the films is 100 nanometers, and the width and length are on the order of micrometers. The diagram of the structures is shown in Figure 1. The external magnetic field $\overline{H_0}$ was directed in two ways: along the x–axis - surface magnetostatic waves (MSSW), along the y-axis - backward volume magnetostatic waves (BVMSW).

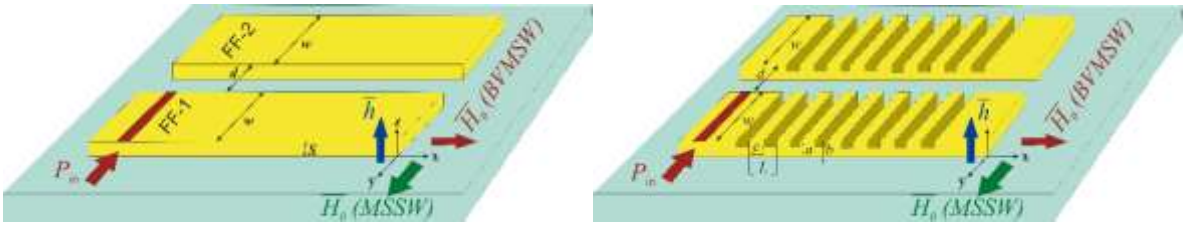

(a) (b)

Figure 1. Diagram of the structure based on laterally bound (a) ferromagnetic films, (b) magnonic crystals.

The main feature of the coupled structure is the propagation of two normal modes, symmetric and antisymmetric, at the same frequency [2]. This leads to periodic pumping of the signal between the layers along the structure length. The coupling length depends on the magnitude of the magnetic field, the orientation of the static magnetization of the waveguides, and the geometry of the structure. The equation for the coupling length can be obtained, for example, by energetically considering of bound MSW [3]:

$$\Lambda = 2\pi/(k_1 - k_2).$$

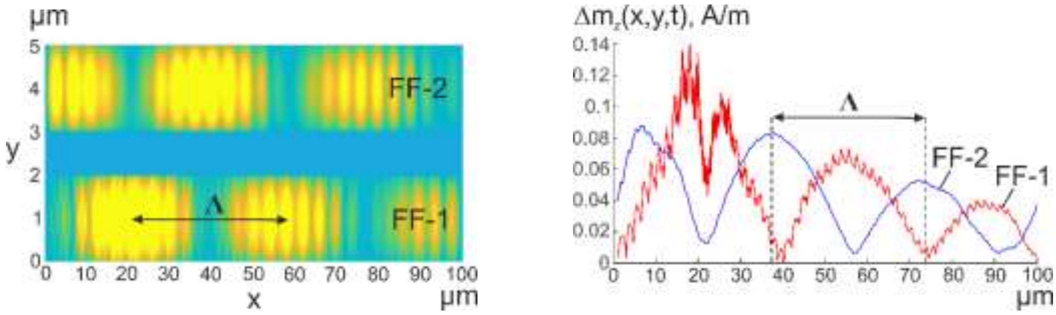

(a) (b)

Figure 2. Spatial distribution of the magnetization deviation $\Delta m_z(x,y,t)$ in the *xy* plane at the fixed *z* for BVMSW. (b) The dependence of the magnetization deviation taken along the center line of each film on the *x* coordinate. Calculation parameters: *w* = 2 microns, *d* = 1 microns.

On the basis of computations in micromagnetic modeling environment MuMax3, the features of propagation of surface and backward volume magnetostatic waves in nanoscale laterally coupled YIG waveguides are investigated.

Figure 3 shows the dependence of the pumping length Λ on the gap between the films *d* for different types of waves. For both BVMSW (Fig. 3a) and MSSW (Fig. 3b), the dependence is nonlinearly increasing. Each graph contains dependencies for different widths of films *w*. It can be seen that the pumping length is proportional to the width of the films *w*: for any gap value *d*, the greater the pumping length, the greater the films’ width. It is also seen that the pumping length for MSSW is greater than the pumping length for BVMSW. In Figure 3c shows the dependence of the difference in pumping lengths for MSSW and for BVMSW on the films' width *w* for different distances between the films *d*. It can be seen that the difference in pumping lengths increases both with an increase in the width of the waveguides and with an increase in the width of the films.

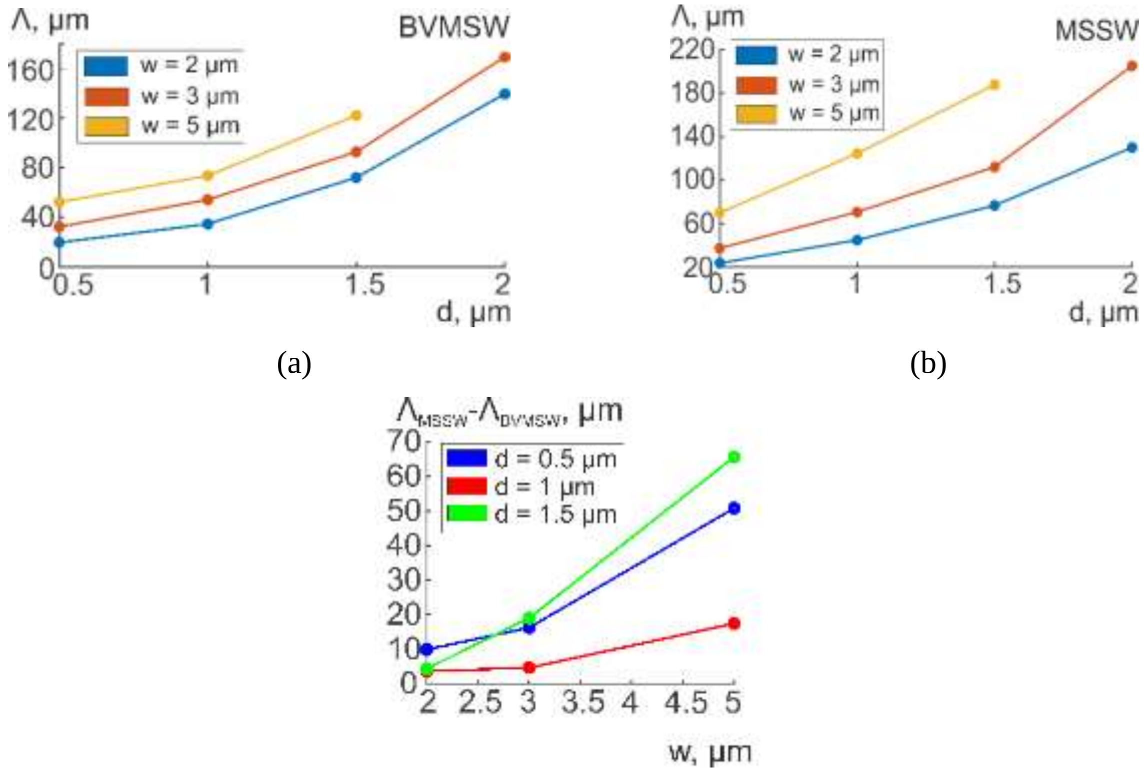

(a) (b)

(c)

Figure 3. The dependence of the pumping length on the gap between the films *d* with different films' widths *w* for (a) BVMSW, (b) MSSW; (c) The dependence of the difference in the pumping lengths of MSSW and BVMSW on the width of the films *w* and at different gap widths *d*.

A pecularity of periodic structures (Fig. 1b) is the presence of bragg resonances, which cause band gaps – non-transmission bands - appear in the spectrum of propagating waves [4, 5]. However, in the coupled structures, including magnonic crystals, the signal supplied to the ferromagnetic film at the band gap frequency is not pumped between the layers.

This feature allows to implement the function of demultiplexing based on the structure investigated. Depending on the frequency, the signal exits through different output ports of the structure, i.e. the structure under study allows for frequency channel separation - demultiplexing. The frequency range coming out to this port is determined by the value of the magnetic field applied to the ferromagnetic layers.

The research was supported by Russian Science Foundation (grant № 23-29-000759).

1. А.В. Вашковский Магнитостатические волны в электронике СВЧ / А.В. Вашковский, В.С. Стальмахов, Ю.П. Шараевский. – Саратов: *Изд –во Сарат. ун –та*, С. 48. (1993).

2. А.В, Вашковский Магнитостатические волны в электронике СВЧ / А.В. Вашковский, В.С. Стальмахов, Ю.П. Шараевский. – Саратов: *Изд –во Сарат. ун –та*, С. 119-121 (1993).

3. М.А. Малюгина (М.А. Морозова), Ю.П. Шараевский / Моделирование нелинейных процессов на магнитостатических волнах в связанных ферромагнитных структурах // *Изв. вузов. Прикладная нелинейная динамика* 8, С. 59-70 (2000).

4. A. Barman, G. Gubbiotti, S. Ladak et al., *J. Phys.: Cond. Matter* **33**, 413001 (2021).

5. A.A. Nikitin, A.V. Kondrashov, A.B. Ustinov et al., *J. Appl. Phys.* **122**, 153903 (2017).

P7

Metal-insulator transition in strongly correlated manganese sulfide

E.D. Chernov[1], A.V. Lukoyanov[1,2]

[1]*M.N. Mikheev Institute of Metal Physics, Ural Branch, Russian Academy of Sciences, 620108 Ekaterinburg, Russia*
chernov_ed@imp.uran.ru

[2]*Ural Federal University named after the first President of Russia, B. N. Yeltsin, 620002, Ekaterinburg, Russia*

Transition metal chalcogenides have the potential to be used as semiconductors [1], capacitors [2] and in catalytic and thermoelectric devices in solar panels [3] due to their optical, thermoelectric and transport properties [4]. Manganese chalcogenides MnX (S, Se, Te), which have several crystalline phases, are of particular interest. For MnS and MnSe, the cubic phase of the NaCl type is stable, while for MnTe, the hexagonal structure of the NiAs type is stable. Phase transitions under pressure were detected in manganese chalcogenides, in particular MnS [4]. These experimental studies link the phase transition with the spin transition of Mn^{2+} ions from a state with high spin $S = 5/2$ to a state with low spin $S = 3/2$. In this work, we present the results of first-principles calculation of the electronic structure and magnetic properties of strongly correlated manganese sulfide and metal-insulator transition under an uniform pressure is demonstrated. To take into account electronic correlations the 3d electronic shell the DFT+U method was used with Coulomb interaction parameter is equal to 6.9 eV and J parameter is equal to 0.86 eV. The calculations were performed for the antiferromagnetic ordering of the Mn atoms. The calculation shows 1.5 eV band gap and manganese magnetic moment is equal to 4.7 μ_B. With a decrease of the MnS cell volume to 70% relative to normal conditions, the insulator-metal transition was found, accompanied by the closure of the band gap, and a decrease in the magnitude of the magnetic moment of manganese ions to 4.5 μ_B. When the cell was compressed to 50% relative to normal conditions, the magnetic moment of manganese in MnS was 3.4 μ_B. Thus, in this work, we demonstrated the effect of pressure on the electronic structure and magnetic properties of manganese sulfide MnS, and metal-insulator transitions was investigated. It was found that with a decrease in the volume of the cell in manganese sulfide, the insulator-metal transition occurs, as well as a transition from a high-spin state to a low-spin one. The work was performed within the framework of the state assignment of the Ministry of Education and Science of the Russian Federation (theme "Electron", No. 122021000039-4).

1. R. Woods-Robinson, Y. Han, H. Zhang, et al., *Chem. Rev.* **120**, 9 (2020).
2. R. Barik, P.P. Ingole, *Curr. Opin. Electrochem.* **21**, 327 (2020).
3. W. Hussain, H. Malik, M. A. Khan, et al., *Mater. Chem. Phys.* **194**, 345 (2017).
4. S. Roychowdhury, M. Samanta, A. Banik, et al., *J. Solid State Chem.* **275**, 103 (2019).

P8

Phase transition in P(VDF-TrFE) copolymer films manufactured by 4D printing

S.I. Gudkov[1], A.V. Solnyshkin[1], N.V. Vostrov[1], E.V. Alexandrov[1], A.N. Belov[2]

[1]*Tver State University, 170100, Tver, Russia*
becauseimaphysicist@yandex.ru

[2]*National Research University of Electronic Technology, Zelenograd, Moscow, Russia*

Polyvinylidene fluoride (PVDF) is a ferroelectric homopolymer in which the ferroelectric to paraelectric phase transition does not occur until the melting point. In contrast, its ferroelectric copolymer with trifluoroethylene P(VDF-TrFE) undergoes a phase transition to the paraelectric phase, and the phase transition temperature decreases with increasing trifluoroethylene content. This paper presents information on phase transitions in 4D printed P(VDF-TrFE) copolymer films.

The copolymer films were prepared by layer-by-layer deposition from the solution containing P(VDF-TrFE) 72/28 onto a heated surface. The films had a thickness of 7 – 15 μm depending on the printing conditions. The manufactured samples did not have macroscopic polarization. To form macroscopic polarization, some of the samples were polarized in a corona discharge. Aluminum electrodes were deposited on the film surfaces. LCR meter E7-30 was used to determine the dielectric characteristics of the films. The measuring signal was equal to 1 V and the frequency varied from 25 to $3\cdot10^6$ Hz.

For the P(VDF-TrFE) 72/28 copolymer, the characteristic temperature of the ferroelectric phase transition is 110 – 112°C. The relative permittivity of the studied unpolarized P(VDF-TrFE) copolymer films increases monotonically with increasing temperature. The relative permittivity reaches maximum value at a temperature of 110°C. This corresponds to the Curie temperature. An increase in the measuring signal frequency causes a decrease in the maximum value of the relative permittivity and an expansion of the Curie region. But at the same time, the temperature at which the maximum value of the relative permittivity is achieved does not depend on the frequency of the electric field, as in classical ferroelectrics.

Polarizing the samples leads to a decrease in relative permittivity by 20 – 25%. This may be the result of a polarization process. Firstly, polarization at a temperature close to the temperature of the ferroelectric phase transition contributes to an increase in the proportion of the polar β-phase, which has a lower relative permittivity. Secondly, the decrease in relative permittivity is associated with the internal electric field, which prevents dipole oscillations and promotes a stable polarized state. This field is due to the space charge that is formed during the film polarization at the interphase boundaries, in particular between the α-phase and β-phase.

A study of the temperature dependence of the dielectric characteristics for polarized P(VDF-TrFE) films showed that the relative permittivity increases with increasing temperature. But the value of the relative permittivity does not exceed the value of the relative permittivity of unpolarized samples. It is important to note that the maximum relative permittivity of polarized samples shifts to the high-temperature region by 10°C. At a temperature of about 120°C, the relative permittivity values for polarized and unpolarized films are the same. With a further increase in temperature, the relative permittivity of both films decreases almost synchronously. Thus, the decay of the unipolar state in polarized samples occurs before the relative permittivity of polarized films reaches the value of the relative permittivity of unpolarized films.

Similar temperature dependences of relative permittivity are typical for ferroelectrics with significant biasing electric fields. Using Wieder's law, the strength of this field was estimated: it is approximately $5\cdot10^5$ V/m. This value is much lower than the coercive field for P(VDF-TrFE)72/28, recorded at room temperature ($3.8\cdot10^7$ V/m). But the strength of this field is sufficient to maintain a stable polarized state formed during polarization by the corona discharge field.

The work was supported by the Russian Science Foundation grant No. 23-22-00224, https://rscf.ru/project/23-22-00224/

P9

Features of conductivity of charged domain walls in chemically reduced lithium niobate crystals

A.M. Kislyuk, I.V. Kubasov, T.S. Ilina, A.V. Turutin, M.D. Malinkovich, V.P. Ivanov,
E.E. Maksumova, V.V. Kuts

National University of Science and Technology MISIS, Moscow, 119049, Leninsky av. 4, Russia
akislyuk94@gmail.com

Charged domain walls (CDWs) in ferroelectric materials are of interest from both fundamental and applied perspectives, as they exhibit electrophysical properties distinct from the bulk material. One of the most interesting materials for the formation of CDWs is the ferroelectric lithium niobate ($LiNbO_3$, LN), which has a uniaxial domain structure in which the vectors of spontaneous polarization of neighboring domains are always antiparallel to each other. The thermal and chemical stability, high Curie temperature (about 1140°C), commercial availability of wafers of various diameters and crystalline cuts with reproducible properties make LN an ideal model object for studying the properties of CDWs. With the correct selection of technological parameters, it is possible to form a single extended isolated CDW located in the middle of the crystal thickness (the so-called "bidomain" crystal). CDWs in bidomain LN crystals of the "head-to-head" (H-H) and "tail-to-tail" (T-T) types are characterized by the presence of a strong local electric field induced by the bound charges of ions. During heat treatment in a reducing atmosphere, small-radius polarons form in congruent LN crystals, which concentrate near H-H type CDWs under the influence of the electric field, resulting in the formation of a conductive channel within the dielectric material. A reductive annealing was performed in a nitrogen atmosphere at a temperature of 1100 °C for 1 hour.

In this work, the conductivity of bidomain reduced LN crystals in the immediate vicinity of CDWs H-H and T-T type was studied using atomic force microscopy methods. It was found that H-H type CDWs have increased electrical conductivity compared to the single-domain area when a positive voltage is applied to the AFM probe, while the current through T-T type CDWs does not differ from the current in the single-domain area.

It has been experimentally shown that with an increase in temperature, the electrical conductivity near H-H type CDWs decreases compared to the monodomain region. For H-H type CDWs, the activation energy of polaron drift mobility is approximately 0,79 ± 0,06 eV. The activation energy of polaron drift mobility in the monodomain region is approximately 0,64 ± 0,04 eV.

Using conductive probe microscopy image processing, the Debye screening length of the H-H type CDW field was determined to be 90 ± 10 nm. The concentrations of charge carriers screening the field of the charged domain wall can be calculated using the proposed model; for the samples of reduced bidomain LN investigated in this work, the concentration of polarons at the charged domain wall of the H-H type exceeds the concentration in the single-domain area by 30 times and is approximately $3,8 \cdot 10^{17}$ cm^{-3}.

The obtained results have fundamental and technological significance for the creation of devices that utilize the properties of CDWs and are at the intersection of optics, electronics, and mechanics.

The study was carried out with financial support from the Russian Science Foundation (grant No. 24-29-20303 https://rscf.ru/project/24-29-20303/).

P10

Variation of bandgap and Urbach tail in proton–exchanged $LiNbO_3$ waveguides, depending on phase composition of $Li_{1-x}H_xNbO_3$

S.M. Kostritskii[1], V.A. Fedorov[1], O.G. Sevostyanov[2], I.M. Chirkova[2]

[1]RPC Optolink, Zelenograd, 124489, Moscow, Russia
skostritskii@optolink.ru

[2]Kemerovo State University, 650000, Russia

It has been established that the absorption edge (AE) and, thus, the direct bandgap energy E_g^d depends on phase composition of $Li_{1-x}H_xNbO_3$ in proton-exchanged waveguides (Fig. 1). Shift of fundamental AE is clear evidence of E_g^d change and, thus, analysis of the optical absorption spectra allowed to determine the variation of E_g^d in the proton-exchanged waveguides [1]. It gave possibility for satisfactory estimation of electro-optic coefficients r_{13} and r_{33} in the $Li_{1-x}H_xNbO_3$ phases [1]. At the same time study of optical absorption spectra may provide data about variation of indirect bandgap E_g^{ind} and Urbach E_U energies at variation of phase composition of $Li_{1-x}H_xNbO_3$. Such data is important to know for nonlinear integrated-optical applications, where nonlinear absorption and scattering may provide some limitations [2].

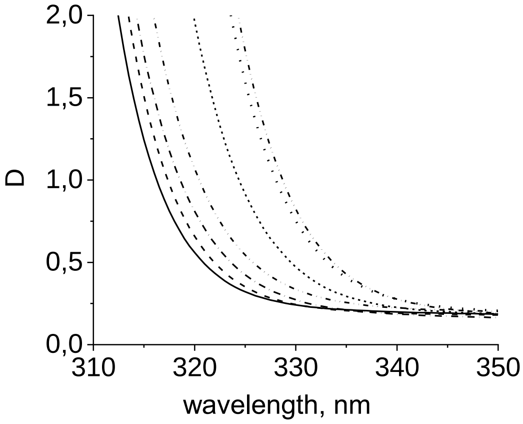

Figure 1. Optical absorption spectra of the samples containing different $Li_{1-x}H_xNbO_3$ phases: cLN, α*, α**, κ_1, κ_2, β_1 and β_2. This samples order corresponds to spectra sequence from left to right side at the optical density $D = 1$. Absorption spectrum of z-cut wafer of a pure congruent $LiNbO_3$ crystal (cLN) is given for reference. α* is the α phase in a strongly annealed waveguide with a small refractive index increment Δn_e, but α** is α phase in a moderately annealed waveguide with a larger Δn_e [1].

To characterise the bandgaps, Tauc relation [3] has been used:

$$\alpha h\nu \sim A(h\nu - E_g)^n$$

where A is a constant, hν photon energy, E_g is the allowed energy gap and n is an exponent determined by the nature of the electron transition during the absorption process. The value of n is ½ for allowed direct transition and 2 for allowed indirect transition.

Optical spectra in transmission mode were measured with a Shimadzu UV- 3101PC spectrophotometer in the visible and near-UV ranges (Fig. 1). The optical absorption spectroscopy data in near UV ranges were used to evaluate the spontaneous polarization P_i in proton-exchanged waveguides, as the shift of fundamental absorption edge, i.e. a marked reduction of energy E_g^d, has been related to the decrease of spontaneous polarization P_0 [4]:

$$P_i / P_0 = (\eta_0/\eta_i)^3 \times \{1 + (\Delta E_{g,i})/aP_0^2\}$$

where $P_0 = 0.71$ C/m^2, η is packing density, $a = -\,0.35$ eV m^4/C^2, $\Delta E_{g,i} = E_{g,0}^d - E_{g,i}^d$, subscripts i and 0 indicate on values for *i*-phase of $H_xLi_{1-x}NbO_3$ and virgin $LiNbO_3$ crystals, respectively. Note, that a red-shift of AE relative to the edge in cLN sample is observed in any *i*-phase studied (Fig. 1). By using the data on the band-gap shift $\Delta E_{g,i}$, the P_i were evaluated for all the $H_xLi_{1-x}NbO_3$ phases (Table 1). The results obtained demonstrate a strong degradation of P_i with increase x. The packing density η = 1.2 for

$LiNbO_3$ and $(\eta_0/\eta_n)^3 = 0.906$ for β_i phases, $(\eta_0/\eta_n)^3 \approx 1.0$ for α^* phase, $0.93 \leq (\eta_0/\eta_n)^3 \leq 0.99$ for α^{**} and κ_i -phases of $H_xLi_{1-x}NbO_3$.

Table 1. The data on E_g^d, E_g^{ind} and the values of spontaneous polarization P_i ($P_i^* = P_i/P_0$) for the various $H_xLi_{1-x}NbO_3$ phases in proton-exchanged $LiNbO_3$ waveguides.

phase	$E_{g,}^{d}$, eV	$\Delta E_{g,}^{ind}$, eV	P_i^*	P_i, C/m^2
cLN	3.930	3.79	1	0.71
α^*	3.921	3.78	0.94	0.67
α^{**}	3.914	3.76	0.88	0.62
κ_1	3.887	3.74	0.67	0.48
κ_2	3.841	3.69	0.43	0.31
β_1	3.802	3.65	0.24	0.17
β_2	3.791	3.64	0.19	0.13

For further insight of defects and disorder on the optical absorption processes near the band edge, logarithm of absorption spectra (lnα) is plotted as a function of incident photon energy. The linear region as observed in the plot near the band edge represents the exponential behavior of photon absorption processes resulting in absorption tail. An exponential character of AE, also known as Urbach tail, is observed in crystalline and amorphous materials. The exponential character of the absorption coefficient α near the fundamental AE is expressed by the Urbach rule [3]:

$$\alpha = \alpha_0 \exp[h\nu/E_U]$$

where α_0 is a characteristic crystal parameters, $h\nu$ is the incident photon energy, and E_U is Urbach energy, which is the width of the tails states in the bandgap associated with the structural defects and disorder within the crystal.

The linear region (exponential tail) is the direct manifestation of the presence of structural defects in the crystal, which result in formation of band tail states below (above) the conduction (valence) band and their density of states falls sharply with energy [3]. The straight line fit of the absorption data near band edge shows that the AE follows the Urbach tail behavior. The inverse of the slope of straight line fit of AE yield Urbach energy E_U: 96 meV (κ_1 and κ_2 phases), 82 meV (β_1 and β_2 phases), 80 meV (α^* and α^{**} phases) and 78 meV (cLN). Note, the Urbach energy of the order of 10–100 meV had been reported for amorphous semiconductors [3]. The observed increase in Urbach energy for κ_1- and κ_2-phases reveal the presence of additional structural or crystalline defects like low angle grain boundaries, additional growth sites on the surface, disorder, oxygen vacancies etc. This is in reasonable agreement with the high resolution X-ray diffraction studies, where higher FWHM is observed for κ_1- and κ_2-phases in comparison to CLN for the (00.6) reflection [5].

Therefore, the fabrication conditions, when using annealed proton exchange technology, should be selected so that the α^*- or α^{**}-phase waveguide is obtained with the appropriate values of E_U and P_i. The results obtained have allowed to optimize the processes of fabrication of integrated-optical devices based on proton-exchanged waveguides in $LiNbO_3$ crystals.

1. S.M. Kostritskii *et al*, *J. Appl. Spectr.* **82**, 234 (2015).
2. F. Laurell, M. G. Roelofs, H. Hsiung, *Appl. Phys. Lett.* **60**, 301 (1992).
3. R. Bhatt, *et al*, *Phys. Stat. Solidi A* **209**, 176 (2012).
4. M. Di Domenico, S.H. Wemple, *J. Appl. Phys.* **40**, 720 (1969).
5. Yu.N. Korkishko, V.A. Fedorov, S.M. Kostritskii, *J. Appl. Phys*. **84**, 2411 (1998).

P11

Contribution of surface and oxygen vacancies to the band structure of barium titanate thin ferroelectric films with resistive switching

M.V. Levichev[1], O.U. Vilkov[2], N.V. Andreeva[1], A.E. Petukhov[3]

[1]*Department of Micro- and Nanoelectronics St. Petersburg Electrotechnical University 'LETI', 197022, Saint Petersburg, Russia*
mvlevichev@etu.ru

[2]*Department of Solid State Electronics St. Petersburg State University, 198504, Saint Petersburg, Russia*

[3]*Research Park St. Petersburg State University, 198504, Saint Petersburg, Russia*

Oxygen vacancies govern the memristive properties of the resistive memory devices (ReRAM) built on thin-film oxides structures. In the case of ferroelectric (FE) thin films, the resistive switching behavior could be induced both by the presence of oxygen vacancies and reversible regulation of FE polarization [1]. However, in thin and ultrathin FE films, surface phenomena involving surface rearrangements and the influence of surface chemistry on the bulk material could also have a significant effect on resistive properties.

This paper presents a combined approach using both experimental and theoretical studies to determine the contribution to the memristive effect in thin FE films from both the atomic and electronic surface structure and the presence of oxygen vacancies in the film.

$SrTiO_3/La_{0.7}Sr_{0.3}MnO_3/BaTiO_3$ heterostructures with ~5 nm –thick epitaxial $BaTiO_3$ film have been studied experimentally by means of scanning tunneling and atomic force microscopies, and X-ray photoelectron spectroscopy (XPS) with ion sputtering. Also, relevant ab initio calculations in the framework of density functional theory (DFT) were carried out.

In Ba 4d and Ti 2p XPS spectra, additional doublets shifted from the main lines appear in investigated compositions. For DFT calculations the periodic slab models with 5.2 nm-thick BTO-film and different surface termination were considered to evaluate the influence of the surface on the electronic structure of the FE-film. The results of DFT calculations on a slab model predict the splitting of Ba 3d and 4d doublets for BTO-film terminated by a BaO layer. In this case Ba-cations on surface have a chemical environment different to the bulk, which inducing the shift of XPS spectra of topmost barium atoms core levels of the Ba $4d_{5/2}$ and $4d_{3/2}$ states towards the higher binding energies compared to the signal from the barium atoms from bulk layers of the film. These results are correlated with data obtained from synchrotron radiation photoemission techniques [2].

Two Ti 2p components revealed experimentally by XPS could be correctly reproduced by the results of DFT calculation of 2x2x2 BTO-supercell with the presence of oxygen vacancy in the BaO and TiO_2 layers. The Ti 2p doublet is shifted towards lower binding energies by a value of about 1.5 eV, and its relative intensity corresponds to an oxygen vacancy concentration of 10-15%. The latter agrees well the quantitative XPS analysis of the BTO-film composition, which gives a lack of oxygen and some excess of barium (about 10%) with respect to the perfect $BaTiO_3$ stoichiometry. Experiments carried out with scanning tunneling and atomic force microscopies confirm the enrichment of the films with barium, which, however, does not lead to the appearance of a separate Ba_2TiO_4 phase.

This research was funded by the Russian Science Foundation, grant number 21-79-20073.

1. N.V. Andreeva, E.A. Ryndin, A.E. Petukhov et al., *Adv. Electron. Mater.* 2300806 (2024).
2. P.-M. Deleuze, H. Magnan, A. Barbier et al., *J. Phys. Chem.* **126**, 37 (2022).

Amplitude and frequency processing of spin-wave signals in structures with magnon crystal and normal metal

N.D. Lobanov, M. A. Morozova

Saratov State University, 410071 Saratov, Russia
nl_17@mail.ru

Modern semiconductor electronics is currently facing a serious fundamental problem in the form of quantum limits. There is an urgent need to create alternative technologies for signal transmission. The developing branches of quantum electronics – magnonics [1,2] and spintronics [3,4] - can be an alternative for classical electronics. The fundamental difference between magnonics and semiconductor electronics is that signal transmission occurs due to precession of magnetic moments, which allows at least avoiding joule losses. And the principles of spintronics allow the use of spin transfer torque (STT) and spin current to change the signal in ferromagnetic layers.

The main structure considered is a model consisting of coupled magnon crystals separated by a normal metal [5]. Magnon crystals are ferromagnetic films with a periodic system of rectangular grooves. The normal metal is a metal with a large value of the spin Hall angle, i.e., the one with the most efficient conversion of electric current into spin current. The field is directed so that surface magnetostatic waves are excited in the ferromagnetic layers.

In this work, the signal passage through the coupled structure and the peculiarities of the spin current influence on the formation of forbidden zones are investigated. When a voltage is applied to a normal metal, an electric current starts to flow through the metal. Due to the applied voltage, the spin Hall effect occurs. The effect consists in the fact that due to spin-orbit interaction, the spins of charge carriers (electrons) are distributed in two opposite directions to the boundaries of the magnon crystal/normal metal interfaces. When the spin in the normal metal is co-directed with the magnetic moment in the normal metal, the wave is weakened, in the case of different directions of the spin in the metal and the magnetic moment in the ferromagnetic, the surface wave is strengthened.

Using the principles of amplification and attenuation, it is possible to effectively redistribute the signal power over different ports, suppress the pumping of spin waves. It is also possible to create and "kill" band gaps (non-transmission bands where the signal is strongly attenuated), to control the position of band gaps.

In general, technologies based on the methods of magnonics and spintronics expand the possibilities for expanding and creating new classes of devices based on the principles of quantum electronics.

This work was supported by the Russian Science Foundation (project № 23-79-30027).

1. S.L. Vysotskii et al., *IEEE Magn. Lett.* **8**, 3706104 (2017).
2. M.A. Morozova et al., *J. Appl. Phys.* **120**, 223901 (2016).
3. A. Brataas et al., *Physics Reports.* **885**, 1 (2020).
4. X. Wang, G. Guo, J. Berakdar, *Nature commun.* **11**, 5663 (2020).
5. X. Wang et al., *Phys. Rev. Appl.* **18**, 024080 (2022).

P13

Influence of impurity phases of the feedstock on the properties of ferroelectric material of the PZT system

M.A. Marakhovskiy, L.A. Dykina, V.V. Fil, A.A. Panich

Southern Federal University,344090, Rostov-on-Don, Russia
marmisha@mail.ru

In the serial production of ferroelectric materials of the PZT system, the presence of various impurity phases in the feedstock is periodically observed. The origin of impurities and their concentration in the feedstock most often vary for a fixed component from batch to batch. The presence of such impurities can significantly affect the final properties of ferroelectric materials and ceramics based on them.

As a result of spectral analysis of the basic feedstock (PbO, ZrO_2, TiO_2) performed on an X-ray fluorescence wave dispersion spectrometer (ARL OPTIM"X 200W), a group of impurity phases (Sb, Na, Bi, K, Fe) of various concentrations was recorded.

The purpose of this work was to study the effect of metal ions of impurity phases of the feedstock on the electrophysical parameters of ferroelectric materials.

A ferroelectric material of the PZT system with a perovskite structure and a nominal chemical formula $Pb_{0,95}Sr_{0,05}(Zr_{0,53}Ti_{0,47})O_3$ + 1% Nb_2O_5 was selected as a model object of research. The specified composition is characterized by high values of relative permittivity ($\varepsilon^T_{33}/\varepsilon_0$ ~ 1800-2000), relatively high values of piezoelectric modulus (d_{33} ~ 380-500 pCl/N), acceptable temperature stability (T_c ~ 290 °C), as well as high reproducibility of properties from batch to batch.

Ferroelectric material of the specified composition was produced by solid-phase synthesis with grinding in a planetary ball mill Fritsch Pulverisette 6. Synthesis of ferroelectric material and sintering of ceramic elements based on it were carried out in a chamber furnace Nabertherm L5/13/P330.

The sintering quality of ceramic elements was assessed based on the results of X-ray phase analysis, microstructure images obtained with a scanning electron microscope (JEOL JSM-6390LA) and density values determined by hydrostatic weighing.

As a result of the study, the dependences of the influence of impurities on the dielectric and electrophysical properties of the ferroelectric material of the CTS system were established. The analysis of the obtained results showed the relevance of the intentional introduction of K and Na impurities in order to reduce the values of relative permittivity by 40-45% (to the values of $\varepsilon^T_{33}/\varepsilon_0$ ~ 720-970). This is accompanied by an increase in the values of the specific voltage sensitivity (g_{33}) by 1.4 times. Such a modified composition of ferroelectric material can be used in electronic acoustic transducers operating in reception mode.

The study was carried out within the framework of the state assignment of the Ministry of Science and Higher Education of the Russian Federation, project No. FENW-2022-0033

1. M. J. Haun, E. Furman, S.J. Jang et al., *J. Appl. Phys.* **62**, 8 (1987).
2. A.Y. Malykhin, L.A. Dynkina, A.E. Oparina, et al., patent No. 2024620147 Russian Federation. 11.01.2024.
3. H.S. Bhatti, S.T. Hussain, Khan, et al., *Appl. Surf. Sci.* 367, (2016).

P14

Monte Carlo studies of magnetic phase transitions in (1-*x*)$BiFeO_3$ – *x*$PbFe_{1/2}Sb_{1/2}O_3$ solid solutions

A.V. Motseyko[1], A.V. Pushkarev[2], N.M. Olekhnovich[2], Y.V. Radyush[2], N.V. Ter-Oganessian[1]

[1]*Institute of Physics, Southern Federal University, 344090, Rostov-on-Don, Russian Federation*
moceyko@sfedu.ru

[2]*Scientific and Practical Center for Materials Science of the NAS of Belarus, 220072, Minsk, Belarus*

Bismuth ferrite, $BiFeO_3$ (BFO), and solid solutions based on it are considered as perspective multiferroics, i.e., materials with simultaneous magnetic and ferroelectric orderings. One of such solid solutions is (1-*x*)$BiFeO_3$ – *x*$PbFe_{1/2}Sb_{1/2}O_3$. $PbFe_{1/2}Sb_{1/2}O_3$ (PFS) is considered multiferroic as it experiences a high maximum of the dielectric constant at 190 K and electric polarization loops below this temperature [1]. The magnetic properties of PFS as well as its magnetic ground state are subject to debates. At temperatures between 150 K and 250 K strongly relaxing superspins are proposed, which transform into a superspin spin glass state below 150 K [2]. In another work a long-range antiferromagnetic ordering below 30 K is observed with the propagation vector (1/2,1/2,0) [2]. The problem of magnetic ordering is also complicated by the strong tendency of PFS to form cation-ordered structures and arguable dependence of magnetic properties on the degree of atomic ordering.

In this work we study the magnetic phase transitions in the (1-*x*)$BiFeO_3$ – *x*$PbFe_{1/2}Sb_{1/2}O_3$ solid solutions using the Monte-Carlo method. We identify the evolution of magnetic phase transition temperature and the type of appearing magnetic ordering in these solid solutions with the PFS concentration *x* and consider different cases of Fe – Sb atomic ordering: disordered, clustered, or with varying degree of atomic ordering.

This study was supported by joint Russia-Belarus scientific project (Russian Science Foundation project 23-42-10024 and BRFFR project T23RNF-086).

1. V.V. Laguta, V.A. Stephanovich, M. Savinov, et al., *New J. Phys.* **16**, 113041 (2014).
2. B. Argymbek, T. Kmjec, V. Chlan, et al., *J. Magn. Magn. Mater.* **477**, 334 (2019).

P15

Magnetic structures of orthonickelates at charge disproportionation

S.V. Nuzhin[1], Yu.D. Panov[1], A.S. Moskvin[1,2]

[1]*Institute of Natural Sciences and Mathematics, Ural Federal University, 620002, Ekaterinburg, Russia*
nuzhin.stepan@urfu.ru

[2]*Institute of Metal Physics, UD RAS 620180, Ekaterinburg, Russia*

Rare-earth orthonickelates $RNiO_3$ (R is a rare-earth element and yttrium) are Jahn-Teller magnetics [1] with perovskite structure. Due to the presence metal-insulator transition in the family of compounds, the question of the magnetic structure and the its formation mechanism remains open [2-4]. We proceed from the idea that the Ni^{3+} ion in the low-spin state $t^6_{2g}e_{1g}$ in the octahedral environment of oxygen forms a Jahn-Teller center with the ground orbital doublet ^2E_g [1]. The removal of orbital degeneracy is carried out in two alternative ways: due to charge disproportionation or the Jahn-Teller effect [5]. The simplified hamiltonian that takes into account both options for removing the degeneracy of the Jahn-Teller center and the exchange interaction is written in the pseudospin formalism in the following form

$$\hat{\mathcal{H}} = \hat{\mathcal{H}}_{ch} + \hat{\mathcal{H}}_{spin},$$

$$\hat{\mathcal{H}}_{ch} = \Delta \sum_{i} \hat{\Sigma}^2_{iz} + V \sum_{\langle i,j \rangle} \hat{\Sigma}_{iz}\hat{\Sigma}_{jz},$$

$$\hat{\mathcal{H}}_{spin} = J_1 \sum_{\langle i,j \rangle} \hat{S}_{iz}\hat{S}_{jz} + J_2 \sum_{\langle\langle i,j \rangle\rangle} \hat{S}_{iz}\hat{S}_{jz},$$

where the i node corresponds to the $|\Sigma\sigma; Sm\rangle$ vector states of the octahedron. $|10;\frac{1}{2}m\rangle$ vector at $m = \pm\frac{1}{2}$ is associated with the octahedral state in the configuration $t^6_{2g}e_{1g}$;E_g, $|1-1;1m\rangle$ vector at $m = \pm1, 0$ and $|11;00\rangle$ vector are mapped to the octahedral state in the configurations $t^6_{2g}e^2_{2g}$;$^3A_{2g}$ and t^6_{2g};A_{1g}, respectively. In the $\hat{\mathcal{H}}_{ch}$ hamiltonian charge part first and second terms consider, respectively, local and nonlocal charge-charge correlations. In the $\hat{\mathcal{H}}_{spin}$ spin part of the hamiltonian, the first and second terms consider the isotropic exchange interaction, respectively, between the first and second nearest neighbors.

In this paper we discuss the differences between the magnetic structure types of orthonickelates with $P2_1/n$ symmetry and magnetic perovskites with space group $Pbnm$. In the mean-field approximation, we have obtained the conditions for the appearance of orthonickelate magnetic structures and their reorientation in the limit of full disproportionation and in the case of the Jahn-Teller effect.

This work was supported by the project FEUZ-2023-0017 of the Ministry of Education and Science of the Russian Federation.

1. A.S. Moskvin, *Magnetochemistry* **9**, 224 (2023).
2. J. L. García-Muñoz, et. al., *Phys. Rev. B* **50**, 978 (1994).
3. M. T. Fernández-Díaz, et al., *Phys. Rev. B* **64**, 144417 (2001).
4. G. Giovannetti, et al., *Phys. Rev. Lett.* **103**, 156401 (2009).
5. I.I. Mazin, et al., *Phys. Rev. Lett.* **98**, 176406 (2007).

P16

Modeling of magnetic and charge ordering in nickelates

Y.D. Panov[1], V.S. Ryumshin[1], V.A. Ulitko[1], A.S. Moskvin[1,2]

[1]*Institute of Natural Sciences and Mathematics, Ural Federal University, 620002, Ekaterinburg, Russia*
yuri.panov@urfu.ru

[2]*Institute of Metal Physics, UD RAS 620180, Ekaterinburg, Russia*

Rare-earth orthonickelates $RNiO_3$ have attracted continuous interest of researchers in the last decades due to the metal-insulator transition found in these compounds, preceding the transition to the magnetically ordered state [1], peculiarities of structural transformations and evidence of phase-separated states [2,3]. Theoretical description of these features within a unified approach is still an unsolved problem.

We consider orthonickelates as Jahn-Teller magnets [4], in which the low-energy state is formed by a charge multiplet. In $RNiO_3$ compounds with ideal NiO_6 octahedra, it is a charge triplet $[NiO_6]^{10-,9-,8-}$ (nominally $Ni^{2+,3+,4+}$) with different spin and orbital ground states. The Ni^{3+} ion in the low-spin configuration of the NiO_6 octahedron $\mathrm{t}_{2\mathrm{g}}^6\mathrm{e}_\mathrm{g}^1$ forms a Jahn-Teller center with a ground orbital doublet ^{2}E. However, the orbital degeneracy in $RNiO_3$ is lifted not due to the local/cooperative Jahn-Teller effect, but due to the charge disproportionation with the formation of Ni^{4+} and Ni^{2+} centers [5,6,7]. In this case, the electronic structure of the orthonikelate can be represented as a system of local composite spin-triplet bosons with the configuration $e_g^2;{}^3\mathrm{A}_{2\mathrm{g}}$ moving in a lattice of non-magnetic centers with the configuration $\mathrm{t}_{2\mathrm{g}}^6$.

The phase diagram for such a system of triplet bosons was obtained in the mean-field approximation [8]. For some values of the model parameters, the phases of charge ordering, antiferromagnetic insulator, and spin-triplet superconductor are realized, as well as the phase-separated state when two order parameters are simultaneously non-zero.

With all the variety of possible phase states, the type of phase transition to the charge-ordered state, as well as the accompanying effects of structure change in nickelates remain beyond the scope of the model [8]. The aim of the present work is to describe these key properties, which leads to the need to include a full octet of low-energy states in the model and to account for the interaction of the electron subsystem with the lattice.

The work was supported under grant FEUZ-2023-0017 of the Ministry of Science and Higher Education of the Russian Federation.

1. M.L. Medarde, *J. Phys.: Condens. Matter* **9**, 1679 (1997).
2. K.W. Post, A.S. McLeod, M. Hepting, et al., *Nature Phys*. **14**, 1056 (2018).
3. B. Mundet, C. Domínguez, J. Fowlie, et al., *Nano Lett.* **21**, 2436 (2021).
4. A. Moskvin, *Magnetochemistry* **9**, 224 (2023).
5. I.I. Mazin, D.I. Khomskii, R. Lengsdorf, et al., *Phys. Rev. Lett.* **98**, 176406 (2007).
6. A.S. Moskvin, *J. Phys.: Condens. Matter* **25**, 085601 (2013).
7. A.S. Moskvin, Y.D. Panov, *Phys. Solid State* **65**, 1081 (2023).
8. V.S. Rumshin, S.V. Nuzhin, Y.D. Panov, A.S. Moskvin, *Phys. Solid State,* to be published (2024).

P17

Asymptotic solution of the Landau-Khalatnikov equation for ferroelectric

A.E. Rassadin

HSE University, 603155, Nizhny Novgorod, Russia
brat_ras@inbox.ru

The relaxation of the initial distribution $\vec{P}_0(\vec{r})$ of the ferroelectric polarization vector is described by the Cauchy problem for the Landau-Khalatnikov equation:

$$\frac{\partial \vec{P}}{\partial t} = -\gamma \, \frac{\delta \Phi[\vec{P}]}{\delta \vec{P}} , \qquad \vec{P}(\vec{r},0) = \vec{P}_0(\vec{r}) , \qquad \vec{r} \in \mathbb{R}^3 , \tag{1}$$

where $\vec{P}(\vec{r},t)$ is ferroelectric polarization vector at time $t > 0$, γ is constant positive coefficient and $\Phi[\vec{P}]$ is thermodynamic potential of ferroelectric.

Further, let one suppose that the ferroelectric crystal has cubic symmetry and $\vec{P} = (0,0,P_z)$, then, within the framework of the Landau-Ginzburg-Devonshire theory, taking into account the spatial fluctuations of the order parameter P_z [1]:

$$\Phi[\vec{P}] = \int \left[\frac{g}{2}(\nabla P_z)^2 + \frac{\alpha\,(T-T_c)}{2}\, P_z^2 + \frac{b}{4}\, P_z^4\right] d^3x , \tag{2}$$

where $\alpha,\ b$ and g are constant positive parameters and T_c is the Curie temperature of the ferroelectric.

Substituting functional (2) in equation (1) one can obtain:

$$\frac{\partial P_z}{\partial t} = \gamma g \Delta P_z + \gamma \alpha (T_c - T) P_z - \gamma b P_z^3 . \tag{3}$$

If temperature $T < T_c$ and the characteristic size of initial distribution $P_{0z}(\vec{r})$ $L \gg \sqrt{g/\alpha(T_c - T)}$, then, according to method, developed in article [2], one can construct the asymptotic solution of equation (3), the leading term of asymptotic expansion being equal to:

$$P_z^{(0)}(\vec{r},t) = \sqrt{\frac{\alpha\,(T_c-T)}{b}}\, \frac{1}{\sqrt{1+\exp[-2\tau - A(\theta,\vec{\rho})]}} , \qquad \tau = \gamma \alpha (T_c - T)\, t . \tag{4}$$

The next term of asymptotic expansion is equal to:

$$\begin{gathered} P_z^{(1)}(\vec{r},t) = \frac{3g}{8L^2\sqrt{\alpha\,(T_c-T)b}}\, \frac{\exp[-2\tau - A(\theta,\vec{\rho})]}{(1+\exp[-2\tau-A(\theta,\vec{\rho})])^{3/2}} \cdot \\ \cdot \left[(\nabla_{\vec{\rho}} A(0,\vec{\rho}))^2 \ln 2 - (\nabla_{\vec{\rho}} A(\theta,\vec{\rho}))^2 \ln(1+\exp(2\tau))\right] \end{gathered} . \tag{5}$$

Function $A(\theta,\vec{\rho})$ in expressions (4) and (5) obeys to the following equation:

$$\frac{\partial A}{\partial \theta} = \Delta_{\vec{\rho}} A + \frac{1}{2}(\nabla_{\vec{\rho}} A)^2, \tag{6}$$

where $\theta = \gamma g t / L^2$ and $\vec{\rho} = \vec{r}/L$.

Equation (6) proves to be the Kardar-Parisi-Zhang equation [3].

The report considers asymptotic solutions of equation (3) with different initial conditions $P_{0z}(\vec{r})$. In particular, for initial conditions rapidly decreasing at infinity, it is shown that at long times the propagation velocity V of the line of the level of function (4) tends to the value:

$$V = 2\gamma\sqrt{g\alpha(T_c - T)} . \tag{7}$$

The relation (7) can be used to measure the parameter γ included in the Landau-Khalatnikov equation (1).

The method proposed in the report can be extended both to other orientations of the polarization vector $\vec{P}$ in ferroelectrics with cubic symmetry and to ferroelectrics with other classes of crystallographic symmetry.

1. B.A. Strukov, A.P. Levanyuk, *The physical basis of ferroelectric phenomena in crystal* (Nauka), 116 (1983).
2. V.S. Berman, *Doklady Akademii Nauk SSSR* **242**, 265 (1978).
3. M. Kardar, G. Parisi, Y.-C. Zhang, *Phys. Rev. Lett.* **56**, 889 (1986).

Monte Carlo study of model nickelate

V.S. Ryumshin[1], Y.D. Panov[1], S.V. Nuzhin[1], A.S. Moskvin[1,2]

[1]*Institute of Natural Sciences and Mathematics, Ural Federal University, 620002, Ekaterinburg, Russia*
[2]*Institute of Metal Physics, UD RAS 620180, Ekaterinburg, Russia*
vitaliy.riumshin@urfu.ru

Nickelates $RNiO_3$ (R – rare earth or yttrium Y) have been the subject of extensive experimental and theoretical investigations over numerous years [1]. These compounds are gaining interest due to their various applications [2]. Theoretical exploration of nickelates is particularly captivating due to their intriguing physical properties, including the metal-insulator transition, unconventional conductivity behavior, and intricate non-collinear magnetic structure. In addition, it is an extremely interesting and convenient model object. The elucidation of the metal-insulator transition mechanism in nickelates remains a topic of active debate among researchers [3].

In our prior study, we examined a model that interprets nickelates as Jahn-Teller magnets. The instability triggered by the anti-Jahn-Teller disproportionation reaction catalyzes the emergence of an effective system of spin-triplet composite bosons [4,5]:

$$\hat{\mathcal{H}} = -t \sum_{\langle ij\rangle\sigma} \left(\hat{B}_i^{\sigma\dagger}\hat{B}_j^{\sigma} + \hat{B}_j^{\sigma\dagger}\hat{B}_i^{\sigma}\right) + V \sum_{\langle ij\rangle} \hat{n}_i\hat{n}_j + J \sum_{\langle ij\rangle} \left(\hat{s}_i, \hat{s}_j\right),$$

where t - boson transfer parameter, V - nonlocal charge correlation, J - exchange integral.

Using the mean field approximation (MFA), we calculated phase diagrams across a spectrum of model nickelate parameters. These diagrams vividly illustrate the competition between charge ordering, an antiferromagnetic insulator, and a spin-triplet superconductor within the system. In addition to these phases, more intricate states can arise when multiple order parameters are concurrently non-zero. These states may manifest themselves either homogeneously or in the form of phase separation. In the extensively studied model of local singlet bosons, numerical simulations demonstrate that the homogeneous phase of a superfluid solid (supersolid) is metastable in relation to phase separation. Within the context of the MFA at finite temperatures for the triplet boson model, it is observed that phase separation is more stable than homogeneous phases. The objective of this study is to validate this assertion, employing Maxwell's phenomenological approach, through numerical simulations using the classical Monte Carlo method, considering the kinematic preservation of boson concentration (Fig. 1), and within the framework of the thermostat algorithm in the grand canonical ensemble.

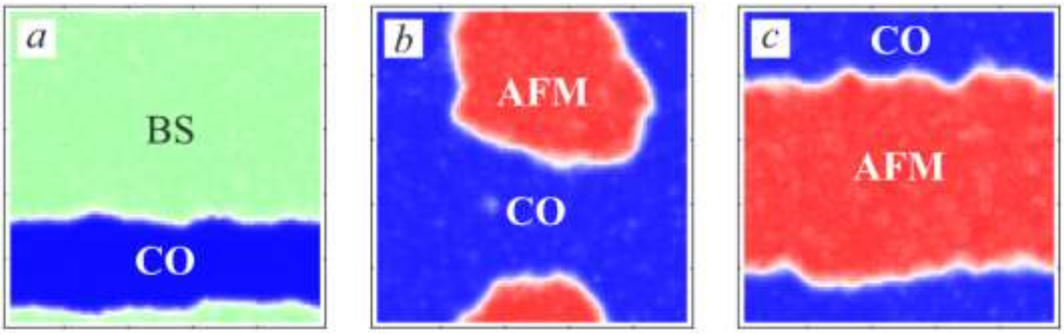

Figure 1. Lattice states of $N = 96\times96$, $z = 4$, $V/J = 4$, $t/J = 1.5$ at (a) $n = 0.25$, $T/T_{c,max} = 0.02$; (b) $n = 0.65$, $T/T_{c,max} = 0.17$; (c) $n = 0.75$, $T/T_{c,max} = 0.25$.

This work was supported by the Ministry of Science and Higher Education of the Russian Federation, project FEUZ-2023-0017.

1. M. L. Medarde, *J. Phys.: Condens. Matter* **9**, 1679 (1997).
2. J. Shi, *Nature Commun.* **4**, 2676 (2013).
3. D.J. Gawryluk et al, *Phys. Rev. B* **100**, 205137 (2019).
4. I.I. Mazin et al, *Phys Rev. Lett.* **98**, 176406 (2007).
5. A.S. Moskvin, *Magnetochemistry* **9**, 224 (2023).

P19

Stochastic model of ferroelectrics switching

V.N. Nechaev, A.V. Shuba

Military Educational and Scientific Centre of the Air Force N.E. Zhukovsky and Y.A. Gagarin Air Force Academy, 394064, Voronezh, Russia
shandvit@rambler.ru

The phenomenon of dielectric hysteresis has a direct association with materials science and determines possible technical applications of ferroelectric materials [1,2]. Its effective application depends on the ability to control the geometric characteristics of hysteresis loops (shape, width, height, points of intersection with the coordinate axes) under experiment conditions. These characteristics and the kinetics of polarization switching $P(t)$ are mainly determined by the structure, and also concentration, distribution and ratio of various types of defects in the material. Modeling the repolarization process permit in choosing the parameters of the sample and the external electric field $E(t)$ and allows to interpret experimental data to obtain information about the domain structure and imperfection of the material. However, there are no simple mathematical models of hysteresis phenomena in frames of which the experimental results could be explained at present.

We assume that switching process in a uniaxial single ferroelectric is characterized by the Markov random process. We use the phenomenological model, shown in Fig. 1, where state «0» corresponds to the initial configuration; «1» is the partial switching state (separation of domain boundaries from point defects with interaction energy W_1); «2» is the partial switching state (separation of domain boundaries from linear defects with interaction energy W_2); «3» and «4» correspond to states «1» and «2» with the opposite direction of the external field $E(t)$; $\lambda_i(t)$, $\mu_i(t)$ are the transitions intensities (i=1,2,3,4), determined by the expressions

$$\lambda_{1,2}(t)=\mu_{3,4}(t)=\omega_0 \exp\left(-\frac{W_{1,2}-E(t)P(t)}{k_B T}\right); \quad \mu_{1,2}(t)=\lambda_{3,4}(t)=\omega_0 \exp\left(-\frac{W_{1,2}+E(t)P(t)}{k_B T}\right), \tag{1}$$

where ω_0 is the number of attempts to separate domain boundaries from defects per unit time; k_B is the Boltzmann constant. After determined the probabilities $p_i(t)$ of the states «0»–«4» from the Kolmogorov system of equations the polarization averaged over the volume was calculated

$$P(t)=P_s\left(p_1(t)\delta+p_2(t)(1-\delta)-p_3(t)\delta-p_4(t)(1-\delta)\right), \tag{2}$$

where δ is the fraction of the crystal volume in which the domain boundaries motion is controlled by point defects; P_s is the spontaneous polarization, and then the hysteresis loop $P(E)$ was built.

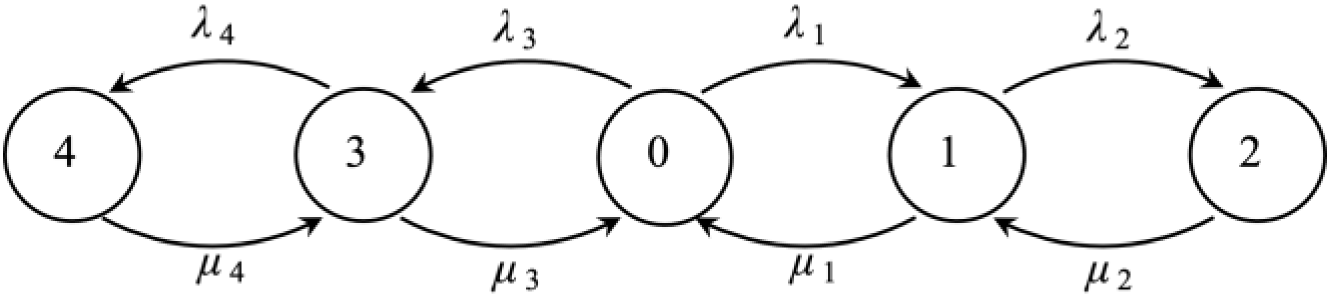

Figure 1. State graph for the polarization switching process in a single crystal.

Comparison of theoretical hysteresis loops, the calculations of which include certain assumptions about the parameters of structure and field $E(t)$, with experimental hysteresis loops allows one to obtain information about the structure of the material.

1. A. Singh, S. Monga, N. Sharma, et al., *J. Asian Ceram. Soc.* **10**, 275 (2022).
2. L. Jin, F. Li, S. Zhang, *J. Am. Ceram. Soc.* **97**, 1 (2014).

P20

Effect of the alignment of Fe nanoparticles in polyvinyl alcohol films on the structure, thermomechanical, and magnetic properties

T.S. Soliman[1,2], S.A. Vshivkov [1], Sh.I. Elkalashy[1,3]

[1]*Ural Federal University, 620000, Ekaterinburg, Russia*
tarek.attia@fsc.bu.edu.eg

[2]*Benha University, 13518, Benha, Egypt*

[3]*Egyptian Atomic Energy Authority, 13759, Cairo, Egypt*

The properties of polymer nanocomposites with embedded magnetic nanoparticles (MNP) are influenced by the orientation or alignment of these nanoparticles within the polymer matrix [1]. The high surface area of these nanomaterials can improve their mechanical, thermal, optical, electrical, and magnetic properties [1]. MNPs like iron (Fe) tend to form agglomerations in the polymer matrix [2]. Many methods have been used to destroy the agglomeration of the nanoparticles, like ultrasonication [1,3]. The high intensity ultrasound waves destroy the aggregates and improve their degree of dispersion. However, ultrasonication alone is unable to produce a homogeneous and stable dispersion. The alignment of metallic nanoparticles along particular directions in a polymer matrix can be realized by applying an external uniform magnetic field [1]. If a uniform magnetic field is applied to a polymer matrix with MNP, the resulting nanocomposites combine between the magnetic and elastic properties. Recently, interest has been focused on exploring a new magnetic polymer with enhanced properties to develop new types of polymer electronics like switches, sensors, magnetic memories, and controlled delivery systems [1,4].

In this work, we reported a method of dispersion of Fe MNP using high speed ultrasound technique and the alignment of Fe MNP in polyvinyl alcohol (PVA) films using a uniform magnetic field. The structural, thermomechanical, and magnetic properties of PVA/Fe MNP nanocomposite films were investigated.

Polymer nanocomposite films were fabricated by a solvent casting method. Iron (Fe) nanoparticles with specific surface area (S_{sp} = 8.3 m^2/g), density (ρ = 7.874 g/cm^3), and a weight average diameter (d_{w} = 150 nm). At first, 1 gm PVA was dissolved in 10 ml distilled water at 70°C. The PVA solution was stirred for two hours, until the PVA was dissolved completely. When the solution dropped to the room temperature, Fe nanoparticles (0.025 gm) were added and dispersed in the PVA solution using high-speed ultrasound (Cole-Parmer ultrasonic processor CPX-750). The dispersion solution was poured on a glass substrate, then it was placed in the center of the gap between the magnets with a uniform magnetic field. The dispersion solution was exposed to a magnetic field with intensity 5.5 kOe for approximately 30 minutes, then left to dry in closed box with dry atmosphere. The Fe MNP in PVA films morphology was studied via a scanning electron microscope (SEM, Carl-Zeiss LEO982) and optical microscope (OLYMPUS-BX51). Optical properties were carried out using UV–VIS–NIR spectrophotometer, type UNICO UV-2800 with an accuracy of ±0.8 nm, wavelength range 190–800 nm. Thermomechanical analysis (TMA) tests were carried out in a NETZSCH TMA-202 thermomechanical analyzer with a silicon probe of diameter 1 mm and the analysis was performed in nitrogen atmosphere.

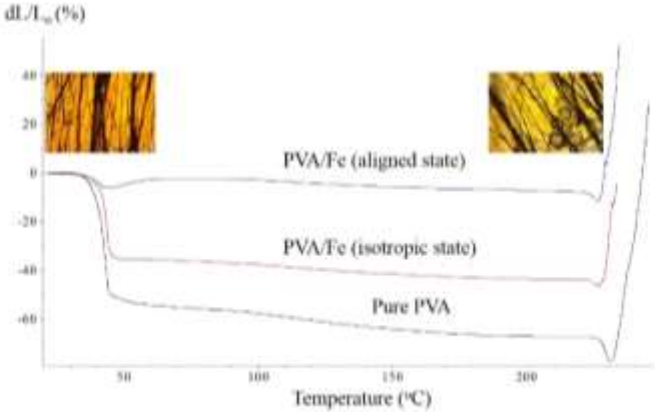

Figure 1. The shrinkage curve for pure PVA and PVA doped with Fe MNP.

The magnetization for the isotropic and aligned samples are 2.75 emu/g and 5.05 emu/g, respectively. The magnetization is larger in the case of the aligned sample.

TMA measures the changes in sample dimensions as a function of temperature under a non-oscillatory load, with a programmed temperature under constant pressure. The sample with aligned MNP in the polymer matrix exhibits less penetration than pure PVA and PVA-Fe MNP (isotropic). Also, from the inset images in Figure 1, which shows the structure of Fe MNP before and after the destruction at 235°C.

It shows that the alignment of Fe MNP was not affected by the heat, which confirms the stability of the polymer films with aligned MNP.

1. A.M. Abdalla, R.P. Sahu, I.K. Puri, *Polym. Compos.* **40**, 779 (2019).
2. T.S. Soliman, S.A. Vshivkov, *J. Non. Cryst. Solids* **519**, 119452 (2019).
3. H. Hong, X. Luan, M. Horton, et al., *Thermochim. Acta* **525**, 87 (2011).
4. K. Huang, H. Yu, M. Xie, et al., *RSC Adv.* **9**, 10599 (2019).

P21

Switching processes in polyvinylidene fluoride films produced by additive technology

A.V. Solnyshkin[1], N.V. Vostrov[1], E.V. Aleksanrov[1], S.I. Gudkov[1], D.A. Kiselev[2], A.N. Belov[3]

[1]Tver State University, 170100, Tver, Russia
a.solnyshkin@mail.ru

[2]National University of Science and Technology MISIS, 119049, Moscow, Russia

[3]National Research University of Electronic Technology – MIET, 124498, Zelenograd, Moscow, Russia

Ferroelectrics due to switchable polarization, remarkable piezo- and pyroelectric properties are the promising materials for functional elements of transducers, touch devices, microelectromechanical systems, and non-volatile memory FeRAM. Additive technologies are increasingly common methods for producing film structures based on ferroelectrics. Compared with traditional methods, additive manufacturing of ferroelectric structures has the following features: producing the complex structure, precise control of thickness and other design parameters for small devices, direct integration of ferroelectric materials with other electronic components, control of parameters and, as a result, increased sensitivity devices, etc. Based on these advantages, additive manufacturing technologies have effectively promoted the development of ferroelectric material devices. This paper presents the results of studies of switching processes at the microscopic and macroscopic levels of polyvinylidene fluoride (PVDF) films produced by 4D printing.

According to the atomic force microscopy, analysis of the surface structure of the PVDF films printed layer-by-layer from a solution revealed the presence of two phases: a non-polar α-phase and a polar β-phase. The latter is characterized by dipole ordering, which determines the ferroelectric properties. The β-phase is observed as rod-like crystals 1–2 μm long and several tens of nanometers thick. However, the degree of crystallinity of the films produced 4D printing is low and equal to ~10 – 20%. Studies of switching processes at the microscopic level by the piezoelectric force microscopy showed the polarization reversal were only observed in the rod-like crystals and presented loops of residual piezoelectric hysteresis.

Switching processes at the macroscopic level were studied using the Sawyer-Tower circuit at a measuring field frequency of 50 Hz. It was found that applying the alternating electric fields with a strength of up to ~600 kV/cm did not lead to processes of the polarization reversal of film samples. The dependence of the polarization value on the applied external field is linear like the response of linear dielectrics that do not have ferroelectric properties. When a field exceeding 600 kV/cm is applied, appearing the dielectric hysteresis loop characteristic to ferroelectric materials begins from unsaturated to saturated loops. Ferroelectric hysteresis loops with pronounced saturation are observed at applying the electric field strengths exceeding 1 MV/cm in an amplitude.

The Preisach model was used to analyze macroscopic dielectric hysteresis loops in PVDF polymer films. The calculation results showed that the average coercive field in rod-like crystals of the printed PVDF film is equal to 630 kV/cm, and the dispersion parameter characterizing the distribution of coercive and internal fields is equal to 210·kV/cm.

The work was supported by the Russian Science Foundation, grant No. 23-22-00224, https://rscf.ru/project/23-22-00224/

P22

Near-electrode processes in lithium niobate crystals $LiNbO_3$

V.E. Umylin[1], N.S. Kozlova[1], M.B. Bykova[1], E.V. Zabelina[1]

[1]*National University of Science and Technology «MISIS», 119049, Moscow, Russia*
v.umylin@mail.ru

Congruent lithium niobate crystal $LiNbO_3$ is a well-known ferroelectric crystal (Curie temperature is 1142°C), which is widely used in the field of optics and acoustics to create electro-optics products, nonlinear optics, surface acoustic wave devices and piezoelectric sensors. $LiNbO_3$ in the ferroelectric phase has pseudoilmenite structure, belongs to the point symmetry group $3m$ and the space symmetry group $R3c$. The elements of symmetry are a third-order axis (the polar axis of the crystal) and three planes, reflection from which is combined with half of the lattice period translation along the third-order axis. The Z axis is parallel to the polar axis (third order axis), the X axis is perpendicular to the m plane, XYZ form a right orthogonal basis.

To create devices based on $LiNbO_3$ elements, various sections of it are used. These samples are covered with current conductive coatings. It is known that the deposition of conductive coatings on the surfaces of crystals leads to aging and degradation, and the nature of conductive coatings significantly affects the measured electrical parameters of polar dielectrics. Aging and degradation of the surface layers of crystals is associated with contact phenomena at the interface between the crystal and the conductive coating. However, the mechanism of such phenomena and the features of their occurrence on different cuts of crystals have been practically not studied.

The purpose of this work was to study the features of near-electrode processes in $LiNbO_3$ samples.

For measurements, samples of $LiNbO_3$ crystals of X, Y, Z-cuts and a 127.8-degree Y cut with different conductive coating materials (In, Ag, Pd) were prepared.

Short circuit currents and their temperature dependences were measured in the temperature range from room temperature to 260°C. Currents were recorded using a low current meter LCM-0.5. To set and maintain a certain temperature regime, a heating chamber, a temperature control system and a heater power supply were used. The furnace temperature was recorded using a chromel-alumel thermocouple. To conduct temperature studies, the samples were kept in short-circuit mode at room temperature until a stationary current value was established, and only after that linear heating began at rates not exceeding 3°/min.

The experiments carried out made it possible to discover the following basic patterns: in $LiNbO_3$ crystals without preliminary external influences, short-circuit currents are observed even at room temperature, which persist for a long time. The magnitude and direction of current flow depends on the material of conductive coatings. Temperature dependences of SCC with different conductive coatings were obtained.

Studies of the electrical properties of $LiNbO_3$ crystals were carried out in the accredited laboratory of semiconductor materials and dielectrics «Single crystals and stock on their base» NUST MISIS with financial support from the Ministry of Education and Science of Russia within the framework of the state assignment to universities FSME-2023-0003.

Markov chains approach for analyzing states of 1D spin systems

D.N. Yasinskaya, Y.D. Panov

Ural Federal University, 620002, Ekaterinburg, Russia
daria.iasinskaia@urfu.ru

One-dimensional spin models, despite their apparent simplicity compared to multidimensional ones, exhibit several unique properties. Exact solutions of these models are essential for understanding the behavior of real physical systems, particularly in the study of phase transitions in statistical physics [1]. The absence of long-range order in low-dimensional spin systems is responsible for their distinct behavior.

Although exact solutions are feasible, analyzing the phase states of one-dimensional systems using standard transfer-matrix formalism can be a challenging task, especially when examining states at the boundaries between different phases. In this study, we propose a novel approach for analyzing ordered and frustrated phase states in one-dimensional spin chains by mapping them to some Markov chains [2]. We consider a chain of Ising spins diluted with two types of charged impurities with density-density interactions [3]. The Hamiltonian includes on-site and inter-site density-density correlations, Ising spin exchange, magnetic field, and chemical potential for impurities.

The considered model exhibits a wide variety of ground state phases, most of them display non-zero residual entropy, indicating frustration. Specifically, in a zero magnetic field, each frustrated phase maps to its own type of Markov chain. In an external field, only 2 types of Markov chains are implemented in the system: periodic with period 2 and aperiodic. Each of these Markov chains possess special properties and identifies the classification of frustrated ground state phases. By using this framework, we are able to elucidate the structural features of frustrated phases that may not be readily discernible through traditional transfer matrix methods.

In phases characterized by periodic Markov chains, a pattern of long-range order is evident on one sublattice while the other sublattice remains disordered. This leads to a unique conjunction of non-zero residual entropy and infinite correlation length. Conversely, in frustrated phases with aperiodic chains, long-range order is absent and the correlation length is finite. It is shown that application of a magnetic field induces the most significant change in the spin chain structure, primarily altering the type of Markov chain.

The work was supported under grant FEUZ-2023-0017 of the Ministry of Science and Higher Education of the Russian Federation.

1. R. J. Baxter, *Exactly Solved Models in Statistical Mechanics* (Academic, London, 1982).
2. Y. Panov, O. Rojas. *Phys. Rev. E* **108**, 044144 (2023).
3. Yu. D. Panov et al. *J. Supercond. Nov. Magn*. **29**, 1077 (2016).

P24

Potential of RF cathode sputtering method for synthesis of lead-containing antiferroelectric films

N.S. Zhukova[1], A.E. Ganja[1], M.A. Knyazeva[1], A.V. Filimonov[1], A.S. Goltaev[2], I.S. Mukhin[1], A.V. Pavlenko[3], R.G. Burkovsky[1]

[1]*Peter the Great Saint-Petersburg Polytechnic University, 195251 St. Petersburg, Russia zhukovaaa3781@gmail.com*

[2]*Saint-Petersburg National Research Academic University named after J.I.Alferov, 194021, St. Petersburg, Russia*

[3]*Southern Federal University, 344006 Rostov-on-Don, Russia*

Ferroelectric (FE) and antiferroelectric (AFE) materials are widely used in various industries: piezo- and pyroelements, electro-optical devices, ferroelectric memory (FeRAM). The potential of AFE materials has not yet been fully realized. Interest in thin films of AFE continues to grow [1], since they are promising in the development of certain industries; for example, based on thin-film AFE structures, new energy storage devices and memory devices can be implemented [2,3]. The most well-known AFE materials are $PbZrO_3$ and $PbHfO_3$. Today, to create heterostructures based on these materials, the pulsed laser deposition (PLD) method is mainly used [4,5]. Using this method, the heterostructure is grown in several stages. Despite the popularity of this method, it has a number of disadvantages that affect the uniformity of films both in thickness and structure. But there is another method that is gradually being introduced into production - the method of radio-frequency cathode sputtering [6]. Unlike PLD, it is a single-stage process, which allows the heterostructure to be grown continuously. At the moment, this method is practically not used for the synthesis of epitaxial films of lead-containing perovskites, including AFE materials, despite the fact that the first epitaxial films have already been obtained for lead-free perovskites using this method. The method of RF cathode sputtering can be significantly more advantageous than PLD in a number of properties, in particular in its availability, according to which it seems useful to develop approaches to its use for the synthesis of lead-containing perovskite films.

The paper examines the potential of using the method of RF cathode sputtering in an oxygen environment for growing thin films of lead-containing perovskites as an alternative to PLD. Two films with the target chemical composition $PbHfO_3$ were synthesized on Si(111) and $SrRuO_3/SrTiO_3/MgO(001)$ substrates at the ” Plasma 50−SE“ installation. The films were characterized using single-crystal X-ray diffraction method with reciprocal space mapping and energy-dispersive X-ray fluorescence analysis (EDX RFX).

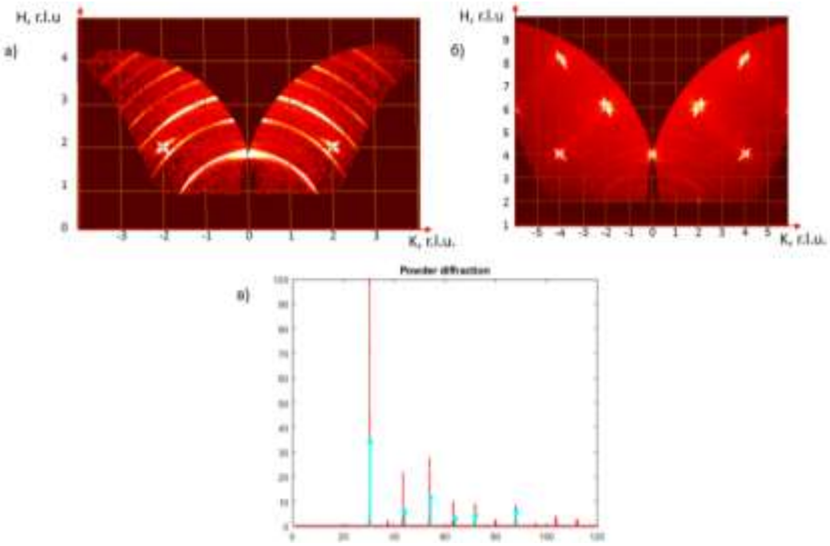

Figure 1. (a) Reciprocal space maps for the film on Si(111) substrate. Reciprocal slice in the H0L plane with reflexes of Si and polycrystalline perovskite on the Cu emission line. (b) Reciprocal slice in the H0L plane with reflexes of presumably Si on the molybdenum emission line. The grid corresponds to the cubic lattice of Si with parameters *a*=*b*=*c*=5.44 Å. (c) powder diffraction pattern for lead hafnate (red - $PbHfO_3$, blue - the film under study).

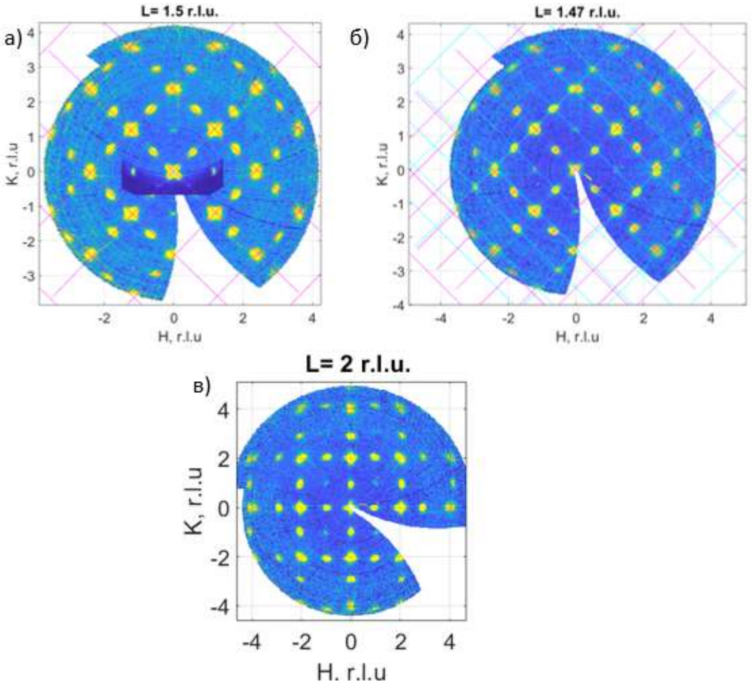

Figure 2. Lattice of unknown epitaxial structure obtained from $PbHfO_3$ target. (a) Reciprocal e slice in HK1.5 plane. (b) Reciprocal slice in HK1.47 plane with superposition of two lattices. (c) Reciprocal slice in HK2 plane, grid with pyrochlore with parameters a=b=5.05 Å

The film grown on a Si(111) is a polycrystalline perovskite, which is confirmed by powder diffraction data and reciprocal space maps (Figure 1). Film based on $SrRuO_3/SrTiO_3$/MgO-epitaxial. The reciprocal lattice of this film is not compatible with perovskite. (Figure 2). Its structure is currently unknown, but it is characterized by an unusually large epitaxial ratio of 5:3, i.e. the intersection of the film and substrate layer nodes occurs through 5 film cells and 3 substrate cells. It is important to clarify that the lattice of the film layer is located at an angle of 45 degrees to the substrate. This seems quite unusual, since epitaxial films usually have simpler epitaxial ratios. According to our results, the synthesis of lead-containing epitaxial perovskites RF cathode sputtering in an oxygen atmosphere presents significant difficulties. To overcome these difficulties, certain technical solutions have to be devised. However, at the same time, this method works for growing polycrystalline lead-containing films and lead-free perovskites. The results of EDX RFX. of our samples showed that each of the crystals under consideration contained all the elements in its composition, and the ratio of molar fractions of lead and hafnium was close to 1, as expected for $PbHfO_3$. However, the presence of individual chemical elements does not guarantee the existence of the $PbHfO_3$ structure.

N.S.Zhukova, A.E. Ganzha, M.A. Knyazeva, A.V. Filimonov and R.G. Burkovsky carried out diffraction characterization of thin-film samples, modeling and interpretation of the results with the support of the Russian Science Foundation (project 20-72-10126).

1. Y. Si, T. Zhang, Ch. Liu, et al., *Prog. Mater. Sci.* **142**, 101231 (2024).
2. M.H. Park, C.S. Hwang. *Ferroelectric-Gate Field Effect Transistor Memories*, Springer, Dordrecht (2016).
3. K. Vorotilov, A. Sigov, *Phys. Solid State* **54**, 894 (2012).
4. R.G. Burkovsky, G.A.A. Lityagin, A.E. Ganzha, et al., *Phys. Rev. B* **105**, 125409 (2022).
5. G.A. Lityagin, A.F. Vakulenko, R. Gao, et al., *J. Phys.: Conf. Ser.* **1236**, 012018 (2019).
6. V.M. Mukhortov, Y.I. Yuzyuk, *Heterostructures based on nanoscale segmentoelectric films* (Rostov-on-Don: Publishing house of the Southern Scientific Center of RAS, 2008. 224 c.

P25

Application of ionic liquids in studies of dielectric microstructure by scanning electron microscopy

A.V. Dudilovskaya, A.I. Ivanova, O.E. Zhuravlev, A.D. Kaftanov

Tver State University, 170100, Tver, Russian Federation
dudilovskayaa@mail.ru

It is known that the physical-mechanical properties of materials are largely determined by their micro- and nanostructure, depending on the electronic structure, chemical composition and technology of their production. Scanning electron microscopy (SEM) is one of the most widespread direct methods of fundamental and applied research in various fields of science and technology: from nanotechnology and materials science to biology and semiconductor physics [1-2]. When studying the microstructure of non-conductive materials by the SEM method, researchers often face the problem of charging samples. Studies of dielectric (non-conductive) samples in a scanning electron microscope are accompanied by electron emission into vacuum, polarization of molecules, and the formation of strong near-surface electric fields and potentials. Charging the surface can lead to image contrast distortion, defocusing, and errors in quantitative microanalysis [3].

The main techniques to solve the charging problem are the use of low vacuum mode, the application of thin films of various metals or carbon on sample surface by thermal vacuum deposition or cathode sputtering. The purpose of this work is to study the technique of using ionic liquid as a coating for dielectric samples and conduct experimental studies. The use of ionic liquids in science and industry is due to their special properties such as electrical conductivity, low vapor pressure, high thermal and electrochemical stability, wide range of liquid state. Ionic liquids are actively used as media for electrochemical deposition of metals, electrolytes in lithium batteries and solar cells, solvents in organic synthesis and catalysis [4-6].

The paper presents the results of using ionic liquid as a thin coating layer to prevent the accumulation of electric charges on non-conductive samples, which helps to improve the quality of electron microscopic studies. The experiments were carried out on non-conductive samples: biological materials, core and powder samples, piezoelectric ceramics and fiberglass. The surface of the samples was treated with a solution of ionic liquid in acetone, after which the samples were air-dried, then attached to a conductive carbon tape to ensure electrical contact of the sample with the instrument table, placed in a microscope chamber and the microstructure of the sample surface was photographed.

In the course of the work, SEM images of the samples were analyzed before and after applying an electrically conductive ionic liquid to them. The results obtained allow us to conclude that ionic liquids can be used to prepare non-conductive samples of various origins for scanning electron microscope examination. Using an electrically conductive ionic liquid on dielectrics gives a comparable result with the method of spraying metal coatings, and often surpasses the quality of SEM images obtained in low vacuum mode.

The advantage of this method is the possibility of obtaining a homogeneous coating layer on samples with complex relief and the simplicity of sample preparation for further studies. Figure 1 shows SEM images of polyhexamethylene izophthalamide fiber obtained by various methods: low vacuum mode (97 Pa), magnetron deposition of platinum (Pt), ionic liquid coating. It is clearly seen from the figure that the image of the initial sample deteriorated due to charging of the surface (Fig. 1a). The low vacuum mode, the use of metal deposition and the application of an electrically conductive ionic liquid make it possible to qualitatively visualize the microstructure of the dielectrics.

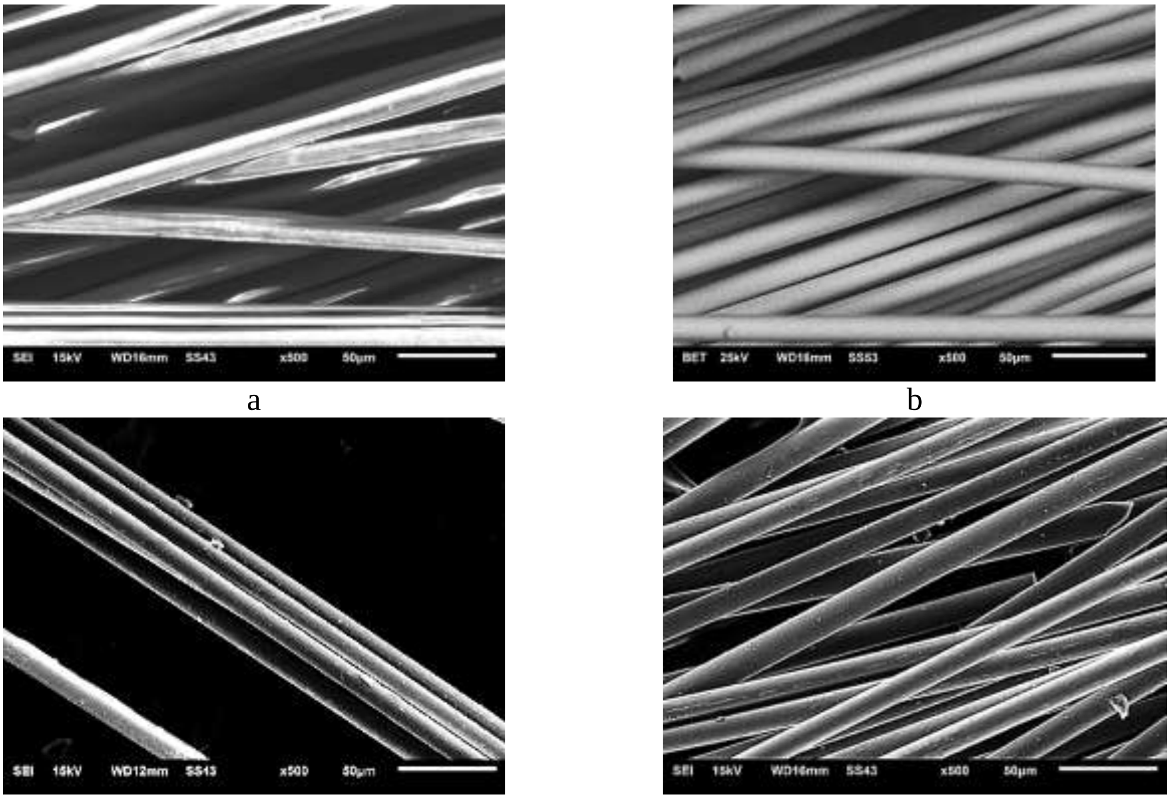

a b

c d

Figure 1. SEM images of the fiber: (a) original sample in secondary electron mode, (b) low vacuum mode, (c) metal deposition (Pt), (d) application of ionic liquid.

The obtained results confirm the effectiveness of using ionic liquid to prevent electrification of non-conductive samples. The advantages of this technique are environmental friendliness, simplicity and rapidity of use, the possibility of obtaining homogeneous coatings on samples with complex topography.

1. J.I. Goldstein, D.E. Newbury, J.R. Michael, et al. *Scanning electron microscopy and X-ray microanalysis* (Springer) 550, (2017).
2. G.M. Zeer, O.Yu. Fomenko, O.N. Ledyaeva, *J. Siberian Federal University. Chemistry* **2**, 287 (2009).
3. O.E. Zhuravlev, A.I. Ivanova, R.M. Grechishkin, *J. Surf. Invest. X-ray, Synch. Neutron Tech.* **9**, 904 (2015).
4. R. Rogers, K. Seddon, *Ionic liquids: Industrial applications to Green chemistry* (Kluwer Academic) 584, (2002).
5. P.C. Howlett, D.R MacFarlane, A.F. Hollenkamp, *Electrochem. Solid-State Lett.* **7**, A97 (2004).
6. H. Sakaebe, H. Matsumoto, K. Tatsumi, *Electrochem. Acta* **53**, 1048 (2007).

P26

High-temperature annealing of ZnO:Ga thin films for neuromorphic applications

D.A. Dzyuba[1,2], Z.E. Vakulov[1], R.V. Tominov[1,2], V.A. Smirnov[1,2]

[1]*Research Laboratory "Neuroelectronics and Memristive Nanomaterials" (NEUROMENA Lab), Institute of Nanotechnologies, Electronics and Electronic Equipment Engineering, Southern Federal University, 347922, Taganrog, Russia*
dmdzyuba@sfedu.ru

[2]*Department of Radioelectronics and Nanoelectronics, Institute of Nanotechnologies, Electronics and Electronic Equipment Engineering, Southern Federal University, 347922, Taganrog, Russia*

In neuromorphic computing systems based on artificial neural networks are emulated the functions of biological synapses and neural systems for energy-efficient computing. Due to the ability to store data and perform computations, memristive structures are a key element of *a memory* computing architecture [1]. It should also be noted that the neuromorphic structure based on memristive structures can operate at low energy (~10 fJ per operation), which emphasises the huge potential of *in-memory* computing compared to the von Neumann architecture [2]. However, despite significant progress and publication activity on topics devoted to neuromorphic electronics, there are currently no systematic studies of the influence of synthesis conditions of doped ZnO thin films obtained by pulsed laser deposition (PLD) on their parameters. These issues prevent the creation of an element base for self-learning adaptive neuromorphic systems, as well as energy-efficient information processing and storage devices with a high degree of integration, and determine the relevance of the study of the regularities of the influence of synthesis conditions of doped ZnO films on their electrophysical and morphological parameters. Moreover, high-temperature annealing of formed films is one of the possible methods of correction for the composition and properties of ZnO:Ga films. Therefore, the purpose of this work is to study the regularities of influence of high-temperature annealing parameters (annealing temperature) on the parameters of the films.

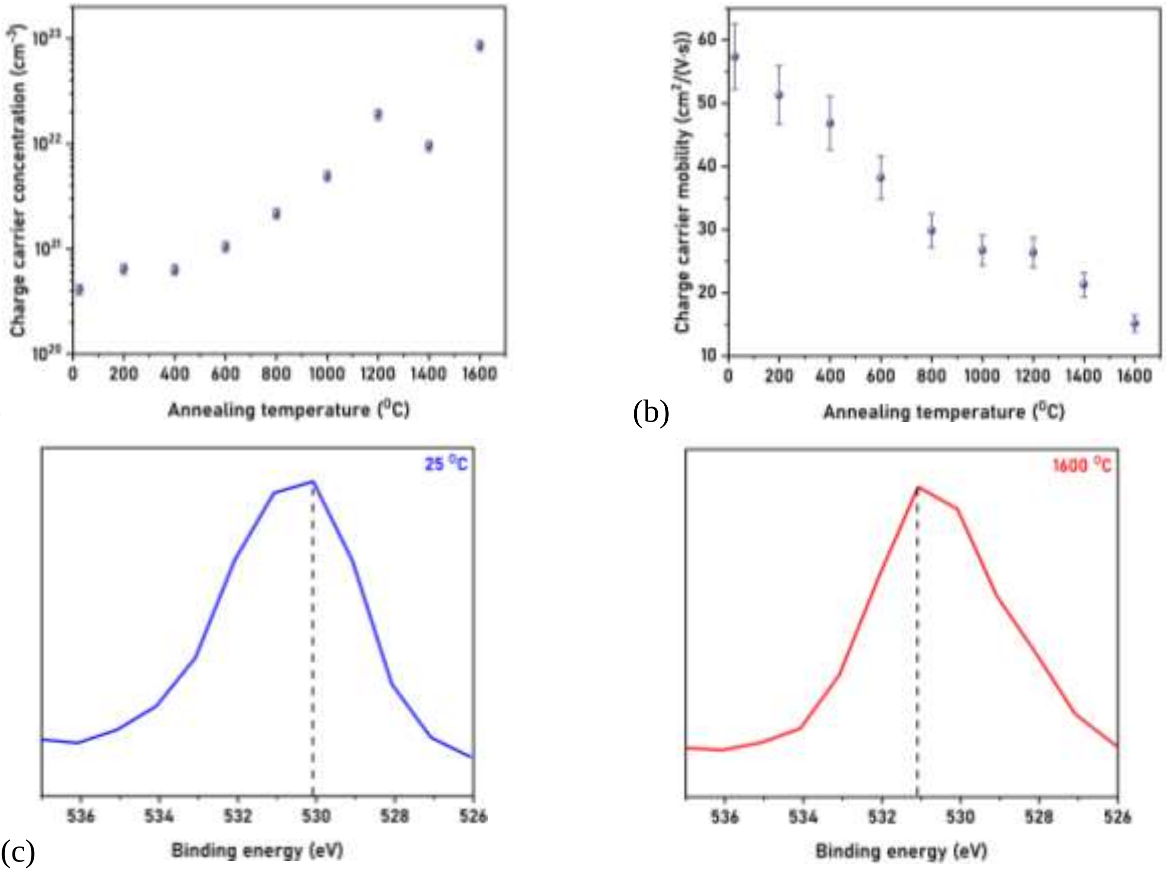

(a)

(b)

(c)

Figure 1. (a) Concentration and (b) mobility of charge carrier dependencies on annealing temperature, (c) the results of XPS study of obtained ZnO:Ga films.

It is shown that when the annealing temperature increases from 25°C (samples without annealing) to 1600°C, the surface roughness of ZnO:In, ZnO:Ga films decreases from 51.1±3.6 nm to 7.4±0.5 nm and from 59.3±3.6 nm to 16.8±1.1 nm, respectively. This fact is explained by the fact that when approaching the sublimation temperature of ZnO (1800°C), activation of the material condensed on the substrate occurs. Additionally, when the annealing temperature increases from 25°C (samples without annealing) to 1600° C in ZnO films: Ga, an increase in the charge carrier concentration was observed from $(4.1\pm0.3)\cdot10^{20}$ cm^{-3} to $(8.6\pm0.3)\cdot10^{22}$ cm^{-3} was observed, while the charge carrier mobility decreases from 57.4±5.2 $cm^2/(V\cdot s)$ to 15.2±1.4 $cm^2/(V\cdot s)$, respectively (Figure 1).

The change in the electrophysical parameters of ZnO:Ga films can also be related to the change in the stoichiometric composition of the films due to the release of oxygen during annealing in a vacuum atmosphere with the subsequent formation of oxygen vacancies, which is confirmed by the results of XPS studies of ZnO:Ga films. Therefore, the peak O 1s at binding energy ~ 530 eV is attributed to O_2- ions in the wurtzite structure of the hexagonal ZnO lattice (Figure 1c), while the peak O 1s at binding energy ~ 531 eV is attributed to O_2- ions in the oxygen-depleted regions of the ZnO matrix, which agrees with the results of measurements of the electrophysical characteristics of the films obtained.

Thus, the regularities of the influence of annealing temperature on morphological and electrophysical parameters of ZnO:Ga films were established. It was found that the change in the electrophysical parameters of ZnO:Ga films can also be associated with a change in the stoichiometric composition of the films because of the release of oxygen during annealing in a vacuum atmosphere with the subsequent formation of oxygen vacancies, which is confirmed by the results of XPS studies of ZnO:Ga films.

The study was carried out with the financial support of the Russian Federation Government (Agreement No. 075-15-2022-1123).

1. F.M. Simanjuntak, T. Ohno, S. Chandrasekaran, et al., *Nanotechnology* **31**, 26 (2020).
2. V.I. Avilov, R.V. Tominov, Z.E. Vakulov, et al., *Nano Research* **16**, 7 (2023).

P27

Optical properties of Cr^{3+} and Mn^{3+} ions in $Ca_3(VO_4)_2$ single crystals: effect of Mg^{2+} ions

L.I. Ivleva, I.S. Voronina, E.E. Dunaeva, M.E. Doroshenko

Prokhorov General Physics Institute of the Russian Academy of Sciences, Moscow, 119991, Russia
ivleva@lst.gpi.ru

A scientific and practical interest is attracted to multifunctional materials that exhibit a complex of various physicochemical properties. These materials include whitlockite-type calcium orthovanadate $Ca_3(VO_4)_2$ (CVO) combining ferroelectric, pyroelectric, piezoelectric, nonlinear optical, and luminescent properties. In the present work we focused our attention on the codoping of CVO crystals by Cr^{3+}/Mg^{2+} and Mn^{3+}/Mg^{2+}. To interpret the influence of Mg^{2+} concentration on properties of codoped crystals we study the CVO:Cr:Mg and CVO:Mn:Mg Czochralski grown crystals of various composition using methods of energy dispersive X-ray spectroscopy, inductively coupled plasma mass spectrometry, selective chemical etching and optical spectroscopy.

CVO crystals were grown from a melt in air along [100] direction using Pt crucibles. The initial charge of stoichiometric composition was prepared by solid-phase synthesis from $CaCO_3$ and V_2O_5 at a temperature of 1100 °C for 4 h. The impurities were introduced into the melt in the form of oxides Mn_2O_3 (0.05-1.00 wt.%), Cr_2O_3 (0.01-0.1 wt.%), MgO (0.5-2.0 wt.%) over stoichiometry. The bulk crystallization rate did not exceed 0.3 cm^3/h. The production of crystals of optical quality with a diameter of 15 mm and a length of 50 mm, free from cracks, bubbles and inclusions of the second phase is ensured. Determination of the effective segregation coefficients of alloying Cr and Mn ions in the CVO matrix showed that the introduction of Mg does not affect $K_{eff.}$Mn and $K_{eff.}$Cr, which are 0.25 and 0.85, respectively. At the same time, $K_{eff.}$Mg in the CVO:Mn:Mg is 0.5, and in the CVO:Cr:Mg is 0.74. As-grown crystals annealing in air at the temperature range of 1000-1200 ° C for 6-24 h leads to significant changes in the optical absorption spectra and crystals color. The general trend is to reduce the absorption intensity in the visible and near-infrared spectral regions with increasing temperature and annealing time. CVO:Mn:Mg blue-green crystals acquire yellow-green color due to 24 hours of annealing at 1000°C. It was shown, that the reduction process of manganese ions $Mn^{3+} \rightarrow Mn^{2+}$ slows down the presence of Mg ions. A similar situation is observed in the case of green CVO:Cr:Mg crystals, for which the transmission in the visible region of the spectrum increases and is accompanied by an increase in yellow coloration. The absorption spectra of nominally pure CVO crystals in IR range of 2700-3100 nm shows one weakly pronounced absorption band of 2794 nm. Introduction into the melt 0.1 wt.% Cr_2O_3 leads to the appearance of a wide 2750-3100 nm absorption band in as-grown crystals, the structure of which consists of three bands with maxima at 2794, 2821 and 2947 nm. Such a three-component structure with a different ratio of band intensities may indicate three slightly different positions of the proton with different O-O bonds and different near surroundings. Introduction into the melt containing 0.1wt.% Cr_2O_3 additionally 0.5% MgO results in one intense peak at 2820 nm. The presence of Mn_2O_3 in the melt leads to a low-intensity absorption band at 2821 nm in CVO:Mn. The intensity of the band increases when MgO is added into the CVO:Mn melt. The kinetics of luminescence attenuation under excitation with 700 nm, were measured at 15 K at a registration wavelength of 1190 and 1250 nm in a CVO:Mn and CVO:Mn:Mg. It was shown that co-activation of the CVO crystal by Mg ions leads to the redistribution of Mn ions between different valence states, but does not cause changes in spectral properties. The results of chemical etching show that all impurities investigated have practically no effect on the CVO ferroelectric domain structure.

This work was supported by Russian Science Foundation, Project №23-23-00383

P28

Characterization of titanium oxide-graphene memristive structures

I.L. Jityaev[1,2], D.J. Rodriguez[1], M.S. Kartel[1], V.A. Smirnov[1,2]

[1]*Southern Federal University, Research Laboratory Neuroelectronics and Memristive Nanomaterials, 347922, Taganrog, Russia*
izhityaev@sfedu.ru

[2]*Southern Federal University, Institute of Nanotechnologies, Electronics and Equipment Engineering, 347922, Taganrog, Russia*

The study of memristive nanostructures based on hybrid heterostructures including graphene and thin films of metal oxides is of significant scientific interest and has high potential for application in promising areas of micro- and nanoelectronics, robotics and artificial intelligence systems. Although resistive switching in bulk metal oxides, caused by spatial modulation of the concentration of oxygen vacancies under the influence of an electric field, is a well-studied phenomenon [1], the mechanisms of resistive switching in graphene and hybrid structures based on it remain poorly studied. In most cases, graphene acts either as a contact material for a memristor structure or as a resistivity-variable memristive layer in the form of an oxide, doped or defective. At the same time, detailed studies of the memristive properties of compositions of thin films of metal oxides and graphene are currently lacking, which opens prospects for fundamental and applied research in this area.

The aim of this work is to study the resistive switching and memristive properties of heterostructures consisting of nanoscale titanium dioxide (TiO_2) films deposited on the surface of graphene synthesized by chemical vapor deposition (CVD) on a copper substrate. It is assumed that the introduction of a graphene layer between a conductive substrate and a thin metal oxide film can lead to the emergence of new resistive switching mechanisms caused by interaction at the graphene/oxide interface and the formation of specific defect states. A comprehensive study of the electrical characteristics of these hybrid structures using modern analytical methods will provide fundamental knowledge about memristive effects in such systems, which opens prospects for the development of new functional materials and devices for use in the field of non-volatile memory, logic circuits, neuromorphic computing, and artificial intelligence.

In this work, heterostructures consisting of 50 nm thick nanoscale TiO_2 films deposited by magnetron sputtering onto the surface of graphene films synthesized on copper substrates via CVD were fabricated. Indium tin oxide pads were formed on the surface of TiO_2 films for electrical measurements. A study of the current-voltage characteristics of the obtained structures revealed the presence of states with high resistance (HRS) and low resistance (LRS) for both TiO_2 films deposited on graphene and graphene films formed on a copper substrate. The observed memristive behavior of graphene may be associated with structural dynamics or chemical functionalization, leading to changes in the electronic properties, including the conductivity of graphene, under the influence of an applied electric field. The copper substrate used in CVD synthesis of graphene and its high electrical conductivity influences the electronic structure of the graphene film. The interaction of graphene with the copper surface, especially in the presence of grain boundaries or defects on the surface of the copper layer, and the migration of ions or defects of the copper substrate to the interface with graphene can lead to modulation of the electronic properties of graphene and the formation of various memristive effects. In addition, during the process of chemical vapor deposition of graphene on a copper substrate, various impurities can be formed in the interface layer between graphene and copper. The results obtained are the initial stage of comprehensive research aimed at identifying the patterns of memristor properties of nanosized oxide films on the surface of graphene. The memristive mechanisms of CVD graphene-based structures, especially with TiO_2, still require a deeper study and understanding, as well as experimental studies to determine the influence of graphene on the characteristics of memristor nanostructures.

The reported study was funded by the Russian Federation Government (Agreement No. 075-15-2022-1123).

1. I. Jityaev, V. Avilov, A. Avakyan, et al., *Proc. 7th Scientific School: Dynamics of Complex Networks and their Applications, DCNA 2023*, 108 (2023).

P29

Resistive switching in transparent ITO/ZnO/ITO memristors deposited by magnetron sputtering

A.V. Saenko, K.A. Kozyumenko, N.V. Polupanov, V.A. Smirnov

Institute of Nanotechnologies, Electronics, and Equipment Engineering, Southern Federal University, 347922, Taganrog, Russia
koziumenko@sfedu.ru

Memristor is a promising non-volatile resistive memory device due to its advantages such as high speed, long-term data storage, low power consumption and multi-level behavior. The memristor is capable of changing its resistance depending on the voltage applied to it and thereby imitating the role of a synapse in the nervous system, which opens up great opportunities for the development of neuromorphic electronic devices, such as universal storage devices (RRAM), computing systems (neurocomputers), as well as biosensors and neural interfaces for robotics. The development of transparent memristors is associated with their use in optoelectronic neuromorphic devices, in particular artificial machine vision systems, where the optical transparency of the memristor and its synaptic behavior are most important, since the memristor directly responds to optical influence, and also has memory and sensor processing data and visual information in real time [1, 2].

Recently, the most promising memristive nanomaterial has been zinc oxide (ZnO), which is non-toxic, has a suitable band gap (3.3-3.4 eV) and a unique combination of optical and electrophysical properties, which are largely determined by the concentration of free charge carriers, controlled by oxygen vacancies (intrinsic defects), and also exhibits synaptic behavior necessary for the creation of artificial vision systems and non-volatile resistive memory devices based on transparent memristive nanostructures [3].

This work is devoted to the formation of transparent ZnO-based memristive nanostructures by radio-frequency (RF) magnetron sputtering in an argon atmosphere at room temperature on glass substrates and the study of their resistive switching for use in artificial vision systems and non-volatile resistive memory devices that have the potential to detect, process and store visual information.

Transparent ITO/ZnO/ITO memristor nanostructures (Fig. 1) were formed by magnetron sputtering using a VSE-PVD-DESK-PRO installation (AcademVac). Thin films of nanocrystalline ZnO with a thickness of 60 nm were deposited on glass substrates with a transparent conducting ITO layer by RF magnetron sputtering of a ZnO ceramic target with a purity of 99.99% in an argon atmosphere at room temperature. The spray power was 75 W, and the operating pressure was $5\cdot10^{-3}$ mbar. ITO films with a thickness of 200 nm (bottom electrode) were deposited on glass substrates by pulsed magnetron sputtering at a frequency of 100 kHz (MF) in an argon atmosphere at room temperature. The spray power was 200 W, and the operating pressure was $2\cdot10^{-3}$ mbar. The top ITO electrode with a thickness of 150 nm and a diameter of 550 μm was deposited on the surface of the ZnO film also by MF magnetron sputtering in an argon atmosphere at room temperature using a metal mask.

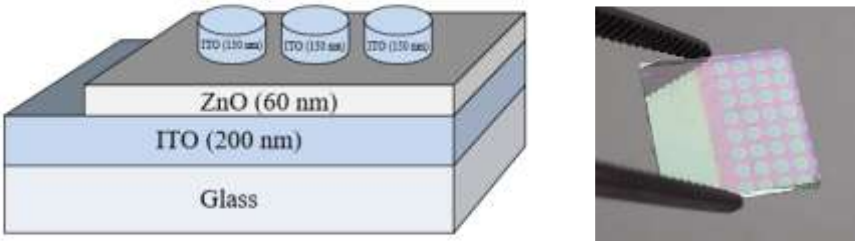

Figure 1. Structure and appearance of a transparent ITO/ZnO/ITO memristor.

The surface morphology of ZnO films was studied using a Nova Nanolab 600 scanning electron microscope (FEI Company) and an atomic force microscope (AFM) in semi-contact mode at the NTEGRA nanolaboratory (NT-MDT). Measurements of the current-voltage characteristics of memristor nanostructures were carried out at room temperature in air using a Keithley 4200-SCS semiconductor parameter measurement system (Keilhley) and an EM-6070A submicron sensing setup with tungsten probes. Voltage was applied to the top electrode of the memristor, and the bottom electrode was grounded.

Analysis of SEM images (Fig. 2) showed that the surface morphology of ZnO films is uniform with an average grain size of 20-30 nm. Analysis of AFM images showed that ZnO films on glass substrates obtained in an argon atmosphere at room temperature have a nanocrystalline structure. In this case, ZnO films have a relatively smooth surface (5 × 5 μm) with an average roughness value of 6.3 ± 0.3 nm.

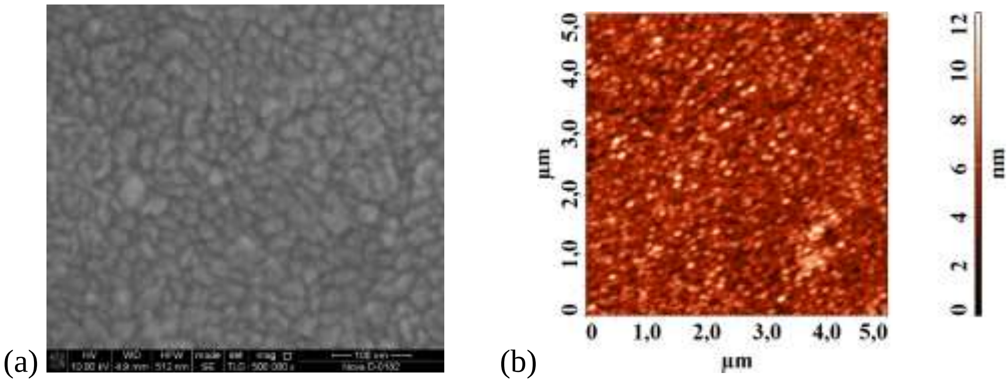

Figure 2. (a) SEM and (b) AFM images of a ZnO film on an ITO glass substrate.

To study the resistive switching of the ITO/ZnO/ITO memristive nanostructure, its current-voltage characteristics were measured. Fig. 3 shows the resulting typical current-voltage characteristic on a logarithmic scale, which shows the behavior of bipolar non-volatile resistive switching without the initial electroforming process.

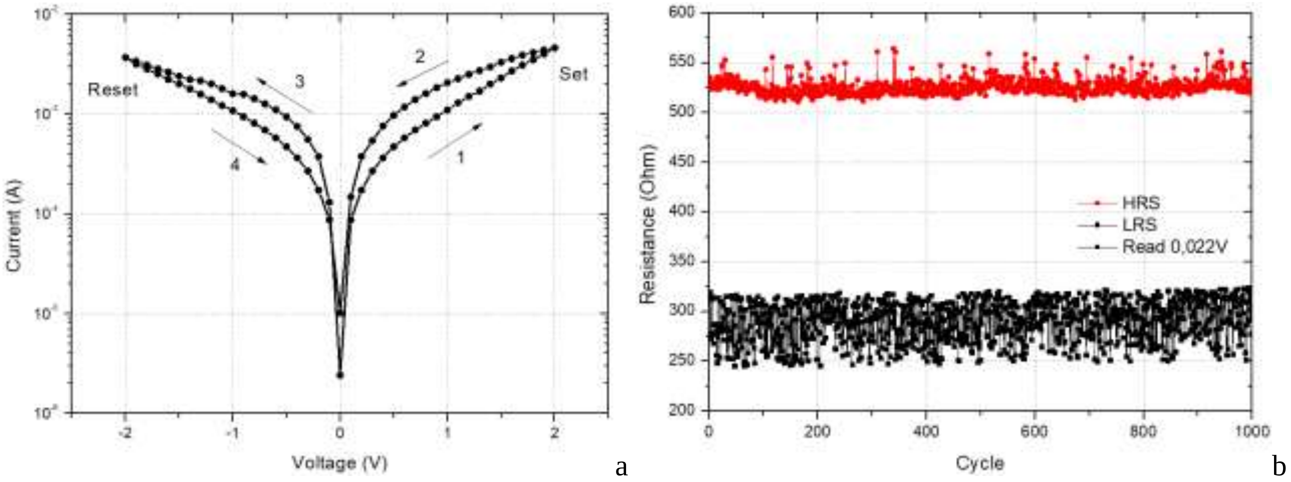

Figure 3. (a) Current-voltage characteristics and (b) resistive switching of the transparent ITO/ZnO/ITO memristor.

Thus, the possibility of creating transparent memristive ITO/ZnO/ITO nanostructures by magnetron sputtering in an argon atmosphere at room temperature on glass substrates for use in artificial vision systems and non-volatile resistive memory devices has been demonstrated. The obtained results of measuring the current-voltage characteristics and studying the resistive switching of memristive nanostructures showed that the change in resistance from the HRS to LRS state occurs at 2.0 ± 0.1 V, and from LRS to HRS at -2.0 ± 0.1 V, while the switching current is of the order of 5 mA. It is shown that HRS is equal to 530 ± 10 Ohm, and LRS is equal to 285 ± 40 Ohm, the ratio of resistances in the states is HRS/LRS = 1.86 at a reading voltage of 0.022 V. The results obtained can be used in the formation of memristive nanostructures, both on glass and on flexible substrates.

The reported study was funded by the Russian Federation Government (Agreement № 075-15-2022-1123) (in part of memristor structures resistive switching investigation). The fabrication of metal oxide thin films by magnetron sputtering were supported by a grant from the Russian Science Foundation № 23-29-00827, https://rscf.ru/project/23-29-00827/, at Southern Federal University.

1. P. Praveen, T. Priya Rose, K.J. Saji, *Microelectronics J.* **121**, 105388 (2022).
2. Zh. Yu, J. Jia, X. Qu, et al., *Molecules* **28**, 5313 (2023).
3. T. Cheng, J. Rao, X. Tang, et al., *Electronics* **7**, 141 (2018).

P30

Capillary flow and liquid spreading dynamics on aluminum surfaces structured by nanosecond laser irradiation

A.S. Bayankina, D.A. Shivarova, D.K. Kuznetsov, V.Ya. Shur

Ural Federal University, Institute of Natural Sciences and Mathematics, 620002, Ekaterinburg, Russia
dimak@urfu.ru

Aluminum surfaces with 1D array of opened microchannels were produced by direct nanosecond laser micro- and nano-structuring. The created surfaces demonstrate excellent drop spreading performance at room temperature. The obtained effects highlight the potential of nanosecond laser structuring in controlling the wettability of metal surfaces for various applications.

The surfaces of 0.5-mm-thick aluminum substrates were treated by precision fiber laser marking system MiniMarker 2 - M20, Laser Center LLC, Russia, with a wavelength of 1064 nm and a pulse duration of 110 ns. The imaging of obtained surface structures was made by Auriga Crossbeam Workstation (Carl Zeiss). The surface wettability was characterized using the static contact angle. The contact angle was measured by a drop shape analyzer DSA25S (KRUSS, Germany) using the sessile drop technique. The liquid spreading dynamics of the produced samples was studied by video imaging capillary spreading of deionized water on a horizontally positioned sample.

The nanosecond laser treatment of aluminum surfaces using scanning mode with line densities in range from 1 to 25 lines per mm leads to formation of periodical microchannels. The inner walls and outer edges of each microchannel are decorated with irregular shapes particles with sizes from several nanometers to several micrometers. Thus, because of processing by laser radiation, a micro- and nanoscale hierarchical structure is created on the surface of aluminum plates.

The developed surfaces were tested for liquid spreading dynamics at room temperature. The tests show that the spreading is not uniform: in the direction of the microchannels, the water has spread much further and faster than in the perpendicular direction. It is revealed that the water spreads with a maximum velocity up to 100 mm/s along the parallel microchannels and strongly depends on microchannel density.

The obtained results showed that the sequence of flow regimes in the hierarchical capillary structure is much more complicated than in simple capillary geometries like tubes and open microchannels with smooth surfaces. The capillary flow velocity undergoes significant fluctuations prior to the Washburn’s regime, making the identification of the sequence of early flow regimes more difficult [1,2].

The detailed investigations of capillary flow showed that spreading dynamic can be divided into two main stages. 1) Flow initiation. The liquid enters the microchannel, forming a front that moves due to capillary and surface forces. The front advances uniformly along the channel, filling it evenly. 2) Secondary front formation. The liquid forms a secondary front due to overflowing through local surface irregularities or defects in the microchannel. This phenomenon is driven by the interaction between capillary forces and hydrodynamic conditions within the channel, leading to the creation of new liquid fronts which spreads perpendicular to main direction. The velocity of secondary front depends on the distance between adjacent microchannels.

The research provides a simple and controllable way to create artificially functional surface that can be used to fabricate micro- and nanoscale functional devices.

The equipment of the Ural Center for Shared Use “Modern nanotechnology” Ural Federal University (reg. no. 2968) was used. The authors are grateful for financial support of the Ministry of Science and Higher Education of the Russian Federation (state task FEUZ-2023-0017).

1. E.W. Washburn, *Phys.Rev.* **17**, 273 (1921).
2. R. Fang, H. Zhu, Z. Li, et al., *Nanomaterials* **10**, 796 (2020).

P31

The calibration of cantilever stiffness of AFM probes

S.A. Melnikov, M.S. Kosobokov, L.V. Gimadeeva, D.K. Kuznetsov, V.Ya. Shur, D.O. Alikin

School of Natural Sciences and Mathematics, Ural Federal University, 620000, Ekaterinburg, Russia
mihail.kosobokov@urfu.ru

The determination of the atomic force microscopy cantilever stiffness is everyday routine in the nanomechanical measurements and other techniques required quantification of the forces acting on the probe. Typically, manufacture provides a range of the values for cantilever stiffness, as the technological process involved in probe fabrication introduces variability that affects the probe's geometry, particularly its thickness. Therefore, it is often the user's responsibility to accurately calibrate the probes. Over the last few decades, reputable metrological institutions have proposed several highly accurate techniques for cantilever calibration, with an average error often below 3% [1,2]. However, many of these techniques present challenges in terms of implementation or require expensive external equipment, which is often not accessible to the average user. Fortunately, there are simpler and more widely available calibration techniques: analytical calculation the stiffness based on dimensional parameters or eigen frequencies, evaluation the stiffness from the parameters of the cantilever's constrained vibration (known as the Sader method) [3], or determination the stiffness through the measurement of thermal noise [4]. Another method involves performing quasistatic measurements of the cantilever stiffness by applying pressure against a reference cantilever with known parameters [5].

In this report, we estimate cantilever stiffness by all mentioned above methods using scanning probe microscopes NTEGRA Aura (NT-MDT, Russia) and Asylum MFP-3D (Oxford instruments, USA). Scanning electron microscope AURIGA CrossBeam (Carl Zeiss, Germany) has been used for precise measuring of the probe geometric parameters. We discovered some probes have thickness variation along length of cantilevers that significantly affects the static and dynamic properties of the cantilever. For example, the mode constant for rectangular cantilever, that is used in thermal noise method, becomes inaccurate when thickness is unevenly distributed. Also, for solving inverse problem by finite element method, neglecting this characteristic can lead to discrepancy in stiffness of up to 9%. Also, we found out that the values of stiffness obtained for reference cantilevers by thermal noise method using Doppler vibrometer have systematic error related to inability to focus laser on the edge of cantilever. A laser spot shift from the edge required for measurement gives an overestimation of the stiffness up to 12% associated with the radius of laser spot on cantilever. Thus, another significant disadvantage of the Doppler vibrometer for stiffness calibration was revealed - sensitive to position of laser on the cantilever relative tip of probe. The last important find is the significant influence of the cantilever incline in microscope on its effective stiffness and the importance of taking into account the length of the tip for correct calculations [6]. Therefore, a FEM simulation offers a robust approach to calibrate cantilever stiffness and sensitivity and avoid direct contact with the surface, thereby preserving the probe's integrity and preventing deformation.

The research funding from the Ministry of Science and Higher Education of the Russian Federation (Ural Federal University Program of Development within the Priority-2030 Program) is gratefully acknowledged. The equipment of the Ural Center for Shared Use “Modern nanotechnology” Ural Federal University (Reg. no. 2968) was used.

1. T.U. Ilmenau, P. Bundesanstalt, IMEKO 23rd TC3, 13th TC5 4th TC22 Int. Conf., Helsinki (2017).
2. R.S. Gates, J.R. Pratt, *Nanotechnology* **37**, 375702 (2012).
3. J.E. Sader, J.A. Sanelli, et al., *Rev. Sci. Instrum.* **83**, 103705 (2012).
4. R. Proksch, T.E. Schäffer, et al., *Nanotechnology* **15**, 1344 (2004).
5. R.S. Gates, M.G. Reitsma, *Rev. Sci. Instrum.* **78**, 086101 (2007).
6. L.O. Heim, M. Kappl, et al., *Langmuir* **20**, 2760 (2004).

P32

Investigation of nanodiamonds as a potential targeted drug delivery system.

P.A. Mutovkin, A.A. Mosunov

Sevastopol State University, 299053, Sevastopol, Russia
pasha.mutovkin2001@mail.ru

Currently, one of the most promising approaches in the treatment of various diseases is targeted drug delivery. This method allows to reduce the unwanted side effects of the medication by decreasing its concentration in non-target organs or tissues. To achieve this, it is essential to ensure reliable binding between the drug and the delivery molecule, while the molecule itself should be biologically inert, to avoid any potential harm to the patient's health [1].

Various allotropic forms of carbon, such as fullerenes, fullerenols, nanodiamonds of different origins, and nanotubes, can act as potential delivery molecules [2]. We previously conducted a study on fullerenes and their aggregates [3, 4], as well as the binding of nanodiamonds synthesized by detonation with one of the standard dye used in biological research - methylene blue (MB) using atomic force microscopy techniques. The results of these studies did not provide a clear answer about the type and nature of the binding between the studied substances. Therefore, in this paper, we continue our research on the possibility of nanodiamond binding to MB using Raman spectroscopy.

The following solutions were prepared for the research: nanodiamonds synthesized by detonation at a concentration of 0.1 mg/mL, methylene blue at a concentration of 10^{-3} mg/mL, as well as several mixtures of these two substances with different concentrations of nanodiamonds (0.1, 0.064, and 0.01 mg/mL) and methylene blue (10^{-3} mg/mL). These solutions were applied to the active parts of SERS substrates produced at the Laboratory "Applied Plasmonics", BGUIR in Minsk, Belarus. The research was conducted on the NtegraSpectra Raman spectrometer at the Research laboratory "Molecular and Cellular Biophysics", Institute for Advanced Studies, SevSU. Analysis was performed using three lasers with wavelengths of 473, 532, and 633 nanometers in accumulation mode (40 scans of 5 seconds each), with a diffraction grating set at 150 lines per millimeter.

Figures 1-3 show the obtained spectra.

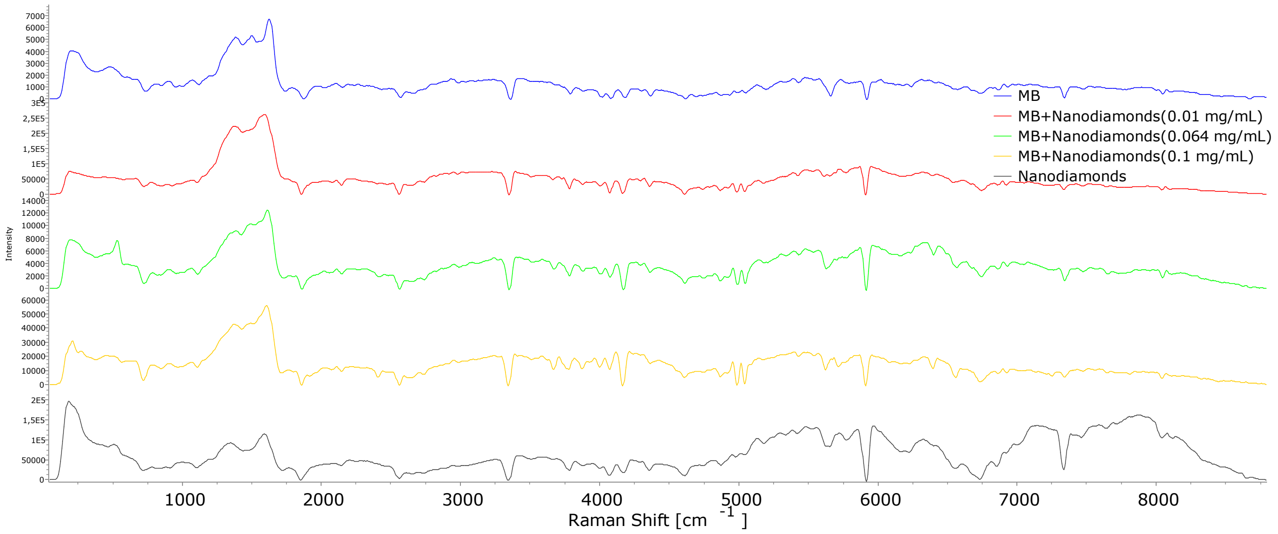

Figure 1. SERS spectra of solutions obtained using a laser with a wavelength of 473 nm.

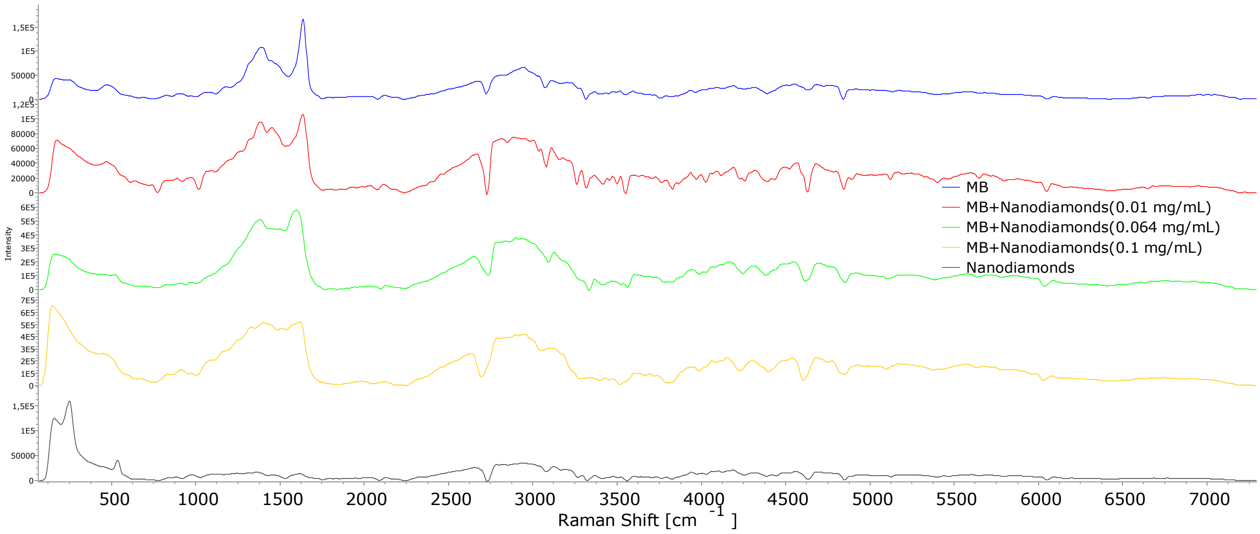

Figure 2. SERS spectra of solutions obtained using a laser with a wavelength of 532 nm.

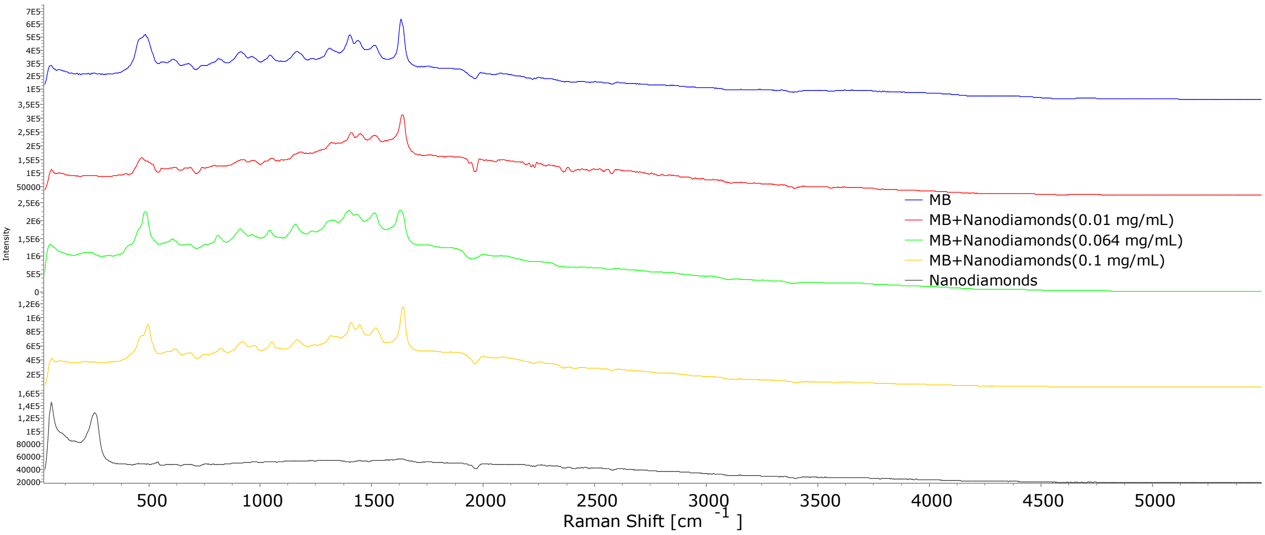

Figure 3. SERS spectra of solutions obtained using a laser with a wavelength of 633 nm.

The spectra of methylene blue and nanodiamonds obtained using a laser with a wavelength of 473 nm are very similar, leading to an overlap of characteristic peaks in the spectra of solutions with different concentrations of nanodiamonds. This makes it challenging to identify the bonds formed in the mixture. The spectra obtained using lasers with wavelengths of 532 and 633 nm show clear peaks for methylene blue, but do not reveal peaks for nanodiamonds, possibly due to their low concentration in the solutions. In order to obtain more information, it is planned to increase the concentration of nanodiamonds and conduct additional experiments using other techniques.

1. E. Valeur, L. Knerr, M. Ölwegård-Halvarsson, et al., *Drug Discovery Today* **22**, 841 (2017).
2. S. Singhal, M. Gupta, Md. S. Alam, et al., *Nanotechnology* **1**, 29 (2022).
3. A. N. Torkhov, *Colloids and Surfaces A: Physicochemical and Engineering Aspects* **687**, 1 (2024).
4. N. Khinevich, K. Girel, H. Bandarenka, et al., *J. Phys.: Conf. Ser.* **917**, 1 (2017).
5. V.Y. Dolmatov, *Russ. Chem. Rev.* **76**, 339 (2007).

P33

Investigation of potential antifouling coatings using scanning probe microscopy.

P.A. Mutovkin, A.A. Mosunov

Sevastopol State University, 299053, Sevastopol, Russia
pasha.mutovkin2001@mail.ru

During the operation of hydraulic structures, ships and vessels [1] are exposed to various environmental factors, such as the mechanical and chemical effects of water and wind, as well as interactions with each other during parking and mooring. To protect them, special paints are often used, which must meet certain requirements, including adhesion to the painted surface, elasticity, resistance to external influences, and effectiveness against fouling [2]. There are several types of such paints: SMT (Soluble Matrix Type Paints) - they are based on the use of rosin as a film former; TBT-free (Selfpolishing) are systems based on copper, silicon or zinc acrylates, without rosin, without tributyltin (TVT); Non-Stick are anti-fouling coatings based on silicon- or fluorine-containing polymers with a low elastic modulus [3].

As an organic matrix, we used formulations based on acrylate and epoxy resins, rosin, polyurethane binders, and other organic materials, as well as the PK-Marine enamel base with the replacement of standard antifouling components with studied nanoparticles. This wide range of organic binders presented certain challenges in conducting experiments and analyzing the results. The nanoparticles used as antifouling agents were ZnO-FeZnO, CuO-FeCuO, $ZnTi_2O_4$-ZnO, $ZnTi_2O_4$-TiO_2 и Ag-TiO_2. The antifouling agent percentage was 10-20% by weight. We chose the mass fraction of nanoparticles in the paint because adding less than 10% does not create a significant antifouling effect, which reduces the effectiveness of the paint. On the other hand, the addition of more than 20% of nanoparticles can lead to their agglomeration, which increases the surface roughness and promotes the growth of biofouling. Additionally, the high content of nanoparticles in the composition can lead to an increase in the rate of curing, potentially making it impossible to apply to the protected surface. Our colleagues from the Tomsk Institute of Strength Physics and Materials Science SB RAS conducted the synthesis of these nanoparticles [4].

Previously, we investigated the physical and mechanical properties of the coating using the Labthink MXD-02 friction machine and the ASTM D1894 measurement method (data is in the process of being published). According to the results of this study, the static and dynamic coefficients of friction for the samples indicate that the lowest values were obtained for the sample coated with Bioplast-52 enamel, and the highest values were obtained for the sample with $ZnTi_2O_4$-ZnO nanoparticles added to the organic base of the Bioplast-52 enamel without an anti-fouling agent. It follows from the studies conducted that coatings containing CuO-FeCuO and Ag-TiO_2 nanoparticles have physical and mechanical parameters similar to those of the Bioplast-52 coating.

In this paper, we continue the study using scanning probe microscopy with the NtegraSpectra atomic force microscope from the Research Institute "Molecular and Cellular Biophysics" at the Institute for Advanced Studies of SevSU. The HAFM/W_2C console was used as the measuring probe. It is a micromechanical silicon device consisting of a rectangular silicon base 3.6×1.6 mm in size with a thickness at the upper edge of 0.4 mm. In the center of the shorter side, there is a beam 223 microns long, 34 microns wide, and 3 microns thick. The upper surface of the beam has a reflective gold coating. At the free end of the longer side of the beam, there is a tip 12 microns high with an angle of about 22 degrees at the apex and a curvature radius of 5 nanometers. This tip serves as the measuring probe. The surface relief measurement, $h = h(x, y)$, was performed in the semi-contact scanning mode. In this mode, the probe makes contact with the surface during scanning at the resonant frequency of the mechanical vibrations of the beam. The amplitude of these vibrations is constant and equal to $A_{\max}$ = const.

Figure 1 shows the scans of the samples. The scanning area is 5×5 microns, the number of points is 500, the speed is 0.5 Hz. Table 1 shows the results of measuring the roughness of samples using the method ASME B46.1.

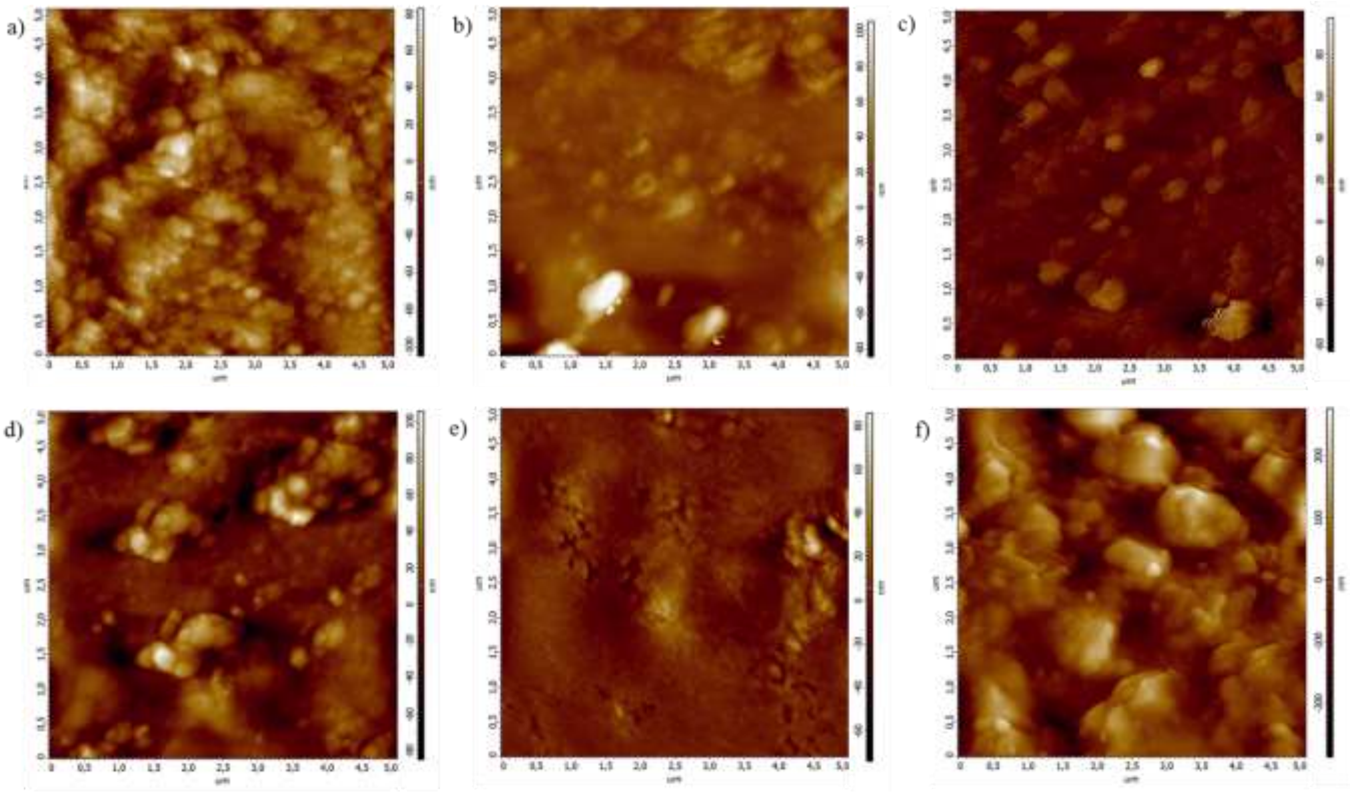

Figure 1. Surface scans of samples: (a) Bioplast; (b) $ZnTi_2O_4$-ZnO; (c) $ZnTi_2O_4$-TiO_2; (d) ZnO-FeZnO; (e) Ag-TiO_2; f) CuO-FeCuO.

Table 1. Roughness results of samples:

Sample	Arithmetical mean deviation of roughness profile R_a, nm
Bioplast-52	14.887
$ZnTi_2O_4$-ZnO	6.754
$ZnTi_2O_4$-TiO_2	7.292
ZnO-FeZnO	6.664
Ag-TiO_2	8.857
CuO-FeCuO	37.996

Based on the results, it can be concluded that the sample with CuO-FeCuO nanoparticles had the highest surface roughness, while the one with ZnO-FeZnO had the lowest. Surface roughness can affect the mechanical properties of a material, such as its wear resistance, friction, and adhesion.

1. Y.Q. Gu, S.W. Yu, J.G. Mou, et al., *Materials* **13**, 444 (2020).
2. M.E. Callow, J.E. Callow, *Biologist* **49**, 10 (2002).
3. A.M.C. Maan, A.H. Hofman, W.M. de Vos, *Adv. Funct. Mater.* **30**, 1 (2020).
4. O.V. Bakina, N. Svarovskaya, L. Ivanova, et al., *Biomimetics* **8**, 1 (2023).

P34

Numerical study of tubular piezoelectric transducer with spiral electrodes made of porous piezoceramics

A.V. Nasedkin[1], A.A. Nasedkina[1], M.E. Nassar[2]

[1]*Southern Federal University, 344090, Rostov-on-Don, Russia*
avnasedkin@sfedu.ru

[2]*Menoufia University, 32952, Menouf, Egypt*

Piezoelectric transducers, which generate predominantly torsional vibrations, have important applications, for example, in micromotors, delay lines, piezoelectric vibration viscometers and other devices. Various designs of torsional transducers are known, for example, spiral-shaped transducers, transducers with multielectrode coating and non-uniform polarization fields, transducers with circumferential polarization, and so on. This investigation presents the results of numerical modelling of a piezoelectric transducer made of porous piezoceramics in the shape of a hollow cylinder with two spiral (helical) wire electrodes located on its outer surface. In such transducer, when a potential difference is applied between the spiral electrodes, due to the piezoelectric effect, coupled axial and torsional displacements are generated, and there are predominantly torsional vibration modes.

For numerical study of this transducer the finite element method and the ANSYS package were used. A special feature of the investigation is the study of the influence of non-uniform polarization and porosity of the piezoceramic material on the efficiency of the transducer. The inhomogeneity of the polarization field was considered separately at the micro and macro levels. Namely, when determining effective moduli at the microlevel in a representative volume of porous piezoceramics, homogenization problems were solved for a nonuniformly polarized piezoceramics, and the inhomogeneity of the polarization field in the vicinity of the pores was taken into account from the preliminary solution of the electrostatics problem, which models the polarization process in a simplified formulation [1]. Further, porous piezoceramics were modeled as a homogeneous continuous material with effective moduli, but at the macro level another heterogeneity was considered. To do this, for the constructed finite element model of a cylinder with the dielectric properties of unpolarized ceramics, the process of its polarization was again simulated, but now with specified spiral electrodes. From the solution of the electrostatics problem, for each finite element the vectors of electric field strength and electric induction were found, from which the elemental coordinate system with the polarization axis parallel to these vectors was determined. Then the dielectric elements were modified into piezoelectric finite elements with material properties calculated from the effective properties of uniformly polarized porous piezoceramics in the original global Cartesian coordinate system according to the formulas for their transformation when transitioning to elemental coordinate systems in accordance with the adopted polarization model. Thus, each finite element of the converter model had its own different material piezoelectric properties.

After this, the operating efficiency of a tubular transducer with spiral properties was studied in static conditions and in steady-state oscillation modes. Numerical results were compared for models of a transducer made of dense piezoceramics, of conventional porous piezoceramics, and of porous piezoceramics with metallized pore surfaces. In the latter case, methods for calculating the effective moduli of porous piezoceramics with metallized pore surfaces, presented in [2, 3], were used.

Calculations of the first frequencies of electrical resonances and antiresonances of torsional vibrations were carried out and the amplitude-frequency characteristics of the electrical impedance of the piezoelectric transducer were constructed in the mode of steady-state oscillations near the operating resonant frequencies for the various models of porous piezoceramic materials described above. As a result of the numerical experiments, it was concluded that a tubular transducer with spiral electrodes made of porous piezoceramics is effective for generating torsional movements.

This study was supported by the Russian Science Foundation, grant number No. 22-11-00302, https://rscf.ru/project/22-11-00302/, at the Southern Federal University.

1. A.V. Nasedkin, A.A. Nasedkina, Y.V. Tolmacheva, *Comput. Contin. Mech.* **16**, 476 (2023).
2. A.V. Nasedkin, A.A. Nasedkina, M.E. Nassar, *Mech. Solids* **55**, 827 (2020).
3. M.E. Nassar, N.A. Saeed, A.V. Nasedkin, *Appl. Math. Model*. **124**, 241 (2023).

P35

Dopant distribution in silicon surface layer after laser hyperdoping

V.I. Pryakhina[1], S.I. Kudryashov[1,2], M.S. Kovalev[1,2], R.F. Saifetdinov[1], A.R. Akhmatkhanov[1]

[1]School of Natural Sciences and Mathematics, Ural Federal University, 620000 Ekaterinburg, Russia
[2]Lebedev Physical Institute, 119991, Moscow, Russia
viktoria.pryahina@urfu.ru

Introducing impurities into the Si lattice with doping is a known way to modify its properties. Increasing the dopant concentration in silicon surface layer to the level higher than the equilibrium solubility, so-called hyperdoping, extends its absorption to near- and mid-infrared range [1-3]. For this purpose, the most promising materials are transient metals and chalcogens. Pulsed laser irradiation of silicon surface covered by thin film of dopant material is one of the methods of hyperdoping. Such laser hyperdoping can be naturally accompanied by annealing which restores crystallinity of the surface layer. Tuning laser processing parameters could facilitate obtaining dopant concentrations, doped layer thickness and doping/annealing conditions for specific applications.

In this work, dopant distribution and chemical state in the Si surface layer, hyperdoped from the pre-deposited metallic film, were studied by X-ray photoelectron spectroscopy (K-Alpha$^+$, ThermoFisher Scientific) and scanning electron microscopy (Auriga CrossBeam, Carl Zeiss) imaging. The crystallinity of the hyperdoped layer was investigated by confocal Raman microspectroscopy (Alpha 300 AR, WiTec). The absorption of hyperdoped samples was characterized by collecting transmittance and reflectance spectra in visible and near-infrared range (Cary 5000, Agilent).

Nominally undoped Si(100) wafers, coated by Au film with thickness from 20 to 100 nm, had been irradiated in the ambient atmosphere by 100-ns laser pulses at 1064-nm wavelength using a MiniMarker-2 M20 marking system (LTC, Russia) equipped with Yb fiber laser (IPG Photonics, IRE-Polus, Russia). The combination laser parameters had been chosen to provide diffusion of dopant into silicon and minimize ablation of materials.

Gold nanocrystallites precipitated on the Si nanograins inside the recrystallized layer and small gold clusters sedimented in the hyperdoped Si layer over the gold diffusion length were observed. The laser-hyperdoped Si samples have shown lower transmittance in the intra-gap spectral range (above 1.1 μm) comparing to the highly transmissive Si wafer which implies the impurity absorption. Resistivity in the hyperdoped samples changed as a result of laser light irradiation at 1550 nm wavelength. The measurements were carried out in the temperature range from -175°C to room temperature. Preliminary measurements of temperature dependence of samples resistivity have revealed the appearance of dopant levels with depth about 0.15-0.2 eV. The obtained results pave the way towards Si detectors for the near infrared range.

The research funding from the Ministry of Science and Higher Education of the Russian Federation (Ural Federal University Program of Development within the Priority-2030 Program) is gratefully acknowledged. The equipment of the Ural Center for Shared Use “Modern Nanotechnology”, Ural Federal University (Reg. no. 2968) was used.

1. S.Q. Lim, J.S. Williams, *Micro* **2**, 1 (2022).
2. J. Fu, D. Yang, X. Yu, *Phys. Status Solidi* **219**, 2100772 (2022).
3. M. Kovalev *et al, Materials* **16**, 4439 (2023).

P36

Local doping of lithium niobate surface layer using femtosecond laser irradiation

V.I. Pryakhina, P.A. Paletskikh, D.E. Tkachuk, B.I. Lisjikh, E.D. Savelyev, A.R. Akhmatkhanov

School of Natural Sciences and Mathematics, Ural Federal University, 620000 Ekaterinburg, Russia

viktoria.pryahina@urfu.ru

Lithium niobate ($LiNbO_3$) crystals are widely used in nonlinear and electro-optical applications. For the applications which exploit waveguides the important role plays the fact that optical properties can be controlled by impurities incorporation [1]. Doping the crystal with specific impurities provides a medium with controlled optical properties. Thus, for optical waveguides titanium diffusion and proton exchange are the two main complex techniques [1,2].

Ultrafast pulsed laser irradiation is a possible alternative for the surface layer doping as it is successfully used with silicon [3]. Focused laser beam allows to localize doped area at the wafer and tuning laser processing parameters could facilitate obtaining dopant concentrations, doped layer thickness and doping/annealing conditions for specific applications.

Congruent lithium niobate z-cut plates covered by Ti film (for Ti doping) or benzoic acid (for proton exchange) layer were exposed to femtosecond laser irradiation of 1064 nm wavelength. The irradiated surfaces were cleaned from residual deposited layers and after that studied by X-ray photoelectron spectroscopy (K-Alpha$^+$, ThermoFisher Scientific) and confocal Raman microspectroscopy (Alpha 300 AR, WiTec) to detect impurities incorporation. The surface morphology was visualized by scanning electron microscopy (Auriga CrossBeam, Carl Zeiss). The transmittance and reflectance spectra were collected in visible and near-infrared range by spectrophotometer (Cary 5000, Agilent).

The analysis of the samples after Ti doping by X-ray photoelectron spectroscopy has confirmed the incorporation of Ti into a surface layer. Raman spectra collected for samples after laser-assisted proton exchange demonstrated the OH^- adsorption band typical for lithium niobate after conventional proton exchange process. The doped surfaces have not received significant damages from laser irradiation. The doped samples have showed decrease in transmittance and reflectance intensities comparing to initial undoped lithium niobate plates.

Presented results demonstrate the first successful application of laser-assisted doping for lithium niobate single crystals.

The research funding from the Ministry of Science and Higher Education of the Russian Federation (Ural Federal University Program of Development within the Priority-2030 Program) is gratefully acknowledged. The equipment of the Ural Center for Shared Use “Modern Nanotechnology”, Ural Federal University (Reg. no. 2968) was used.

1. T.R. Volk, M. Wöhlecke, *Lithium Niobate* (Springer, Berlin, Heidelberg), (2008).
2. N. Courjal, M.-P. Bernal, A. Caspar, et al., *Lithium Niobate Optical Waveguides and Microwaveguides*, in: *Emerg. Waveguide Technol.*, ed by Kok Yeow You (InTech), 153 (2018).
3. S.Q. Lim, J.S. Williams, *Micro* **2**, 1 (2022).

P37

Electromechanical and ferroelectric hysteresis in porous piezoceramics

I.A. Shvetsov, E.I. Petrova, A.N. Reznichenko, N.A. Shvetsova, A.N. Rybyanets

Southern Federal University, 344090, Rostov-on-Don, Russia

arybyanets@gmail.com

Owing to the superior ferroelectric and capacitive properties of ferroelectric ceramics, they are widely used in various applications, such as energy storage devices, high-energy capacitors, night-vision technology, ferroelectric random-access memory, and medical ultrasound. One of the consequences of domain switching in ferroelectrics is the occurrence of ferroelectric hysteresis. The study of hysteresis can provide valuable information about various physical processes occurring in ferroelectric materials, such as space charge relaxation, domain orientation process, pinning of domain walls, and defect ordering. Therefore, extracting saturated displacement-field (*D-E*) and strain-field (*S-E*) hysteresis loops is vital to the study of ferroelectric properties.

Porous ferroelectric ceramics possess usually remarkably less polarizability than dense ceramics; instead, they display high tenability of various physical properties. However, the effect of porosity on the polarization switching behavior of ferroelectrics, which is the fundamental physical process determining their functional properties, remains poorly understood. In part, this is due to the complex effects of porous structure on the local electric field distributions within these materials [1].

In present work, particular aspects of the switching properties of the PZT-type porous piezoceramics with different relative porosity were investigated by comparison with the dense piezoceramics of the same composition. PZT type dense and porous piezoelectric ceramics of the composition $Pb_{0.95}Sr_{0.05}Ti_{0.47}Zr_{0.53}O_3$ + 1% Nb_2O_5 with relative porosity to 40% and average pore size of 30 μm were chosen as the object of the study. Porous PZT samples were fabricated using the pore former burning-out method. A dense PZT samples with the same chemical composition were fabricated by conventional sintering method. Field-dependent polarization and strain loops were recorded at the bipolar electric fields in the range of 0 –5 kV/mm and in the frequency range of 0.001 – 5 Hz using a sinusoidal bipolar waveform. Measurements and analysis were performed by means of the Electromechanical Measurement System (STEPHV) and Electromechanical Response Characterization Program (STEP) from, TASI Technical software Inc., combining large signal modelling of the mechanical and electrical behavior of ferroelectric materials.

Analysis of large-signal displacement-field (*D-E*) and strain-field (*S-E*) hysteresis loops made it possible to obtain full sets of parameters characterizing the switching processes and ferroelectric hysteresis behavior of the porous and dense piezoceramics and understand the effect of porosity on the polarization-field response of ferroelectric materials. It was shown that the differences in switching behavior of dense and porous piezoceramics are due to the specific features of the domain structure and microstructure of porous piezoceramics. The resulting information provides new insights in the interpretation of the physical properties of porous ferroelectric materials to inform future effort in the design of ferroelectric materials for piezoelectric sensor, actuator, energy harvesting, and ultrasonic transducer applications.

The study was financially supported by the Russian Science Foundation Grant No. 22-11-00302, https://rscf.ru/project/22-11-00302/ at the Southern Federal University.

1. A.N. Rybyanets, *IEEE Trans. UFFC*. **58**, 1492 (2011).

P38

Integration and optimization of nanocalorimetric sensors for combined Raman microscopy and nanocalorimetry analysis

I.I. Rulev, A.F. Ahkiamova, A.P. Melnikov, A.F. Abukaev, D.A. Ivanov

NUST MISIS, 119049, Moscow, Russian Federation
irulev@misis.ru

In this study, the development and fabrication of specialized holders for nanocalorimetric sensors to interface a nanocalorimeter and a Raman microscope were conducted. Custom holders for XENSOR's XEN-39390 series MEMS nanocalorimetric sensors were created to facilitate their integration with the Horiba LabRAM Raman microscope. Additionally, essential pharmaceutical substances and consumables, including AB208600-25G Caffeine, 99.7%, ABCR, were procured.

Initial investigations on caffeine, seratrodast, 4-acetamedofenol, and PVDF polymer were conducted using classical methods such as optical microscopy, X-ray diffraction, and thermal analysis. Optimal cleaning techniques for nanocalorimetric sensors from thermal decomposition residues were identified, utilizing standard chemical solvents like chloroform and annealing methods.

To merge the analytical capabilities of the nanocalorimeter and Raman microscope, software and hardware interfacing were achieved using a TTL standard analog signal, with the rising edge of the TTL signal being recognized by the Raman microscope's trigger device. Calibration procedures for nanocalorimetric chips across different operational modes and temperature ranges of the Raman spectrometer were implemented, using tin and indium as calibration standards. This calibration method, performed in situ with the Raman microscope laser active, provided calibration curves indicating melting peak shifts of the standards relative to laser power, thus enabling precise temperature jump assessments on the sensor.

The temperature response of the chips under various laser powers was studied, identifying optimal operational modes for the combined system. Initial tests revealed temperature jumps on the calorimetric sensor caused by laser heating, which could potentially distort experimental data. Continuous recording of the thermocouple signal demonstrated that temperature stabilization on the chip occurred in less than one second, with temperature jumps not exceeding 5°C. However, it was also noted that at 50% laser power, the silicon nitride membrane was damaged.

Functional and technical specifications for the integrated system were established, along with methodologies for combined Raman spectroscopy and nanocalorimetry experiments. These experiments included "Fast heating" mode (ultrafast heating and cooling between 6000 to 600000°C/min) and "Slow heating" mode, suitable for studying sample microparticles at rates typical of classical differential scanning calorimeters.

This research was funded by state support with the K1-2022-035 project in the framework of the strategic academic leadership program “Priority 2030”.

P39

Dielectric response of polar film heterostructure AlGaN/SiC/Si

I.T. Zezyanov[1], A.V. Solnyshkin[1], O.N. Sergeeva[1], Sh.Sh. Sharpfidinov[2],
I.P. Pronin[2], E.Yu. Kapnelov[2]

[1]*Tver State University,170100, Tver, Russia*
o_n_sergeeva@mail.ru
[2]*Ioffe Institute, 194021 Saint-Petersburg, Russia*

Currently, wide-bandgap semiconductors based on nitrides (AlN, GaN, AlGaN) are promising functional materials for laser diodes, microelectronics and photonics devices applications.

In this work, the dielectric properties of complex composite structures comprising $Al_xGa_{1-x}N$ layers were studied. These layers with periodically varied composition (x) were grown on a SiC/Si(110) hybrid substrate by chloride-hydride epitaxy. Analysis of the growth processes of interlayers (the periodic structure of AlGaN) shown that such a structure was a result of self-organization of the composition and the formation of a complex composite material associated apparently with the periodic relaxation of mechanical stresses accumulating during the heterostructure growth [1]. A thickness of the each layer was nearly equal to 70 nm. The upper layers contained AlN comprising low quantity of GaN. It can be assumed that a change in the $Al_xGa_{1-x}N$ composition is accompanied by the formation of heterojunctions and a system of built-in space charges, which should affect the dielectric properties of the above structures.

It was shown there was practically no dispersion of the dielectric constant of the AlN film in the frequency range of the measuring field from 10 to 10^6 Hz (Fig. 1a), while the frequency dependence of the dielectric loss tangent was characterized by a more pronounced dispersion. In $Al_xGa_{1-x}N$ films, a noticeable dispersion of dielectric characteristics is observed (Fig. 1b), which can be associated with both high direct current conductivity and the presence of space charge polarization (high-frequency range).

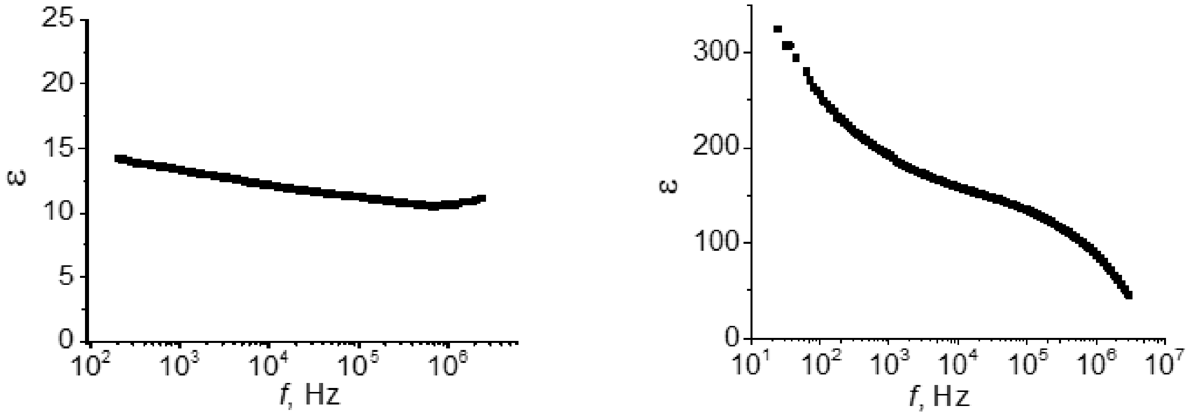

(a) (b)

Figure 1. Frequency dependences of the dielectric constant of the heterostructures: (a) AlN/SiC/Si, (b) AlGaN/SiC/Si.

The capacitance-voltage characteristic of the AlN film indicates a weak dependence of the capacitance on the magnitude and direction of the applied constant bias field. The structure comprising AlGaN layers is characterized by a noticeable dependence of the capacitance on the magnitude and direction of the bias field. For the AlN/SiC/Si structure, the change in capacitance is associated with the injection of charge carriers from the top metal electrode, while for a film comprising AlGaN layers of different compositions, the strong dielectric dispersion is due to the contribution of the capacitance of the interface layers and the injection of charge carriers.

1. S.A. Kukushkin, S.S. Sharofidinov, A.V Osipov, et al., *Phys. Solid State* **63**, 442 (2021).

P40

Elastically stressed state of ferroelectric nanocomposite, caused by the phase transition

V.N. Nechaev, A.V. Shuba

Military Educational and Scientific Centre of the Air Force N.E. Zhukovsky and Y.A. Gagarin Air Force Academy, 394064, Voronezh, Russia
shandvit@rambler.ru

The growing interest to nonuniform materials, as composite with nanofillers, can be explained by two reasons. On the one hand, it is due the potentials of obtaining materials with properties that are absent in uniform materials and with controlling their macroscopic properties [1]. On the other hand, it makes it possible to reveal the formation mechanism of composite macroscopic characteristics if some of its components have at least one characteristic size less than 100 nm [2]. However, the analysis of numerous researches shows absent complete conception of the formation mechanism of the composites properties, the main factors determining the composites macroscopic properties, their relationship with the microstructure, and also the methods for calculating these properties.

The aim of this work is to study the effect of electrostriction on the phase transition temperature in a separate ferroelectric particle in the shape of an ellipsoid located in a dielectric matrix when precisely taking into account depolarizing fields and nonlinear effects.

The thermodynamic potential Φ of a ferroelectric ellipsoid in a dielectric matrix is the sum of four terms: the thermodynamic potential Φ_1, related with the spontaneous polarization appearance $\vec{P}$; the contribution Φ_2 due to the relationship between electrostatic field $\vec{E}$ and polarization $\vec{P}$; the term Φ_3, taking into account electrostriction; the contribution Φ_4, determines the elastic energy of the material.

The equations, describing the distribution of order parameter $\vec{P}(\vec{r})$, electric field $\vec{E}(\vec{r})$ and elastic stress $\sigma_{ik}(\vec{r})$ in the sample, and also the boundary conditions for them, are obtained from the condition the first variation of the thermodynamic potential is equal to zero

$$\delta\Phi = \delta\Phi_1 + \delta\Phi_2 + \delta\Phi_3 + \delta\Phi_4 = 0. \qquad (1)$$

When varying the thermodynamic potential Φ it is necessary to take into account the dependence of its variables and σ_{ik} on each other. They are relationship by elastic equilibrium equations

$$\frac{\partial \sigma_{ik}}{\partial x_i} = 0. \qquad (2)$$

In essence, the interest us problem is the problem of finding the conditional extreme of the functional Φ. This fact and the static boundary conditions

$$\sigma_{ik} n_k \big|_{\Gamma} = F_i \qquad (3)$$

on the particle surface Γ with a unit normal vector $\vec{n}$, at the applied external force $\vec{F}$ to a unit surface area Γ, can be taken into account by the Lagrange multiplier method.

The components of the electric field are related by the equation $\mathrm{rot}\vec{E} = 0$. To exclude the dependence of the electric field coordinates, it should be taken into account the electric potential φ:

$$\vec{E} = -\vec{\nabla}\varphi. \qquad (4)$$

The solution of the problem for a ferroelectric inclusion, obtained after varying the functional Φ, changed in this way, makes it possible to find the shift of the phase transition temperature, the distribution of elastic stress $\sigma_{ik}(\vec{r})$ in the composite, depending on the shape and size of the particle, and on the matrix properties. The estimates of influence of the ferroelectric particles interaction on these effects have been made.

1. Prateek, V.K. Thakur, R.K. Gupta, *Chem. Rev.* **116**, 4260 (2016).
2. Q. Wang, J. Che, W. Wu, et al., *Polymers* **15**, 590 (2023).

P41

Nanometrology in nanomicroscopy

D.I. Yaminsky

Lomonosov Moscow State University, Faculty of Physics, 119991, Moscow, Russia
dyaminsky@nanoscopy.ru

Modern scanning probe microscopes as measuring instruments are gradually moving into the category of metrological equipment. Most scanning systems in these microscopes are built using piezoceramic displacements based on the inverse piezoelectric effect. The inverse piezoelectric effect was theoretically predicted in 1881 by Gabriel Lippmann [1] and brilliantly confirmed experimentally in the same year by Jacques and Pierre Curie [2]. Piezoceramic manipulators in their diversity allow for movements in the range from units to hundreds of microns. In this case, it is possible to provide movement in steps of a thousandth of a nanometer, which is widely used in microscopy for visualizing atoms, molecules, crystal lattices, etc.

In modern microscopes, errors corrections in the realized displacement are achieved using laser interferometers, capacitive and inductive sensors, and precision linear displacement meters. However, these systems can add their own noise, which can be noticeable when providing small sub-nanometer displacements.

For metrological support of scanning probe microscopes, static measures are widely used, which are a substrate with a regular surface relief applied. Dynamic measures, unlike static measures, change their geometric dimensions during the calibration of the microscope. In this case, you can vary not only the amount of movement, but also the speed of movement, as well as the trajectory of movement. As a result, hysteresis and creep have a constant value. In such measures, it is advisable to use a piezoelectric material with low hysteresis. The movement of the piezoceramic plate in the transverse direction (along the Z axis) depends only on the magnitude of the applied voltage U and the piezoelectric module d_{33}: $dZ = U\, d_{33}$.

An example of such a dynamic measure is the nanometer standard. It uses a piezoceramic plate. Metrological accuracy is achieved by the fact that a voltage of the same amplitude and frequency is applied to the electrodes of the plate. The reproducibility of the nanometer standard is at the level of 0.001 nm.

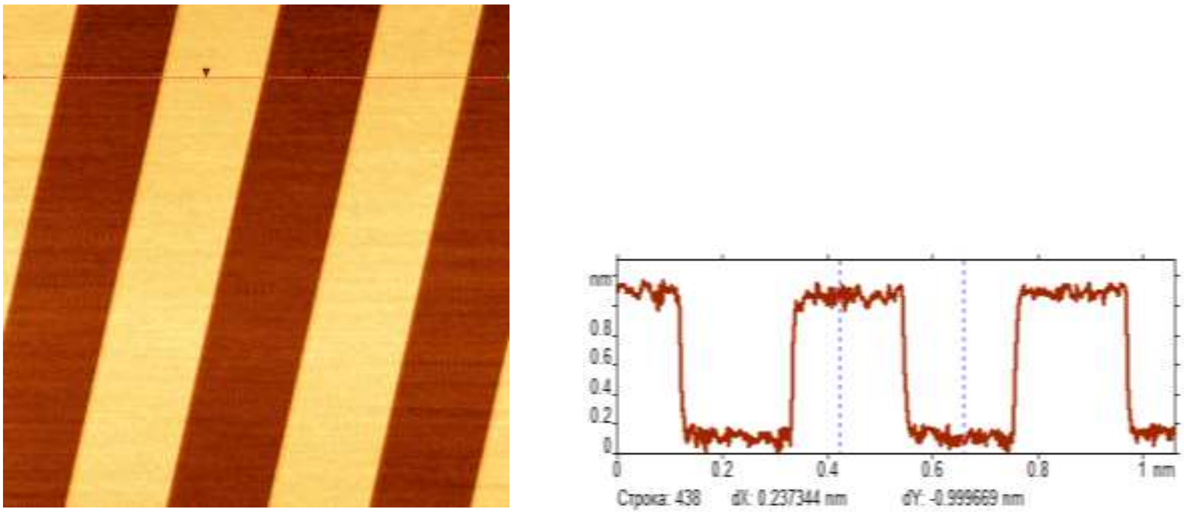

Figure 1. Image of a dynamic nanometer standard, observed in an atomic force microscope: 3D image (left) and cross-section (right).

Probe microscopy has taken the first, albeit confident, steps in the study of networks of living neurons. At the same time, new results, achievements and discoveries in the field of brain research are still ahead.

1. G. Lippmann, *Annales de chimie et de physique* **24**, 145 (1881).
2. J. Curie, P. Curie, *Comptes Rendus* **93**, 1137 (1881).

P42

Local change of the domain structure and conductivity under polarization reversal in BFO thin films

A.S. Abramov, D.O. Alikin, V.Ya. Shur

School of Natural Sciences and Mathematics, Ural Federal University, 620000 Ekaterinburg, Russia

alexander.abramov@urfu.ru

$BiFeO_3$ (BFO) is one of the most attractive multiferroic materials in the form of thin films due to high values of the spontaneous polarization and mobility of charged defects [1]. In BFO, interfaces such as domain walls, phase boundaries and grain boundaries exhibit significantly different electrical properties from the material bulk: enhanced electrical conductivity [2] and memristive effect [3]. At present, there is no consensus on the origin of resistive switching in BFO, which can be associated with the formation of the ionic filaments, variation of the Schottky barrier transparency or pure electronic processes [4, 5]. On the other hand, resistive switching in BFO can be influenced of the conductive domain walls, which are mobile, and their position can be controlled by an external electric field [2]. Understanding the mechanisms of the electronic transport and resistive switching is important for the development of new types of resistive random access memory devices [7,8].

Here, we studied BFO thin films produced by the chemical solution deposition and radiofrequency sputtering in the oxygen atmosphere. Crystal structure, polarization reversal and local conductivity for both sets of the thin films was investigated by the combination of the local and macroscopic techniques.

The first set of thin films had polycrystalline structure. The leakage current, resistive switching and additionally grain boundary conductivity was explored for these thin films. The phenomenon of self-organized formation of clusters consisting of 3-20 domains (grains) with a close direction of spontaneous polarization was observed in the film from first set with thickness about 500 nm. In this case, the conductivity at the boundaries of the clusters was 30-100 times greater than in the inside of clusters. One of the possible reasons of the enhanced conductivity at the boundaries of clusters is a coupling between polarization and stress occurring at the grain boundaries, which results in the mechanical strain.

On the other hand, the films from second set had an island-like structure, where each island had the same orientation of polarization vector. The films are characterized by the appearance of a state with high conductivity, which is activated due to resistive switching in the films. The measurements of local piezoelectric loops revealed strong contributions from electrostatics and backswitching on the shape of loops. For minimizing parasitic contributions, we were able to develop a technique using the modified PUND approach. An increase in the coercive field and bias field was found for films with a thickness of less than 10 nm, also accompanied by a significant decrease in the residual piezoelectric response, which was associated with an increase in the influence of clamping from the substrate for ultra-thin films.

Contrary to many earlier studies, postulating electromigration of the oxygen vacancies, we demonstrate resistive switching in BFO thin films to be caused by the pure electronic processes of trapping/releasing electrons and injection of the electrons by the scanning probe microscopy tip. The electronic transport was shown to be comprehensively described by the combination of the space charge limited current model and the presence of the built-in subsurface charge.

The authors are grateful for financial support of the Ministry of Science and Higher Education of the Russian Federation (state task FEUZ-2023-0017). The work was performed using the equipment of the Ural Center for Shared Use "Modern Nanotechnologies" UrFU (reg. No. 2968).

1. R. Waser, M. Aono, *Nat. Mater.*,**6**, 833 (2007).
2. T. Rojac, A. Bencan et al., *Nat. Mater.* **16**, 322 (2017).
3. A. Sawa, *Mater. Today* **11**, 28 (2008).
4. E. Strelcov, Y. Kim et al., *Nano Lett*. **13**, 3455 (2013).
5. J.M. Luo, S.H. Chen, *J. Alloys Comp.* **601**, 100 (2014).
6. M. Kratzer, O.P. Dimitriev, et al., *J. Appl. Phys*. **125**, 185305 (2019).
7. K.N. Romanyuk, D.O. Alikin, et al., *Ultramicroscopy* **220**, 113147 (2021).

P43

The effect of complete spontaneous backswitching in rubidium titanyl arsenate single crystals

M.A. Chuvakova[1], A.R. Akhmatkhanov[1], I.A. Kipenko[1], L.I. Isaenko[2], S.A. Zhurkov[2], V.Ya. Shur[1]

[1]*School of Natural Sciences and Mathematics, Ural Federal University, 620000 Ekaterinburg, Russia*
m.a.chuvakova@urfu.ru

[2]*Novosibirsk State University, 630090 Novosibirsk, Russia*

The single crystals of potassium titanyl phosphate ($KTiOPO_4$, KTP) family ($MTiOXO_4$, where M is K, Rb, or Cs, and X can be either P or As) are a some of the main materials for nonlinear optics. These uniaxial ferroelectrics with high phase transition temperature and outstanding nonlinear optical properties are widely used for creation of the tailored domain structures (domain engineering). The efficiency of nonlinear optical interactions in these crystals can be improved by periodical poling for realization of quasi-phase matching conditions [1]. Since the discovery, the methods of growth and modification of KTP single crystals have been studied intensively, resulting in appearance of a wide composition family [2]. The potassium rubidium arsenate (KTiOAsO4, KTA) possesses the properties outperforming those of KTP: it has a shorter cut-off wavelength in the UV and a wider IR transmission range [3]. It should be noted that the type of domain structure evolution in KTP family crystals is very promising for creating regular domain structures, since it allows controlling the broadening of the formed stripe domains due to the use of stripe electrodes created by photolithography methods [4-6].

We present the results of spontaneous backswitching processes observations in RTA single crystals by switching current analysis and *in situ* visualization of domain kinetics. We have measured the field dependences of switching time and domain structure stability time – the time interval from the end of switching pulse to the start of spontaneous backswitching process. Polarization reversal experiments were carried out with liquid (saturated aqueous solution of LiCl) and solid (ITO) electrodes within a temperature range from 20°C to 300°C. Spontaneous backswitching was revealed in RTA single crystals in all experiments.

It was found that the domain structure evolution for forward switching consists of the following stages: (1) the formation of oriented narrow stripe domains at the electrode edge with their rapid growth along the Y crystallographic direction to the opposite edge of the electrode, (2) broadening and merging of the stripe domains. Non-uniform formation of stripe domains only at one edge of the electrode was observed. It was shown that the dependence of the switching time on the amplitude of the switching pulse obeys the activation law. The experimental points lie on one curve with the following parameters: $E_{ac} = (120 \pm 20)$ kV/mm, $E_b = (3.4 \pm 0.1)$ kV/mm.

After some time after turning off the external field, which depended on the amplitude of the switching pulse, spontaneous backswitching of the domain structure with complete restoration of the original single-domain state was observed. It was shown that the domain structure stability time is proportional to the field applied during polarization reversal process. The maximum domain structure stability time was 130 s. Holding the crystals under high electric field leads to increasing of backswitching process duration up to 5 min, but the domain structure stability time doesn't change.

The obtained knowledge is important for further development of domain engineering in crystals of KTP family required for creation of high power, reliable, and effective coherent light sources.

The authors are grateful for financial support of the Ministry of Science and Higher Education of the Russian Federation (state task FEUZ-2023-0017). The equipment of the Ural Center for Shared Use “Modern nanotechnology” Ural Federal University (Reg.№ 2968) was used.

1. L.I. Isaenko, A.P. Eliseev, D.B. Kolker et al, *Quantum Electronics* **50**,788 (2020).
2. N.I. Sorokina, V.I. Voronkova, *Crystallogr. Rep.* **52**, 80 (2007).
3 G. Hansson, H. Karlsson, S. Wang, et al., *Appl. Opt.* **39**, 5058 (2000).
4. V.Ya. Shur, A.A. Esin, M.A. Alam, et al., *Appl. Phys. Lett.* **111**, 152907 (2017).
5. A.R. Akhmatkhanov, M.A. Chuvakova, N.A. Dolgushin, et al., *Ferroelectrics* **559**, 1 (2020).
6. A.R. Akhmatkhanov, M.A. Chuvakova, I.A. Kipenko, et al., *Appl. Phys. Lett.*, **115**, 212901 (2019).

P44

Domain shape transition during fast temperature change in lithium niobate single crystal

E.D. Greshnyakov, A.R. Akhmatkhanov, M.S. Kosobokov, V.Ya. Shur

School of Natural Sciences and Mathematics, Ural Federal University, 620000, Ekaterinburg, Russia
evgeny.greshnyakov@urfu.ru

The experimental observation of domain shape transition during fast temperature change in doped 5% MgO congruent lithium niobate (MgO:LiNbO$_3$, MgO:CLN) single crystal plate was demonstrated.

Samples of Z-cut MgO:CLN (Yamaju ceramics, Japan) with 5×5×0.5 mm^3 dimensions were used. Heat treatment was consisted of two stages using of (1) thermo cell THMS600 (Linkam, UK) and (2) setup of rapid temperature changing STE RTA-100 (SemiTEq, Russia). First stage: the sample was placed in thermo cell and heated to 200 °C with rate about 2.5 °C/s, annealing 30 s and then cooled to 25°C with rate about 2.5°C/s. *In situ* domain visualization was performed. Regular and irregular hexagonal shape domains appeared during cooling about temperature 170°C (Fig. 1a,b). Second stage: sample was heated to 270°C with rate about 30°C/s in dry N$_2$ atmosphere, cooling down was performed with rate about 0.3°C. Domain structure was imaged on polar surface by optical microscopy using Olympus BX-51 (Olympus, Japan) and scanning electron microscopy (SEM) using Auriga CrossBeam (Carl Zeiss, Germany) after selective etching in HF 30 s at room temperature (Fig. 1). Before SEM imaging sample surface was covered by 3 nm of Cr by Q 150T S (Quorum Technology, UK) to prevent charging of surface.

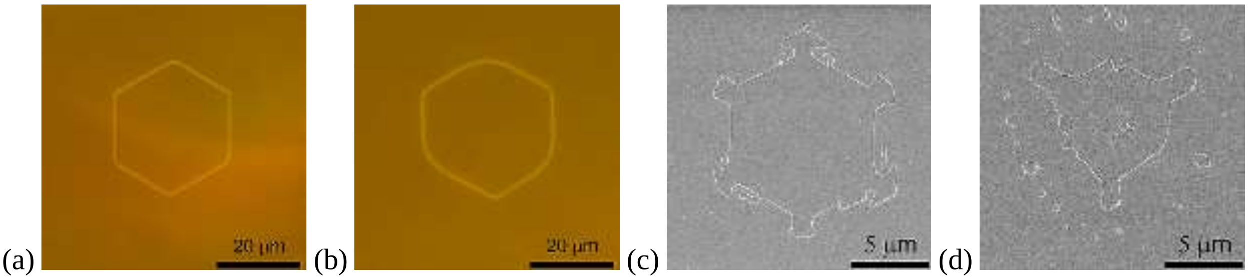

Figure 1. Hexagonal domains appeared after first stage: (a) regular, (b) irregular. Domain shape appeared after second stage: (c), (d).

As a result of the two-stage experiment, isolated domains of an original shape were obtained (Fig. 1c,d). The following changes in the domain shape were revealed: (1) the formation of ledges on six vertices for domains of regular polygon shape (Fig. 1c), (2) the formation of ledges on three domain vertices having the form of irregular polygons (Fig. 1d). To explain the obtained results, it was taken into account that each heating/cooling cycle leads to a hysteresis change in the pyroelectric field [1]. In a single domain sample, domains are formed only upon cooling. With a repeated heating and cooling cycle, isolated domains decrease in size upon heating and grow upon cooling. The formation of domains in the form of regular hexagons is typical for switching in a uniform field at temperatures below 100°C [2] and is attributed by the deterministic generation of steps at the domain vertices. With increasing temperature or increasing electric field, domains in the form of irregular hexagons with a gradual transition to a triangular shape are formed. In this case, ledges on the vertices of the domains are formed due to the generation of steps on the vertices of the domains in the form of polygons [3]. In domains of a regular hexagonal shape, ledges are formed on all six vertices, and in domains in the form of irregular hexagons - only on three vertices (Fig. 1c) The growth of ledges on the vertices is similar to the previously observed formation and growth of domains in the form of twelve-sided (dodecagons) in lithium niobate [3].

The research was made possible by Russian Science Foundation (Project № 24-12-00302). The equipment of the Ural Center for Shared Use “Modern nanotechnology” Ural Federal University (Reg.№ 2968) was used.

1. V.Ya. Shur, M.S. Kosobokov, A.V. Makaev et al., *Acta Materialia* **219**, 117270 (2021).
2. V.Ya. Shur, *Nano- and micro-domain engineering in normal and relaxor ferroelectrics Handbook of Advanced Dielectric, Piezoelectric and Ferroelectric Materials.* Elsevier, 622 (2008).
3. V.Ya. Shur, et al., *Ferroelectrics* **569**, 251 (2020).

P45

Field-induced tripling of a pseudo cubic cell in thin films of lead zirconate

I. V. Khlyupin[1], A.E. Ganzha[1], A.F. Vakulenko[1], Y. Si[2], Z. Chen[2], R.G. Burkovsky[1]

[1]*Peter the Great St.Petersburg Polytechnic University, 195251, St.Petersburg, Russia*
hlyupin.iv@yandex.ru

[2]*School of Materials Science and Engineering, Harbin Institute of Technology, 518055, Shenzhen, PR China*

Functional dielectrics occupy a significant niche in modern electronics. For a large part of such materials, practically significant properties are determined by the presence of structural phase transitions. Due to phase switching in thin-film heterostructures of such materials, it is possible to implement a promising electromechanical, electrocaloric, energy storage and storage devices. Among AFE materials, it is worth noting $PbZrO_3$ films, where excellent thermal [1] and electrical [2] conductivity valve capabilities have been recently discovered and where an unusual field-induced structural changes have been found [3].

Thus, we decided to study field-induced phase transitions in thin films of $PbZrO_3$. The purpose of this study was to verify the results of earlier experiments, where a decrease in the intensity of the reflections with coordinates 1/4(0, 1, 1) (Σ-type reflections) and the appearance of a ferroelectric phase with superstructural reflections with coordinates $\frac{1}{8}$ (0, 1, 1) and $\frac{3}{8}$(0, 1, 1) were observed at field from 150 to 225 kV/cm [4], as well as the study of phase transitions with a larger increase in the electric field.

In the presented work, an X-ray diffraction experiment was carried out on a $PbZrO_3/SrRuO_3/SrTiO_3$ heterostructure when an electric field of up to 285 kV/cm was applied to it. The film together with $SrRuO_3$ electrodes was grown by pulsed laser deposition at Harbin Institute of Technology (Zuhuang Chenna group, Shenzhen, China). The $PbZrO_3$ film thickness is 200 nm, the film surface is oriented in the [0 0 1] direction. The experiment was performed on a SuperNova diffractometer (Rigaku Oxford Diffraction).

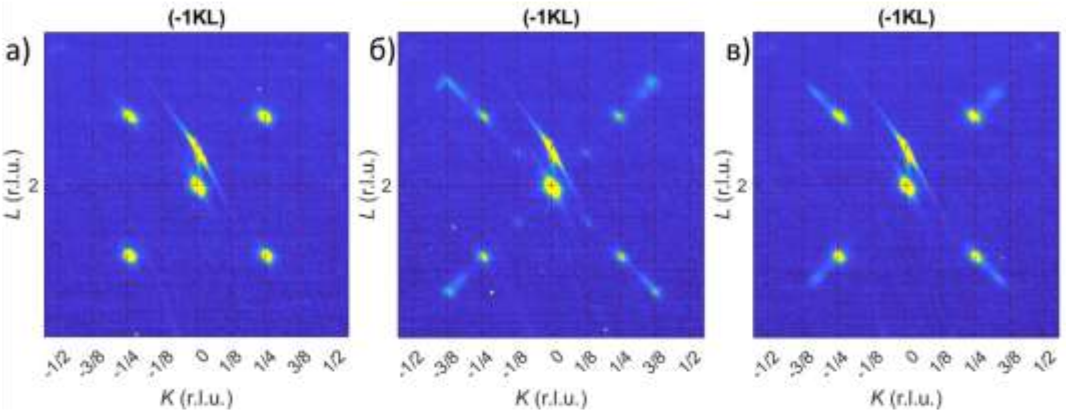

Figure 1. Reciprocal space maps for Q = (-1 0 2) at different electric field: (a) 0 kV/cm at the start of the experiment, (b) 285 kV/cm, (c) 0 kV/cm after decreasing field mode.

At field below 120 kV/cm, the low-temperature AFE phase in $PbZrO_3$ is observed, which manifests itself by superstructural reflections with coordinates $\frac{1}{4}$ (0, 1, 1) (Σ-type reflections), as well as $\frac{1}{2}$(0, 1, 1) (M-type reflections) (Fig. 1a). This phase is characterized by antiphase tilts of oxygen octahedra and antiparallel displacements of lead atoms in the [1 1 0] direction (pattern ↑↑↓↓). As the field increases, the intensity of M- and Σ-type superstructural reflections decreases. For Σ-type reflections, this behavior was observed earlier [4], for M-type reflections it was recorded for the first time.

At field above 120 kV/cm, superstructural reflections occur in $PbZrO_3$ positions of reciprocal space with coordinates $\frac{1}{8}$ (0, 1, 1) and $\frac{3}{8}$ (0, 1, 1). The occurrence of these reflections is interpreted as a phase transition into a ferroelectric phase with displacements of lead atoms described by pattern ↑↑↑↓↑↑↓ [4]. The intensity of these reflections increases with increasing field.

When a field of more than 200 kV/cm is applied, superstructural reflections with coordinates $\frac{3}{9}$ (0, 1, 1) appear (Fig. 1b), these reflections have not been previously reported. The appearance of these reflections may be associated with a phase transition into a ferrielectric phase characterized by displacements of lead atoms described by pattern ↑↑↓. The possibility of this phase to occur in $PbZrO_3$ has been studied with DFT calculations [5]. According to these calculations, such a phase is more energetically advantageous compared to the low-temperature AFE phase, however, other low-symmetric phases may occur under similar conditions [5, 6].

During the experiment in the decreasing field mode, several features have been noted. The intensities of M- and Σ-type superstructural reflections do not reach their initial values at zero electric field. The intensity of reflections with coordinates $\frac{3}{9}$ (0, 1, 1) increases when the electric field decreases to a value at which reflections with coordinates $\frac{1}{8}$ (0, 1, 1) and $\frac{3}{8}$ (0, 1, 1) disappear, after which they begin to decrease. At zero field, only reflections of the low-temperature AFE phase and reflections of the ferroelectric phase, with coordinates $\frac{3}{9}$ (0, 1, 1), are recorded (Figs. 1c,2).

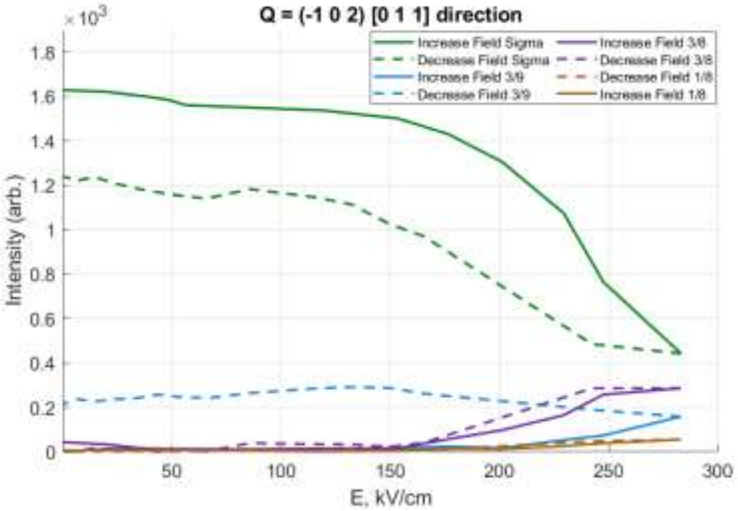

Figure 2. The dependences of the intensity of superstructural reflections with coordinates $\frac{1}{4}$ (0, 1, 1), $\frac{1}{8}$ (0, 1, 1), $\frac{3}{8}$ (0, 1, 1) and $\frac{3}{9}$ (0, 1, 1).

As a result of the study, some of the results obtained earlier were reproduced: transition to phases with a ferroelectric component at high fields. A reflections with coordinates $\frac{3}{9}$ (0, 1, 1) were observed, the presence of which is unexpected, due to its absence in experiments of this kind earlier. The causes of this reflex remain unknown at the moment and require additional study.

The work was funded by the Russian Science Foundation (grant No. 20-72-10126).

1. C. Liu, Y. Si, H. Zhang, et al., *Science* **382**, 1265 (2023).
2. G. Apachitei, J.J. Peters, A.M. Sanchez, et al., *Adv. Electron. Mater.* **3**, 1700126 (2017).
3. A. Roy Chaudhuri, M. Arredondo, A. Hähnel, et al., *Phys. Rev. B—Cond. Matter Mater. Phys.* **84.5**, 054112 (2011).
4. R.G. Burkovsky, G.A. Lityagin, A.E. Ganzha, et al., *Phys. Rev. B* **105**, 125409 (2022).
5. H. Aramberri, C. Cazorla, M. Stengel, et al., *npj Computational Materials* **7**, 196 (2021).
6. J.S. Baker, M. Paściak, J.K. Shenton, et al., *arXiv preprint arXiv:2102.08856* (2021).

P46

Forward domain growth during local switching by focused electron beam in strontium-barium niobate crystal

M.D. Kholodenko, E.A. Pashnina, A.R. Akhmatkhanov, M.S. Nebogatikov,
V.A. Shikhova, A.S. Slautina, V.Ya. Shur

School of Natural Sciences and Mathematics, Ural Federal University, 620000, Ekaterinburg, Russia
kholodenko.maria@urfu.ru

Strontium barium niobate (SBN, $Sr_xBa_{1-x}Nb_2O_6$, $x = 0.61$) single crystals doped with nickel are promising materials for creating electric field-controlled diffraction optical elements [1] and photonic crystals [2]. However, the complex polydomain structure of grown SBN crystals hinders their application in high-performance devices. We have studied the features of domain formation and control in SBN crystals grown by modified Stepanov technique [3] under focused ion beam irradiation.

Single-domain regions were created by raster scanning of a 460x460 μm^2 area by focused electron beam at dose range from 100 to 200 μC/cm^2. Local switching was achieved by focused ion beam. A photoresist layer was deposited on the irradiated surface, and a copper electrode was grounded on the opposite surface. Domains were imaged by second harmonic generation microscopy (SHGM). Irradiation of 5×5 point matrices with a 10 μm period and isolated points at doses from 10 to 50 pC led to the formation of circular domains. Increasing the irradiation dose caused an increase in domain depth and switched area. Isolated domains were smaller than matrix domains (Fig. 1a) due to the influence of neighboring points. Isolated domains penetrated the crystal at doses over 40 pC, while matrix domains - over 10 pC.

Line irradiation at doses 20 - 100 μC/cm formed stripe domains. Higher doses resulted in linear increase of the depth and width (Fig. 1b). Domain stripes in a grid penetrated deeper than isolated ones due to influence of adjacent irradiated areas. Stripe domains penetrated the crystal at doses over 50 μC/cm, whereas isolated ones reached the crystal half. The abiliy of creating domain structures with arbitrary wall orientations for a maximum depth of 370 μm at a dose of 500 μC/cm^2 was demonstrated. With dose increasing, the uniformity of these structures improves, and the penetration depth increases, with central parts of the domain penetrating deeper than the outer ring and rays. This effect can be explained by the additional field contribution generated by charges of the outer ring and rays.

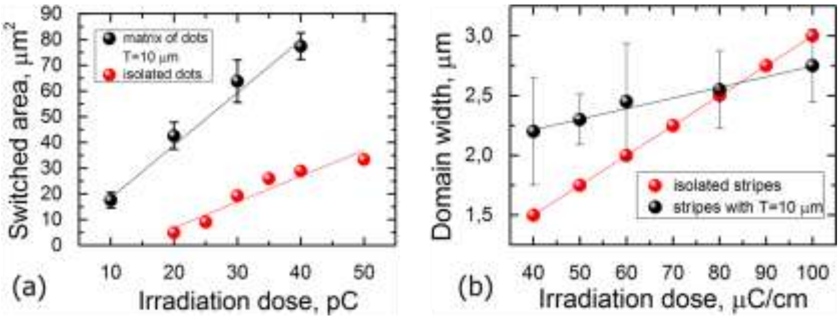

Figure 1. Dose dependences of (a) switched area for dot irradiation and (b) domain width for linear irradiation for isolated domains and domains in a matrix with 10 μm period.

It was shown that the domain width and the width of broad domain boundary (BDB) change with depth: at depths less than 20 μm, they remain constant; with increasing depth, domain width decreases, and BDB width increases, leading to the complete disappearance of a solid domain. At low doses, domain and BDB width behave similarly to isolated lines, but over 300 μC/cm², domain merge at depths up to 130 μm. The obtained results are important for further development of domain engineering methods in SBN crystals and can be used to create highly efficient electro-optical devices.

The authors are grateful for financial support of the Ministry of Science and Higher Education of the Russian Federation (state task FEUZ-2023-0017). The equipment of the Ural Center for Shared Use “Modern nanotechnology” Ural Federal University (Reg.№ 2968) was used.

1. J. Mávita, L.A. Ríos, C.E. Minor, et al., *Appl. Opt.* **57**, 2208 (2018).
2. J. Li, M. Lu, L. Feng, et al., *J. Appl. Phys.* **101**, 013516 (2007).
3. L.I. Ivleva, *Bull. Russ. Acad. Sci.: Phys.* **73**, 1338 (2009).

P47

Superfast domain wall motion in uniaxial ferroelectric single crystals

I.A. Kipenko, A.R. Akhmatkhanov, V.Ya. Shur

School of Natural Sciences and Mathematics, Ural Federal University, 620000, Ekaterinburg, Russia, ilya.kipenko@urfu.ru

Single crystals of lithium niobate family ($LiNbO_3$, LN) and potassium titanyl arsenate ($KTiOAsO_4$, KTA) are widely used ferroelectrics due to unique combination of nonlinear, electrooptic and piezoelectric properties [1,2]. Domain engineering enables the creation of tailored stable domain structures [3]. Formation of spatial modulation of electro-optical, piezoelectric and nonlinear optical properties opens wide opportunities in improvement of main characteristics [2,4]. Basic technology for creation of domain patterns is e-field poling by application of electric field to photolithographically defined electrode structure. Domains merging during e-field poling caused by formation of superfast domain walls impairs accuracy of the domain pattern [5]. An alternative approach to creation of quasi-regular domain structures is polarization reversal under non-equilibrium switching conditions.

The study of superfast domain walls was carried out in single crystals of LN family - congruent (CLN), stoichiometric (SLN), congruent doped with 5 mol% magnesium oxide (MgOCLN), stoichiometric doped with 1.3 mol% magnesium oxide (MgOSLN) compositions - as well as in single crystals of potassium titanyl arsenate (KTA). The unusual domain kinetics during switching from the initial polydomain state and formation of quasiregular dendrite domain structures in crystals with artificial surface dielectric layer at elevated temperatures were investigated in CLN.

We have identified and analyzed the motion of main domain wall types in single crystals of LN family and KTA. All crystals of LN family have domain walls of same three main types: slow, fast and superfast. The field dependences of domain wall velocities in crystals of the LN family obey the activation law (except for slow domain walls in CLN). In KTA, domain kinetics is caused by to the motion of three types of walls. Angular dependences of wall velocities in KTA are caused by the effect of deterministic nucleation. Analysis of simultaneously recorded domain structure evolution and switching current in various LN crystals allows us to reveal that Barkhausen pulses in the switching current correspond to appearance of short-lived superfast domain walls. We found that the merging of domains of comparable sizes leads to “shape stability effect” [6], while the merging of large and small domains results in jerky wall motion [7]. The Flicker-noise in the switching current demonstrates that the evolution of the domain structure in CLN is characterized by self-organized criticality [8].

The comparison of the domain kinetics in CLN for switching from the single domain state and polydomain one representing a matrix of domains located in the nodes of a rectangular lattice, allows to reveal the change of the switching character from persistent to antipersistent [9].

The field dependence of the domain shape occurs in CLN with the artificial surface dielectric layer. "Stars" appeared in low fields by growth of three rays in Y+ directions with their subsequent splitting. "Snowflakes" formed in intermediate fields by growth of rays from hexagonal domain vertices in Y+ directions. "Dendritic snowflakes" arose in high fields by growth of rays in Y+ and Y- directions with branching and splitting.

The reported study was funded by Russian Science Foundation (№24-12-00302). The equipment of the Ural Center for Shared Use "Modern Nanotechnologies" (Ural Federal University) was used.

1. K.K. Wong, *Properties of lithium niobate* (INSPEC), 417 (2002).
2. V.Ya. Shur, E.V. Pelegova, A.R. Akhmatkhanov, et al., *Ferroelectrics* **496**, 49 (2016)
3. R.E. Newnham, C.S. Miller, L.E. Cross, et al., *Physica Status Solidi (a)* **32**, 69 (1975).
4. A. Boes, L. Chang, C. Langrock, et al., *Science* **379**, eabj4396 (2023).
5. V.Ya. Shur, A.A. Esin, M.A. Alam, et al., *Appl. Phys. Lett.* **111**, 152907 (2017).
6. V.Ya. Shur, A.R. Akhmatkhanov, D.S. Chezganov, et al., *Appl. Phys. Lett.* **103**, 242903 (2013).
7. I.S. Baturin, M.V. Konev, A.R. Akhmatkhanov, et al., *Ferroelectrics* **374**, 136 (2008).
8. P. Bak, C. Tang, K. Wiesenfeld, *Phys. Rev. A* **38**, 364 (1988).
9. J. Feder, *Fractals* (Boston, MA: Springer), 283 (1988).

P48

Formation of the domain structure in the bulk of ferroelectric crystals by ultrashort laser pulses

B.I. Lisjikh, M.S. Kosobokov, V.Ya. Shur

Ural Federal University, Institute of Natural Sciences and Mathematics, 620002, Ekaterinburg, Russia
boris.lisikh@urfu.ru

Applications of nonlinear photonic crystals require creation of stable periodical structures with spatially modulated second-order nonlinear susceptibility. One of the ways to reach this is creating of the stable periodical domain structures in ferroelectric crystals by laser irradiation. Recently, the light-only methods of creation of the tailored ferroelectric domain structures by pulse laser irradiation without application of electric field have been demonstrated [1]. The most spectacular achievement is the ability to switch domains in crystal bulk by means of focused NIR femtosecond laser irradiation [2,3].

In this work the domain structures were created by femtosecond and microsecond pulse laser irradiation in uniaxial ferroelectric crystals lithium niobate ($LiNbO_3$, LN) and lithium tantalate ($LiTaO_3$, LT) of different compositions: congruent LN (CLN), Mg-doped CLN (MgOCLN), Mg-doped congruent LT (MgOCLT) and stoichiometric LT (SLT). All samples were monodomain single-crystal plates cut perpendicular to the polar axis. The principal difference between the domain switching mechanism and created domain structure was demonstrated.

Linear absorption coefficient for the NIR spectrum region wavelengths is low in dielectrics therefore long-time laser pulses pass through the medium almost without absorption. But if one uses femtosecond laser then nonlinear multiphoton absorption must be considered: due to the high irradiation intensity because of the very short laser pulses duration NIR irradiation is absorbed by the transparent medium. At the same time energy density also plays important role – the tighter focused irradiation will be absorbed with higher efficiency [3]. Therefore, femtosecond irradiation can be focused in the material bulk which allows local modification to be conducted. Absorption coefficient for the far IR wavelengths is much higher and therefore irradiation is absorbed by the surface layer.

Two types of irradiations have been used: (1) local irradiation in fixed points with various number of pulses and (2) linear scanning with constant velocity.

First, CO_2-laser VLS3.50 (Universal Laser Systems, USA) with 10.6 μm wavelength and pulse duration 350 μs was used to irradiate the monodomain plate of LT covered with conductive layer. The focus point was deposited above the sample to avoid surface damage. Second, Yb-solid state femtosecond laser TETA-10 (Avesta Project, Russia) with 1030 nm wavelength and 250 fs pulse duration was used for in-bulk irradiation using 50x objective with NA = 0.65. Two-stage poling process with additional heating up to 250 °C after laser irradiation was studied in MgOCLN samples.

To conduct domain structure imaging at the polar surfaces scanning electron microscopy after the selective chemical etching was used. 3D domain imaging was carried out by Cherenkov-type second harmonic generation microscopy (SHGM).

Three striped domain structure areas formed after the CO_2-laser irradiation were distinguished by the distance from the laser spot center: 1) central area with weakly pronounced orientation of the curved domain stripes along three Y-axis; 2) straight stripes in the middle area had strict orientation along three Y-axis; 3) external area with parallel domains orientated only along one of the Y-axis. Using SHGM it was shown that the domains had comb-like shape.

LN and LT have strong absorption in the far IR spectral region which leads to the sample surface heating by laser pulse and subsequent cooling. The fast temperature change leads to creation of the strong pyroelectric field [1]. The domain creation and growth occur if its value exceeds the threshold. Three types of the domain structure formed due to spatially nonuniform distribution of the temperature and therefore the pyroelectric field value. The probability of the domain formation and growth are proportional to the field excess above the threshold value. The highest field excess in the central area creates the high concentration of domain nuclei and strong interaction between growing stripe domains leading in curved shape. The moderate field excess in the middle area the domain concentration and the stripe domains were straight due to enough space for their growth. In the external area the field excess value was enough for growth of the domain occurred at the edge of the middle area.

The effect of the multiphoton absorption of the NIR femtosecond irradiation leads to formation of microtracks – amorphous regions [4] inside the crystal bulk, which were imaged by optical microscopy due to the different refractive index. Using SHGM imaging allows to discover the domains localized around the microtracks.

In CLN domains had spindle-like shape and were localized only near the microtracks. The length of microtracks and domains increases with pulse energy and is independent on the pulse number. In MgOCLN for high pulse energy the domains of hexagonal pyramidal shape with charged walls domains start to grow towards Z- polar surface [5]. The length of created domains was up to 400 μm. The domains reached Z- surface transformed to hexagonal prisms with neutral domain walls. It should be noted that for the focusing depth about 200 μm at high pulse energies additional domains appeared and grew from the surface at random positions. At the energy above 6.7 μJ these domains suppressed the domain growth from the microtracks. The domain growth in both polar directions till the surfaces has been achieved by two-step poling with heating of the MgOCLN sample after the femtosecond irradiation.

Irradiation with low energy and pulse number of MgOCLT led to formation of spindle-like domains. With increasing of the irradiation parameters to the domain shape changed drastically. The domain cross-section demonstrates the shape of 3-rays stars with rays orientated along Y+ directions. The linear energy dependence the domain length along polar direction and square-root dependence of the width perpendicular to polar directions were obtained. The revealed logarithmic dependence on the pulse number indicates existence of the cumulative effect: pyroelectric field did not relax completely between the subsequent pulses.

The domain shape in SLT was similar to one obtained in MgOCLN but the domain cross sections were almost circular. The domain length depends linearly and logarithmically on the pulse energy and number, respectively. The obtained difference of domain shapes in studied materials can be attributed to significant difference of thresholds and pyro-coefficients therefore different probabilities of domain nuclei generation and following growth by step generation and kink motion [6].

Linear scanning by femtosecond irradiation in CLN caused the formation of linear microtracks. SHGM visualization revealed double-comb-like structure of stripe domains localized on microtracks. The cross section of domains was the same as in the case of local irradiation. To reveal internal structure of microtracks the sample was cut perpendicular to the scanning direction and polished then scanning force microscopy was applied for visualization. It was shown that microtracks had quasi-periodical substructure of modified regions. For the pulse energy above 1.3 μJ double microtracks formed. The splitting reason consists of birefringence inherent to ferroelectric materials – microtracks corresponded to ordinary and extraordinary refractive indexes.

The quasi-periodical substructures represented non-polar amorphous inclusions with reduced value of spontaneous polarization therefore the bound charges localized at the boundaries created the strong depolarizing field. During the heating process new domains occurred under its action. The following domain growth, which took place in the case of MgOCLN, MgOCLT and SLT, under the action of pyroelectric field induced the field excess above the threshold value.

The obtained results can be used for the creating of 3D nonlinear photonic crystals based on ferroelectrics and in-bulk waveguides with periodical domain structures. Following attempts will be focused on features of domains created under the action of fs-laser irradiation in various ferroelectrics.

The research was made possible by Russian Science Foundation (Project № 24-12-00302). The equipment of the Ural Center for Shared Use “Modern nanotechnology” Ural Federal University (Reg.№ 2968) was used.

1. V.Ya. Shur, M.S. Kosobokov, A.V. Makaev, et al., *Acta Materialia* **219**, 117270 (2021).
2. X. Chen, P. Karpinski, V. Shvedov, et al., *Appl. Phys. Lett.* **107**, 141102 (2015).
3. Y. Sheng, X. Chen, T. Xu, et al., *Photonics* **11**, 447 (2024).
4. Z. Wang, B. Zhang, Z. Wang, et al., *Adv. Mater.* **35**, 2303256 (2023).
5. B. Lisjikh, M. Kosobokov, A. Turygin, et al., *Photonics* **10**, 1211 (2023).
6. V.Ya. Shur, E.V. Pelegova, M.S. Kosobokov, *Ferroelectrics* **569**, 251 (2020).

P49

Electroelastic hysteresis and relaxation in relaxor piezoceramics at low dc electric fields

M.A. Lugovaya, P.A. Abramov, I.A. Shvetsov, N.A. Shvetsova, A.N. Rybyanets

Southern Federal University, 344090, Rostov-on-Don, Russia
arybyanets@gmail.com

The study of domain orientation processes in ferroelectric ceramics and crystals under the influence of a dc electric field is extremely important both for the assessment of the material properties and for the practical use of these materials in ultrasonic transducers, piezoelectric sensors, and actuators. Different methods for studying the electric field dependences of ferroelectrics properties are widely used to estimate coercive field, spontaneous and residual polarization. In our previous paper [1], we have proposed a new method for studying relaxation and transient processes in ferroelectric ceramics under the influence of low dc electric fields based on the measurement and analysis of piezoresonance spectra.

In this work, we studied electroelastic hysteresis and relaxation processes induced by low dc electric field in relaxor piezoceramics based on PZT system. Hot pressed PZT-type piezoceramics of the composition $Pb_{0.96}Sr_{0.04}Zr_{0.042}Ti_{0.435}W_{0.052}Mg_{0.052}Sb_{0.0426}Li_{0.0142}O_3$ were chosen as the object of the study. This composition has relaxor properties when in a depolarized state and exhibits classical ferroelectric properties in a polarized state. The studied composition belongs to the tetragonal boundary of the morphotropic region and characterized by a low coercive field E_C (0.9 kV/mm at 50 Hz). Piezoceramic elements were polarized in air by applying to silver electrodes dc electric field (~1 kV/cm) at heating above Curie temperature (~190°C) and cooling to a room temperature. Precision measurements of the impedance spectra at different amplitudes and polarities of applied dc electric field were performed using Agilent 4294A impedance analyzer and the Piezoelectric Resonance Analysis Program (PRAP) for the thickness vibrational mode of thin piezoceramic disks. The analysis of the dc bias and time dependencies of the complex elastic moduli C_{33}^D and C_{33}^E obtained as a result of processing of successively measured impedance spectra was carried out and a physical interpretation of the results has been proposed.

As a result of the study, it was established that the nature of the field and time dependences of the complex elastic moduli C_{33}^D and C_{33}^E of relaxor piezoceramics under the influence of low *dc* electric fields is mainly due to reversible displacements 90° domain walls. In this case, changes in the real part of the $C_{33}^{D/}$ and $C_{33}^{E/}$ are determined by changes in the residual polarization of the piezoceramics caused by reversible displacements of the 90° domain walls. Changes in the imaginary part of the $C_{33}^{D//}$ and $C_{33}^{E//}$ are caused by the interaction of resonant oscillations of the piezoceramic element with inhomogeneous mechanical stresses caused by displacements of domain boundaries, moving 90° domain walls and space charge carriers.

The proposed method for studying the field and time dependences of the complex constants of piezoceramics under the influence of low dc fields, that is significantly lower than the coercive field, makes it possible to clarify the mechanisms of relaxation and piezoelectric hysteresis in ferroelectric ceramics.

The work was financially supported by the Ministry of Science and Higher Education of the Russian Federation [State assignment in the field of scientific activity, Southern Federal University, 2023, Project No. FENW-2023-0015/(GZ0110/23-08-IF)].

1. I.A. Shvetsov, E.I. Petrova, N.A. Shvetsova, et al., *Ferroelectrics* **561**, 69 (2020).
2. N.A. Shvetsova, S.A. Shcherbinin, M.A. Lugovaya, et al., *Ferroelectrics* **561**, 100 (2020).

P50

The structure of magnetic domain walls during drift in an oscillating magnetic field

D.S. Mekhonoshin, L.A. Pamyatnykh

Ural Federal University, 620026, Ekaterinburg, Russia
dmitry.mehonoshin@urfu.ru

Recently, the dynamics of magnetic domain walls (DWs) has attracted a lot of attention due to the prospects of creating new types of memory devices. [1, 2]. One of the key phenomena required for this is a unidirectional motion of an array of band domains [3] (a drift of domain walls). In this work, changes of the DW structure during drift motion in an oscillating magnetic field in plates with a complex character of magnetic anisotropy has been studied by the method of 2D micromagnetic simulation. The numerical simulation results are compared with experimental results obtained on single crystal iron garnets plates.

A single crystal plate-(111) with cubic magnetocrystalline and induced uniaxial anisotropy was considered, the easy magnetization axis of the induced anisotropy was $[\bar{1}11]$. The sample parameter were: the constants of cubic and uniaxial anisotropy were $K_1 = -6.0 \cdot 10^3$ erg/cm^3 and $K_u = 0.9 \cdot 10^3$ erg/cm^3, the saturation magnetization was $M_s = 19$ G and the plate thickness was $L = 10\ \mu m$. The oscillations of DWs in an alternating magnetic field $H(t) = H_0 \sin 2\pi t$ of frequency $f = 10^6$ Hz applied perpendicular to the plane of the plate were considered. To study the dynamics of DWs, the Landau-Lifshitz-Hilbert equation was solved, the calculations were performed in the micromagnetic simulation package mumax3 [5].

The results of the calculations indicate that the magnetic domain walls at the specified material parameters exhibit an asymmetric vortex character (Fig.1a), near the surface of the plate there are regions of magnetic flux closure. In an alternating magnetic field, the width Δ and shape of DWs change periodically (Fig. 1b), with opposite changes for the DWs with opposite polarities (1-2 and 3-4 in Fig. 1b). If the polarities of the DWs in the plate alternate, then in the oscillating magnetic field, in addition to the oscillations of the DWs, there is their translational motion, i.e. the DWs drift.

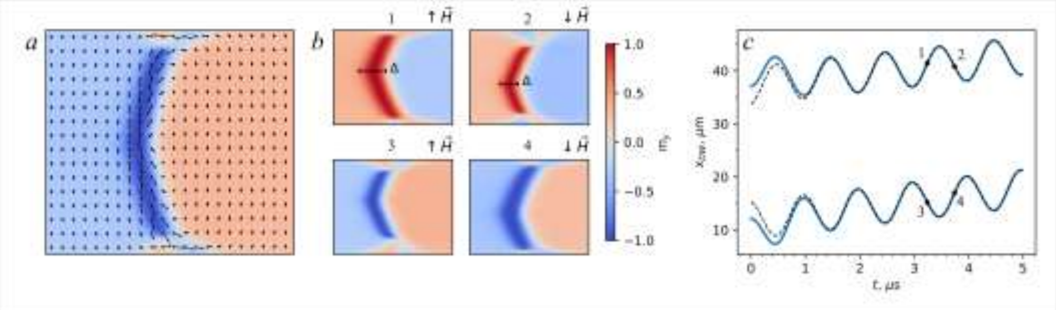

Figure 1. (a) Static distributions of the vertical component of the magnetization vector in the cross section of the plate in the absence of an external magnetic field. (b) Distributions of the y-component of the magnetization vector around DWs during their motion. (c) Dependencies of the coordinates x_{DW} of the domain walls with opposite polarities on time in alternating magnetic field ($H_0 =$ 30 Oe, $f = 10^6\ Hz$).

This work was performed within the framework of the state assignment of the Ministry of Science and Higher Education of the Russian Federation (Project FEUZ 2023-0020).

1. S.S. Parkin, M. Hayashi, L. Thomas, *Science* **320**, 190 (2008).
2. D. Kumar, T. Jin, R. Sbiaa, et al., *Phys. Rep.* **958**, 1 (2022).
3. K.-W. Moon, D.-H. Kim, C. Kim et al., *J. Phys. D: Appl. Phys.* **50**, 125003 (2017).
4. D.S. Mekhonoshin, L.A. Pamyatnykh, *Bull. RAS: Phys.* **87**, 267 (2023).
5. A. Vansteenkiste, J. Leliaert, M. Dvornik, et al., *AIP Advances* **4**, 107133 (2014).

P52

Dielectric hysteresis and relaxation in relaxor piezoceramics at low dc electric fields

E.I. Petrova, I.A. Shvetsov, M.G. Konstantinova, N.A. Shvetsova, A.N. Rybyanets

Southern Federal University, 344090, Rostov-on-Don, Russia
arybyanets@gmail.com

Investigation of transient processes and relaxation phenomena in ferroelectric ceramics under external influences is extremely important both for the assessment of the material properties and for the practical use of these materials materials in ultrasonic transducers, piezoelectric sensors, and actuators. Standard methods (measurement of hysteresis and current loops, reversible dielectric permittivity etc.) are widely used for studying the field dependences of the properties of ferroelectric materials. Hovewer these methods fail clearly when used for studying of transient processes and relaxation phenomena in ferroelectric ceramics under the influence of low dc electric fields. In our previous paper [1, 2], we have proposed a new method for studying relaxation and transient processes in ferroelectric ceramics under low dc electric fields based on the measurement and analysis of piezoresonance spectra.

In this work, we studied dielectric hysteresis and relaxation process in relaxor piezoceramics based on PZT system induced by low dc electric field. Precision measurements of the impedance spectra for the thickness and radial vibrational modes of thin piezoceramic disks at different amplitudes and polarities of applied dc electric field were performed using Agilent 4294A impedance analyzer and the PRAP software. The analysis of the dc bias and time dependencies of the complex dielectric constants ε_{33}^S and ε_{33}^T obtained as a result of processing of successively measured impedance spectra was carried out. PZT-type relaxor piezoelectric ceramics of the composition $Pb_{0.96}Sr_{0.04}Zr_{0.042}Ti_{0.435}W_{0.052}Mg_{0.052}Sb_{0.0426}Li_{0.0142}O_3$ were chosen as the object of the study. This composition has relaxor properties when in a depolarized state and exhibits classical ferroelectric properties in a polarized state. In the phase diagram of concentration states, the studied composition belongs to the tetragonal boundary of the morphotropic region and characterized by a low coercive field E_C (0.9 kV/mm measured at 50 Hz). The domain structure of polarized piezoceramics is characterized by the presence of 90° domain boundaries, predominantly oriented normally to the direction of the polarizing field. Thin discs of polarized hot-pressed piezoceramics (diam. 10 mm and thickness 0.2 mm) were used for the experiments.

It was found that the hystereешс and relaxation nature of temporary changes in the complex dielectric permittivities ε_{33}^S and ε_{33}^T of relaxor piezoceramics under the influence of a dc electric field of different polarities in the weak field region is due to caused by reversible displacements of the 90° domain walls. and space charge relaxation processes that screen the applied electric field. A comparison of various methods for characterizing ferroelectric ceramics under external influences showed that the method of complex electromechanical characterization, based on the analysis of piezoresonance spectra, makes it possible to obtain more accurate data on domain orientation and dielectric relaxation processes occurring in ferroelectric ceramics when exposed to low electric fields, taking into account the out-of-phase response of the material to external influences.

The work was financially supported by the Ministry of Science and Higher Education of the Russian Federation [State assignment in the field of scientific activity, Southern Federal University, 2023, Project No. FENW-2023-0015/(GZ0110/23-08-IF)].

1. I.A. Shvetsov, E.I. Petrova, N.A. Shvetsova, et al, *Ferroelectrics* **561**, 69 (2020).
2. N.A. Shvetsova, S.A. Shcherbinin, M.A. Lugovaya, et al., *Ferroelectrics* **561**, 100 (2020).

P53

Kinetics of the domain structure in uniform electric field in $LiNbO_3$ with surface layer modified by soft proton exchange

E.D. Savelyev[1], A.R. Akhmatkhanov[1], H. Tronche[2], F. Doutre[2], T. Lunghi[2], P. Baldi[2], V.Ya. Shur[1]

[1]Institute of Natural Sciences and Mathematics, Ural Federal University, 620002 Ekaterinburg, Russia
evgeny.savelyev@urfu.ru

[2]Université Côte d'Azur, CNRS, Institut de Physique de Nice, 06108 Nice Cedex 2, France

Lithium niobate ($LiNbO_3$, LN) is a ferroelectric with a well-developed growth technique used in integrated and nonlinear optics. The use of the effect of quasi-phasematching in periodically poled crystal allows generating laser radiation of different wavelengths [1]. The development of domain engineering expands the framework of application of LN crystals [2].

An optical waveguide is a region of a crystal with a modified refractive index. A soft proton exchange (SPE) is one of the simplest ways to change the refractive index in CLN [3]. To carry out proton exchange (PE), the crystal is heated in a proton source. A mixture of benzoic acid (C_6H_5COOH) and lithium benzoate (C_6H_5COOLi) with concentration of more than 2.7% is used. During PE, diffusion of hydrogen ions H^+ into the crystal and of lithium ions Li^+ out of the crystal takes place. A distinctive feature of SPE process is that the distribution of hydrogen in the near-surface layer has a gradient character. The preservation of ferroelectric properties in the SPE waveguide opens the possibility of creating the periodical domain structures for nonlinear integrated optical applications.

The studied samples represent the CLN single-domain plates in which SPE-process was realized at 300°C with a treatment duration from 12 to 48 hours. *In situ* imaging of the domain structure evolution during polarization reversal was realized using optical microscopy. The spatial distribution of the sample composition in the surface layer was determined by confocal Raman microscopy (CRM). The Raman line at 3492 cm^{-1} related to the H^+ ions [4], was analyzed. The static domain structure was imaged in the bulk by the Cherenkov-type second harmonic generation microscopy (SHGM) [5].

We have studied the influence of near-surface H^+ ions concentration gradient on domain kinetics. The observed anomalous evolution of the domain structure represented the formation of stripe domains and their anisotropic growth along three symmetrically equivalent crystallographic directions. The domain imaging in the bulk by the SHGM allowed revealing a comb-like domain shape with toothed charged domain walls. The stripe domains were observed at the depths below 30 μm, whereas the chains of isolated micron-size domains were observed at the depths above 30 μm (30 to 200 μm).

The formation of the comb-like domain was attributed to the repetitive appearance of the domain spikes in the bulk during elongation of the stripe domain. It was demonstrated that with an increase in the SPE process time the composition gradient (dC/dz) increases twofold, which leads to a decrease in the threshold field to 3 kV/mm [6]. This effect was explained by the action of the concentration gradient of H^+ ions which was considered as an analogue of the internal bias field. It was shown that for dC/dz above 0.3 μm^{-1} the internal bias field was proportional to the increase in the gradient of the relative concentration of H^+ ions in the surface layer [6]. The detailed study of domain kinetics can provide new insights into the features of domain structure evolution during periodical poling useful for development of domain engineering.

The research funding from the Ministry of Science and Higher Education of the Russian Federation (Ural Federal University Program of Development within the Priority-2030 Program) is gratefully acknowledged. The equipment of the Ural Center for Shared Use “Modern nanotechnology” Ural Federal University (Reg. no. 2968) was used.

1. D.S. Hum, M.M. Fejer, *Comptes Rendus Phys*. **8**, 180 (2007).
2. V.Ya. Shur, A.R. Akhmatkhanov, I.S. Baturin, *Appl. Phys. Rev*. **2**, 040604 (2015).
3. L. Chanvillard, P. Aschiéri, P. Baldi, et al., *Appl. Phys. Lett*. **76**, 1089 (2000).
4. S.M. Pershin, *Opt. Spectrosc*. **98**, 543 (2005).
5. Y. Sheng, A. Best, H.-J. Butt, et al., *Opt. Express*. **18**, 16539 (2010).
6. E. Savelyev, A. Akhmatkhanov, H. Tronche, et al., *Phys. Rapid Res. Lett.* **18**, 2300420 (2023).

P54

Electrical-field tunable diffraction optical element based on strontium-barium niobate single crystals

V.A. Shikhova[1], M.S. Nebogatikov[1], A.R. Akhmatkhanov[1],
M.A. Chuvakova[1], L.I. Ivleva[2], V.Ya. Shur[1]

[1]School of Natural Sciences and Mathematics, Ural Federal University, 620000, Ekaterinburg, Russia
vera@urfu.ru
[2]Prokhorov General Physics Institute, Russian Academy of Sciences, 119991, Moscow, Russia

Ferroelectric domains have been used extensively for nonlinear optical applications over the past years. On the other hand, the ferroelectric domains with opposite values of spontaneous polarization possess the opposite values of the linear electrooptic effect, which allowed to create the electrical field-controlled diffraction optical elements (DOE) in ferroelectric materials [1].

In this work, we present the design and realization of DOE in strontium-barium niobate $Sr_{0.61}Ba_{0.39}Nb_2O_6$ (SBN) single crystals with precisely tailored ferroelectric domain structure. The tailored ferroelectric domain structure was created by application of a non-uniform electric field using a dielectric spiral-shaped mask deposited by photolithography. The kinetic of domain structures during polarization reversal with tailored electrodes was imaged by polarization optical microscopy, moreover, the switching currents were recorded. The amplitude and duration of the rectangular electric field pulses were selected in such a way that the entire area under the electrode was completely switched. The created domain structure was imaged using Cherenkov-type second harmonic generation microscopy (SHGM) [2] on the crystal surface (Fig. 1a) and in the bulk of the crystal. SHGM allows to visualize the contrast of the domain walls. Thus, the highest SHGM signal was observed at the boundary of the single-domain region switched using electrodes, the signal was absent (black area) in switched single-domain region. The intermediate signal is responsible for the presence of the initial nanodomain structure in the region where the dielectric photoresist was deposited, and switching did not occur. The created structure is through and exactly repeats the given pattern throughout the entire depth of the crystal.

The diffraction patterns obtained as a result of laser irradiation (wavelengths 532 and 632.8 nm) of the domain structure were studied during an electric field application. In the absence of an electric field, the diffraction pattern was not observed. The image of the spiral repeating the domain structure created in the SBN crystal was recorded during electric field application. The diffraction pattern (after background signal subtraction) under action 250 V and $\lambda = 632.8$ nm is presented on Figure 1b. With increasing voltage, the total intensity of the diffraction pattern increased according to a law close to sinusoidal with a maximum at 250 V at a light wavelength of 632.8 nm. This voltage corresponds to the half-wave voltage for SBN single crystals and this wavelength.

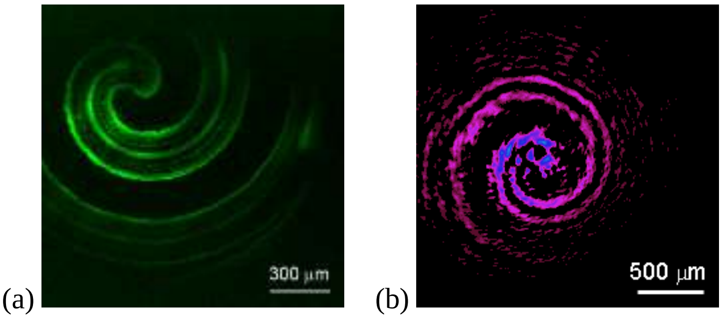

Figure 1. (a) SHGM image of the domain structure created by application of electric field using spiral-shaped mask on the surface, (b) diffraction pattern (after background signal subtraction) on this structure under action U = 250 V, $\lambda = 632.8$ nm.

The authors are grateful for financial support of the Ministry of Science and Higher Education of the Russian Federation (state task FEUZ-2023-0017). The equipment of the Ural Center for Shared Use “Modern nanotechnology” Ural Federal University (Reg. № 2968) was used.

1. J. Mávita, L.A. Ríos, C.E. Minor, et al., *Appl. Opt.* **57**, 2208 (2018).
2. M. Ayoub, P. Roedig, K. Koynov, et al., *Opt. Express* **21**, 8220 (2013).

P55

Micromagnetic simulation of the microstructure parameters influence on the realization of high coercivity state in hard-magnetic MnAl alloys

M.V. Gorshenkov, E.A. Smirnov

[1]*National University of Science and Technology MISiS, 119049, Moscow, Russia*
m2005318@edu.misis.ru

The micromagnetic simulation of a Mn-Al ferromagnetic alloy with a high uniaxial magnetocrystalline anisotropy constant is studied in the work. The objective of the work was to establish the optimum structure parameters for the realization of a high coercive state in an alloy with a nanocrystalline structure, as well as to investigate the influence of the intergrain layer on the magnetic properties. In the course of this work, the dependence of the values of coercive force (H_c) remanent magnetization (M_r/M_s) from the size of the ferromagnetic phase crystal was obtained, and the influence of a strong axial texture on the magnetic hysteresis properties was investigated. Also, the influence of soft-magnetic and non-ferromagnetic interlayers of different thicknesses on the magnetic hysteresis properties was investigated. According to the simulation results, the highest value of the coercive force (H_c=0.5 T) is achieved at the crystal size ranging from 30 nm to 90 nm in ensembles of particles without preferential orientation, with $M_r/M_s \approx 0.59$ (Fig. 1).

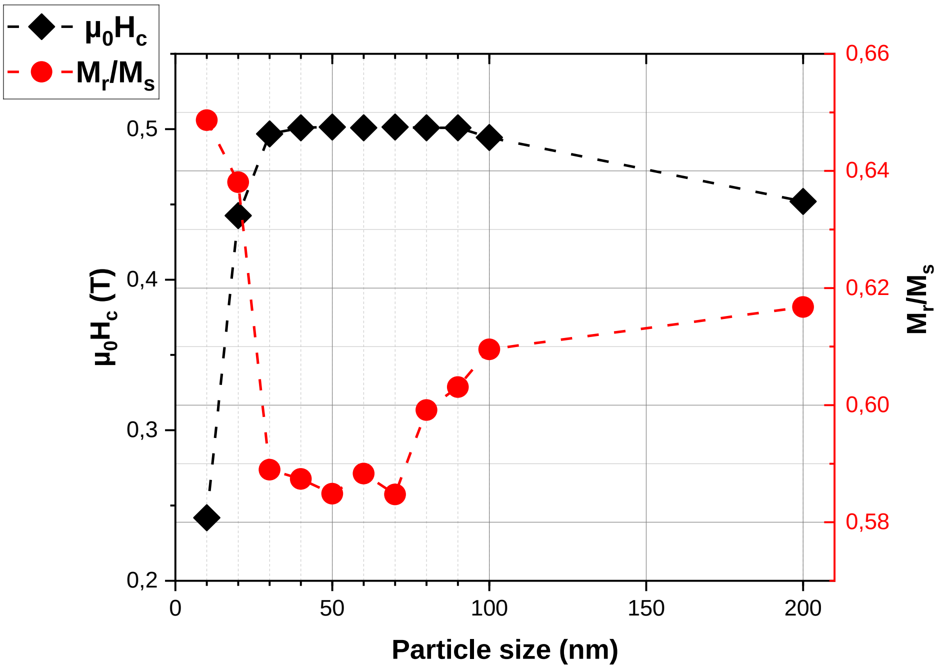

Figure 1. Plots of $\mu_0 H_c(T)$ and M_r/M_s dependence on crystallite size.

Ensembles with strong axial texture show a noticeable increase in magnetic properties (H_c=0.7 T and M_r/M_s =0.74). In both cases, the value of the coercive force is much smaller than the anisotropy field for this phase. The obtained results are in good agreement with the literature data [1].

In ensembles with a non-ferromagnetic interlayer, there is probably an effect of magnetic isolation of crystals. The maximum coercivity is observed at a thickness of 7 nm, and the residual magnetization increases with the growth of the interlayer thickness (Fig. 2).

In ensembles with a soft-magnetic interlayer, no significant increase in the remanent magnetization could be achieved. The coercivity decreases as the interlayer thickness increases (Fig. 3).

Further, the change of the domain structure in the process of remagnetization was investigated. It was possible to confirm the existence of the crystals magnetic isolation effect. To explain the low values of coercivity and remanent magnetization, it is planned to develop a model that considers the influence of crystal structure defects, especially the influence of twins.

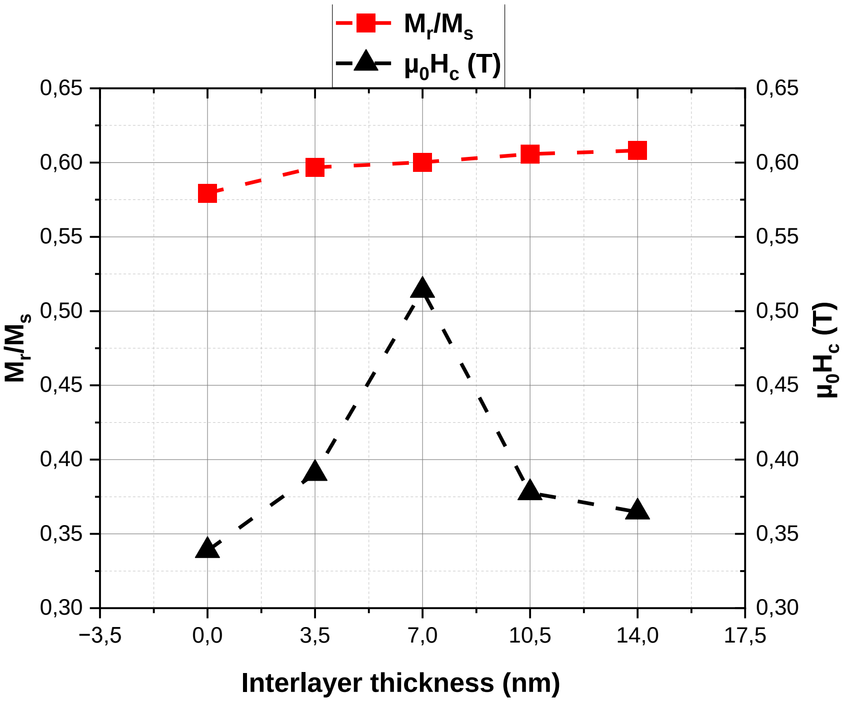

Figure 2. Plots of the coercivity and remanent magnetization dependence on the thickness of a non-ferromagnetic interlayer.

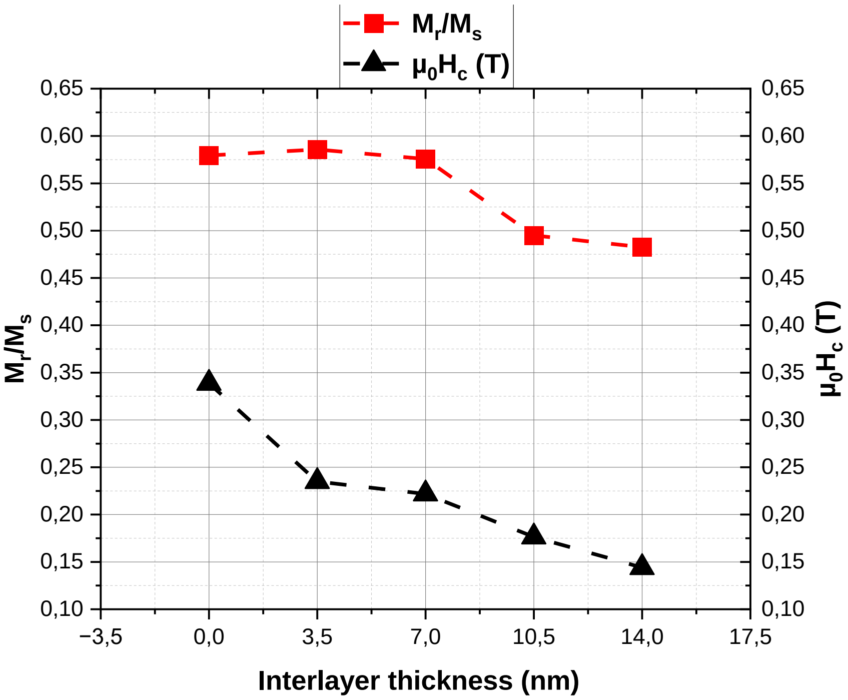

Figure 3. Plots of the coercivity and remanent magnetization dependence on the thickness of a soft-magnetic interlayer.

1. Y. Jia, Y. Wu, Y. Xu, et al., *Acta Materialia* **245**, 2023.

P56

Domain structure and local switching in ceramics and crystals of layered bismuth titanate

A.P. Turygin[1], A.S. Abramov[1], N.A. Shvetsova[2], I.A. Shvetsov[2], A.N. Rybyanets[2], V.Ya. Shur[1]

[1]*School of Natural Sciences and Mathematics, 620000, Ural Federal University, Ekaterinburg, Russia*
anton.turygin@urfu.ru

[2]*Southern Federal University, 344090, Rostov-on-Don, Russia*

Ferroelectric materials are widely used to create various nonlinear optical devices [1], microelectromechanical systems [2], data storage devices [3,4]. One of the important tasks is the creation of high-temperature piezoelectric materials that can operate at temperatures of 400°C and higher [5]. It was reported that bismuth-containing ferroelectrics with a layered structure (Aurivillius phase) have high T_C (> 500°C), high temperature stability of functional properties, low aging rate, which makes them promising for high-temperature applications [6]. Also, one of the potential applications of such ferroelectrics is the creation of non-volatile memory [7]. One of such materials is bismuth titanate ($Bi_4Ti_3O_{12}$, BiT), which has a relatively high ferroelectric phase transition temperature (~675°C) and high spontaneous polarization ($P_s = 50\ \mu C/cm^2$). The polar axis in BiT lies at angle of 5° to the cleavage plane.

In this work, domain structure and local switching in bismuth titanate single crystals and ceramics with composition $Na_{0.5}Bi_{4.5}Ti_4O_{15}$–$PbNb_{0.5}Cr_{0.5}O_3$ were studied. The surface of the BiT crystals was prepared by cleaving the crystals along the cleavage plane. Surface of ceramic samples was thoroughly polished.

The study BiT crystals by the piezoresponse force microscopy (PFM) of as-grown domain structure showed lamella domains with width about several tens on microns. Application of rectangular switching pulses results to formation of lenticular domains. Domain structure in non-polarized BiT consists of blocks of quasi-periodic domains oriented along the long axis of the grain, with a period of about 50-100 nm (Fig. 1a). The characteristic size of the blocks is 0.5-2 μm. In polarized samples the domain structure mainly consists of large domains, 0.5-2 μm wide, oriented perpendicular to the long axis of the grain. Local switching in individual grain with in-plane polarization leads to rearrangement of as-grown domains and formation of mostly uniform switched area with out-of-plane polarization outward to surface (Fig. 1b). In-plane switching occurs on both sides of the probe with the formation of domains on both sides of the probe, separated by tail-to-tail charged domain wall (Fig. 1c).

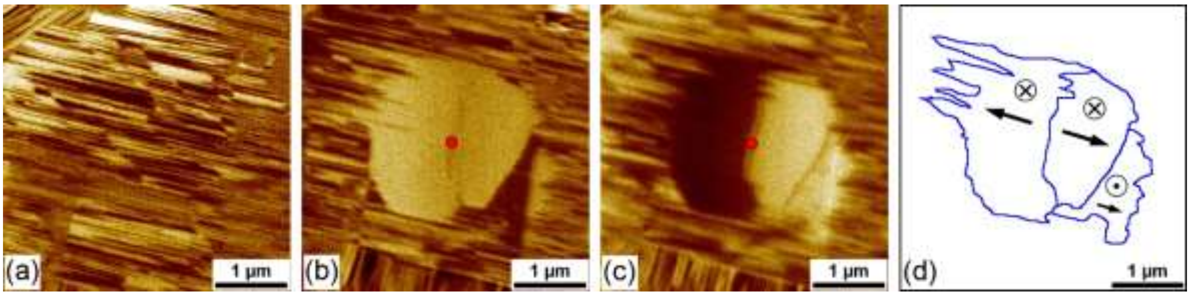

Figure 1. Local switching in unpoled BiT ceramics: (a) initial structure lateral PFM signal, (b) vertical and (c) lateral PFM signal, (d) schematic image. Switching pulse 160 V, 1 s. Red dot indicates point of bias application.

The research was made possible by the Russian Science Foundation (Project No. 24-72-00170). The equipment of the Ural Center for Shared Use “Modern nanotechnology” Ural Federal University (Reg. No. 2968) was used.

1. V.Ya. Shur, A.R. Akhmatkhanov, I.S. Baturin, *Appl. Phys. Rev.* **2**, 040604 (2015).
2. J.F. Scott, C.A. Paz de Araujo, *Science* **246**, 1400 (1989).
3. X. Liu, Y. Liu, W. Chen, et al., *Nanoscale Res. Lett.* **7**, 285 (2012).
4. N. Setter, D. Damjanovic, L. Eng, et al., *J. Appl. Phys.* **100**, 051606 (2006).
5. S.E. Cummins, L.E. Cross, *J. Appl. Phys.* **39**, 2268 (1968).
6. H. Chen, B. Shen, J. Xu, et al., *J. Alloys Compd.* **551**, 92 (2013).
7. H. Watanabe, T. Mihara, H. Yoshimori, et al., *Jpn. J. Appl. Phys.* **34**, 5240 (1995).

P57

Field induced domain evolution in calcium orthovanadate crystals with as-grown domain structure

V.V. Yuzhakov[1], E.V. Shishkina[1], M.A. Chuvakova[1], A.R. Akhmatkhanov[1],
M.S. Nebogatikov[1], E.A. Linker[1], L.I. Ivleva[2], V.Ya. Shur[1]

[1]School of Natural Sciences and Mathematics, Ural Federal University, 620000 Ekaterinburg, Russia
vladimir.juzhakov@urfu.ru

[2]Prokhorov General Physics Institute, Russian Academy of Sciences, 119991 Moscow, Russia

Calcium orthovanadate $Ca_3(VO_4)_2$ (CVO) is a high-temperature ferroelectric with Curie temperature T_C=1110±10°C and spontaneous polarization value $68*10^{-2}$ C/m^2 [1]. Nominally pure and doped with rare earth elements, CVO single crystals possess the nonlinear optical properties, which make them promising materials for second harmonic generation [2,3]. The creation of a periodic domain structure can significantly improve the efficiency of radiation frequency converters, which makes it important to study the domain evolution during polarization reversal in CVO.

The investigated 0.4 mm thick CVO plates were cut perpendicular to the polar axis. The polarization was switched at elevated temperature. Two switching modes were used: (1) a single rectangular pulse with amplitude up to 6.5 kV/mm and a duration up to 10 s, (2) a series of 3,500 to 60,000 rectangular pulses with amplitude range from 2.5 to 6.3 kV/mm, duration 200 μs and frequency 50 Hz. Domain structure evolution was *in situ* optically imaged with simultaneous recording of the switching current. Confocal Raman microscopy and Cherenkov-type second harmonic generation microscopy were used for domain imaging in the bulk.

It was previously shown that the initial domain structure in CVO contains irregularly shaped domains with charged domain walls strongly deviated from the polar direction [4,5]. Isolated round domains are extremely rare, indicating that the optical images of round domains on polar surfaces correspond to cross sections of irregularly shaped domains. The formation of the initial domain structure occurs during cooling near the phase transition.

Polarization reversal in CVO with the initial domain structure consisting of isolated domains with charged domain walls (CDWs) located in the bulk proceeded via formation of the ledges on the CDW and their growth in the polar direction. Analysis of the sequence of instantaneous optical images of the domain structure made it possible for the first time to characterize: (1) the process of growth of individual ledges on the CDW (time dependence of the domain diameter), (2) statistics of the emergence of conical domains on the polar surface (time dependence of the optical current). Statistical analysis of the time dependence of optical currents showed that the rate at which domains reach the surface oscillates and the switching process can be divided into several stages. The obtained time dependence indicates that individual areas of the sample are switched with different delay times caused by to different tilt of the CDWs orientation.

After the top of the growing conical domain touches the polar surface, a current arises along the conductive CDW, which leads to local destruction of the ITO electrode and the formation of a hole, which shape coincides with the domain shape. The reverse switching of the conical domain occurs under the action of the residual depolarizing field $E_{rd} = E_{dep} - E_{scr}$, which, after the formation of a hole in the electrode, grows as a result of the local interruption of external screening. The coincidence of the sizes of the holes and the domains emerging on the surface made it possible to study in detail the domain structure evolution. Analysis of the measured switching currents showed that the contact of the conical domain with the polar surface is accompanied by a current pulse with a duration of about 50 μs. The measured switched charge is close to the value $Q = 2P_SA$, where A is the switched area (hole). The backswitching of the conical domain leads to negative current pulse.

Application of the field pulses series leads to oscillation of the wall, decreasing of the screening efficiency and growth of ledges under the action of partially screened depolarization field [6]. In a CVO with an initial domain structure the polarization reversal under application of the rectangular pulse series happens in three ways: (1) the growth of domains on the surface, as well as (2) the growth of domains completely in the volume and (3) the continuation of their growth after touching the polar surface.

Using statistical analysis of a sequence of instantaneous domains image, an “optical switching charge” was obtained, corresponding to the time dependence of the total area of emerging domains on the surface. An abrupt increase in the switching charge was observed, each step of which corresponded to the appearance of new domains. In this case, the optical switching current, which is the time derivative of the optical switching charge, consisted of isolated pulses, which made it possible to analyze it in terms of Barkhausen pulses. The obtained data on the optical switching current were analyzed by the Korczak method. For the evolution of the field induced domain structure evolution, the values Hurst exponent is about 0.75 was determined, which indicates the persistent nature of the switching process with long-term trend preservation [7].

It was shown that the pulsed laser irradiation of a Mn:CVO sample by far infrared light absorbed in the surface layer led to formation of a twin structure in the irradiation zone induced by fast local surface heating [8]. The influence of twins on the domain structure has been revealed. The interaction of an existing domain wall with a twin led to the formation of a stripe domain of submicron width at the twin boundary. The shift of the domain walls induced by pulsed laser irradiation was also revealed in the irradiated zone. The wall shift dependence on the local curvature has been revealed. The shift was the most significant for the domain wall parts with maximum curvature. The light induced change of the domain structure was attributed to the action of the pyroelectric field appeared as a result of heating by pulsed laser radiation and subsequent cooling.

The research was made possible by Russian Science Foundation (Project № 24-12-00302). The equipment of the Ural Center for Shared Use “Modern nanotechnology” Ural Federal University (Reg.№ 2968) was used.

1. A.M. Glass, S.C. Abrahams, A.A. Ballman, et al., *Ferroelectrics* **17**, 579 (1978).
2. P.S. Bechthold, J. Liebertz, *Optics Communications* **27**, 393 (1978).
3. I.S. Voronina, V.V. Voronov, E.E. Dunaeva, et al., *J. Crystal Growth* **555**, 125965 (2021).
4. E.V. Shishkina, E.D. Greshnyakov, P.S. Zelenovskiy, et al., *Ferroelectrics* **576**, 85 (2021).
5. E.V. Shishkina, V.V. Yuzhakov, M.S. Nebogatikov, et al., *Crystals* **11**, 1508 (2021).
6. E.V. Shishkina, M.A. Chuvakova, V.V. Yuzhakov, et al., *J. Appl. Phys.* **132**, 184101 (2022).
7. V.V. Yuzhakov, M.A. Chuvakova, E.V. Shishkina, et al., *Ferroelectrics* **604**, 99 (2023).
8. E.V. Shishkina, V.V. Yuzhakov, A.R. Akhmatkhanov, et al., *Ferroelectrics* **592**, 83 (2022).

P58

The features of bulk screening process in congruent lithium niobate single crystals

B. Zhu, A.R. Akhmatkhanov, A.D. Ushakov, V.Ya. Shur

Ural Federal University, Institute of Natural Sciences and Mathematics, 620002, Ekaterinburg, Russia
andrey.akhmatkhanov@urfu.ru

Lithium niobate (LN, $LiNbO_3$) single crystals are considered as the main materials of nonlinear optics. The realization of effective nonlinear optical interactions in these crystals requires creation of tailored periodical domain structures in LN by the methods of domain engineering. The stabilization of these structure requires compensation of depolarization field produced by bound charges. This field in ferroelectrics is compensated by two processes: external screening and internal (bulk) screening. Due to existence of dielectric gap (dead layer) in any real ferroelectric, the external screening process is always incomplete. Hence, the residual depolarization field can be fully compensated by slower bulk screening processes only providing the possibility to stabilize any tailored domain structure. That is why the detail characterization of the bulk screening in LN crystals is crucial for domain engineering.

In this work we have studied the bulk screening process in LN single crystals of congruent composition (Jiangxi Shunglang Phot. Tech., China). The samples represented single domain 0.5-mm-thick plates with lateral dimensions 10x15 mm^2 cut perpendicular to the polar axis. Polar surfaces of samples were polished to optical quality.

The bulk screening process was analyzed by measuring the switching current during application of electric field pulse with special shape waveform allowing to vary the delay time between forward and reverse switching. The electric field pulse was applied using Trek 20/20C (Trek Inc., USA) high voltage amplifier using data acquisition board NI PCI-6251 (National Instruments, USA). Electric field was applied using liquid (saturated aqueous LiCl solution) electrodes using special Plexiglass fixture. Switching current analysis allowed to calculate the fields corresponding to current maximum for forward and reverse switching and to extract information about the bulk screening field in the material.

The bulk screening process was studied in the time range from 1 to 10 s. It was shown that in this range the bulk screening field relaxes according to the exponential law. The main limitation of the presented method was the relatively small number of experimental points (about 10) which can be measured due to sample breakdown as a result of cyclic switching. The revealed considerable variation of coercive field among various samples from one wafer didn’t allow to merge data from different samples. The methods of increasing sample durability during cyclic switching are discussed. We have compared the obtained bulk screening parameters with results of previous works [1,2].

Obtained knowledge will be the basis for optimizing the domain engineering methods used in LN single crystals for creation of highly effective nonlinear frequency conversion devices.

The authors are grateful for financial support of the Ministry of Science and Higher Education of the Russian Federation (state task FEUZ-2023-0017). The equipment of the Ural Center for Shared Use “Modern nanotechnology” Ural Federal University (Reg.№ 2968) was used.

1. I.S. Baturin, A.R. Akhmatkhanov, V.Ya. Shur, et al., *Ferroelectrics* **374**, 1 (2008).
2. V.Ya. Shur, A.R. Akhmatkhanov, I.S. Baturin, et al., *Phys. Solid State* **52**, 2147 (2010).

P59

Influence of phase state and microstructure features on magnetic properties of solid solutions of lanthanum-bismuth manganite

A.S. Korolkova[1], D.V. Volkov[2], L.A. Shilkina[3], A.V. Nagaenko[2]

[1] *Southern Federal University, Faculty of Physics, 344090, Rostov-on-Don, Russia*
akorolko@sfedu.ru

[2]*Southern Federal University, Institute of High Technologies and Piezotechnics, 344090, Rostov-on-Don, Russia*

[3]*Southern Federal University, Research Institute of Physics, 344090, Rostov-on-Don, Russia*

Multiferroics are substances that attract the attention of many researchers due to the possibility of coexistence in them of several types of ordering - ferromagnetic, ferroelectric or ferroelastic [1, 2]. At the same time, a complex and interesting object for study is the solid solution of lanthanum-bismuth manganite, which, due to the presence of ferroactive and magnetically active cations in its composition, can demonstrate various types of magnetic and ferroelectric orders. However, the presence of impurity phases and various defects in the form of anionic and cationic vacancies significantly affects the macroresponses observed in these solid solutions. These problems can be partially or completely solved by optimizing the synthesis conditions and introducing various modifiers that facilitate the sintering of ceramics.

In this work, the effect of optimization of synthesis conditions, as well as mechanoactivation [3], which can affect the presence of impurity phases and the kinetics of sintering during the sintering process, is investigated. Mechanical activation is a process in which, as a result of mechanoactivation, as a rule, in the environment of surfactants, the surface potential energy increases and a field of strain stresses appears.

Thus, the purpose of this work was to establish the effect of mechanoactivation on phase formation and structural characteristics and magnetic properties of lanthanum-bismuth manganite solid solution.

All solid solutions were synthesized by two-stage solid-phase synthesis followed by sintering using conventional ceramic technology, including the use of mechanical activation. It was found that a small change in the sintering temperature leads to a significant change in the phase state, leads to a decrease in the average grain size and an increase in the relative density of ceramics [4, 5]. Similar behavior is observed after preliminary mechanoactivation. In all solid solutions at a temperature of 80 K, significant negative magnetic resistance was found, which largely depended on the fineness and homogeneity of the microstructure. Additional conclusions are made about the role of structural features and the observed macroresponses.

The study was carried out with the financial support of the Ministry of Science and Higher Education of the Russian Federation (State task in the field of scientific activity. Project No. FENW-2023-0010/GZ0110/23-11-IF). The equipment of the Center for Collective Use of the Scientific Research Institute of Physics of the Southern Federal University "Electromagnetic, electromechanical and thermal properties of solids" was used. Title of the topic: "Multicomponent intelligent structures: phase transition cross-effects and strategies for accelerated design of eco-systems for technologies for digital design of devices for controlling the parameters of physical media".

1. K. Aizu, *Phys. Rev. B* **2**, 754 (1970).
2. G.A. Smolenskii, I.E. Chupis, *Sov. Phys. Usp.* **25**, 475 (1982).
3. V.A. Poluboyarov, O.V. Andryushkova, I.A. Pauli, et al., *Influence of Mechanical Effects on Physicochemical Processes in Solids* (Novosibirsk: Izd-vo NSU), 604 (2011).
4. D.V. Volkov, I.A. Verbenko, L.A. Shilkina, *Tr. Simp. LFPM* **1**, 92 (2020).
5. A.V. Pavlenko, A.V. Turik, L.A. Reznichenko, et al., *Tech. Phys. Lett.* **39**, 78 (2013).

P60

Mössbauer study of $(1\text{-}x)BiFeO_3\text{-}xAFe_{0.5}B_{0.5}O_3$ (A=Ba, Sr, Pb; B=Nb, Sb) solid solutions

S.P. Kubrin[1], I.N. Lisnevskaya[2], N. M. Olekhnovich[3], A.V. Pushkarev[3], Yu.V. Radyush[3], V.V. Titov[1], S.I. Raevskaya[1] and I. P. Raevski[1]

[1]*Research Institute of Physics and Faculty of Physics, Southern Federal University, Rostov-on-Don, 344090 Russia*
stasskp@gmail.com
[2]*Faculty of Chemistry, Southern Federal University, Rostov-on-Don, 344090 Russia*
[3]*Scientific and Practical Materials Research Centre, National Academy of Sciences of Belarus, Minsk, 220076, Belarus*

The $(1\text{-}x)BiFeO_3\text{–}xBaFe_{0.5}Nb_{0.5}O_3$ (x=0, 0.1, …, 1), $(1\text{-}x)BiFeO_3\text{–}xSrFe_{0.5}Nb_{0.5}O_3$ (x= 0.1, …, 1), $(1\text{-}x)BiFeO_3\text{–}xSrFe_{0.5}Sb_{0.5}O_3$ (x= 0.05, …, 0.9), $(1\text{-}x)BiFeO_3\text{–}xPbFe_{0.5}Sb_{0.5}O_3$ (x= 0.05, …, 0.9) solid solutions were prepared by solid state synthesis. The solid solutions samples with $SrFe_{0.5}Sb_{0.5}O_3$, $PbFe_{0.5}Sb_{0.5}O_3$, $SrFe_{0.5}Nb_{0.5}O_3$ were synthesized under high pressure about 4.5 GPa. The XRS study of prepared samples reviled that all samples are single phase and have perovskite structure.

Room temperature Mössbauer spectra of solid solutions whit x in the range of 0 – 0.2 were decomposed using the model of anharmonic spin – cycloid [1]. This model allows us to obtain the values of anharmonic parameter (m) and the magnetic anisotropy constant (K_u). The analysis of these spectra shows that m value linearly increases with x growing. At x=0.2 the m values are in the range of 0.92 – 0.97. Since the m=1 indicates the absence of spin cycloid in all systems the spatial spin-modulated structure is suppressed near x=0.23. Moreover, the analysis shows that *B*-cations are randomly distributed.

Room temperature spectra of samples with x in the range of 0.3 – 0.7 are Zeeman splitting line. These spectra were fitted by several sextets. Each sextet corresponds to Fe^{3+} ions with different Nb^{5+} or Sb^{5+} ions in near neighborhood. The values of sextet areas are strongly deviated from the probabilities of Fe^{3+} local configuration forming calculated from binominal distribution. This indicates that Fe-rich and Fe-poor regions are forming in the sample. The spectra of sample with x>0.7 are paramagnetic lines. The Nb-contained samples are decomposed on two doublets. The doublets with lager value of quadrupole splitting corresponds to Fe^{3+} ions in Fe-poor regions, the second one associated with Fe^{3+} in Fe-rich regions. The spectra of Sb-contained samples were fitted with singlet and doublet. The singlet corresponds to Fe^{3+} in region with long range compositional ordering. The doublet is represented by Fe^{3+} in region with compositional disordering.

To estimate the magnetic phase transition temperature T_N, the method of temperature scanning was used. The essence of temperature scanning is measuring Mössbauer spectrum line intensity in the course of sequential decrease in temperature. When temperature decreases below magnetic phase transition temperature, the Mössbauer spectra transform from a doublet into Zeeman sextet. This transformation is accompanied by a significant decrease in the magnitude I_m of Mossbauer spectrum intensity within the 0-1.2 mm/s velocity range normalized to its value at 300 K. This drop in the temperature dependence of I_m allows one to obtain the T_N from the Mössbauer experiment.

The obtained by temperature scanning T_N values were summarized into compositional dependencies (Fig. 1). The $T_N(x)$ dependencies of all systems are linearly decreasing in the compositional range of 0 – 0.7. This decreasing of $T_N(x)$ is determined by reduction in the number of $Fe^{3+}\text{-}O^{2-}\text{-}Fe^{3+}$ superexchange magnetic chains due to the substitution of Fe^{3+} ions by Nb^{5+} and Sb^{5+} ions [2]. Near x=0.7 the $T_N(x)$ dependencies change their slope and T_N values reduce faster. The anomaly on $T_N(x)$ near x=0.7 corresponds to the percolation threshold of $Fe^{3+}\text{-}Bi^{3+}\text{-}Fe^{3+}$ magnetic superexchange. When the concentration of magnetoactive Fe^{3+} ions is high and clusterization is weak or absent the magnetic properties mainly determine by $Fe^{3+}\text{-}O^{2-}\text{-}Fe^{3+}$ superexchange. However, the reduction in Fe^{3+} concentration leads to formation of Fe-rich and -poor regions. The Fe-rich regions could connect with each other through Bi^{3+} ions.

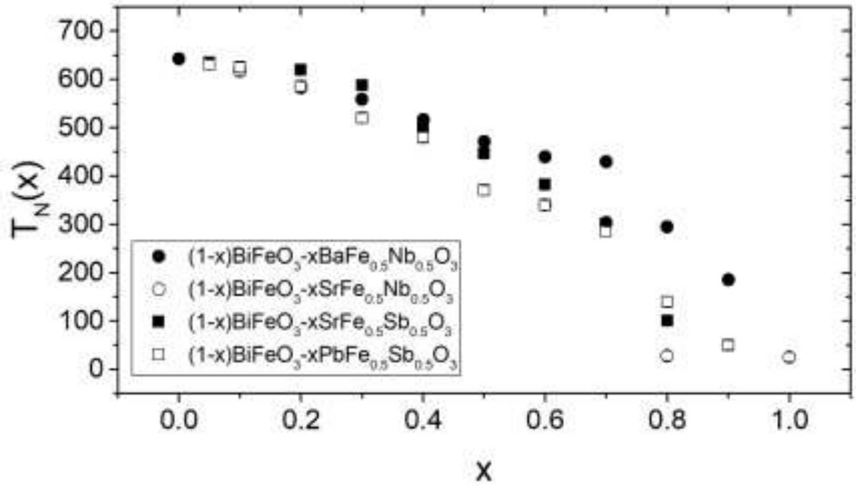

Figure 1. Concentration dependencies of magnetic phase transition temperatures T_N of (1-x)BiFeO$_3$–xAFeBO$_3$ (A=Ba, Sr, Pb; B=Nb, Sb) solid solutions.

The similar phenomenon is observed in $Pb_{1-x}A_xFe_{0.5}Nb_{0.5}O_3$ (A=Ba, Ca) [3,4] where replacing of Pb^{2+} by Ba^{2+} or Ca^{2+} results in lowering of magnetic phase temperature. Moreover, this replacement leads to the changing of magnetic state from antiferromagnetic to spin-glass. In the (1-x)BiFeO$_3$–xAFe$_{0.5}$B$_{0.5}$O$_3$ (A=Ba, Sr, Pb; B=Nb, Sb) systems when x=0.7 the decreasing of Bi^{3+} ion concentration leads to the breakdown of Fe^{3+}-Bi^{3+}-Fe^{3+} connections between Fe-rich regions and reduction in T_N values. It should be noted that in Sb-contained systems T_N decreasing faster that in Nb-contained one. In the Sb-contained samples besides the reduction of Fe^{3+} and Bi^{3+} concentrations the number of magnetic superexchange chains is determined by long range ordering. The growth of Sb^{5+} concentration stimulated compositional order in B-sublattice, which leads decreasing of Fe^{3+}-O^{2-}-Fe^{3+} magnetic chains.

This study was supported by the RNF (Grant 23-42-10024) and Belarusian Republican Foundation for Fundamental Researches (Grant T23RNF-086)

1. M.E. Matsnev, V.S. Rusakov, *AIP Conf. Proc.* **1622**, 40 (2014).
2. J.B. Goodenough, *Magnetism and Chemical Bond* (Interscience, New York) (1963).
3. I.P. Raevski, S.P. Kubrin, S. I. Raevskaya, et al., *Phys. Rev. B* **80**, 024108 (2009).
4. I.P. Raevski, S.P. Kubrin, S. I. Raevskaya, et al., *Ferroelectrics*, **398**, 16 (2010).

P61

Structure, dielectric and magnitodielectric properties of solid solutions of the system based on bismuth ferrite and lithium niobate

D.V. Lymar[1,2], E.V. Glazunova[1], L.A. Shilkina[1], I.A. Verbenko[1], L.A. Reznichenko[1]

[1]Research institute of physics, Southern Federal University, 344090 Rostov-on-Don, Russia
kate93g@mail.ru

[2]Physics faculty, Southern Federal University, 344090 Rostov-on-Don, Russia

Multiferroics are a unique class of compounds that exhibit two or more types of ordering, including ferroelectric, ferroelastic, and magnetic ordering. Due to the heterogeneous nature of these materials, they have attracted the attention of numerous research groups, both in terms of their potential technological applications and in terms of fundamental physics. Among the multiferroics that have been identified to date, bismuth ferrite ($BiFeO_3$) is the most versatile material. It exhibits high antiferromagnetic (T_N) and ferroelectric (T_C) transition temperatures of 643 K and 1100 K, respectively [1]. Nevertheless, it has been established for some time that the magnetoelectric response in bismuth ferrite is relatively weak. This is due to the fact that the different cations present in the structure are responsible for the segmental electric and magnetic response, as outlined in reference [2]. One of the most effective methods for enhancing the electrical and magnetic properties of $BiFeO_3$ is through modification. It has been demonstrated in the literature that non-isovalent modification of $BiFeO_3$ with lithium results in an increase in magnetocapacitance and a reduction in segmental electric losses [3]. Furthermore, it has been demonstrated that doping of $BiFeO_3$-based solid solutions with niobium results in a reduction in the electrical conductivity of the material by six orders of magnitude [4]. A synthesis has been attempted based on the structure of perovskite, using $BiFeO_3$ as a base and ilmenite–$LiNbO_3$ as the second element. A review of the literature reveals that this system of solid solutions is only represented to a limited extent in the existing literature [5, 6]. Moreover, even in the limited number of sources that do exist, there are disagreements concerning the structure and properties of solid solutions of the $BiFeO_3$-$LiNbO_3$ system.

The solid solutions of the $(1\text{-}x)BiFeO_3–xLiNbO_3$ system with $0 \leq x \leq 1$, with a step size of $x = 0.1$, were selected as the objects of study. The fabrication process involved a two-step solid-phase synthesis, followed by conventional ceramic sintering. To optimise the synthesis and sintering conditions, a series of experiments were conducted, in which the temperatures, holding times and application of mechanoactivation were varied. The optimal conditions for obtaining the desired results were found to be as follows: $T_{\text{synt1}} = 550^{\circ}C$, $T_{\text{synt2}} = 800^{\circ}C$, $\tau_{\text{synt1,2}} = 5\text{-}10$ h; $T_{\text{sint}} = 800 - 1100^{\circ}C$, $\tau_{\text{sint}} = 2$ h.

The paper will present the results of X-ray phase analysis, an investigation of the microstructure, dielectric and magnetodielectric properties of solid solutions of the system $(1\text{-}x)BiFeO_3–xLiNbO_3$.

The study was carried out with the financial support of the Ministry of Science and Higher Education of the Russian Federation (State task in the field of scientific activity. Project No. FENW-2023-0010/GZ0110/23-11-IF). The equipment of the Center for Collective Use of the Scientific Research Institute of Physics of the Southern Federal University "Electromagnetic, electromechanical and thermal properties of solids" was used.

1. Y.K. Jun, W.T. Moon, C.M. Chang, et al., *Solid State Commun*. **135**, 133 (2005).
2. D.I. Chomsky, *J. Exp. Theor. Phys.* **159**, 581 (2021).
3. M.M. Shirolkar, C. Hao, X. Dong, et al., *Nanoscale* **6**, 4735 (2014).
4. T. Wang, L. Jin, Y. Tian, et al., *Mater. Lett.* **137**, 79 (2014).
5. M. Dea, S. Hajrab, R. Tiwaria, et al., *Solid State Sciences* **93**, 1 (2019).
6. E.V. Satulova, Y.V. Kabirov, A.G. Rudskaya, et al., *Proc. 4th Int. Interdisciplinary Symp. "Physics of lead-free, piezoactive and related materials"* **2**, 197 (2015).

P62

Crystal structure and properties of ceramics based on $0.55BiFeO_3$-$0.45YMnO_3$ multiferroic system

A.V. Nazarenko[1], Ya.Yu. Matyash[1], D.V. Stryukov[1], A.V. Pavlenko[1,2]

[1]Federal Research Centre the Southern Scientific Centre of the Russian Academy of Sciences (SSC RAS),
344006, Rostov-on-Don, Russia
avnazarenko1@gmail.com

[2]Southern Federal University, 344006, Rostov-on-Don, Russia

Bismuth ferrite ($BiFeO_3$, BFO) is the classical and one of the most studied multiferroic, which combines ferroelectric and antiferromagnetic properties at room temperature [1–4]. It has very high temperatures of antiferromagnetic (T_N = 640 K) and ferroelectric (T_C = 1100 K) phase transitions [5]. $BiFeO_3$ is the basis for various materials in the solid state (for example, solid solutions, composites, thin films, heterostructures, etc.) considering the high interest in it, a wide range of applications and more than half a century of its research [6]. Particularly interesting are the compounds of BFO with other multiferroics, which differ from it not only in structure, but also in the nature of the properties. One of such material is, for example, yttrium manganese oxide ($YMnO_3$, YMO). $YMnO_3$ is a low-temperature multiferroic (T_N ~ 80 K), which exhibits ferroelectric properties at room temperature. It has a high-temperature antiferromagnetic transition (T_C ~ 900 K) [7, 8]. Studies of the entire series of solid solutions based on $(1–x)BiFeO_3–xYMnO_3$ (BFO-xYMO) at $x = 0 \div 1$ concentration range were carried out in 2010-2011 for the first time [9], where it was shown that these materials are complex and multicomponent systems in which perovskite phases coexist against the background of a composite structure. During the studying of these materials properties, there are certain difficulties that are associated not only with complex temperature-frequency behavior, but also with obtaining decent ceramics.

This paper presents the results on the obtaining of dense ceramics of the BFO-xYMO system with $x = 0.45$ using both the two-stage method (“synthesis + sintering”) and the one-stage method (“synthesis with sintering”), and also presents a comparison of their characteristics. During the study, the crystal structure, grain microstructure, as well as temperature-frequency dielectric spectra were studied. In both cases, the obtained materials still have a composite structure, which determines the complex nature of the dielectric spectra, but the significant thing is that it exhibit ferromagnetic properties at room temperature.

The study is funded by Russian Science Foundation (project No. 22-72-00143, https://rscf.ru/project/22-72-00143/) with the use of equipment of the SSC RAS Center for Collective Use (https://ckp-rf.ru/catalog/ckp/501994/).

1. A.I. Zaslavskiy, A.G. Tutov, *Doklady AH SSSR* **135**, 815 (1960).
2. A Filippetti., N.A. Hill, *Phys. Rev. B.* **65**, 195120 (2002).
3. G.A. Smolenskii, V.A. Bokov, V.A. Isupov, et al., *Helvetica Physica Acta* **41**, 1187 (1968).
4. C. Michel, J.-M. Moreau, G.D. Achenbach et al., *Solid State Comm.* 7, 701 (1969).
5. G. Catalan, J.F. Scott, *Adv. Mater* **21**, 2463 (2009).
6. D. Sando, A. Bartheemy, M. Bibes, *J. Phys.: Cond. Matter* **26**, 473201 (2014).
7. Z.J. Huang, Y. Cao, Y.Y. Sun, et al., *Phys. Rev. B* **56**, 2623 (1997).
8. T. Lonkai, D.G. Tomuta, U. Amann, et al., *Phys. Rev. B* **69**, 134108 (2004).
9. A.V. Nazarenko, A.G. Razumnaya, M.F. Kupriyanov, et al., *Phys. Solid State* **53**, 1599 (2011).

P63

Magnetic and magnetocaloric properties of GdMn$_{1-x}$V$_x$Si compounds

S.P. Platonov[1], A.G. Kuchin[1], R.D. Mukhachev[1], A.V. Lukoyanov[1,2], A.S. Volegov[1,3],
V.S. Gaviko[1,3], M.Yu. Yakovleva[1]

[1]*M.N. Mikheev Institute of Metal Physics UB RAS, 620108 Ekaterinburg, Russia*
platonov@imp.uran.ru

[2]*Institute of Physics and Technology, Ural Federal University, 620002 Ekaterinburg, Russia*

[3]*Institute of Natural Sciences and Mathematics, Ural Federal University, 620002 Ekaterinburg, Russia*

Intermetallic RTX compounds, where R is a rare-earth metal and T, X is d or p-element, exhibit a large magnetocaloric effect MCE for various temperatures from helium to room temperature [1]. Magnetic materials with large MCE at room temperature are of particular interest, since they can be used as a working material in household magnetic refrigerators. Replacing conventional freon refrigerators with environmentally friendly magnetic ones is a very urgent task, so there is a permanent search for new materials with high MCE at room temperature.

In this work, the magnetic and magnetothermal properties of GdMn$_{1-x}$V$_x$Si substitution alloys were studied for the first time. The initial GdMnSi compound has a Curie temperature T_C=320 K around room temperature and a noticeable ΔT-effect (i.e. MCE) of 0.5 K during a second-order magnetic phase transition with a field change of 0-13.5 kOe [2].

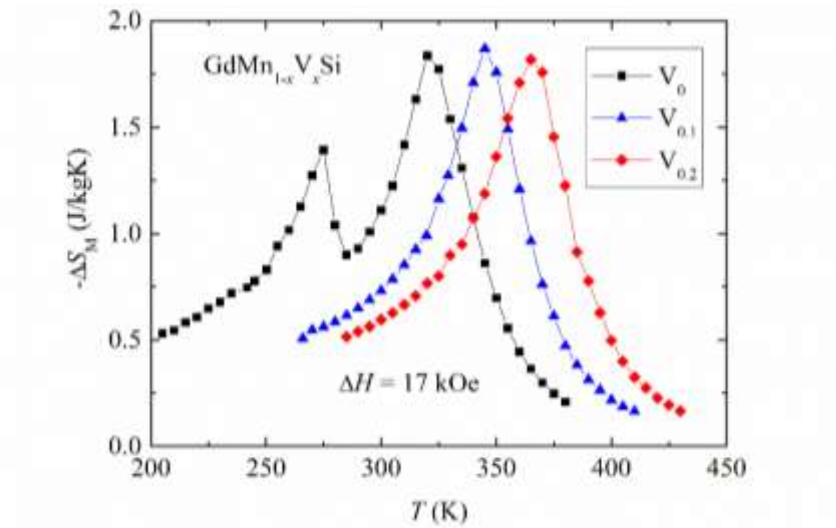

Figure 1. Temperature dependences of the change in magnetic entropy $-\Delta S_M(T)$ for GdMn$_{1-x}$V$_x$Si, x=0, 0.1, 0.2 with a field change of 0-17 kOe.

Temperature dependence of the change in magnetic entropy $-\Delta S_M(T)$ (i.e. MCE) for GdMn$_{1-x}$V$_x$Si exhibits two maxima for x=0 at T of magnetic ordering of the subsystems Gd (at T=270 K) and Mn (at T=320 K) [1] and one maximum for x=0.1, 0.2, as is shown in Figure 1. It can be seen that the Curie temperature noticeably increased by 45 K, while the MCE remained virtually unchanged compared to 1.85 J/kgK for the composition x=0.

This study was supported by the grant of Russian Science Foundation No 24-22-00066, https://rscf.ru/en/project/24-22-00066/.

1. A.G. Kuchin, S.P. Platonov, R.D. Mukhachev, et al., *Metals* **13**, 290 (2023).
2. I.A. Ovtchenkova, S.A. Nikitin, T.I. Ivanova, et al., *J. Magn. Magn. Mater.* **300**, e493 (2006).

P64

Features of the synthesis, structure and properties of $Bi_{1-x}FeO_{3-\delta}$ with $0 \le x \le 0.20$

D.I. Rudskiy[1], I.A. Verbenko[1], Yu.A. Kuprina[1], A.V. Nazarenko[2], Li Zhenyu[3], A.O. Galatova[4],
Yu.V. Kabirov[4], D. Hanov[1], A.R. Lebedinskaya[5], E.N. Sidorenko[4], A.G Rudskaya[4]

[1]*Southern Federal University, Research Institute of Physics, 344090, Rostov-on-Don, Russia*
rudskiy@sfedu.ru

[2]*Southern Scientific Centre of the Russian Academy of Sciences, 344006, Rostov-on-Don, Russia*

[3]*Southern Federal University, International Smart Materials Research Institute, 344090, Rostov-on-Don, Russia*

[4]*Southern Federal University, The Department of Physics, 344090, Rostov-on-Don, Russia*

[5]*Southern Federal University, Academy of Architecture and Arts, 344082, Rostov on Don, Russia*

Among oxide compounds with the chemical formula ABO_3, those that simultaneously possess ferroelectric (FE) and ferro(antiferro)magnetic (FM) properties are of particular interest. As has been established from recent work, such compounds contain bismuth ferrite ($BiFeO_3$, BFO), including those with variations in deviations from stoichiometry.

The preparation of pure BFO by solid-phase reactions is a difficult task, since during the solid-phase synthesis, in addition to BFO, an uncontrolled amount of impurity phases is formed in the form of $Bi_2Fe_4O_9$ (mullite) and $Bi_{25}FeO_{40}$ (selenite). This leads to low repeatability of the properties of the bismuth ferrite ceramic samples.

The main goal of the work was to determine the characteristics of the phase formation of non-stoichiometric $Bi_{1-x}FeO_{3-\delta}$ with a deficiency of Bi_2O_3 from 5 to 20 mol%.

Using the method of the one-stage solid-phase synthesis, the ceramic samples of non-stoichiometric bismuth ferrite $Bi_{1-x}FeO_{3-\delta}$ with $0 \le x \le 0.20$ and a step $\Delta x = 0.05$ were prepared from a mixture of Bi_2O_3 and Fe_2O_3 oxides at a temperature $T = 850$ °C and a synthesis time $\tau = 2$ hours.

In the course of the studies, the phase composition, structural and atomic parameters of the obtained samples were established. In addition to the main rhombohedral phase BFO, all the samples contain impurity phases — the cubic phase $Bi_{25}FeO_{40}$ of the selenite type and the orthorhombic phase $Bi_2Fe_4O_9$ with a mullite-type structure. It has been shown that the behaviour of the BFO rhombohedral phase parameters, depending on the deficiency of the bismuth oxide, is non-monotonic. At $x = 0.05$, all the structural parameters have minimum values: $a = 5.575$ Å; $c = 13.843$ Å; $a_R = 3.960$ Å; $\alpha_R = 89.46°$; $V_R = 62.08$ Å^3 with the perovskite phase concentration $C = 82.8\%$. The concentration of the main BFO phase decreases with increasing x, while the concentration of the $Bi_{25}FeO_{40}$ phase also decreases, and the concentration of the $Bi_2Fe_4O_9$ phase increases in this interval. At a concentration $x = 0.05$, a minimum rhombohedral angle $\alpha_R = 89.46°$ is observed. At other concentrations x, the angle remains virtually unchanged and is approximately 89.50°. As the deficiency of the bismuth Bi^{3+} ions increases, the volumes of the perovskite cells per ABO_3 formula unit decrease at $x = 0.05$ and then linearly increase at $x = 0.10 – 0.20$.

The report will present the results of the structural, microstructural and physical properties of non-stoichiometric $Bi_{1-x}FeO_{3-\delta}$, including the detailed description of the structural features and properties in the concentration range near $x = 0.05$.

The study was carried out with the financial support of the Ministry of Science and Higher Education of the Russian Federation (State task in the field of scientific activity. Project No. FENW-2023-0010/GZ0110/23-11-IF). Title of the topic: "Multicomponent intelligent structures: phase transition cross-effects and strategies for accelerated design of eco-systems for technologies for digital design of devices for controlling the parameters of physical media". The equipment of the Center for Collective Use of the Scientific Research Institute of Physics of the Southern Federal University "Electromagnetic, electromechanical and thermal properties of solids" was used.

P65

Valence state of iron ions in single-crystal compounds $Bi_{1-x}R_xFeO_3$ (R=Eu, Gd, Nd) according to X-ray photoelectron spectroscopy

A.A. Skryabin[1], A.T. Kozakov[1], A.G. Kochur[2], K.A. Googlev[2], S.I. Dudkina[1], L.A. Reznichenko[1]

[1]Research Institute of Physics, Southern Federal University, 344090, Rostov-on-Don, Russia
atkozakov@sfedu.ru

[2]Rostov State Transport University, 344038, Rostov-on-Don, Russia

In recent years, multiferroics have been intensively studied, which simultaneously possessed magnetic and electrical ordering. These properties make such materials potential candidates for the production of memory elements, sensors, and various spintronics devices. Among them, a special place is occupied by bismuth ferrite, $BiFeO_3$, which not only itself has a connection between the magnetic and electrical subsystems, but is also the basis for the creation of other materials based on it.

This work is devoted to the study of the valence state of iron in single crystals of the composition $Bi_{1-x}R_xFeO_3$, where R = Eu, Gd, Nd, using X-ray photoelectron spectroscopy. A description of methods and details for the production of single-crystalline materials of the composition $Bi_{1-x}R_xFeO_3$, where R = Eu, Gd, Nd, is given in work [1].

Bismuth ferrite $BiFeO_3$ belongs to rhombohedrally (symmetry group R3c) distorted perovskites, and already at room temperature it has dipole electric and magnetic long-range order. It retains ferroelectric properties up to temperatures T_c ~ 1103 K or T_c ~ 1123 K. However, the existing helical magnetic ordering of Fe^{3+} ions along the [111] direction is preserved at significantly lower temperatures (T_N ~ 640 K). The spatial helical structure in $BiFeO_3$ can be suppressed by introducing rare earth or alkaline earth ions into its crystal structure, which lead to a significant improvement in its magnetic properties. Eu, Gd, Nd and other elements are often used as such elements.

It has been established that the studied single-crystal samples of the composition $(Bi_{1-x},R_x)FeO_3$ with R = Eu, Gd, Nd, in addition to the main amount of Fe^{3+} ions, also contain a small amount of Fe^{4+} ions. The reasons for the appearance of Fe^{4+} ions are basically the same as those that provoke the appearance of Mn^{4+} in materials $La_{1-x-y}Bi_x A_yMn_\alpha O_{3\pm\delta}$ (A = Ba, Pb), which we discussed in detail in [2]. This is the presence of extended planar defects in the crystal lattice and modulation of the lattice period, leading to the appearance of iron clusters in the defective areas surrounded by oxygen, corresponding to Fe^{4+} ions.

The study was carried out with the financial support of the Ministry of Science and Higher Education of the Russian Federation (State task in the field of scientific activity. Project No. FENW-2023-0010/GZ0110/23-11-IF). Title of the topic: "Multicomponent intelligent structures: phase transition cross-effects and strategies for accelerated design of eco-systems for technologies for digital design of devices for controlling the parameters of physical media". The equipment of the Center for Collective Use of the Scientific Research Institute of Physics of the Southern Federal University "Electromagnetic, electromechanical and thermal properties of solids" was used.

1. V.G. Smotrakov, V.V. Eremkin, A.V. Pavlenko, et al., *Coll. Proc. 1st Int. Interdisciplinary Symp. "Lead-free ferroelectric ceramics and related materials: production, properties, applications (retrospective-present-day-forecasts"*, 254 (2012).

2. A.T. Kozakov, A.G. Kochur, L.A. Reznichenko, et al., *J. Electron Spectroscopy and Related Phenomena* **186**, 14 (2013).

P66

Phase formation, size effects and Maxwell-Wagner relaxation phenomena in bismuth ferrite modified with rare earth elements

A.A. Zubrilin[1], S.V. Khasbulatov[2,3], S.I. Dudkina[4], K.P. Andryushin[3,4],
L.A. Shilkina[4], I.A. Verbenko[4], L.A. Reznichenko[4]

[1]Southern Federal University, Faculty of Physics, 344090, Rostov-on-Don, Russia

zubrilin@sfedu.ru

[2]Chechen State University named after. A.A. Kadyrova, 364094, Grozny, Russia

[3]Comprehensive Research Institute named after. H.I. Ibragimov RAS, 364051, Grozny, Russia

[4]Research Institute of Physics, Southern Federal University, 344090, Rostov-on-Don, Russia

The optimal conditions for the phase formation of high-density, strong, pure ceramics of the $BiFeO_3$/Ln (Ln (x) systems were determined: La, Pr, Nd, Sm, Eu, Gd, Tb, Du, Ho, Er, Tu, Yb, Ln $0.0 \leq x \leq 0.5$, $\Delta x = 0.025...0.10$), obtained by two-stage (with intermediate grinding and granulation of dispersed crystalline products) synthesis followed by sintering using conventional ceramic technology (without externally applied pressure); comprehensively (using various experimental techniques), their structure, grain structure, dielectric spectra, and thermophysical properties were studied in a wide range of external influences.

Phase diagrams of the states were constructed, regions of the coexistence of phases of the different symmetry were identified, and correlations of the macrocharacteristics with the phase and chemical composition of the solid solutions were established.

The influence of size effects (ionic radii Ln) on the form of the phase diagrams of $BiFeO_3$/REE systems, structural nonstoichiometry of the solid solutions, polycrystallinity of ceramics, and dielectric/thermophysical properties of objects has been established.

It is shown that the anomalous “behavior” of the dielectric characteristics ($\varepsilon'/\varepsilon_0$ and tgδ) of $BiFeO_3$/REE is caused by the phenomena of Maxwell–Wagner relaxation [1] due to the spatial inhomogeneity of the structure of the studied media and, as a consequence, the accumulation of free charges on the interface between the components in such environments against the background of interlayer, interphase and intraphase rearrangements. The reason for their development is the natural composite structure of $BiFeO_3$ and $BiFeO_3$/REE, which is formed on the basis of at least four (not counting $BiFeO_3$ itself) Bi,- Fe- containing compounds (Bi_2O_3, Fe_2O_3, $Bi_{25}FeO_{40}$, $Bi_2Fe_4O_9$), which almost always accompany the formation of $BiFeO_3$, remaining in it (in different quantities) in the form of ballast phases and undergoing a series of bifurcations in the above temperature ranges [2].

Based on the experimental results obtained, a group of solid solutions that are promising for use in various microelectronic devices was selected, and methods for their preparation were developed.

The study was carried out with the financial support of the Ministry of Science and Higher Education of the Russian Federation (State task in the field of scientific activity. Project No. FENW-2023-0010/GZ0110/23-11-IF). Title of the topic: "Multicomponent intelligent structures: phase transition cross-effects and strategies for accelerated design of eco-systems for technologies for digital design of devices for controlling the parameters of physical media". The equipment of the Center for Collective Use of the Scientific Research Institute of Physics of the Southern Federal University "Electromagnetic, electromechanical and thermal properties of solids" was used.

1. A.V. Turik, G.S. Radchenko, *Phys. Solid State* **45**, 1060 (2003).
2. S.V. Khasbulatov, *Abstract of dissertation, Ph.D.*, Rostov-on-Don, 24 (2019).

P67

Ferroelectric properties and domain structure of the P(VDF-TrFE) films

D.O. Alikin[1], V.V. Yuzhakov[1], A.D. Ushakov[1], V.S. Shubin[1],
V.A. Agafonov[1], M.V. Silibin[2], A.V. Sysa[2,3]

[1]*School of Natural Sciences and Mathematics, Ural Federal University, 620000 Ekaterinburg, Russia*
denis.alikin@urfu.ru

[2]*Institute of Advanced Materials and Technologies, National Research University of Electronic Technology, 124498 Zelenograd, Moscow, Russia*

[3]*Scientific-Manufacturing Complex «Technological Centre», 124498, Zelenograd, Moscow, Russia*

The ferroelectric polymer poly(vinylidene fluoride) (PVDF) and its copolymers with trifluoroethylene, P(VDF-TrFE), are exceptional materials known for their excellent mechanical compliance and relatively strong dielectric and piezoelectric properties [1]. These characteristics are essential for various devices, including miniature capacitors for telecommunications, high-performance actuators, and contact switches [2]. Despite extensive research into the properties of PVDF and the mechanisms underlying its polarization, the dynamics of its domains and the contributions of domain structure and polarization reversal to its overall ferroelectric and piezoelectric properties remain less understood.

In this study, we investigated P(VDF-TrFE) films with a molar ratio of 70/30 for VDF and TrFE, respectively, produced by polymerization from a dimethylsulfoxide/acetone solution. One film was pre-polarized using corona discharge ("corona poling") [3], while another film was studied in its as-prepared state. A chromium electrode was deposited on top of each film using magnetron sputtering. We measured ferroelectric loops, domain structures, and piezoelectric responses under identical conditions (Fig. 1). A significant increase in the polarization and piezoresponse of the film pre-polarized with corona poling was observed, demonstrating that corona poling is a more effective method for enhancing the piezoelectric properties of PVDF-TrFE films. The variation in macroscopic functional responses was rationalized through the examination of domain structures and local piezoelectric properties using piezoresponse force microscopy.

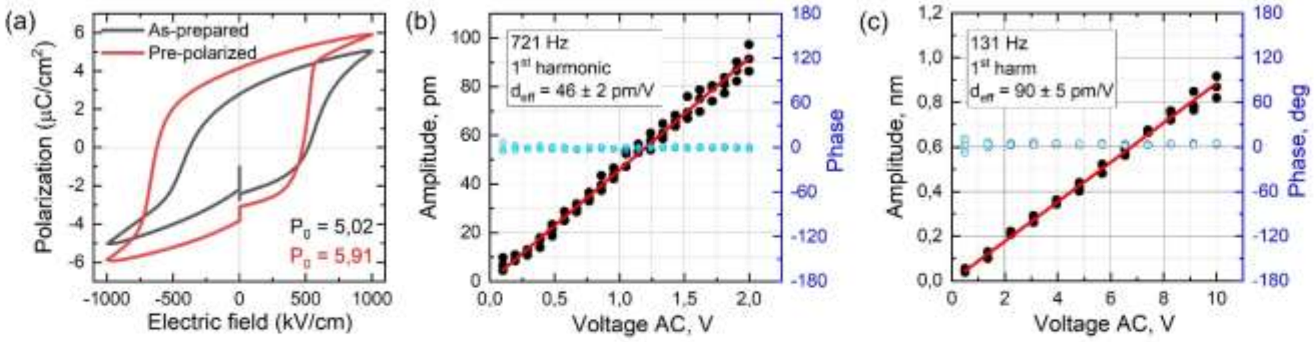

Figure 1. (a) P-E ferroelectric hysteresis loops and (b), (c) piezoresponse for (b) as-prepared and (c) pre-polarized P(VDF-TrFE) films.

The research funding from the Ministry of Science and Higher Education of the Russian Federation (Ural Federal University Program of Development within the Priority-2030 Program) is gratefully acknowledged. M.V. Silibin acknowledges the State assignment 2023–2025, number FSMR-2023-0003. The equipment of the Ural Center for Shared Use "Modern nanotechnology" Ural Federal University (Reg.№ 2968) was used.

1. N. Murayama et al., *Ultrasonics* **14**, 1 (1976).
2. J. Belovickis et al., *Phys. Status Solidi B* **255**, 1700196 (2018).
3. R.A. Hill et al., *Appl. Phys. Lett.* **65** (14), 1733 (1994).

P68

Relationship between domain structure and structural state on the morphotropic phase boundary of the $Bi_{0.5}Na_{0.5}TiO_3$-$PbTiO_3$ ferroelectric ceramics

D.O. Alikin,[1], A.D. Ushakov,[1] A.S. Abramov,[1] L. Zhang,[2]
L.V. Gimadeeva,[1] V.Ya. Shur,[1] Li Jin[2]

[1]*School of Natural Sciences and Mathematics, Ural Federal University, 620000, Ekaterinburg, Russia, denis.alikin@urfu.ru*

[2] *Electronic Materials Research Laboratory, Key Laboratory of the Ministry of Education and International Center for Dielectric Research, Xi'an Jiaotong University, 710049, Xi'an, China*

The sodium-bismuth titanate–lead titanate ($Bi_{0.5}Na_{0.5}TiO_3$-$PbTiO_3$, BNT-PT) system is an important class of lead-free piezoelectric and ferroelectric materials, known for its complex phase behavior near the morphotropic phase boundary (MPB). This boundary is characterized by a rich interplay of structural phases, which can be finely tuned through variations in doping. Understanding the intricate domain structures in BNT-PT ceramics is crucial for optimizing their performance in applications such as sensors, actuators, and energy-harvesting devices.

In this study, we employ advanced microscopic techniques to investigate the structural states of BNT-PT ceramics across the MPB. Using piezoresponse force microscopy (PFM), we examine the domain structures and local electromechanical responses, revealing complex domain patterns and phase coexistence phenomena. Our analysis highlights how dopant concentration and thermal conditions influence the stability and transformation of these phases, leading to varied electrostrictive and piezoelectric responses. The results indicate that BNT-PT ceramics display a combination of polar and non-polar domains, with notable variations in domain size and arrangement depending on the PbTiO3 content. This study provides valuable insights into the domain dynamics and phase transitions in BNT-PT, offering a framework for tailoring material properties to enhance performance. By correlating microscopic observations with macroscopic measurements, we contribute to the fundamental understanding of lead-free piezoelectric materials and pave the way for the development of high-performance ceramics with specific functional attributes.

The equipment of the Ural Center for Shared Use "Modern nanotechnology" Ural Federal University (Reg.№ 2968) was used. The research was made possible by Russian Science Foundation (Project № 23-42-00116). This work was financially supported by the National Natural Science Foundation of China (Grant No. 52261135548).

1. J. Rodel, K.G. Webber, R. Dittmer, et al., *J. Euro. Ceram. Soc.* **35**, 1659 (2015).
2. D. Alikin, A. Abramov, A. Turygin, et al., *Small Methods* **6**, 2101289 (2022).
3. G. Arlt, P. Sasko, *J. Appl. Phys.* **51**, 4956 (1980).

Degradation of sensory elements induced by external potential

S.M. Baraishuk[1], I.A. Pavlovich[1], M. Murodov[2], Kh. Abdulkhaev[2]

[1]*Belarusian state agrarian technical university, 220012 Minsk, Belarus*
bear_s@rambler.ru

[2]*Namangan engineering-construction institute, 160100, Namangan, Uzbekistan*

Potentially induced degradation is the degradation of the silicon substrate or the functional layer of the sensor element formed on it, caused by the appearance of a potential difference between the substrate and the body under irradiation conditions in the visible and infrared range. This phenomenon has the greatest impact on IR sensors, lighting sensors and photocells, causing loss of efficiency of the latter due to the presence of leakage currents. This phenomenon affects the most common silicon-based solar panels. The degradation mechanism known as polarization in circuits having a positive voltage potential relative to ground was discussed in [1-4]. Structural failure is most common for crystalline silicon front junction (n–p) photoconverters, and develops most intensively when the modules are at a negative voltage relative to ground [5].

The decline in efficiency reaches 30% after 3 years of operation. The rate of degradation depends on the operating voltage of the system, humidity, and temperature of the elements. A special feature for photovoltaic panels is the occurrence of induced currents between the photovoltaic panels and the ground, which significantly increases the degradation of parts of the elements connected to the negative or grounded electrode (panel body). The PID phenomenon that occurs in modules with a negative polarity circuit can be completely avoided if the panel frame is made of dielectric, photo-thermal resistant materials with sufficient mechanical strength. There is also a known solution based on anodic grounding [6] to protect silicon wafers by shifting the electrochemical ground potential.

Unlike solar cells, the sensor area is much smaller, and it is necessary to control both the condition of the sensor layer itself and the condition of the substrate. There are several well-known methods for analyzing changes in the effectiveness of properties [7]. In our work, it was proposed to use thin films of molybdenum disilicide as layers of sensor elements, obtained by applying a metal coating accompanied by irradiation with ions of the same metal [8]. Ion bombardment during coating under ion-activated conditions provides mutual mixing at the metal/silicon interface [9]. This method of forming a coating on silicon is accompanied, among other things, by the formation of silicides and is of interest to researchers due to its potentially wide application in electronics. The developed and obtained thin films can find application in the creation of sensor micro-nanosystems for monitoring optical radiation, as well as in other sectors of the national economy, where the problem of converting optical parameters is extremely important and relevant.

In this work, coating-substrate structures were obtained containing molybdenum silicides, having a uniform distribution over the surface, high thermal stability of resistive properties (PID elements are up to 2.7 times smaller compared to other materials), with a wettability of 20^0, which is lower than that of the original substrates. Analysis of the results of hardness measurements showed that the hardness of the coatings themselves is 4.3 times higher than the hardness of the original silicon and is comparable to the hardness of diamond-like coatings and confirms the good strength characteristics of the resulting coatings. The results obtained show the possibility of forming an IR radiation sensor using a group method in the form of a chip cut from a silicon wafer with an increased service life.

1. S. Boulhidja, A. Mellit, S. Voswinckel, et al., *Energies* **13**, 537 (2020).
2. J. Hylsky, D. Strachala, P. Vyroubal, et al., *Microelectron. Reliab* **85**, 1218 (2018).
3. J. Bauer, V. Naumann, S. Grober, et al., *Phys. Status Solidi-Rapid Res. Lett.* **6**, 331 (2012).
4. W. Luo, et al., *Energy Environ. Scince* **10**, 43 (2017).
5. R.M. Swanson, M. Cudzinovic, et al., *Proc. 15th Int. Conf.*, 410 (2005).
6. S. Baraishuk, I. Pavlovich, M. Kakhotsky, *The Age of Science* **24**, (2020).
7. D. Brinkevich, V. Prosolovich, et al., *Pribory i metody izmereniy* 7, 1 (2016).
8. I. Tashlykov, P. Żukowski, et al., *Acta Physica Polonica A* **6**, 125 (2014).
9. S. Baraishuk, V. Gremenok, V. Tulev, *Phys. Chem. Mat. Process.* **1**, 66 (2011).

P70

On the thermal stability of polar state in the modified antimony sulphoiodide above the Curie point

D.V. Chirkova[1], I.V. Lisnevskaya[2]

[1]*Federal Research Centre the Southern Scientific Centre of the Russian Academy of Sciences, 344006, Rostov-on-Don, Russia*
sdanamail@list.ru

[2]*Southern Federal University, Chemistry department, 344015, Rostov-on-Don, Russia*

Antimony sulphoiodide (SbSI) is a material that is interesting both from a fundamental and applied point of view, as it combines ferroelectric, piezoelectric, electro–optical properties, and also, due to its needle structure, that caused high anisotropy of properties. Using synthesis in an aqueous medium, we obtained a number of antimony sulfoiodide samples doped with divalent tin (SbSI:Sn). They demonstrate an elevated phase transition temperature (T_c up to 35°C) in compare with pure SbSI, and a piezomodule d_{33} = 750 - 800 pC/N [1]. Studies of the longitudinal piezoelectric module d_{33} temperature stability above the Curie point were carried out on samples of textured ceramics. For a sample containing 5 mol.% of the dopant d_{33} gradually decreases when heated to temperatures of 90-100°C (Fig. 1). However, even after an 8-hour isothermal exposure of the sample at 90°C, the piezomodule retains a value of up to 80% of the original and depolarizes only after a long (24h) exposure at temperature above 100°C. The temperature dependences of the longitudinal piezomodule for samples with a lower Sn(II) content were of a similar nature, but depolarization in them occurred at lower temperatures. When comparing the XRD patterns of the SbSI:0.05Sn ceramic sample before and after thermal depolarization, no significant differences were found (Fig. 2). Additional structural and dielectric studies are required to clarify the state of the obtained materials above the Curie point.

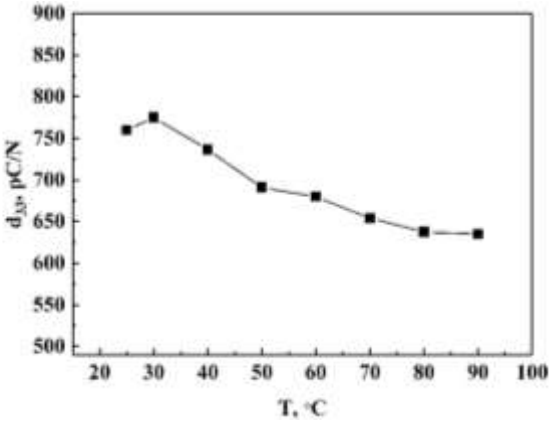

Figure 1. The temperature dependence of the longitudinal piezomodule for SbSI:0.05Sn texture.

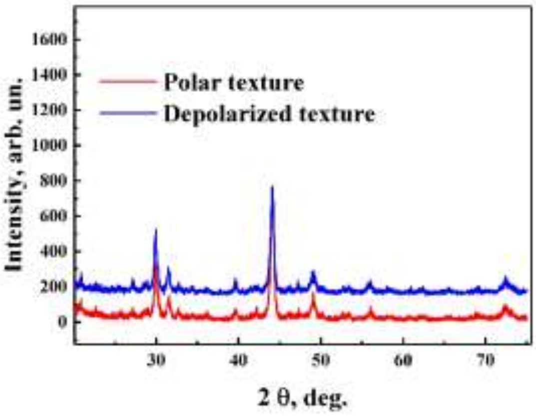

Figure 2. XRD patterns of SbSI:0.05Sn texture before and after thermal depolarization

The work was carried out within the framework of the SSC RAS state task (project number 122020100294-9).

1. D.V. Chirkova, I.V. Lisnevskaya, *Journal of Advanced Dielectrics*, 2350027 (2023).

P71

The effect of Mn_2O_3 modification on the dielectric characteristics of the binary $BiFeO_3$ - $BaTiO_3$ ceramics.

E.S. Esin, N.A. Boldyrev

Research Institute of Physics, Southern Federal University, 344090, Rostov-on-Don, Russia
esin@sfedu.ru

Currently great attention is paid to preparation and study of new materials based on multiferroics. Bismuth ferrite ($BiFeO_3$, BF) is a well-studied compound and representative of this class of materials with perovskite structure and high phase transition temperatures (Curie temperature, T_C = 1083 K, Neel temperature, T_N = 583 K)) [1]. However, the critical dependence of phase composition and characteristics on the synthesis conditions and high conductivity limit the wide application of BF [2]. One way of avoiding these limitations is introduction of modificator on the stage of synthesis. Previously we studied the binary system $(1-x)BiFeO_3$-$xBaTiO_3$ ($0.25 \leq x \leq 0.35$, $\Delta x = 0.05$). [3]. The aim of this work is establishment of regularities of influence of 1% Mn_2O_3 introduction on structure and dielectric characteristics of this binary ceramcis.

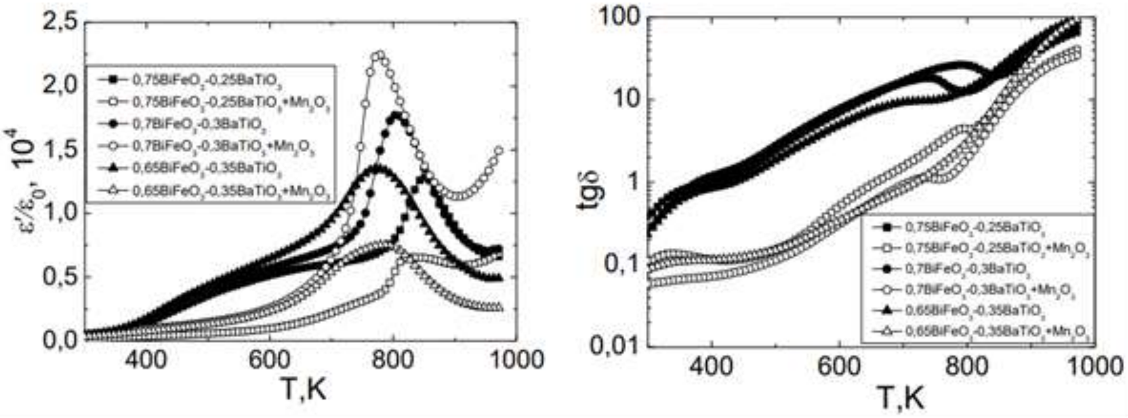

Figure 1. Temperature dependencies of $\varepsilon'/\varepsilon_0$ and tgδ. Black dots – pure solid solution, white – solid solution with Mn_2O_3.

X-ray diffraction study showed that Mn^{3+} is incorporated into the crystal lattice of studied ceramics. In this case, the cell parameters (x = 0.30, 0.35), ceramic density (x = 0.25, 0.35) increased. Figure 1 shows the $\varepsilon'/\varepsilon_0(T)$ and tg$\delta(T)$ dependencies. Modification have led to a shift of the Curie point to the low-temperature region and decrease of the maximum value of $\varepsilon'/\varepsilon_0$ (except for the case with x = 0.25). On the temperature dependences of pure ceramics in the temperature range (450÷700) K, anomalies were observed in the form of inflection points, which are most likely a consequence of the features of the real (defective) structure of the ceramics, leading to the appearance of Maxwell-Wagner polarization and relaxation. No anomalies are observed on similar dependencies in modified objects.

Obtained results indicate complex changes in the crystalline composition of the studied ceramics that associates with the incorporation of manganese cations into the B-position of the perovskite cell of the base compound.

The study was carried out with the financial support of the Ministry of Science and Higher Education of the Russian Federation (State task in the field of scientific activity. Project No. FENW-2023-0010/GZ0110/23-11-IF). with equipment of the Center for Collective Use "Electromagnetic, electromechanical and thermal properties of solids", Research Institute of Physics of the Southern Federal University.

1. P. Fischer, et al., *J. Phys. C: Solid State Phys.* **13**, 1931 (1980).
2. A.P. Pyatakov, A.K. Zvezdin, *Magnetoelectric and Multiferroic Media* **55**, 557 (2012).
3. N.A. Boldyrev, et al., *Bull. Russ. Acad. Sci.: Phys.* **11**, 1303 (2016).

P72

Inverse spin-Hall effect and structural phase transition in $Mn_xPt_{1-x}/Ni_{80}Fe_{20}$ bilayer

A.Kh. Kadikova[1], B.F. Gabbasov[1], I.V. Yanilkin[1], A.I. Gumarov[1], D.G. Zverev[1],
A.G. Kiyamov[1], L.R. Tagirov[1,2], R.V. Yusupov[1]

[1]*Institute of Physics, Kazan Federal University, Kazan, 420008, Russia*
anelyakadikova11@gmail.com

[2]*Zavoisky Physical-Technical Institute, FRC Kazan Scientic Center of RAS, Kazan 420029, Russia*

In the last 10-15 years, an interest to antiferromagnets in the spintronics has increased significantly. This is due to the discovery of the spin-charge transformation effects in them, such as the spin-Hall effects, spin Seebeck effect, and others. In particular, the spin-Hall effect is found in metallic antiferromagnets based on the Mn and a normal heavy metal. The use of such materials can be very promising in perpendicular spin valves for the implementation of "zero field switching" (ZFS), which is achieved utilizing simultaneously the effect of the exchange bias at the FM/AFM interface.

In this report, the inverse spin-Hall effect in epitaxial $Mn_xPt_{1-x}/Ni_{80}Fe_{20}$ bilayer systems was investigated. Ferromagnetic resonance (FMR) spectra were studied using the cavity-based technique. To minimize the contribution of the induction EMF during the experiment in the resonator, a compensating circuit was used. The spin-Hall angles for Mn_xPt_{1-x} layers with various compositions have been evaluated.

To achieve the effect of the exchange bias, the Mn_xPt_{1-x} layer needs to be in an antiferromagnetic state. This state is realized in the chemically-ordered $L1_0$-phase with the tetragonal symmetry. Therefore, a structural phase transition from the cubic A2-phase to the $L1_0$-phase of the Mn_xPt_{1-x} layer was studied. In particular, it has been established that a deposition of Mn_xPt_{1-x} by molecular beam epitaxy in ultrahigh vacuum at 300°C does not result in a formation of a homogeneous $L1_0$-phase in all heterostructures. The structural phase transition may be suppressed by defects in the Mn_xPt_{1-x} layer. It was found that Mn_xPt_{1-x} layers tend to have a low-symmetry type of the epitaxy on $Ni_{80}Fe_{20}$. After annealing, the low-symmetry $L1_0$-phase Mn_xPt_{1-x} structural domains relax to higher-symmetry configurations, forming a texture with the in-plane orientations of {001}, {110} and {100}.

P73

Temperature and field dependences of the dielectric permittivity and converse piezoelectric modulus of $PbFe_{1/2}Nb_{1/2}O_3$ and $PbSc_{1/2}Nb_{1/2}O_3$ ceramics

S.I. Kolosov[1], V.V. Titov[1], Shi Xue[2],G. Li[2], S.I.Raevskaya[1], E.A. Erofeeva[1],
M.A. Malitskaya[1], I.P. Raevski[1],

[1]Physics Research Institute and Faculty of Physics, Southern Federal University, 344090; Rostov-on-Don, Russia
rostov.tea@gmail.com

[2]Shanghai Institute of Ceramics, Chinese Academy of Sciences, 200050, Shanghai, China

Complex perovskites $PbB'_nB''_mO_3$ (m=1-n) are characterized by giant values of piezoelectric, dielectric, electrostrictive, pyroelectric and other responses, which is due to the presence of polar nanoregions, very sensitive to even a small external influence. The critical nature of the field dependence of the direct piezomodulus of (1-x)$Pb(Mg_{1/3}Nb_{2/3})O_3$–$x$$PbTiO_3$ (PMN-xPT) crystals was established earlier, which allows us to significantly increase the piezoelectric response by applying an electric field [1, 2]. In contrast to crystals, in PMN-xPT ceramics it has not yet been possible to achieve giant values of converse piezoelectric moduli for the direct piezoelectric effect even in highly textured samples [3]. At the same time, the values of piezoelectric moduli in the case of the converse piezoelectric effect d^*_{33} (hereinafter referred to as the converse piezoelectric moduli for short) in PMN-xPT, $PbFe_{1/2}Nb_{1/2}O_3$, $PbSc_{1/2}Nb_{1/2}O_3$, and soft multicomponent piezoelectric ceramics samples are comparable to those for PMN-xPT single crystals [4, 5]. This is due to the fact that, unlike conventional ferroelectrics, the contribution of microdomains and polar nanoblasts, as well as electrostriction, to the total value of d^*_{33} in ferroelectric-relaxors is large, so the $d^*_{33}(E)$ dependence is nonlinear and the converse piezoelectric modulus is usually much larger than the direct one, which is promising for practical application. It should be noted that the studies of the $d^*_{33}(E)$ dependences described in [4, 5] were carried out only at room temperature.

In this work, the temperature and field dependences of dielectric permittivity, differential and effective converse piezoelectric modulus d^*_{33} of conventional ferroelectric $PbFe_{1/2}Nb_{1/2}O_3$ and ferroelectric-relaxor $PbSc_{1/2}Nb_{1/2}O_3$ ceramic samples are studied in the temperature range 20-200°C in order to experimentally reveal the hypothesis about the critical nature of giant values of the converse piezoelectric modulus in the relaxor ceramics. The obtained results are compared with the data of similar studies of conventional and textured PMN-0.325PT ceramics [6].

This work was supported by the Russian Science Foundation under Grant 23-22-00194.

1. Z. Kutnjak, J. Petzelt, R. Blinc, *Nature* **441**, 956 (2006).
2. S.I. Raevskaya, A.S. Emelyanov, F.I. Savenko, et al., *Phys.Rev.B.* **76**, 11580R (2007).
3. J. Zeng, K. Zhao, W. Ruan, et al., *Appl. Phys. Lett.* **109**, 052905 (2016)
4. A.V. Turik., A.A. Yesis, L.A. Reznitchenko, *J. Phys.: Condens. Matter* **18**, 4839 (2006).
5. M. Otoničar, A. Bradeško, L. Fulanović, et al., *Adv. Funct. Mater*. **30**, 2006823 (2020).
6. I.P. Raevski, J. Zeng, K. Zhao, et al., *Ferroelectrics* (2024).

P74

Synaptic plasticity in nanocrystalline ZnO films for neuromorphic applications

K.A. Kozyumenko[1], R.V. Tominov[1,2], D.J.S. Rodriguez[1], Z.E. Vakulov[1], V.A. Smirnov[1,2]

[1] *Research Laboratory "Neuroelectronics and Memristive Nanomaterials", Institute of Nanotechnologies, Electronics and Electronic Equipment Engineering, Southern Federal University, 347922, Taganrog, Russia*
tominov@sfedu.ru

[2] *Department of Radioelectronics and Nanoelectronics, Institute of Nanotechnologies, Electronics and Electronic Equipment Engineering, Southern Federal University, 347922, Taganrog, Russia*

The development of technology has led to the era of artificial intelligence and machine learning. As the need for high-performance parallel computing increases, the von Neumann architecture is becoming increasingly inefficient for problems with noisy and unstructured data [1, 2]. One way to address this problem within a compact and energy-efficient platform is a neuromorphic system based on artificial neurons and synapses that has the potential to realize electronic perception and cognitive information processing [3]. One of the main ways of technical realization of neuromorphic systems is integrated circuits based on resistive RAM (ReRAM), which is based on the change of electrical resistance between low-resistance (LRS) and high-resistance (HRS) states. under the action of an external electric field. Resistive switching is observed in many metal oxide materials, but the analysis of literature data has shown that some of the most promising materials for the fabrication of ReRAM elements of neuromorphic systems are HfO_2, TiO_2, and ZnO [4]. It is important to precisely control the parameters of thin oxide films during the fabrication of memristors. There are several methods of thin oxide films fabrication, among which the method of pulsed laser deposition stands out, because it has a large set of technological parameters and allows to obtain films in a wide range of morphological and electrophysical properties. There are still many challenges to be overcome to create neuromorphic systems based on ReRAM cells, one of which is to investigate the amplitude and pulse width of the write voltage on the resistance of ZnO films.

Nanocrystalline zinc oxide films were obtained on the Si/TiN substrate by pulsed laser deposition at the Pioneer 180 unit (Neocera LCC, USA) under the following conditions: substrate temperature: 300°C, distance between the target and the plate: 40 mm, O_2 pressure: 1 mTorr, pulse energy: 350 mJ, laser-pulse repetition rate: 10 Hz, and number of laser pulses: 18 000. Electrical measurements were made using the Keithley 4200-SCS semiconductor measurement system (Keithley, USA). The top and bottom contacts were a tungsten probe and a TiN film, respectively.

Analysis of the experimental results obtained showed that increasing U_{SET} from 1 to 3 V at $t_{USET} = 3$ ms leads to a decrease in the resistances S1-S13 of the nanocrystalline ZnO film from $(1.16\pm0.43)\times10^6$ Ω to $(2.74\pm0.15)\times10^2$ Ω (Fig. 1a). It was also shown that increasing t_{USET} from 1 to 5 ms at U_{SET} = 3 V leads to a decrease in the resistance of the nanocrystalline ZnO film from $(1.67\pm0.17)\times10^6$ Ω to $(1.42\pm0.13)\times10^2$ Ω (Fig. 1b).

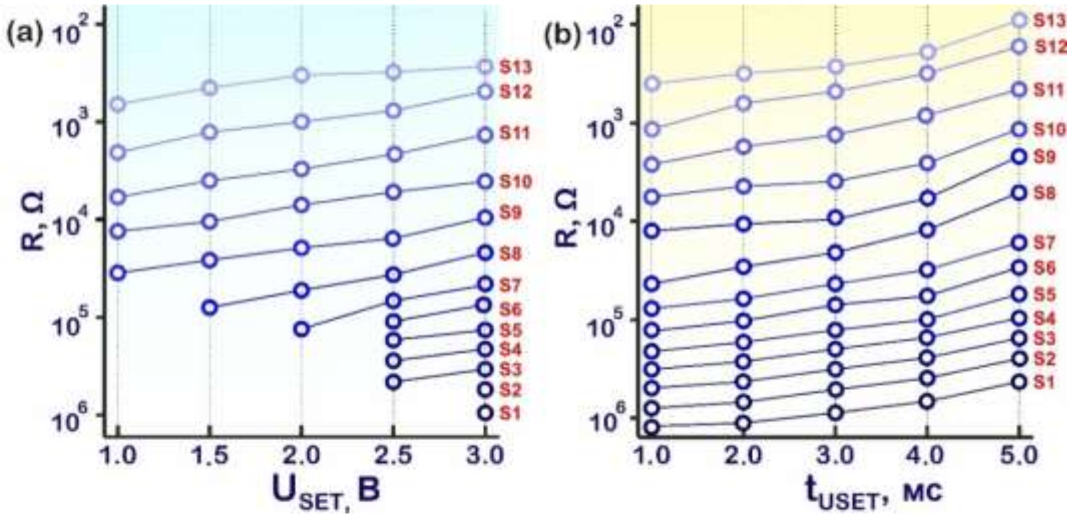

Figure 1. Dependence of the nanocrystalline ZnO film resistance in different states on: (a) U_{SET}; (b) t_{USET}.

The decrease in resistance of the ZnO film with increasing amplitude and pulse duration can be explained by additional Joule heat generation, which leads to an increase in the number of oxygen vacancies.

The study was funded by the Russian Science Foundation grant №. 23-79-10272, https://rscf.ru/project/23-79-10272/ at the Southern Federal University (regarding the growth of nanocrystalline zinc oxide films), as well as with the financial support of the Government of the Russian Federation (Agreement No. 075-15-2022-1123) (regarding electrical measurements of nanocrystalline zinc oxide films).

1. V.I. Avilov, R.V. Tominov, Z.E. Vakulov, et al., *Nano Research* **16**, 7 (2023).
2. R.V. Tominov, V.I. Avilov, Z.E. Vakulov, et al., *Adv. Electronic Materials* **8**, 2200215 (2022).
3. S.G. Stavrinides, I.P. Antoniades, J. Georgiou, et al., *Microelectronic Engineering* **216**, 111026 (2019).
4. X. Duan, Z.Cao, K. Gao, et al., *Adv. Materials* **1**, 2310704 (2024).
5. C. Prakash, L. R. Gupta, A. Mehta, et al., *Materials Advances* **4**, 5882 (2023).

P75

Combined experimental and theoretical study of cobalt-doped strontium titanate

A.I. Lebedev, I.A. Sluchinskaya

Lomonosov Moscow State University, 119991 Moscow, Russia
swan@scon155.phys.msu.ru

The search for new multiferroics is one of the actual problems of modern physics of the solid state. Strontium titanate $SrTiO_3$, which has long been the object of intense studies and various applications, can be considered as a potential material to solve this problem. It is known that the 3*d* doping elements in strontium titanate can have different oxidation states and substitute atoms at different lattice sites [1-6]. If these magnetic impurities become off-center, then $SrTiO_3$ can acquire the properties of a multiferroic, in which the ferroelectric and magnetic states coexist simultaneously and result in magnetoelectric interaction. The possibility of creating dipole moments when doping $SrTiO_3$ with 3*d* elements is quite possible if the impurity atom enters the *A* site of the perovskite structure and becomes off-center (the ionic radii of all 3*d* elements are noticeably smaller than that of Sr).

The position of an atom in the unit cell and its local environment can significantly affect the magnetic moment of an ion. In addition, atoms of 3*d* transition elements are characterized by the possibility of their existence in several oxidation states which depend on their atomic position, the local environment (an isolated atom or complexes with various defects), as well as on the presence of other donors and acceptors in the samples. For practical applications, it is necessary to be able to control the position and oxidation state of these impurities. To achieve this goal, synthesis under various conditions, deviation from stoichiometry, and additional doping with donor or acceptor impurities can be used.

The aim of this work is to experimentally and theoretically study the structure of the impurity complexes formed by Co atoms in $SrTiO_3$ samples synthesized under various conditions and in stoichiometric samples additionally doped with Nb. To solve the experimental part of this problem, the XAFS spectroscopy technique was used.

$SrTiO_3$ samples with an impurity concentration of 2–3% Co and various deviations from stoichiometry, as well as stoichiometric $SrTiO_3$ samples with Co concentration of 3% codoped with 6% Nb were prepared by solid-phase synthesis method in air and annealed at temperatures of 1100–1600°C. The quality of the samples was controlled by X-ray method. Fluorescence EXAFS and XANES spectra were recorded at the KMC-2 station of the BESSY synchrotron radiation source at the Co *K* edge (7.709 keV) at 300 K. The XAFS spectra were processed in a traditional way.

To select structural models when analyzing EXAFS spectra, the first-principles modeling of the local environment of impurities was used. Calculations of the geometry, magnetic and electronic structure of cobalt-containing impurity centers were carried out within the density functional theory using the ABINIT program in the LDA+*U* approximation on 80-atom cubic supercells, in which one of the Ti^{4+} ions at the *B* site or the Sr^{2+} ones at the *A* site is substituted by a cobalt ion. To change the oxidation state of Co, donor or acceptor impurities as well as the oxygen vacancies were introduced into the unit cell. These calculations were necessary to confirm the physical feasibility of the impurity complexes configurations found in the EXAFS data analysis, and to predict their other (magnetic, optical) physical properties for comparison with the available experimental data.

X-ray phase analysis of obtained samples showed that all studied samples of $SrTiO_3$(Co) and $SrTiO_3$(3%Co, 6%Nb) had a cubic perovskite structure at 300 K. All $SrTiO_3$(Co) samples were single-phase. Samples of the stoichiometric composition of $SrTiO_3$(3%Co, 6%Nb) annealed at 1500ºC were also single-phase, whereas in samples of the same composition annealed at 1100ºC, additional peaks were observed in their diffraction patterns.

Studies of the XANES and EXAFS spectra of synthesized samples showed that, depending on the preparation conditions, cobalt can enter both the *A* and *B* sites of the perovskite structure and can be in different oxidation states in them [3,4] (the oxidation state was determined from the shift of the X-ray absorption edge in XANES spectra). The redistribution of the impurity atoms between the two sites can be controlled by changing the stoichiometry and annealing temperature of the samples.

The experimentally found interatomic distances and oxidation states of Co impurities were compared with the results of calculations of the geometry and electronic structure of a number of Co-containing structural defects. Taking into account other properties of doped samples available in the literature, models that adequately describe the observed properties were proposed. Since cobalt ions have a non-zero magnetic moment according to the literature data, the structure of $\mathrm{Co}^{3+}{}_{\mathrm{Ti}}$ ions was interpreted as $\mathrm{Co}^{3+}{}_{\mathrm{Ti}}$ complexes with the nearest oxygen vacancies, which have a magnetic moment of $S = 1$ according to our calculations. The $\mathrm{Co}^{2+}{}_{\mathrm{Sr}}$ ions turned out to be off-center (Co is displaced by ~1.0 Å from the *A* site in the [100] direction) and are in a high-spin state ($S = 3/2$). Calculations of the electronic structure of various Co-containing defects show that the $\mathrm{Co}^{3+}{}_{B}$–V_{O} complexes as well as the $\mathrm{Co}^{2+}{}_{A}$ ions and the $\mathrm{Co}^{2+}{}_{B}$–V_{O} complexes can produce strong optical absorption which explains the intense color of the doped samples.

In stoichiometric $\mathrm{SrTiO_3}$(3%Co, 6%Nb) samples, regardless of the annealing temperature, the X-ray absorption edge shifts to the low-energy region, which indicates a change in the Co oxidation state to +2 induced by Nb donors. According to the EXAFS data, the impurity atoms are located at the Ti sites and remain on-center. A change in the oxidation state of Co in niobium-doped samples is accompanied by an increase in the distance between the impurity atom and the nearest oxygen atoms by ≈0.1 Å, which is consistent with the results of first-principles calculations. In this state, the magnetic moment of the impurity becomes equal to $S = 3/2$. The calculations predict also another configuration of the $\mathrm{Co}^{2+}{}_{B}$ impurity with $S = 1/2$ and a small Jahn-Teller distortion, but the energy of this configuration is 135 meV higher.

In summary, the performed studies show that the combination of XAFS spectroscopy with first-principles calculations makes it possible to obtain reliable information on the local structure and oxidation state of 3*d* elements in $\mathrm{SrTiO_3}$. Information about the influence of specific preparation conditions on the structure of defects in $\mathrm{SrTiO_3}$ can be used for targeted control of the properties of this material.

1. A. Tkach, P.M. Vilarinho, A.L. Kholkin, *Acta Materialia* **53**, 5061 (2005).
2. A.I. Lebedev, I.A. Sluchinskaya, A. Erko, et al., *JETP Lett.* **89**, 457 (2009).
3. I.A. Sluchinskaya, A.I. Lebedev, *Phys. Solid State* **61**, 390 (2019).
4. I.A. Sluchinskaya, A.I. Lebedev, *J. Alloys and Compounds* **820**, 153243 (2020).
5. I.A. Sluchinskaya, A.I. Lebedev, *Phys. Solid State* **64**, 345 (2022).
6. A.I. Lebedev, I.A. Sluchinskaya, *Ferroelectrics* **604**, 116 (2023).

P76

Leakage currents in two-layer heterostructures based on ferroelectrics with the tetragonal tungsten bronze structure

N.V. Makinyan[1,2], A.V. Pavlenko[1,2]

[1]*Federal Research Center The Southern Scientific Centre of the Russian Academy of Sciences, 344006, Rostov-on-Don, Russia*
norair.makinyan@yandex.ru

[2]*Research Institute of Physics, Southern Federal University, 344090, Rostov-on-Don, Russia*

With the development of electronic technology, there is an increase in requirements for the characteristics of functional materials used or planned to be used, in particular for leakage currents, which often determine the range of applicability of materials [1]. In ferroelectric materials made in the form of nanoscale films, almost all physical processes occurring under the influence of an external electric field are closely related to the influence of leakage currents, therefore, a detailed study of the latter is important both from a fundamental and applied points of view.

In this work, we studied leakage currents in two-layer structures combining layers n this work, we studied leakage currents in two-layer structures combining $Sr_xBa_{1-x}Nb_2O_6$ (SBN) and $Ba_2NdFeNb_4O_{15}$ (BNFNO) layers with the TF Analyzer 2000 E measuring system at a field voltage from -25 to 25 V (Fig. 1). Single-layer SBN and BNFNO thin films have been studied by us previously.

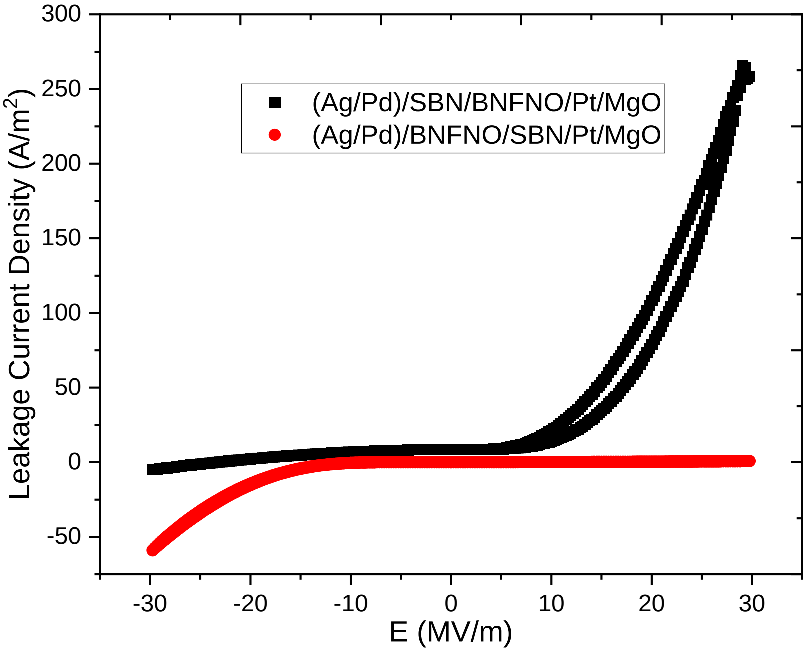

Figure 1. Leakage currents in two-layer heterostructures based on BNFNO and SBN.

After analyzing the obtained dependences, it was shown that the differences in the values of leakage current in bilayers are due both to different conduction mechanisms of SBN and BNFNO separately, and to the contribution of conductivity from the near-electrode region. This can be explained by the different values of the work function and, accordingly, by the different potential difference at the boundaries of the sections between the conductive and ferroelectric layers. The paper discusses the relationship of the observed differences with the actual structure of materials.

1. F.-C. Chiu, *Advances in Materials Science and Engineering* **2014**, 1-18 (2014).

P77

Development of magnet feedstock based on polymers and Nd-Fe-B magnetic powder for 4D additive manufacturing of magnetic devices

G.M. Vieira[1], R.L. Souza[2], B.L. Fertig[3], M.A. Rosa[3], P.A.P. Wendhausen[3], M.D. Martins[1]

[1]*Center for the development of the nuclear technology (CDTN), Belo Horizonte, Brazil*
mdm@cdtn.br

[2]*Universidade Federal dos Vales do Jequitinhonha e Mucuri (UFVJM), Janaúba, Brazil*

[3]*Universidade Federal de Santa Catarina (UFSC), Florianópolis, Brazil*

In recent years, new 3D printing techniques that include the application and manipulation of magnetic fields during the printing process of parts have emerged, and such technique has been named "4D printing" [1]. The localized application of magnetic fields during the manufacturing process of the component aligns the randomly dispersed magnetic particles within the material matrix according to the direction of the applied magnetic field [2]. Such technique allows for the production of materials that have applications in structural reinforcement, precision motors, magnetically controlled robots and many others [3]. Therefore, the present work aimed at obtaining a composite polymer-based magnetic material suitable for 4D-printing. Different composite formulations were obtained through the dispersion of commercial or recycled nanocrystalline Nd-Fe-B powders into a commercial non-rigid photopolymer resin. The recycled Nd-Fe-B powder were prepared by hydrogen processing: hydrogen decrepitation (HD) followed by hydrogenation disproportionation desorption recombination (HDDR) of end-of-life Nd-Fe-B magnets. An UV laser was adapted at the head of a FDM 3D printer, which allowed the production of samples and magnetic soft robots. During the printing process, magnetic field was applied to specific areas allowing to introduce magnetic anisotropy within the device (a schematic of the methodology can be seen in Figure 1a).

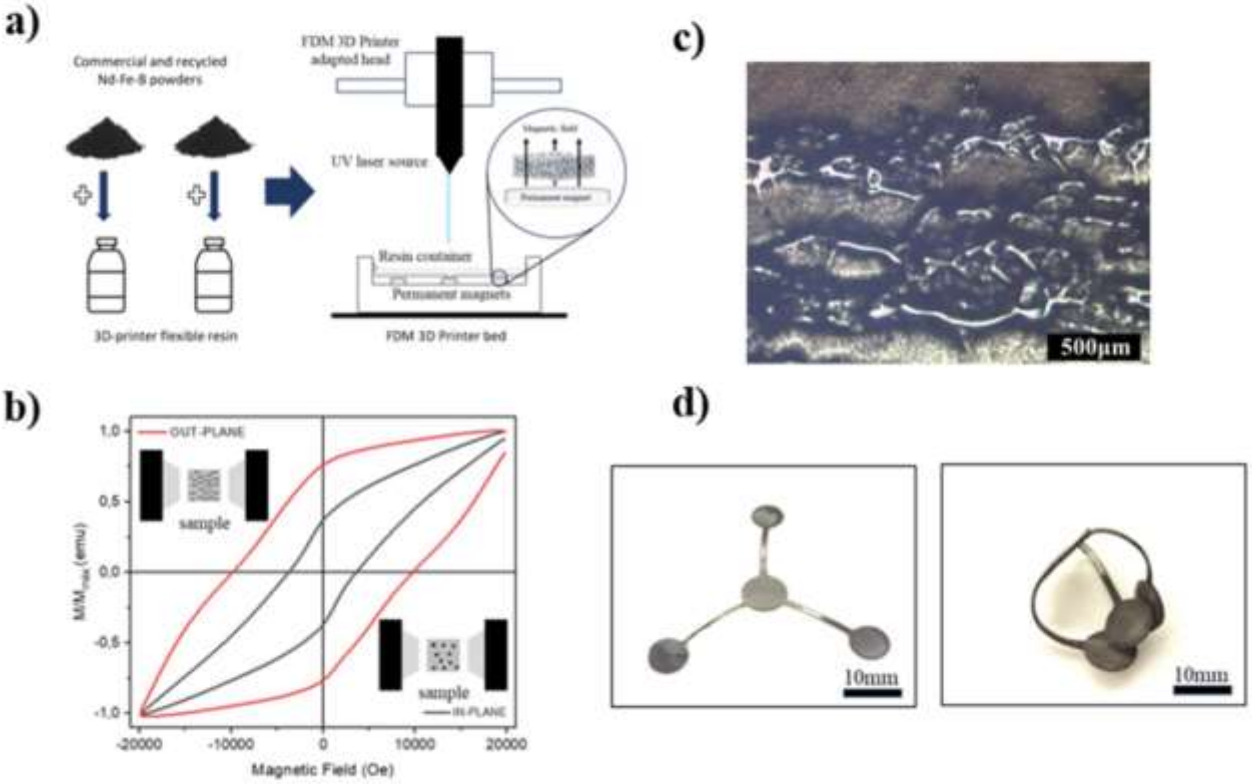

Figure 1. (a) Schematic illustrating the methodology employed for producing the bonded magnetic materials, (b) Hysteresis loops of bonded permanent magnet obtained with HDDR powder in directions parallel and perpendicular to the sample plane, (c) Nd-Fe-B chains aligned along the applied field during printing, (d) digital images of magnetic soft robot showing its ability to deform under magnetic field application.

The obtained materials were characterized by both open circuit magnetometry, using a vibrating-sample magnetometer (VSM). Figure 1b shows the M-H hysteresis loop of flexible photocurable resin blended with HDDR powder in an approximate volume ratio of 10%. The microstructure of the powders and robots was assessed via optical microscopy, scanning electron microscopy (SEM) and digital pictures. The composite materials showed attenuated magnetic properties compared to the powders, due to its dispersion in the polymeric resin. The induced magnetic anisotropy correlates with the alignment of Nd-Fe-B particles into chains in the direction of the magnetic field applied during the printing process, as seen in figure 1c. The soft magnetic robots proved to be responsive to magnetic fields and were able to be controlled to perform simple tasks (as seen in Figure 1d).

The authors acknowledge the financial support of Brazilian agencies CAPES, CNPq, FAPEMIG, and FINEP.

1. I. Cooperstein, E. Sachyani-Keneth, E. Shukrun-Farrell, et al., *Adv. Materials Interfaces* **22**, 1800996 (2018).
2. C. Zhang, X. Li, L. Jiang, et al., *Adv. Functional Materials* **31**, 2102777 (2021).
3. A. Ahmed, S. Arya, V. Gupta, et al., *Polymer* **228**, 123926 (2021).

P78

Electrophysical properties of ferroelectric ceramic materials based on the PZT system obtained by slip casting technology

A.A. Martynenko, A.A. Pavelko, L.A. Dykina, K.P. Andryushin,
E.V. Glazunova, A.V. Nagaenko, L.A. Reznichenko

Southern Federal University, 194, Stachki Ave., Rostov-on-Don, 344090, Russia
e-mail: alekmar@sfedu.ru

The search for new pyroelectric materials that have a set of parameters (minimum values of specific heat capacity, relative dielectric constant and dielectric losses in combination with a high pyroelectric coefficient) is an important task of modern physical materials science, the solution of which will improve the characteristics of existing pyroelectric detectors. Work on improving the quality characteristics of the IR receiver is also inextricably linked with reducing the thickness of the pyroelectric layer. Thus, making ceramics as thin as possible is one of the main technological tasks when creating detector materials. Based on the totality of parameters, the best pyroelectric materials, in most cases, are ferroelectrics; however, difficulties may arise on the way to their creation due to high technological requirements during their synthesis and sintering. A promising basis for pyroelectric materials are multicomponent solid solutions based on the $PbZrO_3$-$PbTiO_3$ (PZT) system, including relaxor components such as $PbNb_{2/3}Zn_{1/3}O_3$-$PbTiO_3$ [1-3] and $PbNb_{2/3}Mg_{1/3}O_3$-$PbTiO_3$ [4-7].

The objects of study were ceramic samples of solid solutions of the composition $PbTiO_3$-$PbZrO_3$-$PbW_{1/2}Mn_{1/2}O_3$-$PbNb_{2/3}Mn_{1/3}O_3$. The preparation of solid solutions was carried out by a two-stage solid-phase synthesis method. The selection of optimal technological modes was carried out on a series of experimental samples with x-ray control of the phase composition of the samples. The optimal synthesis modes were $T_{\text{sint1}} = 820°C$, $T_{\text{sint2}} = 850°C$, $\tau_{\text{sint1}} = \tau_{\text{sint2}} = 5$ hours. Mechanical activation (MA) of the synthesized solid solution powders was carried out at the stage of manufacturing press powders prepared for sintering. MA was carried out in a high-energy grinding planetary ball mill AGO-2 (Russia). Grinding was carried out in an alcohol medium for 15 minutes, the drum rotation speed was 1820 rpm.

In order to obtain pyroelectric materials with a thickness of about 100 microns, which have stable characteristics, we used the slip casting method, which consists in preparing a slip from the synthesized powder, which is a suspension of the material in a high-molecular 5% solution of rubber in mixtures of organic solvents (gasoline-acetone-toluene), taken in strictly defined proportions. In this case, the ratio of solid and liquid phases of the slip is 3:1. In addition, dispersants (organic acids) and plasticizers (esters of sebacic or phthalic acids) are introduced into the slip. The slip is prepared by mixing the components in a closed drum in a roller mill for at least 2...2.5 hours.

From the resulting slip, a film is cast using a squeegee method onto a moving conveyor belt. Cast and naturally dried film with a thickness of 0.08...0.2 mm is cut into pieces, calibrated and collected in bags, which are then rolled to achieve the required density and thickness. From the rolled film, blanks of experimental samples are formed in the form of thin disks with a diameter of 0.7 mm, which are then sintered at a temperature of 1150°C for 1.5 hours. To study the electrical properties of the resulting samples, electrodes were applied to opposite faces.

X-ray structural studies were carried out by powder diffraction on a DRON-3 diffractometer using CoKα radiation. The cell parameters were calculated using the standard method, the error in measuring the parameters was: $\Delta a = \Delta b = \Delta c = \pm 0.003$ Å, $\Delta V = \pm 0.05$ Å^3, where a, b, c are the cell parameters, V is the cell volume.

To study the microstructure of the samples, a JSM-6390L scanning electron microscope (Japan) with a microanalyzer system from Oxford Instruments (UK) was used. The resolution of the microscope was 1.2 nm at an accelerating voltage of 30 kV (image in secondary electrons), the accelerating voltage range was from 0.5 to 30 kV, the magnification was from ×10 to ×1000000, and the beam current was up to 200 nA.

The dielectric, piezoelectric and pyroelectric properties of the obtained samples were studied in a wide temperature range. The study of relative dielectric constant ($\varepsilon/\varepsilon_0$) and dielectric losses (tgδ) was carried out in the temperature ranges $T = 20...350°C$ and measuring signal frequencies $f = 20...10^6$ Hz on a specially designed stand, including a high-temperature furnace, an SRS PTC10 thermal controller with a sensor temperature PT-100, as well as an LCR meter Agilent E4980A. Piezoelectric characteristics were measured automatically on the same stand using a Keysight E4990A impedance meter; the resonance-antiresonance method was used to calculate the piezoelectric parameters [8]. To study the pyroresponse, various methods were used: quasi-static method, temperature wave method and radiation method [9-12].

As a result of the studies, it was shown that the resulting ceramic samples have exceptional pyroelectric properties, pyroelectric parameters pHW, pHW$\times\varepsilon_0/\varepsilon^T_{33}$ (pyroelectric detectivity) and pHW/$|d_{31}|$ (pyroelectric resistance to vibration interference) at room temperature are 3.3×10^{-4} C/($m^2\times$K), 1.0×10^{-6} C/($m^2\times$K) and 13.2×10^6 N/($m^2\times$K), respectively. Such excellent pyroelectric properties are maintained in the temperature range of 30...200°C, which makes this material promising from the point of view of practical applications.

The results of this work can be used in the future in the development of pyroelectric detectors used for remote measurement of the temperature of heated bodies, including moving ones (rolling mills, high-frequency furnaces for hardening or tempering steel; plastic production; food industry, etc.); for measuring power systems; control of overheating of rubbing parts, etc.); in protection systems (from fire, from intruders), which determines the relevance and significance of the results obtained in the work.

The study was supported by the Russian Science Foundation grant No. 23-12-00351, https://rscf.ru/project/23-12-00351/.

1. I.N. Andryushina, et al., *Ceram. Int.* **39**, 753 (2013).
2. I.N. Andryushina, et al., *Ceram. Int.* **39**, 1285 (2013).
3. I.N. Andryushina, et al., *Ceram. Int* .**39**, 2889 (2013).
4. I.N. Andryushina, et al., *Materials Sci. Eng.: B* **283**, 115804 (2022).
5. A. Pavelko, L. Shilkina, L. Reznichenko, *J. Adv. Dielectrics* **10**, 2060011 (2020).
6. A.A. Pavelko, *Bull. Russ. Acad. Sci.: Phys.* **78**, 802 (2014).
7. Y.N. Zakharov, et.al. *Ferroelectrics* **399**, 20 (2010).
8. *IEEE Standard on Piezoelectricity* ANSI/IEEE Std 176-1987, New-York, 1988.
9. R. Whatmore, *Dordrecht: Springer Netherlands*, 65-86 (2014).
10. L.E. Garn, E.J. Sharp, *J. Appl. Phys.* **53**, 8974 (1982).
11. L.E. Garn, E.J. Sharp, *J. Appl. Phys.* **53**, 8980 (1982).
12. A.G. Chynoweth, *J. Appl. Phys.* **27**, 78 (1956).

P79

Electrophysical properties of high-temperature ferroelectric solid solutions of the (1-x)$BiScO_3$-x$PbTiO_3$ system

A.A. Martynenko, A.A. Pavelko, E.V. Glazunova, L.A. Shilkina, L.A. Reznichenko

Southen Federal University, 194, Stachki Ave., Rostov-on-Don, 344090, Russia
alekmar@sfedu.ru

High-temperature piezoelectric ceramics are widely used in various industries, namely: structural health monitoring, non-destructive testing of new generation gas turbine engines, in internal combustion engines with high pressure injection systems, etc. [1,2]. Currently, widely used high-temperature piezoelectrics are ceramic solid solutions based on $PbZrTiO_3$ (PZT). The main advantages of these solid solutions are the high Curie temperature ($T_C \approx 360°C$) and high values of the piezoelectric modulus ($d_{33} \approx 350$ pC/N) near the morphotropic phase boundary, however, the maximum operating temperatures do not exceed 230°C, which significantly limits their use in devices operating at higher temperatures [3,4]. An alternative to these solid solutions can be high-temperature piezoelectric ceramics $BiScO_3$-$PbTiO_3$. This compound has been known for a long time, it has fairly good electrophysical properties and has a fairly high Curie temperature $T_C \geq 450°C$ [5], which exceeds the performance of PZT-based ceramics. The main disadvantage of this system is the difficulty of obtaining it, as well as the tendency to self-destruction [6]. However, solid solutions in a certain range of component concentrations can be synthesized using conventional ceramic technology, while possessing outstanding electrophysical properties.

This work is part of a study aimed at developing high-temperature piezoelectric materials based on the binary system of $(1-x)BiScO_3–xPbTiO_3$ solid solutions.

The research samples were solid solutions of ceramics with $x = 0.63, 0.64, 0.65, 0.7$. The solid solutions were prepared by two-stage solid-phase synthesis followed by sintering using conventional ceramic technology. The selection of optimal technological modes was carried out on a series of experimental samples with x-ray control of the phase composition and relative density ($\rho_{rel.}$) of the samples. The optimal synthesis modes were $T_{synt1} = 800°C$; $T_{synt2} = 900°C$; $\tau_{synt1} = \tau_{synt2} = 4$ hours. Optimal sintering modes - $T_{sint.} = 1050°C$-1150°C (depending on composition), sintering time $\tau_{sint.} = 2$ hours. Also, during the manufacturing process, before synthesis, the method of mechanical activation of powders was used, but this had virtually no effect.

The work addresses the issues of obtaining and comprehensive study of the crystal structure, grain structure, dielectric and piezoelectric properties of ceramic samples of solid solutions of the $(1-x)BiScO_3–xPbTiO_3$ system with $x = 60...70\%$.

The research was carried out with the financial support of the Ministry of Science and Higher Education of the Russian Federation (State assignment in the field of scientific activity 2023). Project No. FENW-2023-0010/ (GZ0110/23-11-IF).

1. D. Darnjanovic, *Curr. Opin. Solid State Mater. Sci.* **3**, 469 (1998).
2. F. James, S.A. Tressler, R.E. Newnham, *J. Electroceram.* **2**, 257 (1998).
3. I.N. Andryushina, L.A. Reznichenko, V.A. Alyoshin, et al., *Ceram. Int*. **39**, 753 (2013).
4. Y. Dong, Z. Zhou, R. Liang, et al., *J. Am. Ceram. Soc*. **105**, 1558 (2022).
5. R.E. Eitel, C.A. Randall, T.R. Shrout, et.al., *Jpn. J. Appl. Phys.* **40**, 5999 (2001).
6. A.A. Belik, M. Azuma, T. Saito, et.al., *Chem. Mater.* **17**, 269 (2005).

P80

Microwave absorption properties of multicomponent solid solutions based on lead zirconate titanate

A.S. Masliaev[1], P. A. Astafev[2], K. P. Andryushin[2], A. A. Pavelko[2]

[1]*Department of Physics, Southern Federal University, Rostov-on-Don, 344006, Russia*

[2]*Research Institute of Physics, Southern Federal University, Rostov-on-Don, 344090, Russia*
l.6.e.9.w.4.a.9.p@yandex.ru

Multicomponent solid solution (SS) systems based on the lead zirconate titanate $PbZrO_3$–$PbTiO_3$ (PZT) have higher efficiency and manufacturability compared to simple systems and can significantly expand the possibilities of choosing materials with a given combination of parameters [1, 2]. This is possible due to the presence of complex morphotropic regions (MO) in many compositions, in which extreme values of electrical and piezoelectric properties are observed. One of such systems is PZT–PZN–PMN [3, 4], designed for low-frequency applications. The complex domain structure and phase composition of such materials, in addition to enhancing the electrical characteristics at low frequencies, can lead to increased microwave losses.

In this regard, the purpose of this study was to establish the patterns of formation of a high level of microwave losses in the SS of system PZT–PZN–PMN modified with Ba and Sr.

The objects of the study were the SS of system PZT–PZN–PMN, modified Ba and Sr, corresponding to the chemical formula $(Pb_{1-\alpha_1-\alpha_2}Sr_{\alpha_1}Ba_{\alpha_1})[Ti_xZr_y\langle(Nb_{2/3}Zn_{1/3})(Nb_{2/3}Mg_{1/3})\rangle_{1-x-y}]O_3$, where α_1=0.02÷0.12; α_2=0.0036÷0.073; x=0.385÷0.430; y=0.402÷0.447 [5]. The materials were obtained by two-stage solid-phase synthesis followed by sintering using conventional ceramic technology. The samples are made in the form of cylinders with a diameter of 10 mm and a height of 1 mm.

Radiophysical measurements were performed using a P9375A “Keysight” vector network analyzer (USA, California), which has an operating frequency range of 300 kHz – 26.5 GHz, and a measuring cell, which is a straight section of a microstrip line. The dissipation coefficient of electromagnetic wave energy by a sample, including radiation losses and ohmic losses in the samples under study, was calculated according to [6, 7]. The main parameter characterizing microwave losses in the materials under study was the loaded quality factor of the resonant maxima, calculated by the formula $Q_i = \frac{f_{max}}{\Delta f}$, where Δf is the width of the maximum at half the power level [8].

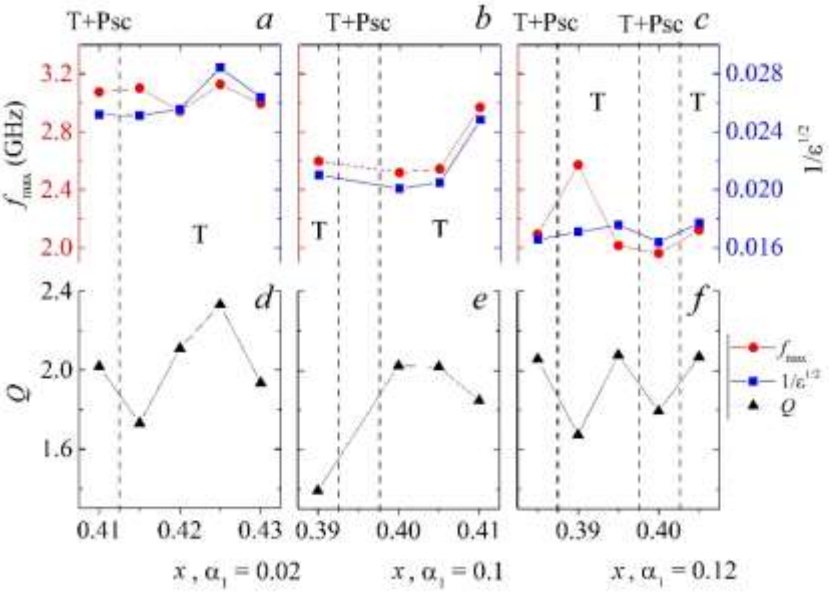

Figure 1. Dependences of the frequency of the first resonant maxima, the inverse root of the dielectric constant at low frequency and the quality factor of the first resonant maxima on the molar fraction of Ti.

The position of the first resonant maxima correlates with the value of the inverse root of the dielectric constant at low frequencies (Fig. 1a,b,c), which indicates the identity of the dielectric constant ratios of the materials under study at high frequencies, in the vicinity of 2-3.2 GHz. In this case, compositions with α_1=0.02 have on average the lowest values of dielectric constant in the specified frequency range among all materials studied in this work, and compositions with α_1=0.12 have the highest. The highest level of losses is achieved in the regions of coexistence of the tetragonal and pseudocubic phases, as evidenced by a decrease in the quality factor of the resonant maxima (Fig. 1d,e,f).

The study was carried out with the financial support of the Ministry of Science and Higher Education of the Russian Federation (State task in the field of scientific activity in 2023). Project No. FENW-2023-0010/(GZ0110/23-11-IF).

1. C.-H. Wang, et al. *Jap. J. Appl. Phys.* **42**, L595 (2003).
2. M. Kobune, Y. Tomoyoshi, A. Mineshige, et al., *J. Ceram. Soc. Jap.* **108**, 633 (2000).
3. R. Muanghlua, S. Niemchareon, W.C. Vittayakorn, et al., *Adv. Mater. Res.* **55**, 125 (2008).
4. J.S. Han, C.W. Gal, J.M. Park, et al., *J. Manufacturing Processes* **28**, 235 (2017).
5. K.P. Andryushin, et al., *Ceram. Int.al* **45**, 16855 (2019).
6. D. Micheli, C. Apollo, R. Pastore, et al., *Composites Science and Technology* **70**, 400 (2010).
7. Z. Wang, G.-L. Zhao, *J. Materials Chemistry C* **2**, 9406 (2014).
8. D. Kajfez, P. Guillon, *Dielectric Resonators* (Artech House, Norwood, 1986).

P81

Nanostructure and ferroelectric properties of multilayer heterostructures based on SBN and BNFNO materials

Ya.Yu. Matyash[1], A.V. Pavlenko[1,2]

[1]*Federal Research Centre the Southern Scientific Centre of the Russian Academy of Sciences, 344006, Rostov-on-Don, Russia*
matyash.ya.yu@gmail.com

[2]*Research Institute of Physics of Southern Federal University, 344090, Rostov-on-Don, Russia*

Among materials with a tetragonal tungsten bronze structure, barium strontium niobate (SBN) and barium neodymium ferroniobate (BNFNO) are of particular interest. BNFNO is a promising compound for use in microelectronics and shows interesting multiferroic and dielectric properties [1, 2]. The ability to control the magnetoelectric effect in multiferroics is of great fundamental and applied importance. Therefore, single-layer and multilayer thin films of ferroelectrics and multiferroics are important objects of research. In that paper features of the topography and local ferroelectric properties of a four-layer heterostructure and a two-layer heterostructure, obtained by RF-cathode sputtering, are considered.

The results of studying the samples topography with a total thickness of ~720 nm are presented in Figure 1. For a four-layer heterostructure, the surface is represented by large blocks, which in-plane have the shape of polygons with clear sharp edges. The average size of growth blocks is 122 nm (Fig. 1a), the surface roughness is 10.8 nm. In a two-layer heterostructure, elongated branched regions are observed, forming “ridges” against the background of homogeneous regions of smaller height. The roughness and average crystallite size for the two-layer heterostructure were 14.91 nm and 203 nm (Fig. 1b), respectively. For samples, studies of switching processes and relaxation of regions induced by applied voltage were carried out using piezoresponse force microscopy. During the polarization process, a “box-in-box” structure is formed on the heterostructures surface by applying positive and negative voltages. As a result, stable regions with different directions of polarization (toward and away from the substrate) were created, which indicates the ferroelectric nature of the samples. In the case of a four-layer heterostructure, after 48 minutes, polarized regions are clearly visualized in vertical piezoresponse scans. The vertical piezoresponse magnitude remained virtually unchanged for the entire induced structure. The vertical piezoresponse of the heterostructure unpolarized part has positive values, which may indicate the polarization vector direction from the film to the substrate. The piezoresponse of a two-layer film is less than the piezoresponse of a four-layer heterostructure. For a two-layer heterostructure, there is an asymmetry in the magnitude of the piezoresponse signal for positively and negatively polarized regions, which may indicate spontaneous polarization. It should be noted that the relaxation of induced regions in a two-layer heterostructure occurs faster than in a four-layer heterostructure.

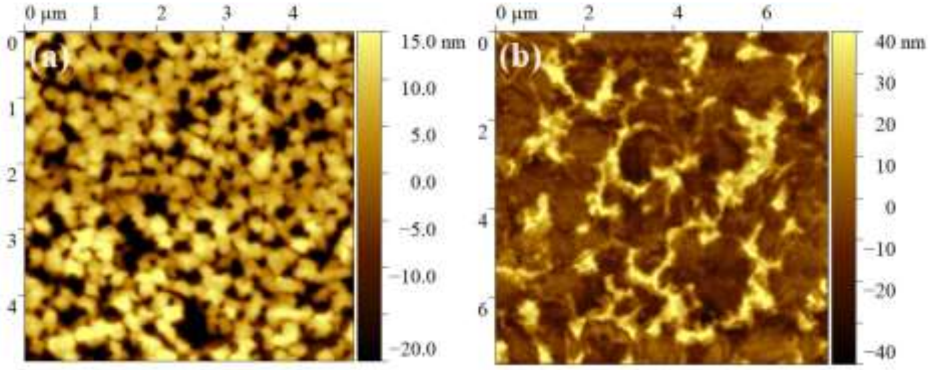

Figure 1. Topography of SBN60/BNFNO/SBN60/BNFNO/SRO/MgO (a) and SBN60/BNFNO/SRO/MgO (b) heterostructues.

This work was financially supported by the Russian Science Foundation [project No. 21-72-10180].

1. M. Josse, O. Bidault, F. Roulland, et al., *Solid State Sciences* **11**, 1118 (2009).
2. T. Hajlaoui, C. Chabanier, C. Harnagea, et al., *Scripta Materialia* **136**, 1 (2017).

P82

Features of the nanostructure and ferroelectric properties of multilayer films based on materials with the tetragonal tungsten bronze structure

Ya.Yu. Matyash[1], A.V. Pavlenko[1,2], D.V. Stryukov[1]

[1]*Federal Research Centre the Southern Scientific Centre of the Russian Academy of Sciences, 344006, Rostov-on-Don, Russia*
matyash.ya.yu@gmail.com

[2]*Research Institute of Physics of Southern Federal University, 344090, Rostov-on-Don, Russia*

During the high pace of development of functional microelectronics and optoelectronics, single-layer and multilayer thin films of multiferroics and ferroelectrics are becoming high-demand. Using these materials in the form of thin-film structures on dielectric or semiconductor substrates, it becomes possible to control the properties of such a structure due to the deformation that occurs in the thin layer [1, 2]. Some of the most interesting representatives of multiferroics and ferroelectrics are materials with the tetragonal tungsten bronze (TTB) structure [3], in particular $Sr_{0.4}Ba_{0.6}Nb_2O_6$ (SBN60) and $Ba_2NdFeNb_4O_{15}$ (BNFNO).

The topography and local ferroelectric properties of the heterostructure were studied using an atomic force microscope "Ntegra Academia". Using an NS15/50 cantilever in semi-contact mode, the relief of surface areas 4 μm^2 in size was scanned. Using a conductive cantilever NSG01/Pt, two rectangular areas were polarized on the surface of the heterostructures with a voltage of ±10 V. After this, the relaxation of voltage-induced areas was studied in the Kelvin mode using a two-pass technique.

The results of studying the surface morphology showed that the heterostructure with a thickness of 720 nm is characterized by roughness values of 10.5 nm (less than 1.5% of the total thickness). The sample surface is represented by large interconnected growth blocks, the size of which varies from 200 to 380 nm, which indicates the island growth mechanism of Volmer-Weber films.

As can be seen from Figure 1, polarization of the heterostructure in the contact mode did not lead to a change in the surface topography of SBN60/BNFNO/SBN60/BNFNO/SRO/MgO. However, voltage-induced regions of different polarization directions are clearly visualized in surface potential scans. A relaxation study of the surface potential signal from polarized regions in the Kelvin mode showed that the polarized states in the heterostructure are stable for 60 min, and after 80 min they begin to "spread" and after 120 min there are practically no traces of polarization. In addition, the surface potential of the unpolarized part of the heterostructure had positive values, which may indicate spontaneous polarization of the films.

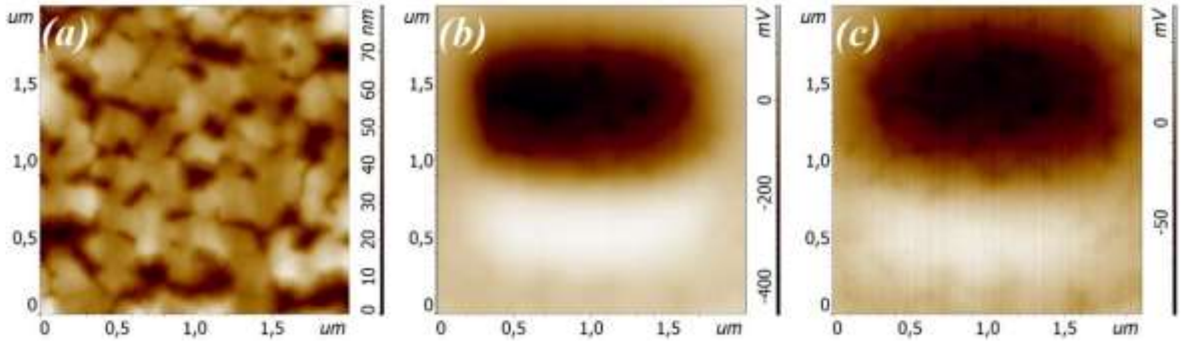

Figure 1. Topography (a) and surface potential of a four-layer heterostructure obtained immediately after polarization (b) and 80 minutes after polarization (c).

The work was carried out within the framework of the state assignment (topic number of state registration 122020100294-9) of the South Scientific Center of the Russian Academy of Sciences.

1. P.E. Janolin, *J. Mater. Sci.* **44**, 5025 (2009).
2. J. Haeni, et al., *Nature* **430**, 758 (2004).
3. X. Zhu, et al., *Chem. Mater.* **27**, 3250 (2015).

P83

Physical properties and sintering features of high temperature piezoelectric ceramics $0.36BiScO_3$-$0.64PbTiO_3$

P.A. Pankratiev[1], E.G. Guk[1], E.P. Smirnova[1], A.V. Sotnikov[1,2], V.N. Klimov[3],
N.V. Zaitseva[1], E.E. Mukhin[1]

[1]*Ioffe Institute,* ***194021****, Saint-Petersburg, Russia*
pavel-pankratiev@yandex.ru
[2]*Emperor Alexander I St. Petersburg State Transport University (PGUPS), 190031, Saint- Petersburg, Russia*
[3]*Central Research Institute of Structural Materials Prometey, National Research Centre Kurchatov Institute, 191015, Saint-Petersburg, Russia*

The manufacturing process of ferroelectric ceramics significantly affects its properties. Thus, production technology of such materials is constantly being developed, modified and discussed in numerous publications. Conventional ceramics technique involves calcination, pressing and final one-step high temperature sintering. A new method of two - step sintering of ceramics was proposed [1]. It involves heating of samples to a high temperature T_1 for a short time t_1, rapid cooling to a lower temperature T_2 and subsequent long sintering at temperature T_2 for a time $t_2 >> t_1$. New sintering technique allowed to control the growth of ceramic grains, i.e. to form high density samples. This technique is widely used in the manufacture of piezoelectric ceramics with improved material parameters, such as piezoelectric constant d_{33}. The temperature decrease from T_1 to T_2 is carried out with forced rapid cooling, at a rate of 20-30°C/min that requires complex equipment, which makes its use difficult.

In this study, a modified two-step sintering technology is proposed to produce ceramics without forced cooling from the first stage to a lower temperature second step. The effect of cooling conditions between two sintering steps on piezoelectric constants was investigated. High temperature piezoelectric ceramics $0.36BiScO_3$-$0.64PbTiO_3$ (BSPT) was synthesized by the modified technique, for comparison, with the conventional one. Structural, dielectric and piezoelectric properties of the resulting ceramics were studied. It is shown that regardless of technology ceramics has a tetragonal phase (P4mm) and the composition is close to the morphotropic phase boundary. Ceramics produced by modified technique possesses high density (97% of the theoretical value and the average grain sizes are within the 0.8-1.0 μm, in contrast to 7-10 μm for one-step sintering samples. The temperature dependences of BSPT dielectric properties fabricated by both techniques were studied. Curie temperature T_c varied from 450°C to 440°C for piezoceramics produced by conventional technique and by two- step sintering, respectively. Regardless of the production technology, a rapid increase of the loss tangent at temperatures above 300°C, which narrows the operating temperature range of ceramic temperatures, is observed. Poling of the samples was carried out in silicon oil as follows: electric field E = 4 kV/mm, temperature 115°C (30 minutes), then the samples were cooled down to 40°C under the same field for several hours. Piezoelectric and elastic properties were measured using the resonance impedance spectroscopy by a PSM1735 frequency response analyzer with an impedance interface, according to the IEEE (1987) standard. The obtained parameters are summarized in the Table below.

Sintering technique	$tg\delta$	$\varepsilon_{33}^T/\varepsilon_0$	s_{11}^E, 10^{-12} m^2/N	s_{33}^E, 10^{-12} m^2/N	d_{33} pC/N	$-d_{31}$ pC/N	k_p	k_{33}^t	Q_m
Conventional	0.032	905	17.35	13	350	70	0.34	0.46	67
Two step	0.028	1379	17.08	8.6	525	111	0.48	0.42	30

The proposed method demonstrates the possibility and advantages of manufacturing BSPT piezoceramics by a simplified two-step sintering technique with natural cooling from temperature T_1 to T_2 instead of forced cooling. The proposed modified method of two - step sintering may be successfully applied for the production of piezoelectric ceramics of other compositions.

1. I.W. Chen, X.H. Wang, *Nature* **404**, 168 (2000).

P84

Fabrication and properties of STO thin films grown by RF sputtering in an oxygen atmosphere

A.V. Pavlenko[1,2], D.V. Stryukov[1]

[1]*Federal Research Centre the Southern Scientific Centre of the Russian Academy of Sciences, 344006, Rostov-on-Don, Russia*
Antvpr@mail.ru

[2]*Research Institute of Physics of Southern Federal University, 344090, Rostov-on-Don, Russia*

Ferroelectrics in the form of ceramics, single crystals and thin films are widely used in modern technology, from sensors for various purposes to complex elements of microelectromechanical systems.

Among the materials intensively studied in recent years, quantum ferroelectrics based on $SrTiO_3$ (STO) can be distinguished [1].

This work is devoted to establishing the formation principles of phase composition and crystal structure of STO thin films grown on Al_2O_3 single-crystal substrates.

For this purpose, $SrTiO_3$ heteroepitaxial pure films ~120 nm thick on an Al_2O_3(001) substrate were obtained by RF cathode sputtering. When studying heterostructures using X-ray diffraction analysis, only bright reflections related to the STO film and the Al_2O_3(001) substrate were detected. No traces of impurity phases were found. In the θ-2θ X-ray pattern (Fig. 1), in normal scattering geometry for the STO film, only reflections of the $(hhh)_c$ family are detected, which indicates the orientation of the $[111]_c$ axis along the normal to the substrate surface ([001]Al_2O_3 axis).

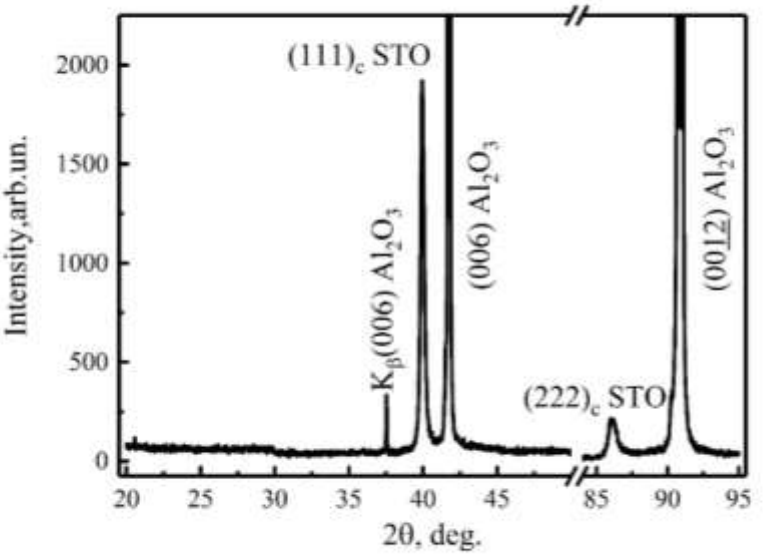

Figure 1. θ-2θ X-ray pattern of STO/Al_2O_3(001) thin film in normal scattering geometry.

It was revealed that the $SrTiO_3$ unit cells, as in the bulk material, have cubic symmetry, its deformation is insignificant and does not exceed 0.2%. These unit cells are oriented in such a way that the [111] axis of $SrTiO_3$ is parallel to the [001] axis of the substrate, the $[1\text{-}10]_c$ axis of $SrTiO_3$ is rotated relative to the [100] axis of the substrate by 30°.

The work was carried out within the framework of the state assignment (topic number of state registration 122020100294-9) of the South Scientific Center of the Russian Academy of Sciences.

1. V.A. Gritsenko, D.R. Islamov, *Physics of dielectric films: mechanisms of charge transport and physical basis of memory devices* (Parallel, Novosibirsk), 351 (2017) [in Russian].

P85

Dielectric characteristics of multilayer heterostructures based on SBN thin films

A.V. Pavlenko[1,2]

[1]*Federal Research Center Southern Scientific Center, Russian Academy of Sciences, 344006 Rostov-on-Don, Russia*

[2]*Scientific Research Institute of Physics, Southern Federal University, 344090 Rostov-on-Don, Russia*
Antvpr@mail.ru

Thin films of ferroelectrics and multiferroics with a tetragonal tungsten bronze structure have been studied quite intensively in recent years, due to the prospects for their use in electronics. Among them there are barium strontium niobate ($Sr_xBa_{1-x}Nb_2O_6$, SBN) and barium neodymium ferroniobate ($Ba_2NdFeNb_4O_{15}$, BNFN). The fabrication of multilayer heterostructures based on these materials can make it possible, on the one hand, to combine the advantages of each material separately, and on the other, to realize new combinations of their properties. The studying of the dielectric properties of such heterostructures in a wide temperature range is the aim of this work.

For this purpose, a four-layer BNFN/SBN/BNFN/SBN heterostructure on an SRO/MgO(001) substrate with BNFN and SBN layer thicknesses of about 200 nm was fabricated by RF cathode sputtering using intermittent deposition technology. According to X-ray diffraction data, it was established that all layers in the heterostructure were grown epitaxial and pure. Figure 1 shows the temperature-frequency dependences of the relative dielectric constant (ε) and loss tangent (tgδ) of the heterostructure.

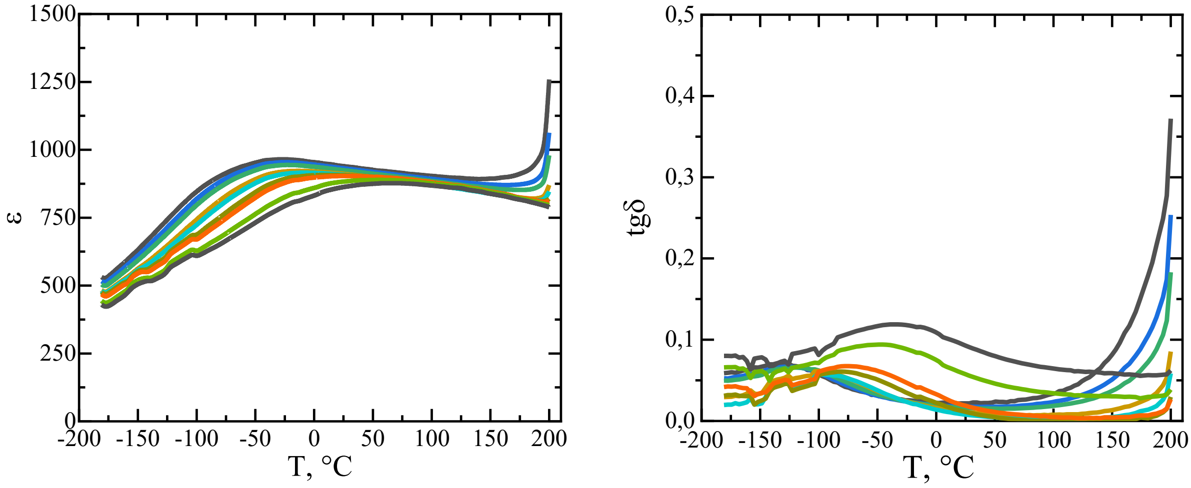

Figure 1. $\varepsilon(T)$ and tgδ dependencies for BNFN/SBN/BNFN/SBN/SRO(001)/MgO(001) heterostructures at 200-10^6 Hz.

The studied SBN composition is a ferroelectric-relaxor, and BNFN is a ferroelectric with a diffuse phase transition. In the multilayer structure it is seen that there are all the signs of relaxor-like behavior (dielectric relaxation of the non-Debye type in the $\varepsilon(f)$ and tg$\delta(f)$ dependencies, fulfillment of the Vogel-Fulcher law for the $T_m(f)$ dependency), but the transition region was more blurred. The reasons for the identified patterns and their differences from single-layer BNFN and SBN films of the same thickness are discussed.

The work was carried out within the framework of the state assignment of the SSC RAS project No. 122020100294-9. The equipment of the Center for Collective Use of the SSC RAS was used.

P86

Complex electromechanical characteristics of ceramic matrix composites

A.N. Rybyanets[1], N.A. Shvetsova[1], I.A. Shvetsov[1], E.I. Petrova[1], N.A. Kolpacheva[2]

[1]*Southern Federal University, 344090, Rostov-on-Don, Russia*
arybyanets@gmail.com

[2]*Don State Technical University, 344000, Rostov-on-Don, Russia*

Over the past years, considerable advances have been made to improve the mechanical properties of ceramics using ceramic matrix composite (CMC) approaches. Numerous technologies based on incorporation of functional ceramics into structural ones and vice-versa have been developed, and a novel design idea have applied in the field of functional ferroelectric ceramics [1]. However, the problem of property trade-off, i.e., the deterioration of electromechanical properties, remains unsolved. In the last few years, new design concepts and ceramic compositions for composites have been developed in the field of functional CMC. The main problem in developing piezoactive CMC is the compromise between mechanical and functional properties, in particular the deterioration of such important parameters as piezoelectric and electromechanical characteristics.

This paper presents the results of experimental study of the concentration dependences of the complex electromechanical characteristics of CMC fabricated using a previously developed method [2]. CMC was fabricated by joint sintering of synthesized piezoceramic powder (PZT matrix) of the composition $PbTi_{0.41}Zr_{0.49}Nb_{0.057}Zn_{0.0235}W_{0.006}Mn_{0.011}O_3$ (C-1) and crushed particles of sintered piezoceramics (PZT filler) of the composition $Pb_{0.95}Sr_{0.05}(Zr_{0.53}Ti_{0.47})O_3$ + 1% Nb_2O_5 (C-2) was chosen as the object of the study. The filler particles size was equal to 50 – 250 μm at a concentration of 0 – 60 vol%.

The density of the samples was measured using the hydrostatic weighing method, as well as by measuring the weight and volume of the sample The CMC samples were made in the shape of disks 20 mm in diameter and 1 mm thick. Electrodes were deposited on the main surfaces of the CMC by firing a silver paste. CMC samples were polarized in air by applying a constant electric field (~1 kV/mm) to the electrodes at a temperature above the Curie point with cooling under the field to room temperature.

Complex dielectric characteristics of CMC elements were measured on standard samples using an Agilent 4294A impedance analyzer and the Piezoelectric Resonance Analysis Program (PRAP). Analysis of experimental piezoresonance spectra of the thickness and radial vibrational modes of disk samples made it possible to obtain dependences of complex elastic, dielectric and electromechanical parameters of CMC on the volume concentration and size of filler particles.

Analysis of obtained concentration dependences showed that the real and imaginary parts of complex electromechanical characteristics of CMC exhibits anomalous behavior typical for percolation transitions in heterogeneous media. We have shown that the additional porosity of the ceramic matrix resulting from sintering of the CMC masks the elastic, dielectric, and electromechanical percolation transitions occurring at the volume concentrations of filler particles close to percolation thresholds (V~ 1/2 and V ~ 1/3).

The study was financially supported by the Russian Science Foundation Grant No. 24-22-00063, https://rscf.ru/project/24-22-00063/ at the Southern Federal University.

1. A.N. Rybyanets, A.A. Rybyanets, *IEEE Trans. UFFC*. **58**, 1757 (2011).
2. A.N. Rybyanets, I.A. Shvetsov, E.I. Petrova, et al., *Ferroelectrics* **605**, 88 (2023).

P87

Size effect of the piezoelectric properties, crystal structure and memristive effect in $BiFeO_3$ thin films

V.A. Safina[1], A.S. Abramov[1], E.D. Greshnyakov[1], V.Ya. Shur[1], A.V. Pavlenko[2], D.O. Alikin[1]

[1]*Ural Federal University, 620002, Ekaterinburg, Russia*
v.a.safina@urfu.ru

[2]*Research Institute of Physics SFU, 344090, Rostov-on-Don, Russia*

$BiFeO_3$ (BFO) is unique material known for its high spontaneous polarization and antiferromagnetic behavior at room temperature [1,2]. BFO thin films exhibit a pronounced memristive effect, with a significant increase in conductivity following activation by a DC bias [3]. This makes them an ideal candidate for ferroelectric memory and memcomputing devices that require electrical and magnetic writing and reading capabilities. However, producing ultra-thin epitaxial BFO films that retain ferroelectric properties is challenging due to phase instability and high leakage currents.

Here, we used the method of the radio-frequency sputtering in an oxygen atmosphere to produce hetero-epitaxial bismuth ferrite thin films. We studied size effect of the piezoelectric properties, crystal structure and memristive effect employing combination of the angle-resolved Raman spectroscopy and quantitative piezoresponse force microscopy. Large enhancement of the coercive fields in the film with the thickness below 10 nm has been found, while nevertheless film retained ferroelectric properties and rhombohedral structural symmetry. Despite of the evident reduction of the polarization, polarization reversal and associated memristive effect can be easily detected, which make BFO film promising for the polarization-controlled memristive devices.

The research funding from the Ministry of Science and Higher Education of the Russian Federation (Ural Federal University Program of Development within the Priority-2030 Program) is gratefully acknowledged. The equipment of the Ural Center for Shared Use “Modern nanotechnology” Ural Federal University (Reg.№ 2968) was used.

1. G. Catalan, J.F. Scott, Adv. Mat. **21**, 2463 (2009).
2. S. Fujino et al., Appl. Phys. Lett. **92**, 202904 (2008).
3. A. Chen et al. Adv. Funct. Mater. **30**, 2000664 (2020).

P88

Composite polyvinylcarbazole films with zinc oxide nanoparticles formed by the Langmuir–Blodgett method

D.V. Sapsaliou, G.B. Melnikova, M.I. Douhal, T.N. Tolstaya, S.A. Chizhik

A.V. Luikov Heat and Mass Transfer Institute of the National Academy of Sciences of Belarus, 220072, Minsk, Republic of Belarus

dsapsalev@list.ru

The design of portable, cost-effective, technologically advanced devices based on polymers and their composites often requires their preparation in the form of thin nanostructured coatings. The Langmuir–Blodgett (LB) method makes it possible to controllably obtain nanometer-thick coatings on planar substrates [1, 2].

LB films of poly(9-vinylcarbazole) (PVK, Sigma-Aldrich, average M = 1,100,000) were formed from its solution in chloroform with a concentration of 0,75 mg/ml. In order to obtain films with a more developed surface, zinc oxide nanoparticles (ZnO NPs, SigmaAldrich, d < 100 nm) were introduced into the composition of polymer coatings. The mole content of NPs in suspensions for the formation of coatings was of $1{,}13 \cdot 10^3$; $2{,}26 \cdot 10^3$; $4{,}53 \cdot 10^3$; $9{,}05 \cdot 10^3$; $18{,}11 \cdot 10^3$ (per 1 mole of PVK). The surface structures of the formed coatings was investigated by atomic force microscopy (AFM, NT-206, ALC “Microtestmaschines”, Republic of Belarus) using silicon cantilevers, according to [3].

Based on the analysis of PVK compression isotherms, the optimal surface pressure (π) for the formation of LB coatings was established. It was 15 mN/m, which corresponds to the middle of the linear section of the compression isotherm, corresponding to the “solid crystal” phase state. The dense packing of PVK macromolecules in a monolayer at a given π is also confirmed by a decrease in the compressibility (k) of the monolayer from 0,0208 (section π = 1,8–4,6 mN/m) to 0,0148 (π = 5,0–10,4 mN/m) and 0,0122 (π = 10,8–18,4 mN/m). According to AFM data, the release of the LB coating of PVK at π = 15 mN/m leads to the formation of a dense, homogeneous coating with a small number of defects (Fig. 1).

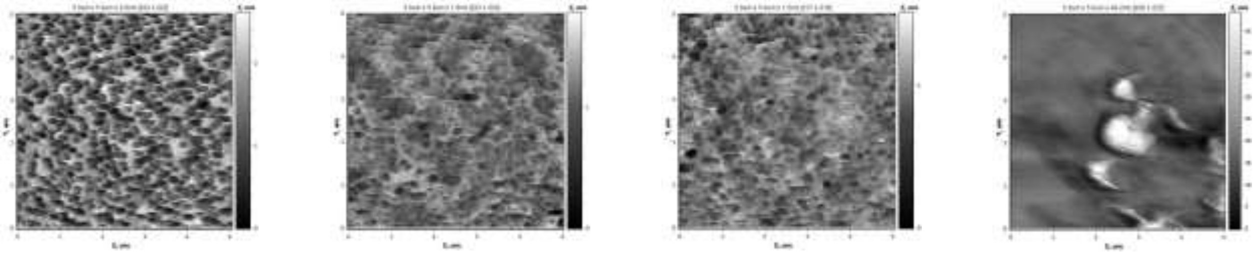

a *b* *c* *d*

Figure 1. Structure of PVK film (a) and nanocomposite coatings PVK–ZnO NPs ($1{,}13 \cdot 10^3$ – (b); $4{,}53 \cdot 10^3$ – (c); $9{,}05 \cdot 10^3$ – (d) mole of NPs per 1 mole of PVK), formed by the LB method at π = 15 mN/m.

It has been established that the optimal content of zinc oxide NPs in the working suspension for the formation of coatings is up to $4{,}53 \cdot 10^3$ mole. An increase in the content of zinc oxide leads to the formation of large conglomerates of both elongated and spherical shapes (Fig. 1, *b*–*d*).

Thus, the optimal conditions for the formation of PVK-based LB films were established: concentration of PVK in solution/suspension is of 0,75 mg/ml; π = 15 mN/m; ZnO NPs content up to $4{,}53 \cdot 10^3$ mole (per 1 mole of PVK). An increase in the NPs content is accompanied by the formation of large conglomerates, which is associated with the aggregative instability of suspensions.

The investigation was performed within the Programs of State Research "Energy and Nuclear Processes and Technologies", subprogram 1.2. "Energy Processes and Technologies", pr. 2.25, 2021–2025 yrs.

1. A. Shakeel, K. Rizwan, U. Farooq, et al., *Chemosphere* **303**, 134923 (2022).
2. S. Choudhury, V. Saxena, S.K. Gupta, et al., *Thin Solid Films* **493**, 267 (2005).
3. D.V. Sapsaliou, G.B. Melnikova, T.N. Tolstaya, et al., *Butlerov Commun.* **72**, 131 (2022) (Russian).

P89

Composite polyvinylcarbazole coatings with silicon dioxide nanoparticles formed by spin-coating method

D.V. Sapsaliou, G.B. Melnikova, T.N. Tolstaya, S.A. Chizhik

A.V. Luikov Heat and Mass Transfer Institute of the National Academy of Sciences of Belarus, 220072, Minsk, Republic of Belarus
dsapsalev@list.ru

Polyvinylcarbazole (PVK) and its nanocomposites are of interest for various fields of science and technology (photonics, optoelectronics, sensors, etc.). The creation of technological devices based on polymers often requires the production of thin functional coatings. Spin-coating is an easy-to-implement and cost-effective method for forming polymer and nanocomposite coatings [1, 2].

Poly(9-vinylcarbazole) (Sigma-Aldrich, average M = 1,100,000) coatings were formed by spin-coating method on the pre-hydrophilized silicon substrates from its solutions in chloroform with concentrations of 0,03125–1 mg/ml according to the [3]. Nanocomposite coatings were obtained by introducing SiO_2 nanoparticles (NPs) into the polymer structure. For this purpose, a solution of PVK (c = 0,125 mg/ml) was mixed with a suspension of SiO_2 NPs (Sigma-Aldrich, d = 10–20 nm) in chloroform. The content of nanoparticles in suspensions for the formation of coatings was of $73{,}3 \cdot 10^3$; $146{,}7 \cdot 10^3$; $293{,}3 \cdot 10^3$; $586{,}7 \cdot 10^3$ (per 1 mole of PVK). The surface structures of the formed coatings was investigated by atomic force microscopy (AFM, NT-206, “Microtestmaschines”, Republic of Belarus) using silicon cantilevers, according to [3].

Based on the AFM data, it was found that the most dense, homogeneous coatings are formed by spin-coating from a solution with a polymer concentration of 0,0625 mg/ml (Fig. 1a). It has been shown that the PVK–SiO_2 NPs nanocomposites have a homogeneous structure with uniformly distributed conglomerates of nanoparticles when the content of SiO_2 NP is up to $293{,}3 \cdot 10^3$ mole. The nanoroughness values of nanocomposites increase with increasing NPs content in the coating composition and are of R_a = 0,55 nm, R_q = 0,73 nm (PVK0,0625 mg/ml); R_a = 0,58 nm, R_q = 0,81 nm ($73{,}3 \cdot 10^3$ mole SiO_2) and R_a = 0,77 nm, R_q = 1,16 nm ($586{,}7 \cdot 10^3$ mole SiO_2), respectively. An increase in the SiO_2 NPs content above $293{,}3 \cdot 10^3$ mole leads to the formation of large conglomerates of both spherical and irregular shapes (Fig. 1b–d).

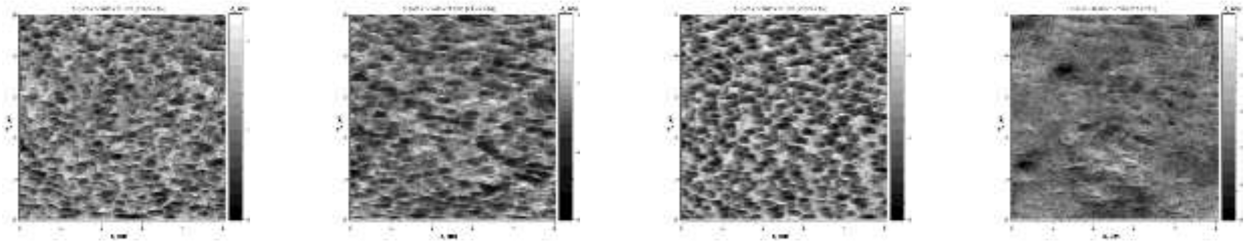

a *b* *c* *d*

Figure 1. (a) Structure of PVK films (c = 0,0625 mg/ml) and PVK–SiO_2 NPs nanocomposites ($73{,}3 \cdot 10^3$ – (b); $293{,}3 \cdot 10^3$ – (c); $586{,}7 \cdot 10^3$ – (d) (mole per 1 mole of PVK)) formed by spin-coating method

Thus, as a result of the work, the optimal concentration of PVK in the solution for the formation of dense, uniform coatings was established – 0,0625 mg/ml. It has been shown that the spin-coating method can be successfully used to obtain composite coatings based on PVK with SiO_2 nanoparticles. Optimal content of SiO_2 NPs in the working suspension for the formation of coatings up to $293{,}3 \cdot 10^3$ mole per 1 mole of PVK.

The investigation was performed within the Programs of State Research "Energy and Nuclear Processes and Technologies", subprogram 1.2. "Energy Processes and Technologies", pr. 2.25, 2021–2025 yrs.

1. P.D’Angelo, M. Barra, A. Cassinese, et al., *Solid-State Electronics* **51**, 123 (2007).
2. R. Das, A. Chanda, *Fabrication and Properties of Spin-Coated Polymer Films*, 283 (2016).
3. D.V. Sapsaliou, G.B. Melnikova, V.A. Lapitskaya, et al., *J. Belarus. State University. Chem.* **2**, 36 (2021) (Russian).

P90

Recrystallization of the perovskite phase in spherulitic films of lead zirconate titanate

S.V. Senkevich[1,2], D.A. Kiselev[3], A.S. Elshin[4], A.R. Valeeva[1,4]

[1]*Ioffe Institute, 194021, St. Petersburg, Russia*
SenkevichSV@mail.ioffe.ru

[2]*Herzen State Pedagogical University of Russia, 191186, St. Petersburg, Russia*

[3]*National University of Science and Technology «MISiS», 119049, Moscow, Russia*

[4]*Russian Technological University MIREA*

Previously, a number of studies have investigated the features of crystallization (recrystallization) of the perovskite phase and the physical properties of thin films of lead zirconate titanate (PZT), characterized by an ring spherulite microstructure [1]. Recently, studies have been carried out on spherulites with a radially radiant microstructure, characterized by a rotation of the crystal lattice caused by the action of tensile mechanical stresses that are formed due to differences in phase densities during crystallization of the perovskite phase [2]. In the work, the effect of recrystallization of the perovskite phase in radially radiant thin PZT films on their physical properties was studied.

PZT films were deposited onto platinized substrates by RF magnetron sputtering at low temperature and then annealed at high temperature to crystallize the perovskite phase. The composition of the films corresponded to the region of the morphotropic phase boundary with the elemental ratio Zr/Ti=54/46. Crystallization of the perovskite phase occurred through the nucleation and growth of spherulites. During the spherulite growth, two phase transitions were sequentially observed: low-temperature pyrochlore phase - perovskite phase (I) and perovskite phase (I) - perovskite phase (II), which were accompanied by an increase in the density of the thin film.

Phase transformations were studied using an EVO-40 scanning electron microscope (Zeiss) (microstructure, growth orientation, phase state and composition of the formed films), atomic force microscopes MFP-3D SA (Asylum Research) and Ntegra Prima (NT-MDT) (morphology surfaces, normal and lateral piezoelectric responses (Fig. 1a), surface potential (Fig. 1b)) and nonlinear optical confocal microscope alpha 300 (WiTec) (local second harmonic optical response (Fig. 1c)). It is shown that radially radiant microstructure is a result of recrystallization of perovskite phase.

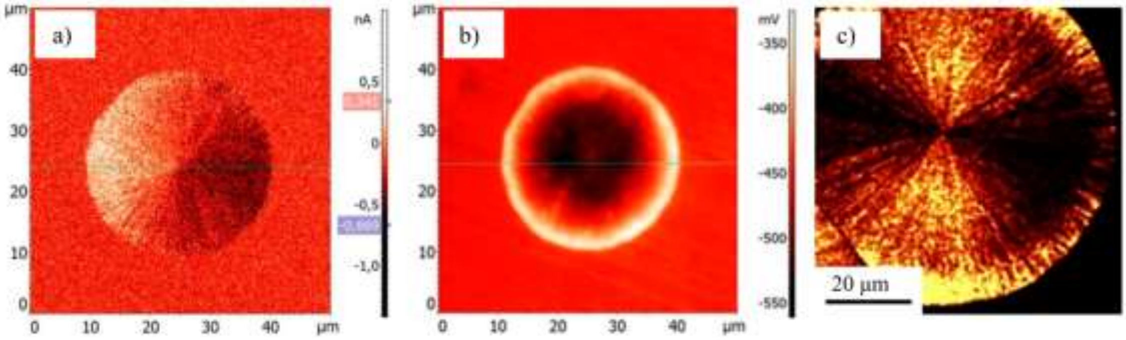

Figure 1. Second optical harmonic response (a), lateral piezoelectric response (b) and surface potential (c) of peroskite spherulite island in a pyrochlore matrix.

The work was carried out using the equipment of the shared core facilities Modern physical and chemical methods of formation and research of materials for the needs of industry, science and education of the Herzen University.

The research was supported by a grant from the Russian Science Foundation 23-72-01110.

1. I.P. Pronin, E.Yu. Kaptelov, S.V. Senkevich, et al., *Phys. Solid State* **52**, 132 (2010).
2. A.S. Elshin, M.V. Staritsyn, I.P. Pronin, et al., *Coatings* **13**, 247 (2023).

P91

Microstructure, complex electromechanical parameters and dispersion characteristic of porous piezoceramics

I.A. Shvetsov[1], N.A. Shvetsova[1], N.A. Kolpacheva[2], B.M. Lagutin[3], A.N. Rybyanets[1]

[1]*Southern Federal University, 344090, Rostov-on-Don, Russia*
arybyanets@gmail.com

[2]*Don State Technical University, 344000, Rostov-on-Don, Russia*

[3]*Rostov State Transport University, 344038, Rostov-on-Don, Russia*

Porous ceramics are heterogeneous media with unique microstructures that provide original, effective properties on which many different applications are based. In particular, porous ceramics combine general characteristics associated with the geometry and topology of porous microstructures with the characteristic properties of ceramics as a specific class of materials. Porous piezoceramics based on different piezoceramic compositions are widely used now in ultrasonic transducers and sensors for various technical applications. Recently, new family of porous ceramics based on ferroelectrically hard PZT compositions with properties combining better parameters of PZT ceramics and 1-3 composites for high intensity ultrasonic applications are developed [1]. However, despite lengthy studies, many aspects of the relationship between the microstructure peculiarities and electromechanical parameters of porous piezoceramics are still unclear.

This paper presents the results of an experimental study of the microstructure peculiarities, complex electromechanical parameters and their frequency dependences for PZT-type hard piezoelectric ceramics of the composition $PbTi_{0.41}Zr_{0.49}Nb_{0.057}Zn_{0.023}W_{0.008}Mn_{0.012}O_3$ + 0.1 m% GeO_2 with different relative porosity in the range of 0 - 30 % and average pore size of 10 - 20 μm. The complex elastic, dielectric, and electromechanical parameters of the piezoceramics elements were measured at radial and thickness extensional modes of standard piezoceramic discs using impedance analyzer Agilent 4294A (Agilent Technologies, USA) and the PRAP software. To study the frequency dependences of the complex parameters of experimental samples in the range from 2 up to 20 MHz we used the method of analysis of piezoelectric resonance spectra at the fundamental frequency and higher-order resonances of thickness extensional modes. Microstructural studies were performed on chipped surfaces of porous piezoceramics samples using the scanning electron microscopes (JEOL JSM-6390LA).

As the result of SEM microstructure analysis, it was found that the following microstructural features of porous piezoceramics define the dielectric, piezoelectric and electromechanical properties of porous piezoelectric ceramics: branched flexible three-dimensional piezoceramics skeleton and quasi-rod piezoceramics structure in the direction of residual polarization of porous piezoceramics. The regions of elastic and electromechanical dispersion, characterized by anomalies in the frequency dependences of the imaginary and real parts of the complex constants of porous piezoceramics were found. It was revealed that the anomalous dispersion of the elastic properties of porous piezoceramics is due to its microstructural features, namely, the presence of a rigid three-dimensional piezoceramic structure and a quasi-rod structure. A change in the ratio of the wavelength of resonant oscillations and the scale of the spatial inhomogeneity of the porous microstructure with increasing frequency leads to an increase in the contribution of the quasi-rod structure to the effective parameters of the porous piezoceramics.

The study was financially supported by the Russian Science Foundation Grant No. 24-22-00063, https://rscf.ru/project/24-22-00063/ at the Southern Federal University.

1. I.A. Shvetsov, E.I. Petrova, M.A. Lugovaya, et al., *Advanced Materials* (NY: Springer Proceedings in Physics), 33 (2018).

P92

Ferroelectric hysteresis and switching process in relaxor type PZT piezoceramics

I.A. Shvetsov[1], N.A. Shvetsova[1], B.M. Lagutin[2], A.N. Rybyanets[1]

[1]*Southern Federal University, 344090, Rostov-on-Don, Russia*
arybyanets@gmail.com

[2]*Rostov State Transport University, 344038, Rostov-on-Don, Russia*

Relaxor ferroelectrics form a peculiar class of ferroelectric materials [1]. The relaxor ferroelectrics show the abnormal behavior as compared to normal ferroelectrics in terms of dielectric, piezoelectric, ferroelectric properties and, subsequently, receive much attention by the scientific community. One of the basic properties distinguishing a relaxor ferroelectrics is a slim/constricted ferroelectric hysteresis loop caused by the presence of nanosized and randomly oriented polar islands known as polar nanoregions. Like conventional ferroelectrics, relaxor ferroelectrics show permanent dipole moment in domains. However, these domains are on the nano-length scale, unlike conventional ferroelectrics domains that are generally on the micro-length scale, and take less energy to align. Consequently, relaxor ferroelectrics have very high specific capacitance and attract thus generated interest in the fields of energy storage. Furthermore, due to their slim hysteresis curve with high-saturated polarization and low remnant polarization, relaxor ferroelectrics have high discharge energy density and high discharge rates.

This paper presents the results of a study of the switching behavior of five-component relaxor piezoceramics of the composition $Pb_{0.96}Sr_{0.04}Zr_{0.042}Ti_{0.435}W_{0.052}Mg_{0.052}Sb_{0.0426}Li_{0.0142}O_3$. This composition has relaxor properties when in a depolarized state and exhibits classical ferroelectric properties in a polarized state. In the phase diagram of concentration states, the studied composition belongs to the tetragonal boundary of the morphotropic region and characterized by a low coercive field E_C (0.9 kV/mm measured at 50 Hz). Polarized and nonpolarized discs of porous and dense piezoceramics (diam. 10 mm and thickness 1 mm) were used for the experiments. Piezoceramic elements were polarized in air by applying to silver electrodes dc electric field (~1 kV/cm) at heating above Curie temperature (~290°C) and cooling to a room temperature. The initial polarization of the piezoceramics leads to a shift in the hysteresis (P-E) loop and distortion of the deformation (S-E) loop, but allows one to analyze and determine the main parameters of the switching processes. Ferroelectric polarization and strain loops were recorded at the bipolar electric fields in the range of 0-5 kV/mm and in the frequency range of 0.001-5 Hz using a sinusoidal waveform. Measurements and analysis were performed by means of the Electromechanical Measurement System (STEPHV) and Electromechanical Response Characterization Program (STEP) from TASI Technical software Inc., combining large signal modelling of the mechanical and electrical behavior of ferroelectric materials.

Analysis of ferroelectric hysteresis and strain loops under application of bipolar ac field by means of STEP made it possible to obtain full set of parameters characterizing the switching behavior of the relaxor piezoceramics below the freezing temperature and clear the effect of measuring frequency on the D-E and S-E responses of relaxor piezoceramics. As a result of the study, it was found that the coercive field, remnant and saturation displacement, area of hysteresis loops and relative strain values are strongly dependent on frequency. It was attributed to the features of the nanopolar domain structure of the relaxor piezoceramics. The obtained experimental results can be used in the design of ferroelectric materials for piezoelectric sensor, actuator, energy harvesting, and ultrasonic transducer applications.

The study was financially supported by the Russian Science Foundation grant No. 22-11-00302, https://rscf.ru/project/22-11-00302/ at the Southern Federal University.

1. A.A. Bokov, Z.-G. Ye, *J. Mater. Sci.* **55**, 16451 (2020).

P93

Electromechanical hysteresis and relaxation in PZT piezoceramics in low electric fields

N.A. Shvetsova, I.A. Shvetsov, A.N. Reznichenko, M.A. Lugovaya, A.N. Rybyanets

Southern Federal University, 344090, Rostov-on-Don, Russia
arybyanets@gmail.com

The study of polarization reversal and domain-orientation processes in ferroelectric ceramics under the influence of a dc electric field is important both for the characterization of materials and for development of ultrasonic transducers, piezoelectric sensors and actuators with a stable and predictable response [1]. One of the consequences of domain switching in ferroelectrics is the occurrence of ferroelectric hysteresis. With the exception of memory device applications that rely on polarization switching and hysteretic polarization-electric field relationships, hysteresis is undesirable in high-precision sensors, actuators, and capacitors. The consequence of the irreversible component of this movement is a nonlinear and hysteretic piezoelectric response even at relatively low external electric fields and pressures. Understanding the mechanisms of electromechanical and ferroelectric hysteresis is an important and complex task from both practical and theoretical points of view. In previous paper [2], we proposed a new method for studying relaxation and transient processes in ferroelectric ceramics under the influence of low dc electric fields based on the measurement and analysis of piezoresonance spectra.

In this work, we studied electromechanical hysteresis and relaxation effects induced by low dc electric fields in the PZT system piezoceramics of the composition $Pb_{0.95}Sr_{0.05}Ti_{0.47}Zr_{0.53}O_3$ + 1% Nb_2O_5. The studied composition belongs to the tetragonal boundary of the morphotropic region and characterized by a low coercive field E_C (1.2 kV/mm measured at 50 Hz). Piezoceramic elements were polarized in air by applying to silver electrodes dc electric field (~1 kV/cm) at heating above Curie temperature (~290°C) and cooling to a room temperature. Precision measurements of the impedance spectra at different amplitudes and polarities of applied dc electric field were performed using Agilent 4294A impedance analyzer and the Piezoelectric Resonance Analysis Program (PRAP) for the thickness and radial vibrational modes of thin piezoceramic disks. The analysis of the dc bias and time dependencies of the complex electromechanical coupling factors k_p, k_t, and elastic modulus C_{33}^D obtained as a result of processing of successively measured impedance spectra was carried out and a physical interpretation of the results has been proposed.

It was found that the character of the field and time dependences of the complex electromechanical coupling factor k_p, k_t and elastic modulus C_{33}^D of PZT piezoceramics under the influence of low dc electric fields is mainly due to reversible displacements 90° domain walls. In this case, changes in the real part of the $k_p^{/}$, $k_t^{/}$ and elastic modulus $C_{33}^{D/}$ are determined by changes in the residual polarization of the piezoceramics caused by reversible displacements of the 90° domain walls. Changes in the imaginary part of the $k_p{}^{/}$, $k_t^{//}$and elastic modulus $C_{33}^{D//}$ are caused by the interaction of resonant oscillations of the piezoceramic element with inhomogeneous mechanical stresses caused by displacements of domain boundaries, moving 90° domain walls and space charge carriers.

The study was financially supported by the Russian Science Foundation Grant No. 22-11-00302, https://rscf.ru/project/22-11-00302/ at the Southern Federal University.

1. I.A. Shvetsov, E.I. Petrova, N.A. Shvetsova, et al., *Ferroelectrics* **561**, 69 (2020).
2. N.A. Shvetsova, S.A. Shcherbinin, M.A. Lugovaya, et al., *Ferroelectrics* **561**, 100 (2020).

P94

$Sr_{0.6}Ba_{0.4}Nb_2O_6$ thin films on Si(110) substrate fabricated by RF-cathode sputtering

D.V. Stryukov, Ya.Yu. Matyash, A.V. Pavlenko

Federal Research Center Southern Scientific Center, Russian Academy of Sciences, 344006 Rostov-on-Don, Russia
strdl@mail.ru

Active dielectrics, which include ferroelectrics, are currently being successfully introduced into various microelectronic devices. Particular attention is paid to thin-film structures, where it is possible to control the properties of the material by using the effects of deformation and domain engineering. This occurs by changing the film growth mechanism and/or material thickness, creating sublayers, and choosing a substrate. One of the promising ferroelectrics for use is strontium barium niobate $Sr_{0.6}Ba_{0.4}Nb_2O_6$ (SBN), which has high dielectric, piezoelectric and optical characteristics. However, SBN thin films is produced on various substrates, but mainly on the (001)-cut substrates. The use of substrates of other orientations can both change the deformation of the unit cell and obtain new phases, which in turn will affect the properties of the material.

In this work, SBN thin film was obtained on a (110)Si substrate by RF cathode sputtering in an oxygen atmosphere. A θ-2θ X-ray diffraction pattern of the obtained film is presented in Figure 1.

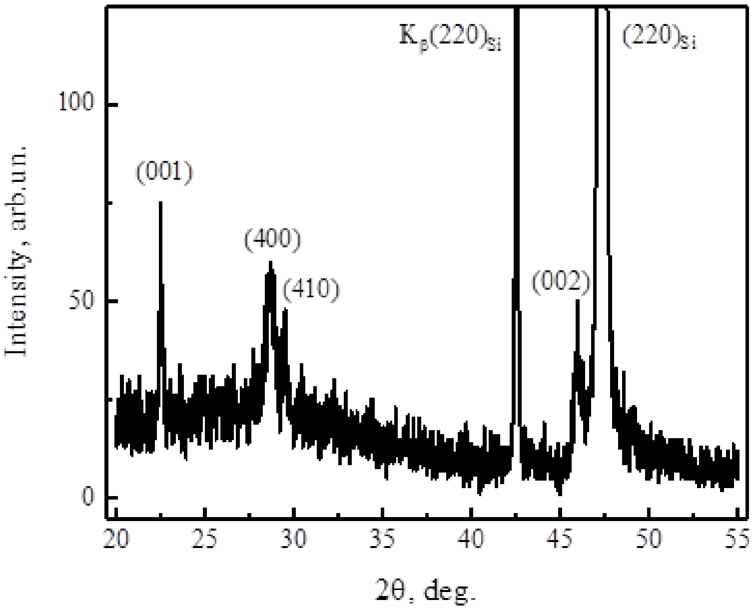

Figure 1. θ-2θ X-ray diffraction pattern of SBN/Si(110) thin film.

From the obtained data it is clear that the film grows as a polycrystalline textured film, where the brightest reflections are the (001) and (400). Since SBN is a uniaxial ferroelectric with a polar “c” axis, the film contains both crystallites with out-of-plane polarization and crystallites with in-plane polarization. This has a strong influence on the electrophysical characteristics of the film. Moreover, the lattice parameters practically do not differ from the parameters of the bulk material

This work was supported by the Russian Science Foundation under Grant [No. 23-22-00389, https://rscf.ru/project/23-22-00389/].

Intermittent deposition of $Ba_2NdFeNb_4O_{15}$ thin films

D.V. Stryukov, A.V. Pavlenko, Ya.Yu. Matyash

Federal Research Center Southern Scientific Center, Russian Academy of Sciences, 344006 Rostov-on-Don, Russia
strdl@mail.ru

Thin film structures are of great interest from both fundamental and applied points of view. They have the properties of traditional functional materials, which can be tuned by deformation and domain engineering methods. One approach is the manifestation of the size effect by changing the film thickness. In this work, multiferroic $Ba_2NdFeNb_4O_{15}$ (BNFN) with a tetragonal tungsten structure was used. By RF-cathode sputtering a series of films were produced in which layers of the BNFN were sequentially deposited. The thickness and number of layers were varied so that the total film thickness remained constant. Single-layer, four-layer, ten-layer and twenty-layer films were obtained. The layer thicknesses varied from 6 to 120 nm. Figure 1 shows the diffraction patterns of the (002) reflection of the resulting thin films.

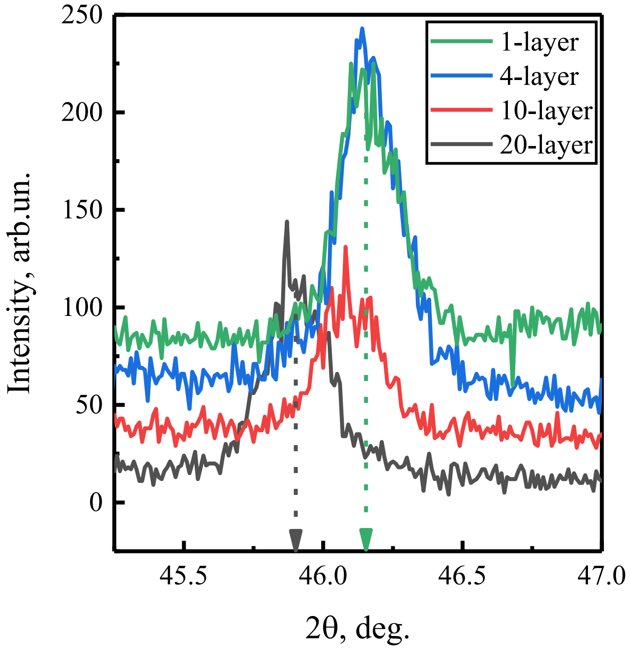

Figure 1. θ-2θ X-ray diffraction pattern of 1-layer, 4-layer, 10-layer and 20-layer BNFN/MgO(001) thin film.

From the obtained diffraction patterns, a shift in the angular positions of the maxima with a layer thickness decrease is noticeable, which corresponds to an increase in the unit cell parameter. Thus, during intermittent deposition of BNFN films, by reducing the layer thickness from 120 to 6 nm, it is possible to further increase the out-of-plane tensile strain of the unit cell (strain was obtained by comparison to the bulk unit cell parameter) by 0.55%. This deformation persists if the thickness of each subsequent layer does not exceed the thickness of the first layer.

This work was funded as part of a state order to the Federal Research Centre The Southern Scientific Centre of the Russian Academy of Sciences, project No 122020100294-9.

P96

Understanding the phase heterogeneity and functional responses in the relaxor BNT-ST ceramics

A.D. Ushakov[1], V.A. Safina[1], A.S. Abramov[1], J. Ruiyi[2], L. Jin[2], V.Ya. Shur[1], D.O. Alikin[1]

[1]*School of Natural Sciences and Mathematics, Ural Federal University, 620000, Ekaterinburg, Russia, bddah@ya.ru*

[2] *Electronic Materials Research Laboratory, Key Laboratory of the Ministry of Education and International Center for Dielectric Research, Xi'an Jiaotong University, 710049, Xi'an, China*

A typical lead-free ferroelectric with excellent dielectric properties, (Bi,Na)TiO_3 (BNT), is considered to be the most promising and competitive eco-friendly ceramic material and has become a focus of research in recent years for dielectric energy storage [1]. The strontium titanate-doped binary ceramics of BNT, $(1-x)(Bi_{0.5}Na_{0.5})TiO_3$–$xSrTiO_3$ (BNT-*x*ST), has been extensively investigated since the first work of Sakata *et al.* [2] which reported the so-called *antiferroelectric phase*.

In this study, we present the results of an experimental investigation of the BNT-xST ceramics family near the morphotropic phase boundary region [3,4]. We employed a combination of complementary microscopic and macroscopic techniques to evaluate phase heterogeneity and its correlation with macroscopic responses. Our analysis involved macro and micro techniques applied to a series of BNT-xST ceramics with x values of 20, 22, 24, and 26%.

It is well-known that relaxor ferroelectric systems exhibit phase and composition inhomogeneity, despite having a nominal composition. In our study, we interpret the relaxor state as a mixture of polar and non-polar volumes, enabling us to differentiate grains of compositions close to ferroelectric, paraelectric, and two types of relaxor states (polar inclusions in non-polar volumes, and non-polar inclusions in polar volumes). By combining macroscopic P-E loop measurements (Fig 1a), local loop measurement modes of piezoresponse force microscopy (PFM) (Fig 1b), and backscattered scanning electron microscopy (SEM) (Fig 1c), we developed a unique method for phase characterization of ceramics.

This approach provides deep insights into the mechanisms underlying the superior performance of these energy-harvesting materials.

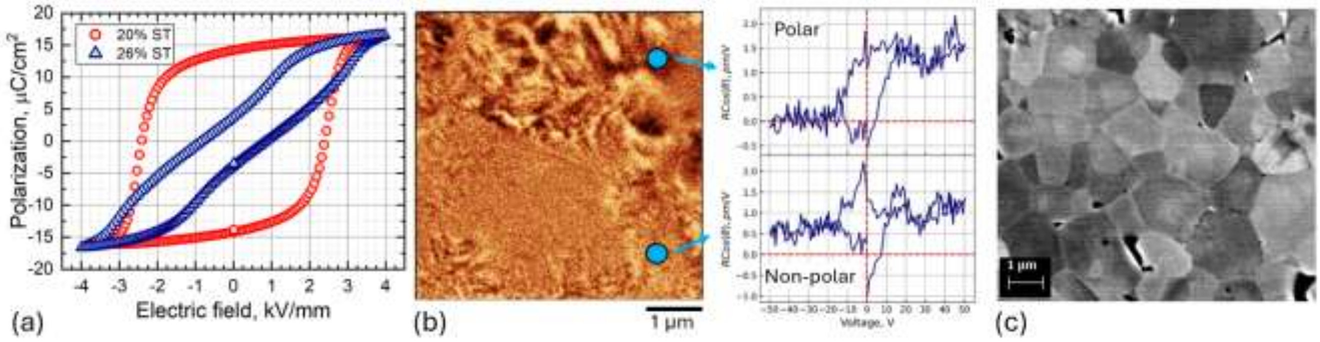

Figure 1. (a) Macroscopic P-E loops of 20 and 26%ST samples. Sample with 26% ST: (b) PFM image and loops measured locally at points marked with dots. (c) SEM image of the surface.

This work was supported by the Russian Science Foundation (Project No. 23-42-00116) and the Natural Science Foundation of China (Grant No. 51761145024). The work was performed using the equipment of the Ural Center for Shared Use "Modern Nanotechnologies" UrFU (reg. No. 2968).

1. W. Zhu, Z.Y. Shen, W. Deng, et al., *J. Mater.***10**, 863 (2024).
2. K. Sakata, Y. Masuda, *Ferroelectrics* **7**, 347 (1974).
3. D. Rout, K.S. Moon, S.J.L. Kang, et al., *J. Appl. Phys.* **108**, 084102 (2010).
4. Y. Hiruma, Y. Imai, Y. Watanabe, et al., *Appl. Phys. Lett.* **92**, 262904 (2008).

P97

Estimation of the band gap in multilayer heterostructures based on SBN and BNFN

K.M. Zhidel, A.V. Pavlenko

Federal Research Centre The Southern Scientific Centre of the Russian Academy of Sciences, 344006, Rostov-on-Don, Russia
karinagidele@gmail.com

In modern electronics, heterostructures based on multiferroic and ferroelectric films are the most popular. Such materials include barium-neodymium ferroniobate ($Ba_2NdFeNb_4O_{15}$, BNFN) and barium-strontium niobate ($Sr_{0.61}Ba_{0.39}Nb_2O_6$, SBN) with a tetragonal tungsten bronze structure. An analysis of literature sources showed that there is no information on the optical parameters of multilayer heterostructures based on SBN and BNFN.

The objects were heteroepitaxial multilayer structures [SBN/BNFN] and [BNFN/SBN], obtained by sequential deposition of 5 bilayers with a thickness of 12–18 nm each by high-frequency sputtering according to the layer growth mechanism on single-crystal MgO substrates with a (001) orientation of 0.5 mm thickness. The optical properties were studied using an SF-56 spectrophotometer at room temperature. Scanning was carried out in the range of 190–110 nm with a step of 1 nm. The resulting multilayer structures were considered as single-phase films of total thickness, having material constants common to the entire multilayer structure. The absorption spectra $\alpha(h\nu)$ was calculated from the transmission spectra using the Lambert–Beer law. To estimate the band gap E_g, the Tauc method was used [1–2].

An analysis of the optical absorption spectra of heteroepitaxial multilayer structures [SBN/BNFN] and [BNFN/SBN] with different thicknesses, assuming direct and indirect allowed transitions, is presented in Figure 1. It can be seen that the [SBN/BNFN] and [BNFN/SBN] multilayer structures with thicknesses of 60 and 90 nm have similar optical band gaps E_g^{dir}. Assuming indirect transitions, it is not possible to reveal an explicit dependence of the E_g^{ind} on the thickness or sequence of layers.

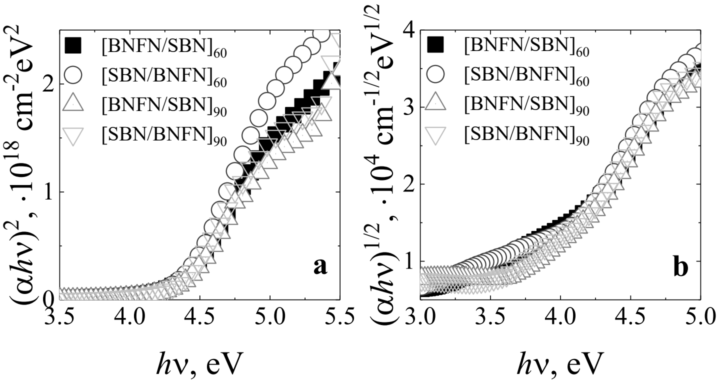

Figure 1. Determination of the optical absorption edge of samples in the model of direct and indirect allowed transitions.

Thus, the results obtained make it possible to observe two energy gaps (one direct E_g^{dir} and one indirect E_g^{ind}) when analyzing the optical region of the spectrum near the fundamental absorption edge for all structures.

The work was performed with the use of equipment of the Center for Collective Use «Integrated Centre of scientific-technological equipment SSC RAS (research, development, approval)», the Southern Scientific Centre of the Russian Academy of Sciences (No. 501994).

The research was funded by the Russian Science Foundation (project No. 21-72-10180).

1. J. Tauc, R. Grigorovici, A. Vancu, *Physica Status Solidi B* **2**, 627 (1966).
2. J.G. Solé, L.E. Bausa, D. Jaque, *An Introduction to the Optical Spectroscopy of Inorganic Solids* (John Wiley & Sons, Ltd.), 304 (2005).

P98

Transmission spectra of SBN61 thin films in the low temperature region

K.M. Zhidel[1], A.V. Pavlenko[1,2]

[1]*Research Institute of Physics, Southern Federal University, 344090, Rostov-on-Don, Russia*
karinagidele@gmail.com

[2]*Federal Research Centre The Southern Scientific Centre of the Russian Academy of Sciences, 344006, Rostov-on-Don, Russia*

The study of heterostructures based on thin films of barium-strontium niobate ($Sr_xBa_{1-x}Nb_2O_6$, SBN) is of great scientific interest and is promising for many technical applications, in particular as the basis for non-volatile memory, microelectromechanical systems, phase shifters and new optoelectronic devices. It is known that SBN solid solutions at strontium concentration x from 0.2 to 0.8 have the structure of tetragonal tungsten bronze. When the Ba/Sr concentration ratio changes, the lattice parameters change, and the filling of channels with Ba and Sr atoms redistributes. In this case, the dielectric, optical and electro-optical properties undergo changes. We did not find any information in the literature about changes in the optical properties of thin-film structures of this material, which confirms the relevance of our research.

This paper presents the results of studying the temperature dependence of the transmission spectra of thin films of barium-strontium niobate with the composition $Sr_{0.61}Ba_{0.39}Nb_2O_6$ (SBN61) when cooled from room temperature (RT) to –180°C.

The objects were heteroepitaxial films of SBN61 on MgO (001) substrates, obtained by high-frequency cathode sputtering in an oxygen atmosphere. Measurements of the transmittance of SBN61 films in the optical wavelength range 190–1100 nm were carried out on an SF-56 spectrophotometer. For temperature measurements, a nitrogen filled optical cryostat LN-121-SPECTR was used. The temperature range varied from RT at +21°C to –180°C.

The transmission spectra of SBN61/MgO heterostructures are presented in Fig. 1. As can be seen from the figure, the spectrum boundary (absorption edge) of the films shifts to the region of short wavelengths as the temperature decreases, which should correspond to a change in the band gap of the films, and a change in the level of transmittance should correspond to a change in the optical constants of the material, respectively.

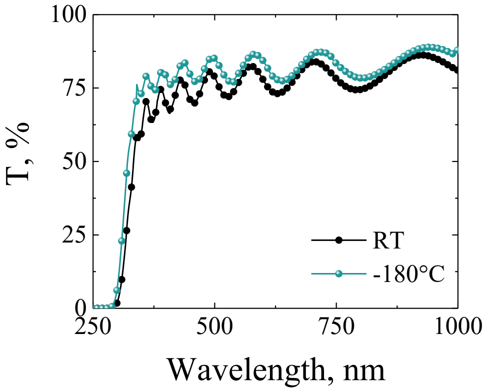

Figure 1. Transmission spectra of SBN61 films on a MgO substrate depending on temperature.

The work was performed with the use of equipment of the Center for Collective Use «Integrated Centre of scientific-technological equipment SSC RAS (research, development, approval)», the Southern Scientific Centre of the Russian Academy of Sciences (No. 501994).

The study was carried out with the financial support of the Ministry of Science and Higher Education of the Russian Federation (State task in the field of scientific activity. Project No. FENW-2023-0010/GZ0110/23-11-IF). Title of the topic: «Multicomponent intelligent structures: phase transition cross-effects and strategies for accelerated design of eco-systems for technologies for digital design of devices for controlling the parameters of physical media».

P99

Diphenylalanine peptide nanotubes as substrates for surface-enhanced Raman spectroscopy

V.S. Bystrov[1], E.V. Paramonva[1], O.R. Ledeneva[2], O.E. Bagrova[3], P.S. Zelenovskiy[4]

[1]*Institute of Mathematical Problems of Biology - Branch of Keldysh Institute of Applied Mathematics, Russian Academy of Sciences, 142290 Pushchino, Russia*
vsbys@mail.ru

[2]*Faculty of Computer Science, National Res. University Higher School of Economics,109028 Moscow, Russia*

[3]*Faculty of Physics, Lomonosov Moscow State University, 119991 Moscow, Russia*

[4]*School of Natural Sciences and Mathematics, Ural Federal University, 620000 Ekaterinburg, Russia*

Surface-enhanced Raman spectroscopy (SERS) is a powerful and highly sensitive technique for enhancing the Raman scattering of molecules supported on the nanostructured materials [1]. It enables the detection of the structural fingerprints of analyte molecules at low concentrations [1]. In the original versions of the SERS technique, the most important factor is the SERS substrate, typically a metal surface (silver or other noble metals) with nanoscale characteristics. The type of metal and the nanoscale features of the substrate largely determine the overall Raman enhancement. However, the development of this method is now progressing towards simpler SERS substrates, portable analytical instruments, and point-of-sample analysis. The SERS signal depends on the materials used to fabricate the substrate, and semiconductor-based SERS-substrates have received significant research interest as a means of mitigating the costs associated with noble metal nanoparticles and utilizing a chemical enhancement mechanism to improve the SERS signal through charge transfer processes.

In this regard, several studies [2] have demonstrated that nanotubes made from the diphenylalanine peptide (FF PNT), which also possess semiconductor properties, can serve as a SERS substrate capable of detecting concentrations as low as 10^{-7} M for various molecules, including mononucleotides. Therefore, bioinspired semiconductor FF PNT have attracted considerable interest as SERS substrates due to their biocompatibility, piezoelectric and pyroelectric properties, as well as their thermal and chemical stability and wide bandgap. These properties of FF PNT has also been studied in a number of our works [3,4]. Furthermore, we have extensively studied their photoelectronic properties [5], which are crucial for their utilization as a SERS-substrates.

In this work, based on the research and calculations, we investigated the mechanism for the potential detection of small molecules, such as Methylene blue (MB), using FF PNT as SERS substrates. The calculations were performed using the semi-empirical RM1 RHF method in the HyperChem software package, similar to our previous works [3-5]. The results indicate that when the MB analyte molecule is in proximity to the FF PNT surface, charge is captured and transferred from the HOMO energy level of the FF PNT to the HOMO energy level of the MB molecule. Consequently, the total width of the band gap (E_g) decreases, and upon excitation by a laser with energy E_l = 2.33 eV (532 nm), a resonant enhancement of the SERS signal occurs due to the chemical bond formation. As an illustration, we present the following data for the "D-FF/L-FF + MB" system:

Object	E_HOMO, eV	E_LUMO, eV	E_g, eV	λ, nm	ΔE_g, eV	$\Delta\lambda(E_g)$, nm	$\Delta E=E_l-E_g$, eV	$\Delta\lambda$, nm
MB	-4.242	-0.006	4.236	293				
D-FF	-5.812	-2.450	3.362	369				
D-FF + MB	-4.566	-2.417	2.149	577	1.213	208	0.181	44
L-FF	-5.857	-2.618	3.239	383				
L-FF + MB	-4.372	-2.523	1.849	670	1.390	287	0.48	138

1. X.X. Han, R.S. Rodriguez, et al., *Nat. Rev. Methods Primers* **1**, 87 (2021).
2. S. Almohammed, A. Fularz, M.B. Kanoun, et al. *ACS Appl Mater Interfaces* **14**, 12504 (2022).
3. P. S. Zelenovskiy, A. S. Nuraeva, S. Kopyl, et al., *Cryst. Growth Des*. **19**, 6414 (2019).
4. V. Bystrov, J. Coutinho, P. Zelenovskiy, et al., *Nanomaterials* **10**, 1999 (2020).
5. V. Bystrov, E. Paramonova, P. Zelenovskii, et al., *Symmetry* **15**, 504 (2023).

P100

Experimental validation of one-dimensional model of an ideal bimorph actuator provided on bidomain lithium niobate

I.V. Kubasov, I.S. Syrykh, A.V. Turutin, A.M. Kislyuk, V.V. Kuts,
A.A. Temirov, M.D. Malinkovich, Y.N. Parkhomenko

Laboratory of Physics of Oxide Ferroelectrics in the University of Science and Technology MISIS, Moscow, Russia
kubasov.ilya@gmail.com

We experimentally demonstrate that the dynamic characteristics of piezoelectric bimorph actuators based on bidomain lithium niobate single crystals are accurately described by an analytical 1D model of an ideal bimorph. Our observations show that displacements and an electric impedance of the single-crystal bimorphs can be predicted without use of any sophisticated lumped circuit models, equations with handpicked "effective" values of material's constants or finite element analysis within the frequency range containing at least the first three bending resonances. The experimental data were measured by means of laser interferometry and impedance spectroscopy from a cantilevered y+128°-cut bidomain crystal. To validate the correspondence between the measured data and theoretical predictions, we solved the inverse problem by fitting the experimental points with the equations predicted by the 1D model using a simulated annealing algorithm. This technique allowed us to calculate the transverse piezoelectric coefficient, longitudinal mechanical compliance, dielectric permittivity, and piezoelectric coupling coefficient of the material. The obtained values of the material constants of the lithium niobate y+128°-cut crystal cut are d_{23} = 25 pC/N, s_{33}^{E} = 7.58 TPa^{-1}, ε_{22}^{T} = 52.7ε_0 , and k_{23}^{2} = 0.18, which are in excellent agreement with the literature data. The demonstrated accuracy, stability, and predictability of bimorphs based on bidomain lithium niobate single crystals offer a pathway towards advanced actuators with enhanced precision and reliability. Leveraging the unique properties of bidomain lithium niobate crystals holds promise for expanding the possibilities of both sensing and actuation applications in diverse fields.

This study was performed with financial support from the Russian Science Foundation (grant no. 24-19-00876, https://rscf.ru/project/24-19-00876/).

P101

Features of porous piezoceramics polarization by point sources of electric field

D.I. Makarev, A.N. Reznichenko, N.A. Shvetsova, A.N. Rybyanets

Southern Federal University, 344090, Rostov-on-Don, Russia
dmakarev@rambler.ru

The intensive development of additive technologies has affected many industries, including the fabrication of elements from active materials and products on their base. One of the promising additive technologies for the production of piezoelectric elements is the technology of layer-by-layer gluing of powders. It can be used for the manufacture of composite piezoelements based on a polymer matrix with inclusions of piezoactive particles. Using this technology, a layer of powder is applied to the working table of the installation, which is glued in the right places with polymer glue. The cartridge with this glue is delivered to the desired point by a mechanical programmable coordinate system. Instead of powder, you can use particles of porous piezoceramics, and instead of glue, you can use a two-component polymer binder. The result is a composite of the “porous piezoceramics-polymer” system. Particles of porous piezoceramics PCR-1 were used as piezoactive particles, and a two-component acrylic-based polymer was used as glue. However, this composite did not have a piezoelectric effect. The lack of piezoelectric properties in such composites is explained by the presence of irremovable polymer layers between the piezoceramic particles, along with the huge difference in the dielectric constants of the piezoceramic particles and the polymer binder. These layers prevent the electric field from effectively penetrating the particles during polarization and operation of the samples. This circumstance can be overcome by introducing conductive particles into the polymer matrix. These particles are capable of providing electrical contact between particles of porous piezoceramics. However, such contact is point-wise. This significantly reduces the effectiveness of the material. The longitudinal piezoelectric modulus of such composite is only 10% of the piezoelectric modulus of the original piezoceramics.

The purpose of this work was to study the dependence of the polarization of porous piezoceramics on the geometric dimensions and concentration of sources of the polarizing electric field. It should be noted that the topology of porous piezoceramics resembles the structure of coral and can be imagined as consisting of many intertwined quasi-unidimensional rods. This circumstance contributes to the polarization of such ceramics by point field sources. Research has shown that the piezoelectric properties of porous piezoceramics depend on the linear density of point sources of electric field and the magnitude of the electric field strength. Compared with the electromechanical coupling coefficients of thickness vibrational mode and longitudinal piezoelectric modulus, the electromechanical coupling coefficients of planar vibration mode and transverse piezoelectric modulus depend much more strongly on both the discreteness of the field sources and the degree of symmetry of their location on the surface of the samples. The overall anisotropy of the piezoelectric properties of porous piezoceramic samples increases with a decrease in the number of polarization field sources on the samples.

Supported by the Ministry of Science and Higher Education of the Russian Federation; the state task in the field of scientific activity No. FENW-2022-0001.

P102

Stress of annealed proton exchange waveguides in mixed lithium niobate-tantalate single crystals

A.V. Sosunov[1], E.V. Miasnikova[1], I.V. Petukhov[1], M. Kuneva[2]

[1]*Perm State University, 614990 Perm, Russia*
alexeisosunov@gmail.com

[2]*Institute of Solid State Physics, Bulgarian Academy of Sciences, 1784 Sofia, Bulgaria*

To manufacture single-mode waveguides in mixed single crystals, it is necessary to choose a technological regime depending on the structure and composition of the samples. In this work, we analyze the lattice stresses and the increment of the refractive index for lithium niobate (LN) and mixed crystals obtained under identical conditions. The crystal was grown by the Czochralski method from the $LiNb_{0.97}Ta_{0.03}O_3$ (LNT) charge in Pt crucibles at the Institute of Microelectronics Technology and High Purity Materials of the Russian Academy of Sciences using NIKA-3M system [1]. The experimental samples LNT had a size of 10×10×1 mm and *X*- and *Z*-cut crystallographic orientation. Annealed proton exchange (APE) waveguides were created in zirconium reactor in pure molten benzoic acid at 190 °C during 2 hours and subsequent air annealing at temperature 370 °C – 8 hours (*X*-cut) and 350 °C – 5 hours (*Z*-cut). XRD, prism coupling method and selective chemical etching with optical microscopy were applied for research.

The deformations of the crystal lattice of the APE waveguides were determined by the broadening of the XRD lines. The results are given in Table 1.

X-cut: α-phase is formed with an increment of the refractive index $\Delta n_e < 0.025$ [2] and almost identical deformations of the crystal lattice with LN. To form single-mode waveguides in LN and LNT, similar proton exchange and annealing regimes can be applied.

Z-cut: for the non-polar LNT sample, the temperature regime that was chosen for the formation APE waveguides allows to the α-phase with low crystal lattice deformations is sufficient. However, we observed κ_1-phase for LN sample with a high degree of stress in the crystal lattice (4.6×10^{-4}). Thus, a gentler regime of proton exchange and annealing of LNT makes it possible to form an α-phase, unlike LN. The results of dislocation density on the rate of proton diffusion and stresses of the crystal lattice of APE waveguides in LNT crystals are discussed.

Table 1. Results

Crystallographic orientation	LN		LNT	
	ε, 10^{-4}	Δn_e	ε, 10^{-4}	Δn_e
X-cut	3.3	0.019	3.3	0.018
Z-cut	4.6	0.032	3.4	0.022

This work was funded by Ministry of Education and Science of the Perm Region № C-26/37

1. E.V. Zabelina, A.A. Mololkin, N.S. Kozlova, et al. *Crystallogr. Rep.* **68**, 1173 (2023).
2. Yu.N. Korkishko, V.A. Fedorov, *Crystallogr. Rep.* **44**, 237 (1999).

P103

2D mapping technique of non-uniform magnetic fields using self-biased magnetoelectric composites based on “bidomain $LiNbO_3$/Ni/Metglas” structures

V.V. Kuts[1], A.V. Turutin[1], I.V. Kubasov[1], A.A. Temirov[1], A.M. Kislyuk[1], E.E. Maksumova[1],
F.A. Fedulov[2], Y.K. Fetisov[2], M.D. Malinkovich[1], Y.N. Parkhomenko[1]

[1]Laboratory of Physics of Oxide Ferroelectrics, National University of Science and Technology MISIS, 119049 Moscow, Russia
aturutin92@gmail.com

[2]MIREA – Russian Technological University, Moscow 119454, Russia

Magnetoelectric (ME) composites are extensively researched for magnetic field detection, typically characterized by interactions with homogeneous magnetic fields. However, practical applications often involve non-uniform magnetic fields. In this study, we developed and validated a technique for 2D mapping non-uniform magnetic fields (NMF) using ME sensors. The primary focus was on mapping the magnetic field generated by a single wire carrying an alternating current (AC). The experimental setup included a bidomain $LiNbO_3$/Ni/Metglas ME structure, which demonstrated a non-zero ME coefficient of 0.83 V/(cm·Oe) at 117 Hz. The ME structure was characterized using both quasi-static and dynamic methods, with the mapping performed at a frequency of 232 Hz, chosen to ensure a linear response and minimize resonance effects. Our measurements revealed that the maximum signal from the ME sensor was consistently shifted from the central position of the wire (0 mm on the X-axis), even though the maximum integral magnetic field intensity is theoretically achieved at this position. Specifically, the maximum response from the ME sensor exhibited a shift of 5 mm and 2 mm along the X-axis when scanning along the B-A-B and A-B-A paths, respectively. This shift was attributed to the deformation of the ME structure and the redistribution of the magnetic flux along the sample, as confirmed through modeling. Further, the measured 2D mapping of the NMF from the wire closely matched the theoretical distribution, displaying axial symmetry but with a persistent shift of 2-3 mm along the X-axis across different Z-levels. The distribution also extended along the X-axis as the ME signal level varied slightly with a 2-mm shift. These effects were linked to the linear dimensions and clamping methods of the ME structure.

Overall, our experimental results closely correlated with theoretical data and the COMSOL model, demonstrating that ME composites are effective for NMF detection and mapping. Future work will aim to reduce the dimensions of the ME structure using MEMS technology to minimize the observed shift effects in the measurements.

The study was performed with financial support from the Russian Science Foundation (grant No. 22-19-00808, https://rscf.ru/project/22-19-00808/).

P104

Extremely large strain response under low driving electric fields in lead-based textured piezoelectric ceramics

H. Jia, Zh. Li, L. Wang

Electronic Materials Research Laboratory, Key Laboratory of the Ministry of Education and International Center for Dielectric Research, School of Electronic Science and Engineering, Xi’an Jiaotong University, Xi’an, 710049, P. R. China
lhwang@xjtu.edu.cn

Precision positioning technology is one of the key technology to achieve precision manufacturing, precision measurement and precision drive, and it has been receiving great attentions and widely used in optical engineering, aerospace, semiconductor industry and many other high-tech fields. As the key part of precision positioning system, micro-displacement actuator plays an important role in sensitivity and resolution of precision positioning system. In order to achieve large driving force and high-precision displacement of micro-displacement actuator, it is particularly necessary for piezoelectric ceramics to possess a high strain value and low strain hysteresis under small driving electric fields. Up to date, it remains grand challenge for piezoelectric ceramics to simultaneously possess large strain response and low strain hysteresis under low driving electric fields. At present, texture technique, which can make ceramic grains oriented along specific crystallographic orientation, is considered one of the most promising means to significantly improve the strain response of piezoelectric ceramics. In this work, we adopted a combination strategy of composition design and texture technique to develop a novel textured ceramics to address this challenge. In this paper, 1%Sm-PMN-30PT textured ceramics with highly [001]c orientation was successfully manufactured and an ultrahigh strain response of 0.27% and a low strain hysteresis of 15% at 2 kV/mm were obtained concurrently.

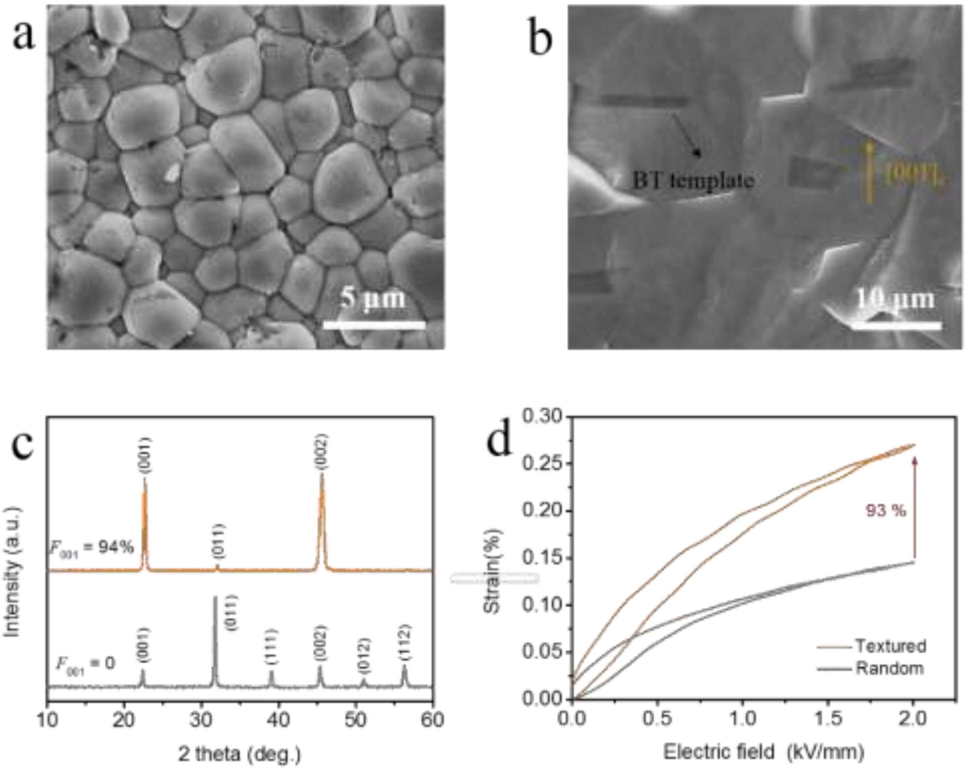

Figure 1. Structural and strain characterizations of 1%Sm-PMN-30PT ceramics. (a) Surface SEM image of random ceramics. (b) Fracture surface SEM images of textured ceramics. (c) XRD patterns of random and textured ceramics. (d) Unipolar strain curves of random and textured ceramics.

P105

The structure and preferred orientation of the 180° domain walls in uniaxial ferroelectrics lithium niobate and lithium tantalate

E.L. Rumyantsev

School of Natural Science and Mathematics, Ural Federal University, 620026, Ekaterinburg, Russia
evgenij.rumyantsev@gmail.com

The single domains arising during polarization reversal in the uniaxial lithium niobate and lithium tantalate often demonstrate the regular shape at the cross-section with the surface. The regular hexagons and equilateral triangles so as domain rays with orientations strictly subjected to the symmetry of the crystal are observed. The theoretical consideration of the possible physical reasons for formation of such regular shapes is presented to our knowledge only in the following papers [1-3]. In [1,2] the structure, energetics and ferroelectric properties of the infinite plane domain walls as the function of orientation have been investigated within Landau-Ginzburg-Devonshire (LGD) approach. The breaking of the uniaxial symmetry by the obtained polarization profile in this approach has been attributed to the interaction of polarization and elastic subsystems. In [2,3] the similar polarization profiles of Bloch and Neel types differing from simple Ising-type have been obtained within microscopic Density-Functional Theory (DFT) calculations.

The purpose of our paper is to show that the main results of DFT can be reproduced if qualitatively using trial variation functions in the analysis of LGD functional. The main difference with the results of LGD in [1] is that we take into account the interaction of the critical system only with the orthogonal to the optical axes polarization subsystem. Such consideration is based on the existence of the specific invariant $P_z(P_x^2 P_y - P_y^3)$ in the LGD expansion arising only for the point D_{3d} group which is the symmetry of the crystals of interest. We reproduce qualitatively the spatial behavior of the mixed Ising-Bloch and Ising-Neel types within proposed approach for Y and X oriented walls [3] correspondently. We show within such simplified LGD version that the neutral Y walls are always energetically favored over the charged X walls if the excess contribution to the surface energy due to in-plane polarization is accounted for in accord with [1-3]. As the surface energy value is a crucial parameter determining the equilibrium wall orientation, it means that the domains with X walls are forbidden within LGD and DTF approaches. Nevertheless, the triangular domains with X walls are observed experimentally.

We discuss this apparent theoretical paradox and propose the physical conditions under which the arising of the triangle domain shapes could be made possible. We ascribe the main difference in Y and X walls kinetics to the possibility of the simultaneous movement of the two walls of the same type in the opposite directions. The enhanced contribution of the depolarization energy for such movement of X walls which according to the theory bear opposite charges (one is of head-to-head type and other is tail-to-tail one) forbids their simultaneous existence. There is no such problem for the neutral Y walls thus comprising hexagons as a result. The existence of charged X walls can be attributed to screening of the depolarization field through the bulk conductivity.

The author is grateful for financial support of the Ministry of Science and Higher Education of the Russian Federation (state task FEUZ-2023-0017).

1. D.A. Scrymgeour, V. Gopalan, A. Itagi, et al., *Phys. Rev. B* **71**, 184110 (2005).
2. D. Lee, R.K. Behera, P. Wu, et al., *Phys. Rev. B* **80**, 060102 (2009).
3. D. Lee, H. Xu, V. Dierolf, et al., *Phys. Rev. B* **82**, 014104 (2010).